Université de Neuchâtel **Faculté des Sciences**

Dimers of the columnar mesomorphic 2-substituted benzene-1,3,5,-tricarboxamide (BTA) unit: study of the liquid crystallinity in the bulk and of the self-assembly in solution

---

Thèse soutenue le 1 juin 2015 pour l'obtention du titre de Docteur ès Sciences
par

Christian INVERNIZZI

Titulaire d'un Master Degree in Chemical Sciences
de Università degli Studi di Milano, Milan, Italie

Membres du jury:

Prof. Reinhard NEIER	(Directeur de thèse)
Prof. Robert DESCHENAUX	(Rapporteur interne)
Dr. Claudio DALVIT	(Rapporteur interne)
Prof. Cesare GENNARI	(Rapporteur externe)

FNSNF
FONDS NATIONAL SUISSE
SCHWEIZERISCHER NATIONALFONDS
FONDO NAZIONALE SVIZZERO
SWISS NATIONAL SCIENCE FOUNDATION

unine
UNIVERSITÉ DE
NEUCHÂTEL

Institut de Chimie, Juin 2015

UNIVERSITÉ DE NEUCHÂTEL

Faculté des sciences
Secrétariat-décanat de Faculté
Rue Emile-Argand 11
2000 Neuchâtel - Suisse
Tél: + 41 (0)32 718 2100
E-mail: secretariat.sciences@unine.ch

IMPRIMATUR POUR THESE DE DOCTORAT

La Faculté des sciences de l'Université de Neuchâtel autorise l'impression de la présente thèse soutenue par

Monsieur Christian INVERNIZZI

Titre:

"Dimers of the columnar mesomorphic 2-substituted benzene-1,3,5-tricarboxamide (BTA) unit: study of the liquid crystallinity in the bulk and of the self-assembly in solution"

sur le rapport des membres du jury composé comme suit:

- Prof. Reinhard Neier, directeur de thèse, Université de Neuchâtel
- Prof. Robert Deschenaux, Université de Neuchâtel
- Dr Claudio Dalvit, Université de Neuchâtel
- Prof. Cesare Gennari, Università degli Studi di Milano, Italie

Neuchâtel, le 23 juillet 2015

Le Doyen, Prof. B. Colbois

Acknowledgments

The work of this PhD project has been carried out from April 2010 until June 2015 at the Institut de Chimie of the University of Neuchâtel under the supervision and in the laboratory of Professor Reinhard Neier. I really would like to thank him for the great chance he gave me to work with him in his research group on a such challenging project. I would like to thank him as well for the freedom and confidence that he has given to me.

I would like to thank Professor Robert Deschenaux for have accepted to be part of the jury and corrected my manuscript. Moreover I would like to thank him for the kind discussions spent with me.

I would like to thank Professor Cesare Gennari for have accepted to be part of the jury and corrected my manuscript, and moreover for his passionate teaching of organic chemistry.

I address a special thanks to Dr. Claudio Davit for have accepted to be part of the jury and, especially, I would like to thank him for all his teaching and the all discussions we had together.

During doctoral studies I had the opportunity to work with different apprentices that enormously contributed to the development of this project. My thanks are addressed to Sebastien Mendes, Maude Stein and Tracy Rosselet.

During the last five years I had the privilege to work in a very friendly and professional research group. I would like to thank all the present and the former members of the Neier's group. In particular I thanks the Post-Doc I met during this time, especially for their teaching and advices. My thanks are addressed to Dr. Frederic Bruyneel, Dr. Anca Pordea, Dr Damien Thevenet, Dr. Christophe Letondor, Dr. Maria Kolympadi and Dr. Ana-Maria Buciumas.
My gratitude is also addressed to the PhD students that were with me in the lab: William Maupillier, Sara Santi, Ewa Banach, Dr. Guillaume Journot, Dr. Christelle Schenk, Dr. Inga Kolod and Dr. Lucia Cerisoli.

I would like to thank all the Neuchâtel Platform of Analytical Chemistry (NPAC). In particular, I would like to thank Dr. Claudio Dalvit for the NMR analyses, Dr. Armelle Vallat-Michel for the Mass analyses and Professor Helen Stoeckli-Evans for the X-Ray diffractions. I also would like to thank Professor Robert Deschenaux and his group, especially Dr. Sebastiano Guerra, Dr. Thi Luyen Vuong and Steeve Albert, for having allowed me to use their instruments (DSC and polarized-light microscope) and their essential assistance.

I would like to thank all the other members of the Institut de Chimie of the University of Neuchâtel for have been spent unforgettable moments with me during these years.

I would like to thank all the founding agencies that supported my project, especially the Swiss National Science Foundation (FNS), the University of Neuchâtel and the Canton of Neuchâtel.

I would like to thank all the friends I met during all these five years in Switzerland because they made my stay in Switzerland an extraordinary experience. Thanks to all of you.

Finally, I would like to thank all my family for their support and encouragement during this doctoral experience and during all the other moments of my life.

You are urgently warned against allowing yourself to be influenced in any way by theories or by other preconceived notions in the observation of phenomena, the performance of analyses and other determinations.

(Hermann Emil Fisher)

General Information

This manuscript has been written and edited according to the publication format. Each chapter has its own reference list. However, for an easy reading, the compounds have been assigned a sequential ordering.

Part of the figures and schemes reported in this manuscript have been directly extracted from the referenced original work subjected to copyright. According to the "Statements on the fair use of images for teaching, research and study" reported by the Visual Resources Association, US, all the figures and other material subjected to copyright have been properly referenced and the sources have been clearly indicated.

List of Abbreviations

M.p.	Melting Point
B.p.	Boiling Point
TLC	Thin Layer Chromatography
NMR	Nuclear Magnetic Resonance
DOSY	Diffusion-Ordered Spectroscopy
ppm	Part-per-million
R_f	Retention Factor
HR-MS	High-Resolution Mass Spectroscopy
IR	Infrared
BTA	Benzene-1,3,5-tricarboxamide
ESI	Electron Spray ionization
aq.	Aqueous
MALDI	Matrix-assisted laser desorption/ionization
Col	Columnar Liquid Crystal
I	Isotropic Liquid
r.t.	Room Temperature

Key Words

Benzene-1,3,5-tricarboxyamides; Hydrogen Bonds; π-π stacking; columnar liquid crystals; Self-Assembly; Structure-Properties Relationships; Dimers.

Summary

The self-assembly of *N,N',N''*-trialkylbenzene-1,3,5-tricarboxyamides (BTAs) has been reported to lead to supramolecular columnar-stacked structures with attractive material properties. The formation of the columnar liquid crystalline phases (mesophases) along a broad range of temperature is one of the most interesting properties shown by BTAs. In this thesis, the formation of dimeric structures from the BTA unit was carried out to investigate the stabilization effect on the columnar supramolecular aggregation.

The first challenge concerned the functionalization of the BTA scaffold in order to introduce an "anchoring site" and achieve the formation of dimers. In this context, in the literature, the introduction of alkoxy groups has been demonstrated to reinforce the self-assembly process. For this reason, we synthetized a mono-2-substituted BTA carrying a pentynyloxy group. We investigated the aggregation process of the newly synthetized 2-substituted BTAs in the bulk and in solution by means of DSC, POM, X-ray diffraction and concentration-induced ^{1}H-NMR experiments. The presence of this single substituent significantly influenced the self-assembly process. Moreover, those measurements revealed that the self-assembly was impaired by H-bond accepting substituents and strengthened by non-H-bonding substituents.

In the second part, the 2-substituted BTA derivative was employed in the construction of covalently-connected dimers. The study of the self-assembly process of the dimers was carried out in solution by employing concentration-induced NMR analyses. These measurements revealed the enhancement of the association process upon dimerization. However, none of the dimeric structures presented liquid crystallinity. Therefore, we synthetized a library of 2-substituted BTA dimers with different aromatic linkers and modifications on the amide side-chains. Finally, we screened the ability of these dimeric compounds to form mesophases with the goal of establishing an empirical structure-properties relationship.

Table of Contents

Introduction

Table of Contents

Understanding the mechanisms that create molecular order from simple building-blocks is a prerequisite for deepening our knowledge of fundamental processes in biological and material sciences.[1] The availability of new materials showing properties in a programmed fashion (e.g. charge transporting materials, self-aggregating materials) could be exploited and utilized in a broad scope of potential applications from photovoltaics to biomedical applications.[2]

Nowadays the majority of the synthetic organic materials that found industrial uses and large scale applications are polymers. However, polymers are not good starting materials for creating ordered structures due to lack of knowledge in their non-covalent aggregation mechanism. Therefore only few examples of controlled supramolecular assembly of covalent polymers have been reported so far.[3]

On the other hand the use of the self-assembly process leading to supramolecular (aggregated) polymers could potentially solve the challenges in providing materials with controlled properties. The self-assembly process occurs in natural biological systems (e.g. DNA, proteins) and it has already been successfully used in abiotic artificial systems.[4] Typically, the relatively small number of interactions responsible for self-assembly is combined with the wealth of empirical data for the creation of "designed" structures with predictable shapes and properties. "*Our ability to predict the structural features and the functional outcome of the assembled materials is still limited and most of the learning is done in retrospect*".[5] In-depth understanding of natural phenomena is the ultimate goal of fundamental research. At the moment that the natural phenomenon is sufficiently mastered, its exploitation in artificial applications on large scale will be possible. "*An important prerequisite to evolve from an academic curiosity into a viable platform for advanced, functional materials is the synthetic accessibility of the supramolecular building blocks and an in-depth understanding of how small changes in the molecular structure affect the aggregation properties".*[6]

The use of reversible non-covalent interactions toward the construction of supramolecular architectures presents the advantages of reduced synthetic costs, high modifiability and rapid access to new structures. Due to the pioneering work of the Nobel laureate Jean-Marie Lehn from the University of Strasbourg, the understanding of supramolecular non-covalent interactions has changed and evolved dramatically.[7] Since then, a large variety of functionalized monomers have been reported in the literature.[8] Different types of intermolecular forces that bind monomers to form supramolecular polymers have also been identified. These interactions are mostly based on $\pi-\pi$ stacking,[9] H–bonds,[10] metal-ligand interactions[11] or a symbiotic combination of several different interactions (e.g. H-bonds and $\pi-\pi$ stacking).

Trialkyl benzene-1,3,5-tricarboxamides BTAs: A journey into the world of self-assembly.

Trialkyl benzene-1,3,5-triacarboxamides (or more simply and commonly called BTAs) are a promising class of organic compounds used in the preparation of highly organized supramolecular structures (Scheme 1). Although BTAs were synthesized for the first time in 1915 by Curtius[12] their application in the field of supramolecular chemistry did not started until late 1980s. At that time the group of Matsunaga discovered that BTAs form hexagonal columnar liquid crystalline phases (Col_h).[13] It has been shown that BTAs organize in columnar mesomorphic phases over a wide temperature range

when the three side chains **R** (Scheme 1) are composed of at least five carbon atoms (pentyl group).[10]

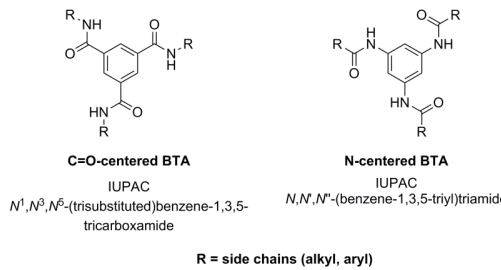

Scheme 1. General structures of benzene triamide derivatives BTAs.

In the last decade, trialkyl benzene-1,3,5-triacarboxamides have become the subject of extensive studies (Graph 1), mostly because of their potential technological applications (e.g. discotic liquid crystals DLC, organogels, MRI contrasting agents).[6]

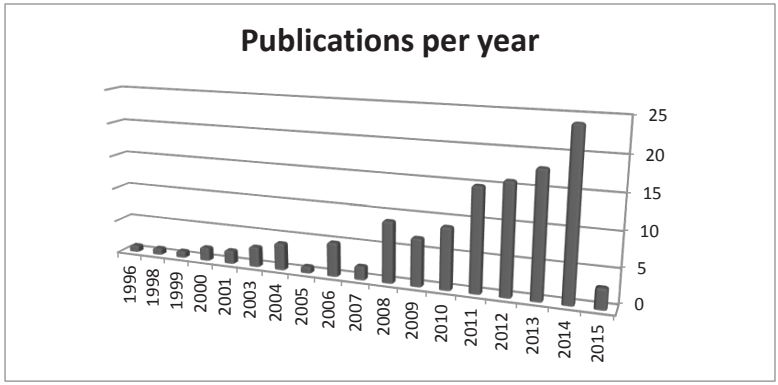

Graph 1. Number of publications per year presenting the concept of "Benzene-1,3,5-tricarboxamide". The key word was searched on the program Scifinder® chemical abstract on the 1st May 2015. A total of 92 publications were found.

The extensive use of BTAs in the design of materials for new applications became possible thanks to the understanding of the mechanism of BTAs self-aggregation that results in well-defined supramolecular architectures.[14]

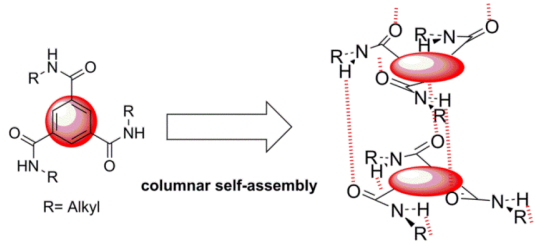

Figure 1. Schematic representation of C=O-centered BTAs columnar aggregation.

The skeleton of benzene-1,3,5-tricarboxamide is composed of a central C_3-symmetrically substituted aromatic ring (*discotic unit*) functionalized by three amide groups (containing alkyl *chains*). The amide groups can be connected to the aromatic ring in two different positions generating two distinct isomers (Scheme 1). When the connection to the aromatic ring is made via the nitrogen atom, *N*,*N*′,*N*′′-(benzene-1,3,5-triyl)-triamides, commonly called *N*-centered BTAs, are obtained. When the connection is made via the carbonyl group however, N^1,N^3,N^5-(trisubstituted) benzene-1,3,5-tricarboxamides, called C=O-centered BTAs, are formed. This study deals exclusively with C=O-centered BTA derivatives, nonetheless for the sake of completeness, crystal structures, aggregation mechanisms and major synthetic approaches of *N*-centered BTAs will be discussed as well. In a simplified model, the aromatic rings are kept in place by a $\pi-\pi$ stacking type of interactions. The three amide groups stabilize the columnar intermolecular arrangement by forming H-bonds with both neighbors (Figure 1). The process of aggregation was studied in the solid state, by means of X-ray diffraction, and in solution using NMR and UV-spectroscopic techniques. The major results and conclusions of the solid structure elucidation and of the analysis of the aggregation mechanism by Meijer will be presented in this chapter.

X-ray structure

C=O-centered BTAs

More than hundred crystal structures of C=O-centered BTAs have been reported in the literature so far. In this paragraph we focus the attention on the description of just a few BTA crystal structures to explain the necessary parameters that enable columnar organization. In our approach we investigate the influence of the intermolecular H-bonds on the conformation of amide group (N-H--O=C distance, amide dihedral angle φ, aromatic inter-ring distance and interplanar dihedral angle). The goal of the discussion is to highlight the important factors deduced from the analysis of simple model compounds.

Generally *N*-alkyl benzamides are showing a coplanar conformation between the aromatic π-system and the π-orbitals of the amide group, creating an optimal overlap (Scheme 2).

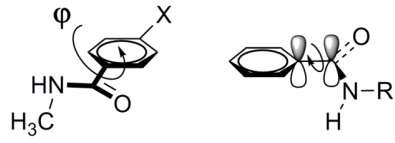

Scheme 2. Schematic representation of the benzamide torsion angle and the conjugation between the π-orbitals.

The planarity can be distorted by electronic effects or, especially, by the formation of strong H-bond networks. Compiling the measured torsion angle of *p*-substituted *N*-methylbenzamide we found that electron donating groups (e.g. -Me, -OMe and -OH) induce a small tilt ($0° < \varphi < 15°$) from coplanarity between the amide bond and the aromatic ring. On the other hand electron withdrawing groups like -F or $-CF_3$, consistently show a greater tilt ($15° < \varphi < 30°$).

The second important observation is that H-bond distances reported for the interaction N-H--O=C are between 1.58 to 2.05 Å.[15]

Since the publication of the pioneering work of Matsunaga, the columnar aggregation of BTA molecules was proposed as model for the supramolecular structure. The occurrence of a helical columnar aggregation was confirmed in 1999, by Lightfoot *et al*., when the X-ray structure of the non-mesogenic *N,N′,N′′*-(2-methoxy)-ethyl-BTA **1** was reported (Figure 2).[16] Typical distances compatible with H-bonds were measured for the N-H--O=C bonds (2.196, 2.127 and 2.092 Å). Surprisingly, very large torsion angles for the carbonyl groups with respect to the main aromatic plane were measured (C_{Ar}-C_{Ar}-C=O 38°, 43° and 47°). The strong H-bond network twists the carbonyl groups of **1** out of planarity. The large amide twist angle observed in **1** is the result of mutual opposing effects: the conjugation between the aromatic ring and the amides favoring planarity and the intermolecular H-bonds imposing a tilt of the amide groups. The fact that all the three amide groups are tilted with roughly the same dihedral angle and that they orient towards the same direction compared to the aromatic ring is due to the helicity and to the propeller-type columnar organization (Figure 1 and 2).

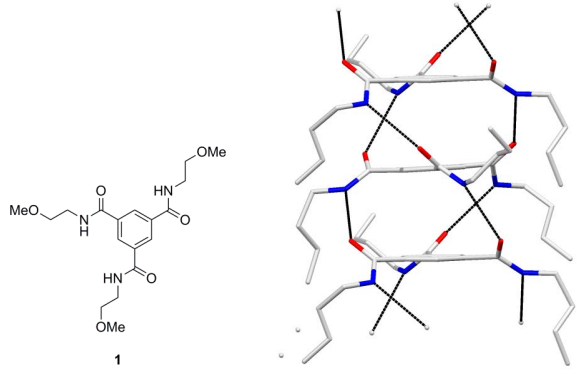

1

Figure 2. X-ray structure of the propeller-type crystal packing of the model-BTA derivative **1** reported by Lightfoot *et al*. [16] Hydrogen atoms have been omitted for the sake of clarity. Black dashed lines represent intermolecular H-bonds. The carbonyl groups are depicted in red and the N-H groups in blue in order to accentuate the helicity of the column (same sense of propagation). The figure illustrates the large twist angles of the three amides.

The aromatic rings are separated by a short centroid inter-ring distance of 3.62 Å and the measured interplanar dihedral angle of 2.8° indicates good coplanarity between the aromatic rings. These two observations are compatible with the occurrence of strong aromatic π–π stacking interactions.

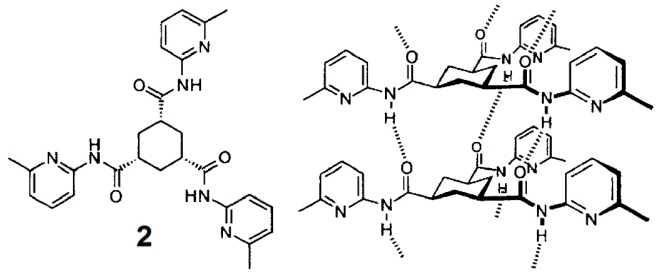

Figure 3. Cyclohexyl triamide **2** reported by Hamilton and co-workers. The figure was extracted from the original work of Hamilton. [17]

In 1995 the group of Hamilton reported an X-ray structure of the cyclohexyl triamide **2**-the hydrogenated derivative of **1** (Figure 3).[17] The crystal structure analysis shows that the carbonyl groups are all oriented in the same direction with respect to the main plane of the cyclohexyl ring forming a torsion angle of 90°. This perpendicular arrangement maximizes the H-bond network. The absence of the aromatic ring suppresses the effect of the conjugation between the amide groups and the central ring. As a result, cyclohexyl triamide **2** demonstrates the strong stabilizing effect originating from the simultaneous formation of the three intermolecular H-bonds. The arrangement directs all the dipoles formed by the amide bonds of one column into the same direction.

In conclusion, the measured dihedral angle value of the amide group is an important indirect indication of the strength of the intermolecular H-bonds.

Despite its columnar crystal packing, the model BTA **1** structure does not show mesomorphic properties due to the short aliphatic side-chain. The crystallization of BTAs substituted with longer alkyl side-chain is not an easy task owing to the disordered packing of the alkyl chains.

The group of Chu recently reported the crystal structure of the *N,N′,N′′*-trioctyl-BTA **3**.[18] The X-ray diffraction of **3** shows nano-sheet structures (Figure 4) where every BTA is connected to six other BTAs via H-bonds. The measured N--O=C distances are compatible with typical intermolecular H-bond distances (Table 1), and they are slightly shorter when compared to the six H-bonds formed in the helical structure of **1** (Table 1). In contrast to the model BTA **1,** the structure of BTA **3** shows that one of the amide groups points in the opposite direction compared to the plane of the aromatic ring. This prevents the coherence of the H-bonds needed to create their helical arrangement. Despite the difference in the X-ray structure, BTA **3** shows columnar liquid crystallinity over a broad range of temperatures[10] (see Table 3). The crystal structure of **1** has been postulated to be representative of the columnar organization despite the fact that compound **1** does not form mesophases. This example emphasizes the difference between the solid state structures and the columnar organization of BTA molecules in the mesophase.

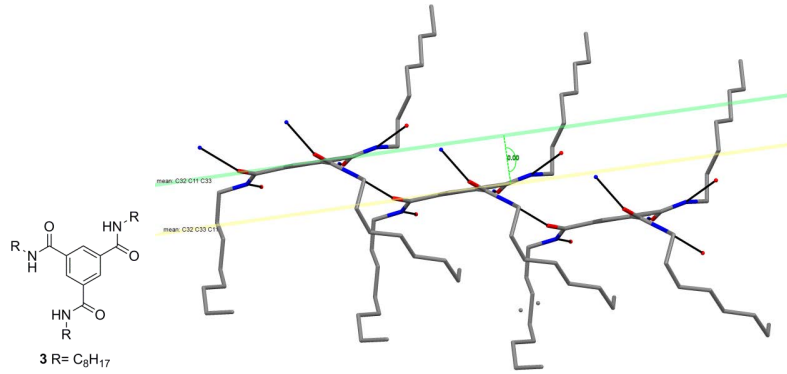

Figure 4. X-ray of the nano-sheet structure of **3** reported by Chu.[18] Black dashed lines indicate intermolecular H-bonds. The calculated interplanar dihedral angle is 0° indicating perfect coplanarity.

BTA[Ref.]	R	Torsion angle ϕ (°)	*d* H-bond (N-H--O=C) (Å)	Crystal packing
4[19]	Et	-8; 14; 45	2.053, 2.040, 2.048	Supramolecular sheets
1[16]	CH_2-CH_2-OMe	38; 43; 47	2.196, 2.127, 2.092	Columns
3[18]	C_8H_{17}	15; 16; 34	2.103, 2.016, 2.047	Chiral nano-sheets

Table 1. Comparison of different trialkyl-substituted C=O-centered BTAs.

In 2009 Jimenez *et al*. reported the crystal structure of BTA **4** substituted by ethyl side chains (Figure 5). As in the case of the trioctyl substituted BTA **3**, the amide groups in **4** are slightly tilted from the plain of the aromatic ring plane (Table 1). Also in this case one carbonyl group is oriented towards the opposite side with respect to the aromatic plane. The measured interplanar dihedral angle is equal to 0°, but the aromatic rings are too far away to exhibit π–π stacking. Therefore, the crystal packings of BTA **3** and **4** are predominantly driven by the intermolecular H-bond interactions. The columnar organization however is the result of co-operating effects between H-bonds and π-π interactions.

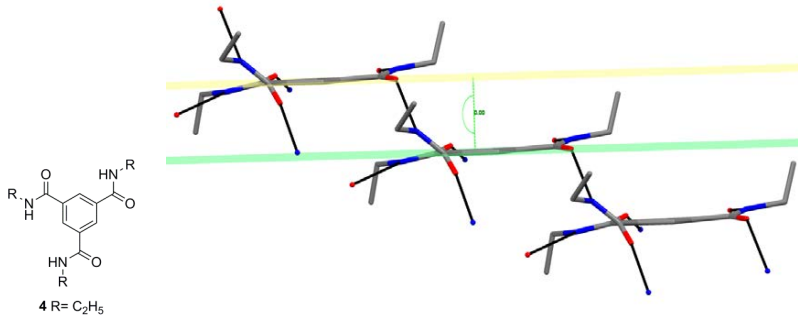

Figure 5. X-ray structure showing the sheets formed by of triethyl-BTA **4**. Black dashed lines refer to intermolecular H-bonds. Hydrogens are omitted for simplicity.[19] The crystal structure shows the sheets induced by the intermolecular H-bonds. The calculated interplanar dihedral angle is 0° indicating a perfect coplanarity

N-centered BTAs

Only six crystal structures of N-centered BTAs have been reported in the literature so far. This lack of data hinders extensive comparative studies as in the case of C=O-centered BTA. The change in connectivity of the amide groups in BTA derivatives (*N*- vs. *C=O*-centered) strongly influences the nature and the strength of the intermolecular interactions (in particular the H-bonds). To highlight this differences, we present a comparison between the BTA structures **5** and **6** (Scheme 3). Both compounds are substituted by *tert*-butyl groups either connected to a C=O-centered BTA **5** [20] or to a N-centered BTA **6**. [21]

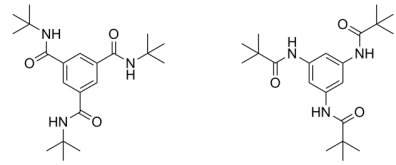

Scheme 3. The structures of the *tert*-butyl substituted C=O-centered **5** and N-centered **6** BTAs.

BTA[Ref.]	Centroid distances (Å)	Torsion angle φ	H-bond distances (Å)	Crystal packing
6 [21]	3.402	31.63°; 31.46°; 34.56°	2.110; 2.044; 2.144	Columnar

Table 2. Crystallographic data of the N-centered **6** *tert*-butyl substituted BTAs.

The X-ray structures of **5** and **6** show that both BTAs present helical columnar packing similar to the BTA derivative **1**. The amide groups of the N-centered derivative have a slightly smaller torsion angle with respect to the C=O-centered BTA **4** analogue. [20] The distances found in the NH--O=C bonds are 0.3 Å longer in **6** indicating weaker intermolecular H-bonds. This type of connectivity weakens the intermolecular H-bonds as indicated by the longer N-H--O=C distances and the smaller amide torsion angles characteristic for weaker interactions.

In conclusion, the helical columnar assembly of BTA derivatives has been well documented with the help of data from the crystal structure of the model compound **1**. The intermolecular H-bonds are arranged as a triple helix around the aromatic core hold together by π-stacking interactions. The tilt angle of the amide groups towards the plane of the aromatic ring is a good probe for the strength of the intermolecular H-bonds. Deducing the propensity to form mesophases by analyzing the crystal packing obtained from the XRD study is still difficult. The data available is not sufficient to predict the mesophase formation with a high enough degree of certainty.

Mechanism of aggregation

Understanding the mechanism of the supramolecular aggregation should provide the rules needed for rational design, controlled aggregation and thereby predicting the properties of the resulting materials.[14]

Different techniques have been used to monitor the BTA aggregation process, such as concentration-dependent[14] and temperature-dependent UV-vis spectroscopy[22] as well as circular dichroism (CD) spectroscopy studies on BTAs substituted with side chains containing chiral centers.[22] Considerable progress has been made at elucidating the mechanism of supramolecular polymerization.[23] Different mathematical models have been proposed to describe the formation of

supramolecular aggregates.[14, 24] The supramolecular aggregation of BTA derivatives follows one of the two different mechanisms: Isodesmic or Cooperative mechanism (Figure 6).

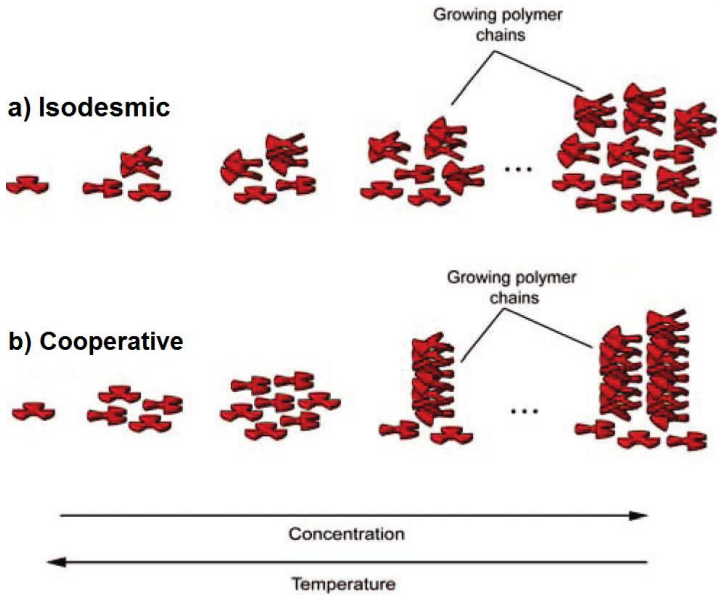

Figure 6. Schematic representation of supramolecular polymerization. a) Isodesmic model. b) Cooperative supramolecular polymerization. The figure was extracted and modified from the original review of Meijer and co-workers.[14]

Cooperative aggregation

Most of the BTA derivatives are found to polymerize according to the cooperative mechanism.[14] This type of aggregation proceeds *via* two distinct steps: nucleation step, characterized by an association constant K_n, followed by an elongation step with an equilibrium constant K_e. As soon as the concentration of the monomer species (or the temperature of the solution) enables the self-assembly process, the formation of a first aggregated supramolecular oligomer takes place (nucleation step) (Figure 7).

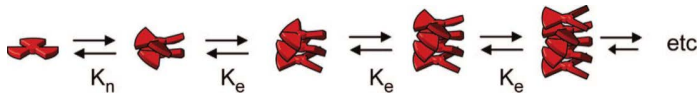

Figure 7. Schematic representation of cooperative supramolecular polymerization. The two different equilibrium (association) constants, nucleation constant K_n and the elongation constant K_e, are highlighted. The figure was extracted from the review of Meijer and co-workers.[14]

Once this first step is accomplished, the supramolecular polymerization continues with the second step (elongation). The supramolecular polymerization constant, characterizing the elongation, is higher in value than the nucleation constant ($K_e > K_n$).[25]

$$M_1 + M_1 \overset{K_2}{\rightleftharpoons} M_2 \qquad [M_2]=K_2[M_1]^2$$

$$M_2 + M_1 \overset{K}{\rightleftharpoons} M_3 \qquad [M_3]=KK_2[M_1]^3$$

$$\cdots \qquad\qquad \cdots$$

$$M_{i-1} + M_1 \overset{K}{\rightleftharpoons} M_i \qquad [M_i]= K_2K^{i-2}[M_1]^i = \sigma K^{-1}(K[M_1])^i \quad i = 2, 3,\ldots,\infty$$

Scheme 4. Different thermodynamic equilibrium constants as postulated for the cooperative mechanism are shown. The scheme was extracted from the review of Meijer and co-worker.[14]

To study the supramolecular polymerization mechanism of BTA derivatives temperature-dependent circular dichroism (CD) and UV-Vis spectroscopy were used. These techniques allowed to distinguish whether the aggregation follows the isodesmic or cooperative mechanism.[22, 26] Temperature-dependent UV spectra recorded for temperatures between 90 and 20 °C revealed occurrence of a hypochromic shift in the absorption maximum indicating the formation of aggregates (Figure 8a). Further investigations carried out for different concentrations of **3** revealed the occurrence of two distinct events upon cooling the solution (Figure 8b and c). At higher temperatures (around 90 °C) the absorbance value remains almost constant with changing temperature and then drops upon further cooling. The first event corresponds to the nucleation step that is characterized by an association constant K_n. In this stage **3** is present in the non-aggregated (monomeric) form. Temperature decrease enlarges the rate of spontaneous self-aggregation of **3**. This is so-called elongation step characterized by an association constant K_e that has the same value for each consecutive aggregation step but differs from K_n. The plotted curves show non-sigmoidal relationship between absorbance and temperature. This is characteristic of a cooperative aggregation mechanism. This result is in accordance with the findings from temperature-dependent CD measurements for BTA **3** solutions.

When a chiral aliphatic amine ((*R*)-3,7-dimethyl-octylamine) was introduced as the side chain of **7**, the aggregation process was followed employing both temperature-dependent circular dichroism CD and UV-vis experiments (Figure 8c). Non-sigmoidal curves, characteristic of a cooperative type of assembly were obtained in both cases.

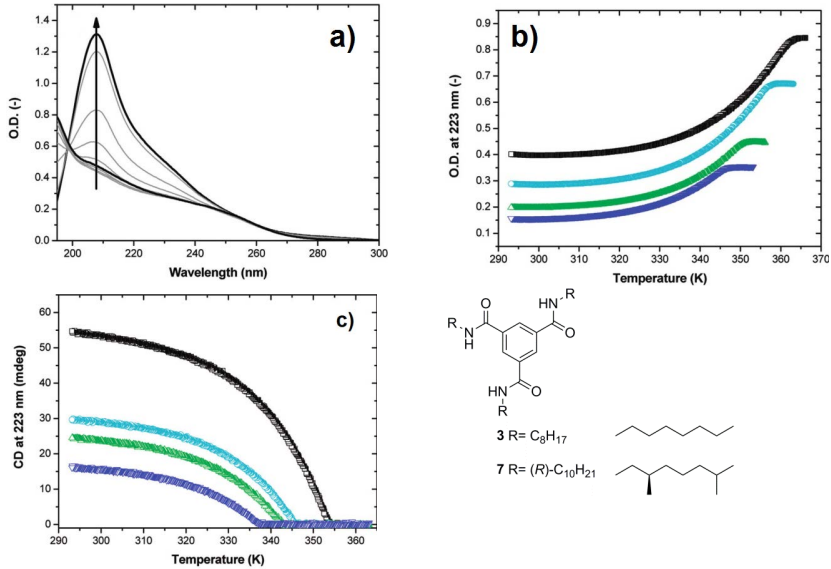

Figure 8. a) Temperature-dependent UV-Vis absorption spectra of **3** at 3.5 x10^{-5} M from 90 °C to 20 °C (the arrow indicates the direction of the heating) in heptane. b) Temperature-dependent UV-Vis adsorption spectra of **3** at 223 nm. (Black curve 4.2 x10^{-5} M; cyan curve 3.5 x10^{-5} M; green curve 2.2 x10^{-5} M; blue curve 1.8 x10^{-5} M). c) Temperature-dependent circular dichroism experiments of **7** at 223 nm at 1.4 x10^{-5} M. The figures were extracted from the original work of Meijer and co-workers.[26b]

Origin of the cooperativity

The origin of the cooperative nature of BTAs supramolecular aggregation were studied by de Greef and co-workers employing quantum mechanical *DFT* calculations.[26a, 27] The results indicated a concomitance of *long range non-nearest neighbor dipole-dipole interactions* and *non-pairwise short range polarization* resulting from H-bonds. The calculated electron-density maps indicate a global addition of the single induced-dipole moments redistributing the local polarization along the supramolecular BTA aggregate (Figure 9).[27]

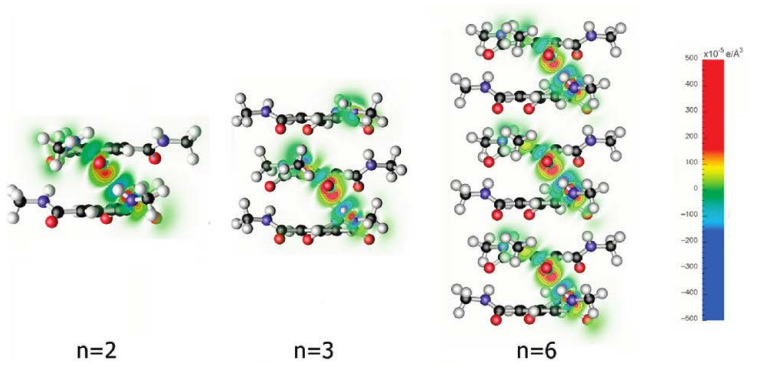

Figure 9. Electron-density differences calculated by subtracting the electron density of the individual monomer from the electron density of the constituting oligomer (dimer, trimer and hexamer). The figure was extracted from the original work of de Greef and co-workers.[27]

According to the quantum mechanical simulation, the first nucleation step produces an anisotropic electron density and induces a *macro*-dipole moment[28] variation in the BTAs dimer (n= 2). Once the dimer is formed, the supramolecular growth (*elongation*) occurs without variation of the induced *macro*-dipole moment or the electron density of the native polymer (n= 3 and n= 6). At this point all further aggregation steps proceed as for the isodesmic mechanism (Scheme 5), where all the polymerization steps have the same association constant.

Isodesmic aggregation

The isodesmic model is the second mechanism occurring in the aggregation process of BTA derivatives. It is also called the "equal-*K*" model because it assumes that during the polymerization every single step has the same association constant *K* value (Figure 10 and Scheme 5a). It represents the linear supramolecular aggregation of a vast number of organic molecules (e.g. perylene bisimide derivatives, Scheme 5b),[29] however only bipyridyl-substituted BTA derivatives were found to aggregate according to the isodesmic model.[30] From a mechanistic point of view, the initial aggregate formation does not modify the affinity of the molecular assembly towards the polymerization.

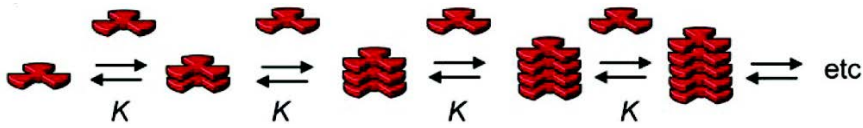

Figure 10. Representation of the isodesmic polymerization model, where all association constants *K* are equal. The figure was extracted from the review of Meijer and co-workers.[14]

The supramolecular aggregation proceeds following the same thermodynamic equilibrium constant for all the steps (equal-*K*). The temperature-dependent UV-vis titration gives a sigmoidal curve from which only one thermodynamic constant can be deduced (Figure 11b).

a)

$$M_1 + M_1 \overset{K}{\rightleftharpoons} M_2 \qquad [M_2]=K[M_1]^2$$

$$M_2 + M_1 \overset{K}{\rightleftharpoons} M_3 \qquad [M_3]=K^2[M_1]^3$$

$$M_{i-1} + M_1 \overset{K}{\rightleftharpoons} M_i \qquad [M_i]=K^{-1}(K[M_1])^i \quad i = 1, 2,...,\infty$$

b)

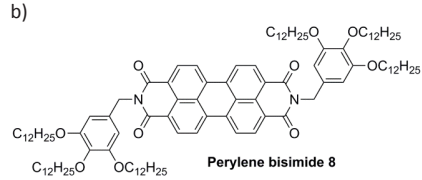

Scheme 5. a) Isodesmic polymerization mechanism. The thermodynamic equilibrium (aggregation) constant K is the same for every polymerization step. The scheme was extracted from the review of Meijer and co-workers.[14] b) Perylene bisimide **8**, a molecule forming a discotic mesophase aggregating according to an isodesmic mechanism.[29g]

The three different bipyridyl-substituted BTAs **9**-**11** (Figure 11) have been found to aggregate according to an isodesmic mechanism. When BTA **10** was analyzed by means of concentration and temperature-dependent CD spectroscopy, the normalized curve of the *e.e*. vs. the net helicity gave a diagnostic sigmoidal curves, typical of an isodesmic aggregation mechanism (Figure 11).[30]

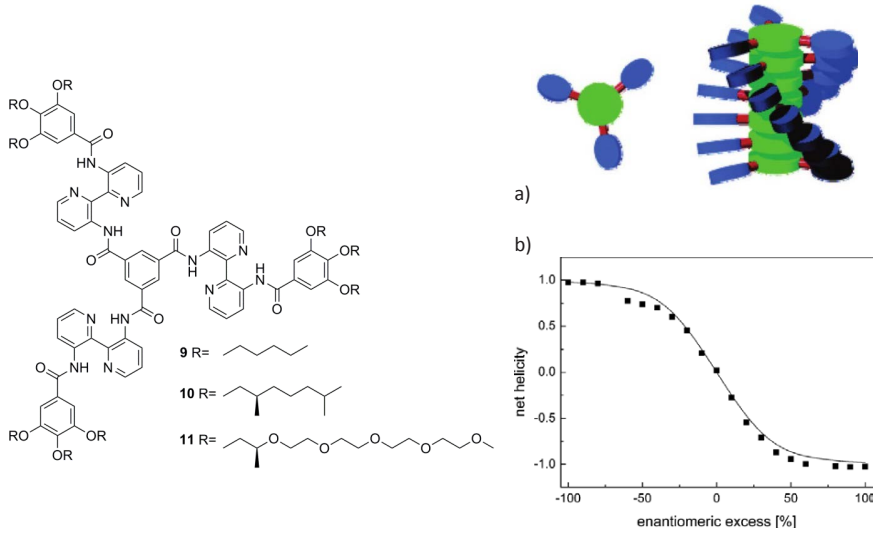

Figure 11. BTA derivatives substituted by pyridyl side chains reported by Meijer and co-workers. a) Proposed model for the self-assembly of the planar BTA. b) Normalized CD results of BTA **10** in octane at 20 °C. The sigmoidal curve clearly indicates an isodesmic aggregation mechanism. The figure was extracted from the publication of Meijer and co-workers.[30]

This atypical self-assembly mechanism has been analyzed by quantum-mechanical *ab initio* calculations. MP2 *ab initio* calculations indicated the formation of strong intramolecular H-bonds between the N—H of the aromatic central core and the nitrogen atom on the bipyridine system.[31] The result of these intramolecular interactions is a coplanar arrangement of the BTA derivatives, where the dihedral angles of the three amides are almost 0° with respect to the plane of the central

aromatic ring. The self-assembly process is not driven by intramolecular H-bonds but by π–π stacking and solvophobic effects.

Fully-substituted "crowded" arenes BTA

The study of BTA **10** showed that other intermolecular interactions like π-stacking and solvophobic interactions can be exploited to drive the self-assembly of BTA derivatives. H-bonds however still play the major role in the self-assembly of BTA derivatives. Nuckolls and co-workers introduced three substituents on the aromatic core of the BTA scaffold. By doing so they forced the amide groups out of the planarity and they facilitated intermolecular H-bond formation. This approach lead to a new class of 2,4,6-trisubstituted BTA called "crowded aromatics".[32] The first reported crowded aromatic (2,4,6-trialkoxy-BTA) **12** showed an enhanced capability to form intermolecular H-bonds (Figure 12).[33]

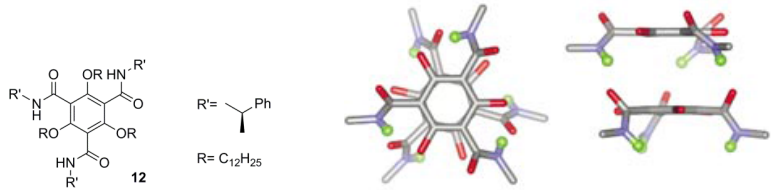

Figure 12. Modeling of crowded arene BTA **12** showing the energy minimized structure. The figure was extracted from the publication of Nuckolls and co-workers.[33]

Molecular mechanics energy minimization of **12** (Figure 12) indicated that the three amide groups are tilted away from planarity (calculated dihedral angle of ~60°) facilitating the occurrence of intermolecular H-bond interactions. The amide groups try to avoid steric strain by directing the N—H group away from its nearest neighbor -the oxygen of the alkoxy group. Concomitantly, the oxygen atom of the carbonyl group tries to avoid Coulomb repulsion with its neighbor thereby increasing the forces preferring high dihedral angles. Temperature-dependent CD aggregation analyses on BTA **12** showed the cooperative nature of the supramolecular self-assembly mechanism of BTA **12**.[34]

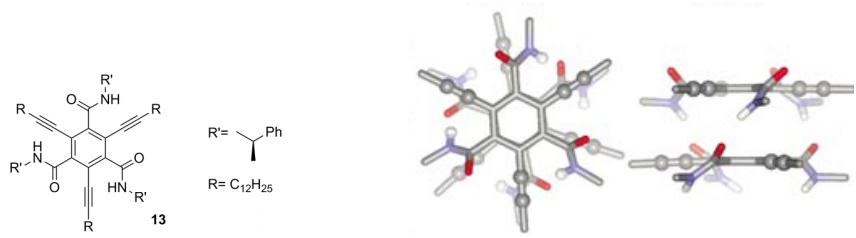

Figure 13. Crowded arene **13** substituted by the introduction of alkyne chains. The figure was extracted from the original publication of Nuckolls and co-workers.[35]

Another example of the crowded arene is 2,4,6-trialkynyl-BTA **13** (Figure 13).[35] Analysis of the aggregation employing fluorescence spectroscopy indicated the formation of supramolecular architectures in dichloromethane. No aggregation was observed in an apolar solvent, such as dodecane. If the supramolecular aggregation would have been driven by intermolecular H-bonds, the

aggregation should be enhanced in apolar aprotic solvents like dodecane. The authors explained their results as a consequence of enhanced solvophobic effects. Indeed, the apolar dodecane stabilizes the monomer thereby decreasing length of the aggregate. This result indicates that both H-bonds and solvophobic effects play a fundamental role in the self-assembly process.

Aggregation of N-centered BTA

Few studies on the supramolecular aggregation mechanism of N-centered BTA derivatives has been carried out by Meijer and co-workers.[36] The well-established temperature-dependent CD and UV-Vis analysis was used to study the aggregation process of N-centered BTAs.[36] Interestingly, the same cooperative supramolecular aggregation mechanism, explainable by two association constants K_n and K_e, as for C=O-centered BTA was found. Quantitative spectroscopic analyses indicated a smaller enthalpy change associated with the elongation step compared with the analog C=O-centered derivative **1**.

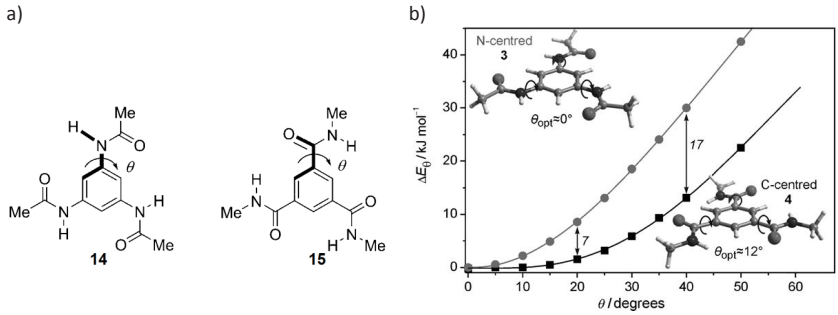

Figure 14. a) Torsion angle θ of the C_{Ar}-N and C_{Ar}-C bonds of N-centered **14** and C=O-centered BTA **15** derivatives. b) Potential energy profiles for the torsion angle between the C_{Ar}-N and C_{Ar}-C bonds of N-centered and C=O-centered BTA derivatives. The figures were extracted from the publication of Meijer and co-workers.[36]

Density functional theory DFT calculations were carried out in order to rationalize the reasons of the observed phenomena. A lower cohesive energy for the aggregation process of **14** was found compared with the C=O-centered **15** (ΔE of 10 kJmol^{-1}). Temperature-dependent infrared measurements and theoretical calculation indicated the occurrence of longer distances for the N—H H--O=C bonds of N-centered BTA. This increased distance is interpreted as a sign of the decrease of the intermolecular H-bond strength.[37] These theoretical calculations showed that the rotation along the C_{Ar}—N bond (N-centered BTA) is less favorable then the rotation of the C_{Ar}—C bond (C=O-centered). At a dihedral angle of 40° the difference of energy induced by torsion strain between the two types of BTA is 17 kJ mol^{-1} (Figure 14b).[36] In accordance with these analyses the N-centered BTA **14** showed a reduced propensity and efficiency towards supramolecular aggregation when compared to the C=O-centered BTA **15** (Figure 14).

Applications

The applications of BTA derivatives are closely related to the nature of the side chains. C=O and *N*-substituted BTAs carrying alkyl groups form hexagonal columnar liquid crystals, depending on the length and the nature (linear or branched) of the alkyl chain.[10, 38] Matsunaga reported in his pioneering work the effects of the chain length on the temperature range of mesomorphic behavior of alkyl-substituted BTAs (Table 3).[10] The measured temperature for the melting to the isotropic liquid phase transition of the different BTA derivatives is quasi constant (between 204 and 216 °C). However the occurrence of the first liquid crystalline phase is correlated to the length of the chains. This transition seems to go through a minimum for the chain length C_{10} and stabilizes around a temperature between 73 and 88 °C. An alteration of the temperature between chain length composed of a paired number of carbon atoms and chain length composed of an unpaired number of carbon atoms can be observed. The temperature of 61 °C reported for the chain length C_{14} may be an outlier.

R	Transition Temperature (°C) and Enthalpy (kJ mol^{-1})	ΔT (°C) Range of LC
C_5H_{11}	**Cr** 75(6) 119(10) **Col$_h$** 206(6) **I**	87
C_6H_{13}	**Cr** 99(12) **Col$_h$** 205(22) **I**	106
C_7H_{15}	**Cr** 116(16) **Col$_h$** 208(12) **I**	92
C_8H_{17}	**Cr** 102(19) **Col$_h$** 204(17) **I**	102
C_9H_{19}	**Cr** 65(17) **Col$_h$** 215(15) **I**	150
$C_{10}H_{21}$	**Cr** 49(47) **Col$_h$** 208(20) **I**	159
$C_{11}H_{23}$	**Cr** 72(32) **Col$_h$** 216(15) **I**	144
$C_{12}H_{25}$	**Cr** 21(11) 88(36) **Col$_h$** 212(16) **I**	124
$C_{13}H_{27}$	**Cr** 32(7) 81(27) **Col$_h$** 216(13) **I**	135
$C_{14}H_{29}$	**Cr** 61(59) **Col$_h$** 209(15) **I**	148
$C_{15}H_{31}$	**Cr** 88(56) **Col$_h$** 214(14) **I**	126
$C_{16}H_{33}$	**Cr** 73(68) **Col$_h$** 205(12) **I**	132
$C_{17}H_{35}$	**Cr** 87(66) **Col$_h$** 211(9) **I**	124
$C_{18}H_{37}$	**Cr** 78(68) **Col$_h$** 206(12) **I**	128

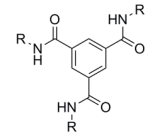

R= from pentyl (C_5H_{11}) to octadecyl ($C_{18}H_{37}$)

Table 3. Transition temperature and relatives enthalpy of alkyl BTAs extracted from the Matsunaga's work.[10] **Cr** indicates the crystal state. **Col$_h$** indicate the columnar liquid crystalline state. **I** indicates the isotropic liquid state. ΔT expresses the temperature difference (in °C) of the mesophases.

Liquid crystalline trialkyl benzene-1,3,5-tricarboxyamides (BTAs) have been reported to form a large polarization of 10 mC/m^2 in the amorphous solid phase at 70 °C (below the mesophases formation temperature).[39] Indeed BTAs are known to form a macro-dipole along the columnar axis (Figure 15).[28, 40]

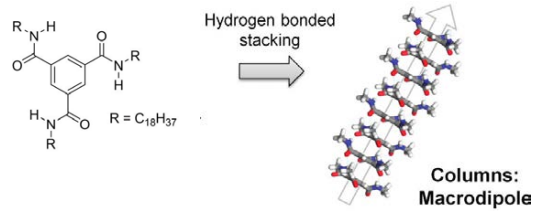

Figure 15. Schematic representation of the formed macrodipole along the supramolecular axis. The figure was extracted from the publication of Sijbesma and co-workers.[40a]

This property could be exploited for the fabrication of non-volatile memory devices.[41]

The BTA scaffold found other important applications. When the lateral chains consists of branched alkyl groups, the formation of organogel (in organic solvents) is favored over liquid crystals.[42] The group of Palmans patented the use of BTA-based organogels to produce insulating layers for electrical cables.[43] When the branched side chains are polar enough to allow the dissolution of BTAs in water, the formation of hydrogel is observed.[44]

Fiber-like needles were obtained when the side chains are composed of a bulky aliphatic group such as the *tert*-butyl group (e.g. **5** and **6**). This property made such bulky substituted BTAs effective nucleating agents for the clarification of isotactic polypropylene *i*PP.[45] Adding a small amount of the nucleating agent (ca. 200 ppm) the crystallization temperature of *i*PP increases making the material less opaque. N-centered *t*-butyl BTA **6** was found to be an effective derivative for the clarification of *i*PP.[46] The German company *BASF* commercialized **6** under the name of *Irgaclear XT 386*.

Recently water soluble BTA derivatives (gadolinium-based complexes) [47] found an application in the biomedical field as contrasting agents for MRI diagnostic.[48] The use of BTA derivatives in the drug delivery has also been studied. [49]

Exhaustive literature reviews have been published by the groups of Meijer[8] and more recently of Palmans[6] working in Eindhoven.

Closing Remarks

A large amount of research has been done so far on BTA derivatives and a lot of empirical data are available in the open literature. This was possible because the synthesis of the BTA derivatives is easy and the structural variations are simple. The formation of H-bonds has been postulated to be the key factor responsible for the supramolecular assembly of BTAs. This proposition has been largely corroborated by spectroscopic and diffraction analyses. The effects of the side chains on the crystal packing and, consequently on the supramolecular organization has been demonstrated. In conclusion, the properties of the BTA could be designed by modifying the nature of the lateral chains introduced on the amide group.

BTAs as building blocks forming columnar liquid crystals

Generality and Classification of Columnar Liquid Crystals

The liquid crystalline phase is a state of the matter intermediate between solid and liquid. Liquid crystalline materials belong to the family of soft matter where the distinctive properties of both the liquid and the crystal phases are combined: rigidity from the solid and flexibility from the liquid (Scheme 6).

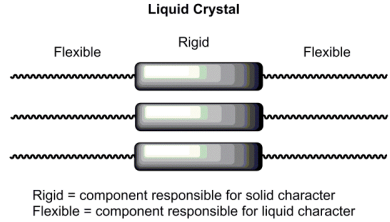

Scheme 6. Generic representation of a (columnar) liquid crystalline compound as a combination of order (rigidity) and disorder (flexibility).

The identification of the liquid crystalline (LC) phase was achieved almost hundred and thirty years ago by the German chemist Otto Lehmann.[50] Since that time the world of liquid crystals evolved from a pure academic research into a field with many important industrial applications. This new type of phase was classified in a systematic fashion.

The first classification is based on the nature of the mesophase formation. This can be induced either by varying the concentration of the self-assembling molecules (*lyotropic* LCs) or by changing the temperature (*thermotropic* LCs). Examples of the first class are micelles made of amphiphilic tensioactive phospholipids.

Our description of the systematic classification refers to thermotropic LCs exclusively which is the largest family of mesomorphic compounds.

Depending on the shape of the molecules, different types of mesophases are formed (Figure 16). Rod-like molecules give rise to nematic phases; disk-like molecules generate discotic liquid crystals (=DLC) (Figure 16). Each type of LC presents its own characteristic and potential applications (Figure 16). We focused exclusively on discotic liquid crystals (*DLCs*) since BTAs form thermotropic columnar mesophases.

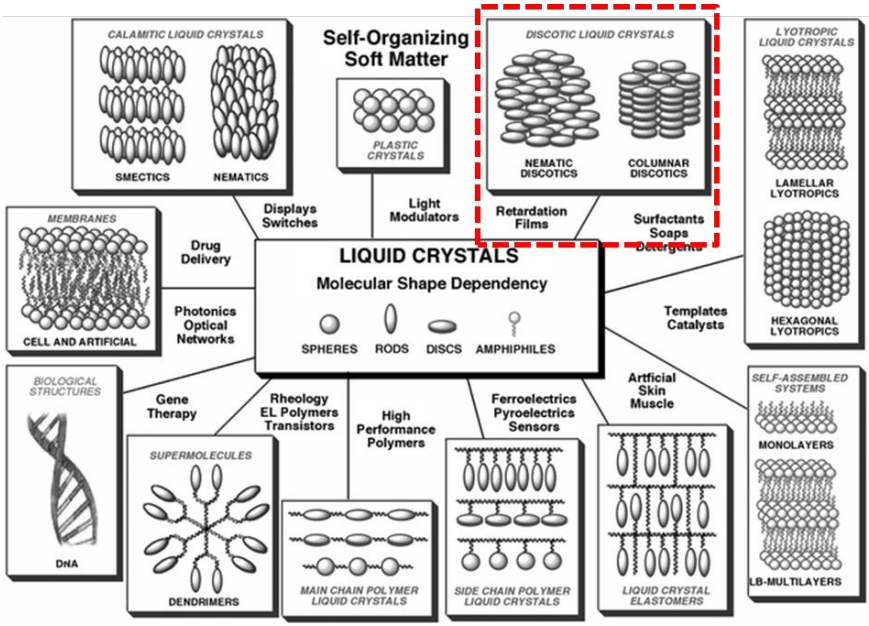

Figure 16. Schematic classification of the different types of thermotropic liquid crystals and their applications. The dashed red square indicates the family of DLC, which are of interest to us. The figure was extracted and modified from the original publication of Goodby. [51]

Discotic Liquid Crystals

Chandrasekhar observed in 1977 for the first time a discotic liquid crystalline phase DLC.[52] He analyzed the mesomorphic properties of the benzene-1,2,3,4,5,6-hexacarboxylic acid hexalkyl ester (Figure 17a). This first molecule defines the typical morphology that enables the formation of columnar organizations:

- ✓ a rigid aromatic central core
- ✓ flexible lateral alkyl chains (typically longer than five carbons)

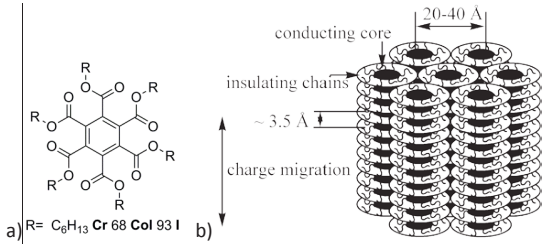

Figure 17. a) Structure of the benzene-1,2,3,4,5,6-hexacarboxylic acid hexalkyl ester.[52] b) Schematic representation of the columnar liquid crystals. The central aromatic cores are surrounded by the flexible aliphatic chains. Figure 17b was extracted from the review of Kumar.[53]

The aromatic central cores drive the columnar assembly by forming π-π interactions ("rigid" contribution) whereas the aliphatic lateral chains contribute to the "flexibility". Disk-shaped molecules can exhibit three different mesophases:

- ✓ Nematic: The following classes have been observed: Nematic Discotic N_D, Chiral Nematic $\mathbf{N_D}$* and Columnar Nematic $\mathbf{N_{Col}}$.
- ✓ Lamellar
- ✓ Columnar: This type is divided into the following classes: Hexagonal $\mathbf{Col_h}$, Rectangular $\mathbf{Col_r}$, Oblique, Plastic $\mathbf{Col_p}$ and Helical (Figure 18).

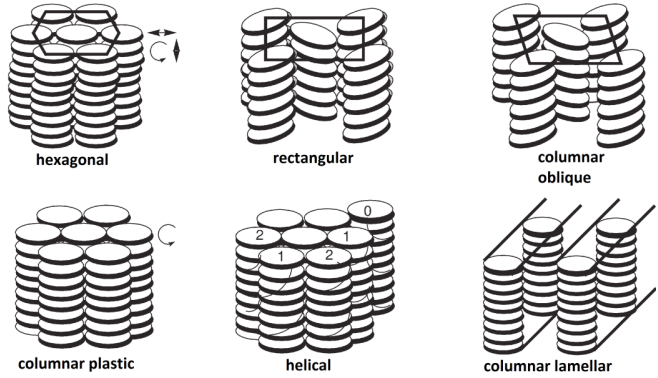

Figure 18. Schematic representation of the different types of columnar phases. The figure was extracted and modified from the original review of Kumar.[53]

Characterization of the Liquid Crystalline Phase

Liquid crystals are organic molecules and consequentially they can be characterized using the classical analytical techniques such as NMR, IR, and MS spectroscopy. Characterization of the supramolecular structures and their material properties necessitates the use of specialized techniques.

Polarized Light Microscope (POM) and Small Angle X-ray Scattering (SAXS)

Typically, the first test carried out on a sample expected to form mesophases is to examine the birefringence of the compound. When a polarized light beam crosses an anisotropic material birefringence is observed. The refractive index of such material depends on the polarization and on the direction of the light propagation. Therefore an incident light beam is split in two components with different propagation speed. Liquid crystals are anisotropic materials, therefore birefringent, and they split the incident light beams in different components depending of the local polarization of the LCs. The light passing a sample containing a LC material creates textures and colors, which can be easily observed. Columnar liquid crystalline compounds are known to be birefringent materials that form characteristic pseudo-focal conic textures (Figure 19a). This type of analysis of the liquid crystalline phase is extremely powerful because it is inexpensive and fast. It allows to identify different mesophases by evaluating the observed textures which are specific for a given type of mesophase.

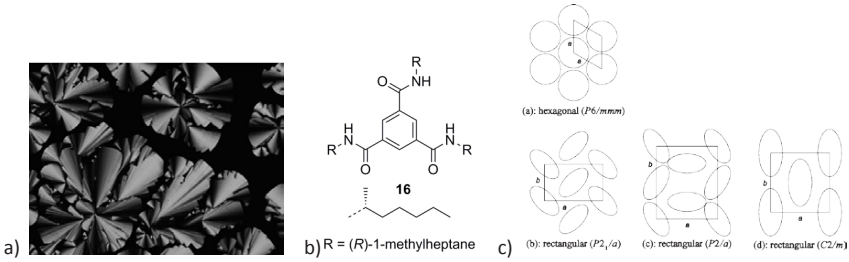

Figure 19. a) Typical pseudo-focal conic texture of the chiral BTA derivative **16** at 217 °C.[38] b) Chemical structure of **16**. c) Example of 2D lattice of columnar mesophases adapted from the publication of Laschat *et al*.[54]

Unfortunately this technique is not adapted to determine the symmetry of the supramolecular structure (2D lattice). For example BTA derivatives form hexagonal columns. The POM analysis shows the typical pseudo-focal conic textures. To gain information on the symmetry of the columns (2D lattice) other techniques have to be used (Figure 19c). In order to determine the symmetry of the hexagonal columns Small Angle X-ray Scattering (SAXS) analyses are required.[55] This technique is based on the recording of the elastic scattering of X-ray radiation at very small angles (0.1° – 10°) through the analyzed sample. The scattering of the X-ray radiation by the material depends of the density and geometry of the packing. This technique enables the structural determination of heterogeneous and disordered materials.

Differential Scanning Calorimetry (DSC)

The DSC is a calorimetric method used to analyze quantitatively the temperature and the enthalpy of a thermal phase transition. DSC measures the transition temperature and the associated relative energies (exchanged heat ΔH) for the LCs studied. In a typical DSC analysis a heating cycle followed by a cooling cycle are recorded. A thermal transition (e.g. melting point) is expected to be present in both cycles. Such transitions are called enantiotropic. However there are cases where such phase transition is observed exclusively on the heating or cooling cycle. Those types of transitions are called monotropic.

Importance of Columnar Discotic LC (DLC): organic semiconductors

Nematic liquid crystals were the first class of LCs that found industrial application in the sixties of the last century. Today fluorinated nematic LCs are employed on a large scale in electronic devices like liquid crystal displays (*LCD*).[56] *Discotic Liquid Crystals* (DLC) are promising candidates for organic-based semi-conducting materials replacing expensive inorganic semiconductors. Therefore DLCs are objects of intensive research in academia. This class of LCs shows charge transport along the columnar axis.[57] This feature might be exploited for the fabrication of *photovoltaic systems* (PV)[58] and *field-effect transistors* (FETs).[59] When the aromatic cores in DLCs are separated by a distance of around 3.5 Å, an overlap between the π^*–π^* LUMOs (Lowest Unoccupied Molecular Orbital) along the columnar axis occurs forming a conducting bands facilitating charge mobility (Figure 20a).[54]

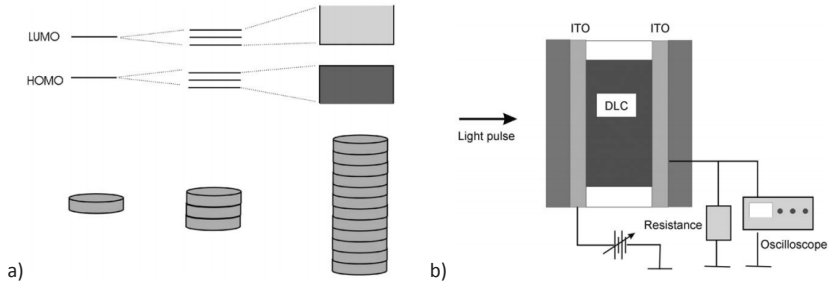

Figure 20. a) Schematic representation of the energy separation of the conducting bands in discotic liquid crystals. The columnar aggregation of the discotic units allows the overlap of the π*-π* LUMO of each unit forming a conduction band along the columnar axis. b) Schematic representation of TOF experiment. The figure was extracted from the review of Laschat and co-workers.[54]

When a photoactive material is irradiated, electrons (e^-) can be promoted into the conduction band leaving an electron hole in the valence band (p^+). The generated electric charges can be transported and thereby separated along the organic material. If full charge separation is achieved, the photovoltaic device can generate electric current. The recombination of electrons and holes in organic semiconductors has been used to create organic light emitting diodes (OLED).

The transport of the electric charge in organic materials (semiconductors) can take place by two mechanisms: *i*) hole migration or *ii*) electron migration. Hole migration occurs typically in electron-rich aromatics that are able to stabilize the electric holes, called *p*-type organic semiconductors. The most important examples of *p*-type semiconductors are 2,3,6,7,10,11-hexalkoxy-triphenylene derivatives, coronene, hexabenzocoronene *HBC* (Scheme 8).

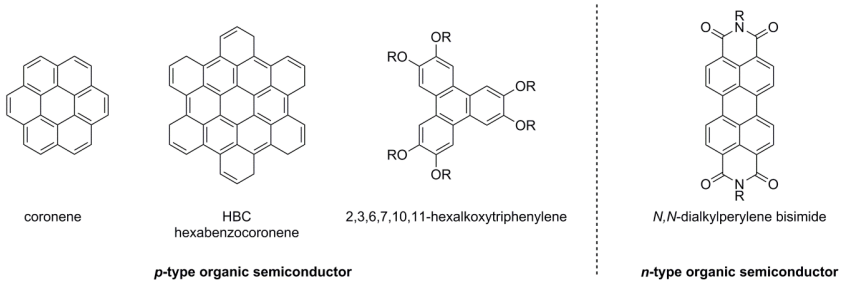

Scheme 7. Examples of *p*-type (left) and *n*-type (right) DLCs as organic semiconductors.

Electron migration is typical for electron poor aromatics, called *n*-type organic semiconductors. Representative examples of *n*-type semiconductors are perylene derivatives (Scheme 7).[60]

Precisely measuring the charge transport is of fundamental importance. Two different techniques have been developed to reliably measure the charge transport in organic materials. The first technique is the *time-of-flight* (TOF) electron mobility measurement (schematic representation of the apparatus system shown in Figure 20b)[54]. The mesomorphic material, in its liquid crystalline state, is irradiated by a pulsed light producing the formation of electric charges in the sample. An external electric field is applied to induce the charges to move. The transient current is recorded. These types

of measurements allow to identify the charge carrier (holes or electrons). The charge mobility can be determined as well. To obtain reliable results from TOF electron mobility measurements good alignment of the molecules in the mesophase is crucial.

The second technique developed is called pulse-radiolysis time-resolved microwave conductivity technique PR-TRMC.[61] The electric charge is generated by exposing the sample to a very short and very intense electron pulse (0.5 – 50 ns of 3 MeV). This pulse perturbs the microwave absorbance of the analyzed material. The charge transport can be calculated from the observed change in microwave absorption. PR-TRMC techniques do not require the perfect alignment of the aromatic molecules in the columnar mesophases.

References

[1] G. M. Whitesides, B. Grzybowski, *Science (Washington, DC, U. S.)* **2002**, *295*, 2418-2421.

[2] T. Aida, E. W. Meijer, S. I. Stupp, *Science (Washington, DC, U. S.)* **2012**, *335*, 813-817.

[3] D. Tanner, J. A. Fitzgerald, B. R. Phillips, *Angew. Chem.* **1989**, *101*, 665-670.

[4] D. Philp, J. F. Stoddart, *Angew. Chem., Int. Ed. Engl.* **1996**, *35*, 1155-1196.

[5] S. I. Stupp, L. C. Palmer, *Chem. Mater.* **2014**, *26*, 507-518.

[6] S. Cantekin, T. F. A. de Greef, A. R. A. Palmans, *Chem. Soc. Rev.* **2012**, *41*, 6125-6137.

[7] aJ. M. Lehn, *Prix Nobel* **1988**, 129-176; bJ. M. Lehn, *Angew. Chem.* **1990**, *102*, 1347-1362 (See also Angew. Chem., Int. Ed. Engl., 1990, 1329(1311), 1304-1319).

[8] L. Brunsveld, B. J. B. Folmer, E. W. Meijer, R. P. Sijbesma, *Chem. Rev. (Washington, D. C.)* **2001**, *101*, 4071-4097.

[9] aM. Weck, A. R. Dunn, K. Matsumoto, G. W. Coates, E. B. Lobkovsky, R. H. Grubbs, *Angew. Chem., Int. Ed.* **1999**, *38*, 2741-2745; bH. Bengs, M. Ebert, O. Karthaus, B. Kohne, K. Praefcke, H. Ringsdorf, J. H. Wendorff, R. Wuestefeld, *Adv. Mater. (Weinheim, Fed. Repub. Ger.)* **1990**, *2*, 141-144.

[10] Y. Matsunaga, N. Miyajima, Y. Nakayasu, S. Sakai, M. Yonenaga, *Bull. Chem. Soc. Jpn.* **1988**, *61*, 207-210.

[11] A. G. Serrette, C. K. Lai, T. M. Swager, *Chem. Mater.* **1994**, *6*, 2252-2268.

[12] T. Curtius, *J. Prakt. Chem. (Leipzig)* **1915**, *91*, 39-102.

[13] Y. Matsunaga, Y. Nakayasu, S. Sakai, M. Yonenaga, *Mol. Cryst. Liq. Cryst.* **1986**, *141*, 327-333.

[14] T. F. A. De Greef, M. M. J. Smulders, M. Wolffs, A. P. H. J. Schenning, R. P. Sijbesma, E. W. Meijer, *Chem. Rev. (Washington, DC, U. S.)* **2009**, *109*, 5687-5754.

[15] H.-B. Bürgi, J. D. Dunitz, *Structure Correlation, Vol. 2*, VCH, **1994**.

[16] M. P. Lightfoot, F. S. Mair, R. G. Pritchard, J. E. Warren, *Chem. Commun. (Cambridge)* **1999**, 1945-1946.

[17] E. Fan, J. Yang, S. J. Geib, T. C. Stoner, M. D. Hopkins, A. D. Hamilton, *J. Chem. Soc., Chem. Commun.* **1995**, 1251-1252.

[18] X. Hou, M. Schober, Q. Chu, *Cryst. Growth Des.* **2012**, *12*, 5159-5163.

[19] C. A. Jimenez, J. B. Belmar, L. Ortiz, P. Hidalgo, O. Fabelo, J. Pasan, C. Ruiz-Perez, *Cryst. Growth Des.* **2009**, *9*, 4987-4989.

[20] M. Kristiansen, P. Smith, H. Chanzy, C. Baerlocher, V. Gramlich, L. McCusker, T. Weber, P. Pattison, M. Blomenhofer, H.-W. Schmidt, *Cryst. Growth Des.* **2009**, *9*, 2556-2558.

[21] M. Schmidt, J. J. Wittmann, R. Kress, D. Schneider, S. Steuernagel, H.-W. Schmidt, J. Senker, *Cryst. Growth Des.* **2012**, *12*, 2543-2551.

[22] M. M. J. Smulders, M. M. L. Nieuwenhuizen, T. F. A. de Greef, P. van der Schoot, A. P. H. J. Schenning, E. W. Meijer, *Chem. - Eur. J.* **2010**, *16*, 362-367, S362/361-S362/315.

[23] A. Ciferri, *Macromol. Rapid Commun.* **2002**, *23*, 511-529.

[24] R. B. Martin, *Chem. Rev. (Washington, D. C.)* **1996**, *96*, 3043-3064.

[25] aA. Arnaud, J. Belleney, F. Boue, L. Bouteiller, G. Carrot, V. Wintgens, *Angew. Chem., Int. Ed.* **2004**, *43*, 1718-1721; bO. Colombani, L. Bouteiller, *New J. Chem.* **2004**, *28*, 1373-1382; cM. De Loos, J. Van Esch, R. M. Kellogg, B. L. Feringa, *Angew. Chem., Int. Ed.* **2001**, *40*, 613-616.

[26] aA. J. Markvoort, H. M. M. ten Eikelder, P. A. J. Hilbers, T. F. A. de Greef, E. W. Meijer, *Nat. Commun.* **2011**, *2*, 1517/1511-1517/1519; bM. M. J. Smulders, A. P. H. J. Schenning, E. W. Meijer, *J. Am. Chem. Soc.* **2008**, *130*, 606-611.

[27] I. A. W. Filot, A. R. A. Palmans, P. A. J. Hilbers, R. A. van Santen, E. A. Pidko, T. F. A. de Greef, *J. Phys. Chem. B* **2010**, *114*, 13667-13674.

[28] R. Q. Albuquerque, A. Timme, R. Kress, J. Senker, H.-W. Schmidt, *Chem. - Eur. J.* **2013**, *19*, 1647-1657.

[29] aZ. Chen, V. Stepanenko, V. Dehm, P. Prins, L. D. A. Siebbeles, J. Seibt, P. Marquetand, V. Engel, F. Wuerthner, *Chem. - Eur. J.* **2007**, *13*, 436-449; bM. Kastler, W. Pisula, D. Wasserfallen, T. Pakula, K. Muellen, *J. Am. Chem. Soc.* **2005**, *127*, 4286-4296; cS. Lahiri, J. L.

Thompson, J. S. Moore, *J. Am. Chem. Soc.* **2000**, *122*, 11315-11319; dR. P. Sijbesma, F. H. Beijer, L. Brunsveld, B. J. B. Folmer, J. H. K. K. Hirschberg, R. F. M. Lange, J. K. L. Lowe, E. W. Meijer, *Science (Washington, D. C.)* **1997**, *278*, 1601-1604; eS. Stoncius, E. Orentas, E. Butkus, L. Oehrstroem, O. F. Wendt, K. Waernmark, *J. Am. Chem. Soc.* **2006**, *128*, 8272-8285; fY. Tobe, N. Utsumi, K. Kawabata, A. Nagano, K. Adachi, S. Araki, M. Sonoda, K. Hirose, K. Naemura, *J. Am. Chem. Soc.* **2002**, *124*, 5350-5364; gJ. Van Herrikhuyzen, A. Syamakumari, A. P. H. J. Schenning, E. W. Meijer, *J. Am. Chem. Soc.* **2004**, *126*, 10021-10027; hW. Wang, J. J. Han, L.-Q. Wang, L.-S. Li, W. J. Shaw, A. D. Q. Li, *Nano Lett.* **2003**, *3*, 455-458; iF. Wurthner, C. Thalacker, S. Diele, C. Tschierske, *Chem. - Eur. J.* **2001**, *7*, 2245-2253.

[30] J. van Gestel, A. R. A. Palmans, B. Titulaer, J. A. J. M. Vekemans, E. W. Meijer, *J. Am. Chem. Soc.* **2005**, *127*, 5490-5494.

[31] T. Metzroth, A. Hoffmann, R. Martin-Rapun, M. M. J. Smulders, K. Pieterse, A. R. A. Palmans, J. A. J. M. Vekemans, E. W. Meijer, H. W. Spiess, J. Gauss, *Chem. Sci.* **2011**, *2*, 69-76.

[32] M. L. Bushey, T.-Q. Nguyen, W. Zhang, D. Horoszewski, C. Nuckolls, *Angew. Chem., Int. Ed.* **2004**, *43*, 5446-5453.

[33] M. L. Bushey, A. Hwang, P. W. Stephens, C. Nuckolls, *J. Am. Chem. Soc.* **2001**, *123*, 8157-8158.

[34] T.-Q. Nguyen, R. Martel, P. Avouris, M. L. Bushey, L. Brus, C. Nuckolls, *J. Am. Chem. Soc.* **2004**, *126*, 5234-5242.

[35] T.-Q. Nguyen, M. L. Bushey, L. E. Brus, C. Nuckolls, *J. Am. Chem. Soc.* **2002**, *124*, 15051-15054.

[36] P. J. M. Stals, J. C. Everts, R. de Bruijn, I. A. W. Filot, M. M. J. Smulders, R. Martin-Rapun, E. A. Pidko, T. F. A. de Greef, A. R. A. Palmans, E. W. Meijer, *Chem. - Eur. J.* **2010**, *16*, 810-821, S810/811-S810/816.

[37] aS. J. Grabowski, *Chem. Phys. Lett.* **1999**, *312*, 542-547; bS. J. Grabowski, *J. Phys. Chem. A* **2000**, *104*, 5551-5557; cM. Rozenberg, A. Loewenschuss, Y. Marcus, *Phys. Chem. Chem. Phys.* **2000**, *2*, 2699-2702.

[38] P. J. M. Stals, M. M. J. Smulders, R. Martin-Rapun, A. R. A. Palmans, E. W. Meijer, *Chem. - Eur. J.* **2009**, *15*, 2071-2080.

[39] A. Sugita, K. Suzuki, A. Kubono, S. Tasaka, *Jpn. J. Appl. Phys.* **2008**, *47*, 1355-1358.

[40] aC. F. C. Fitie, W. S. C. Roelofs, M. Kemerink, R. P. Sijbesma, *J. Am. Chem. Soc.* **2010**, *132*, 6892-6893; bC. F. C. Fitie, W. S. C. Roelofs, P. C. M. M. Magusin, M. Wuebbenhorst, M. Kemerink, R. P. Sijbesma, *J. Phys. Chem. B* **2012**, *116*, 3928-3937.

[41] aA. Sakamoto, D. Ogata, T. Shikata, O. Urakawa, K. Hanabusa, *Polymer* **2006**, *47*, 956-960; bM. L. Bushey, T.-Q. Nguyen, C. Nuckolls, *J. Am. Chem. Soc.* **2003**, *125*, 8264-8269.

[42] T. Shikata, D. Ogata, K. Hanabusa, *J. Phys. Chem. B* **2004**, *108*, 508-514.

[43] O. Steinar, H. M. Janssen, P. M. Fransen, M. A. J. Veld, A. R. A. Palmans, EP, 2009, 2, 254 26 A1

[44] aS. Lee, J.-S. Lee, C. H. Lee, Y.-S. Jung, J.-M. Kim, *Langmuir* **2011**, *27*, 1560-1564; bA. Bernet, R. Q. Albuquerque, M. Behr, S. T. Hoffmann, H.-W. Schmidt, *Soft Matter* **2012**, *8*, 66-69; cN. Shi, H. Dong, G. Yin, Z. Xu, S. Li, *Adv. Funct. Mater.* **2007**, *17*, 1837-1843.

[45] F. Abraham, S. Ganzleben, D. Hanft, P. Smith, H.-W. Schmidt, *Macromol. Chem. Phys.* **2010**, *211*, 171-181.

[46] M. Blomenhofer, S. Ganzleben, D. Hanft, H.-W. Schmidt, M. Kristiansen, P. Smith, K. Stoll, D. Maeder, K. Hoffmann, *Macromolecules* **2005**, *38*, 3688-3695.

[47] aP. Besenius, G. Portale, P. H. H. Bomans, H. M. Janssen, A. R. A. Palmans, E. W. Meijer, *Proc. Natl. Acad. Sci. U. S. A.* **2010**, *107*, 17888-17893, S17888/17881-S17888/17819; bP. Besenius, K. P. van den Hout, H. M. H. G. Albers, T. F. A. de Greef, L. L. C. Olijve, T. M. Hermans, B. F. M. de Waal, P. H. H. Bomans, N. A. J. M. Sommerdijk, G. Portale, A. R. A. Palmans, M. H. P. van Genderen, J. A. J. M. Vekemans, E. W. Meijer, *Chem. - Eur. J.* **2011**, *17*, 5193-5203, S5193/5191-S5193/5126.

[48] P. Besenius, J. L. M. Heynens, R. Straathof, M. M. L. Nieuwenhuizen, P. H. H. Bomans, E. Terreno, S. Aime, G. J. Strijkers, K. Nicolay, E. W. Meijer, *Contrast Media Mol. Imaging* **2012**, *7*, 356-361.

[49] K. E. Broaders, S. J. Pastine, S. Grandhe, J. M. J. Frechet, *Chem. Commun. (Cambridge, U. K.)* **2011**, *47*, 665-667.
[50] O. Lehmann, *Zeitschrift für Physikalische Chemie* **1889**, *4*, 462.
[51] J. W. Goodby, *Chem. Soc. Rev.* **2007**, *36*, 1855-1856.
[52] S. Chandrasekhar, B. K. Sadashiva, K. A. Suresh, *Pramana* **1977**, *9*, 471-480.
[53] S. Kumar, *Chem. Soc. Rev.* **2006**, *35*, 83-109.
[54] S. Laschat, A. Baro, N. Steinke, F. Giesselmann, C. Haegele, G. Scalia, R. Judele, E. Kapatsina, S. Sauer, A. Schreivogel, M. Tosoni, *Angew. Chem., Int. Ed.* **2007**, *46*, 4832-4887.
[55] E. Fontes, P. A. Heiney, M. Ohba, J. N. Haseltine, A. B. Smith, III, *Phys. Rev. A: Gen. Phys.* **1988**, *37*, 1329-1334.
[56] M. Hird, *Chem. Soc. Rev.* **2007**, *36*, 2070-2095.
[57] aV. Coropceanu, J. Cornil, D. A. Da Silva Filho, Y. Olivier, R. Silbey, J.-L. Bredas, *Chem. Rev. (Washington, DC, U. S.)* **2007**, *107*, 926-952; bW. Pisula, M. Zorn, J. Y. Chang, K. Muellen, R. Zentel, *Macromol. Rapid Commun.* **2009**, *30*, 1179-1202.
[58] L. Schmidt-Mende, A. Fechtenkotter, K. Mullen, E. Moons, R. H. Friend, J. D. MacKenzie, *Science (Washington, DC, U. S.)* **2001**, *293*, 1119-1122.
[59] W. Pisula, A. Menon, M. Stepputat, I. Lieberwirth, U. Kolb, A. Tracz, H. Sirringhaus, T. Pakula, K. Muellen, *Adv. Mater. (Weinheim, Ger.)* **2005**, *17*, 684-689.
[60] aF. Wuerthner, *Chem. Commun. (Cambridge, U. K.)* **2004**, 1564-1579; bH. Langhals, *Helv. Chim. Acta* **2005**, *88*, 1309-1343; cQ. Ye, J. Chang, K.-W. Huang, C. Chi, *Org. Lett.* **2011**, *13*, 5960-5963.
[61] J. M. Warman, A. M. Van De Craats, *Mol. Cryst. Liq. Cryst.* **2003**, *396*, 41-72.

Objectives and strategy

Table of Contents

A key feature of BTAs in the context of material sciences is the formation of columnar discotic LCs (DLCs). The ferroelectric nature of those columnar DLC produces a macroscopic dipole moment along the supramolecular axis.[1] The electron poor aromatic system confers to the materials made from the BTA scaffold the status of good candidates for the construction of *n*-type heterojunction materials for photovoltaics (*PV*) and field-effect transistor (*FETs*)[2] or for non-volatile memory devices.[3] All of these potential applications depend strongly of the ability of BTAs to self-aggregate in a highly organized supramolecular arrangement. Organic molecules show very low charge mobility (ca. 10^{-6} $cm^2V^{-1}s^{-1}$)[4] compared to inorganic conducting materials like graphite (3 $cm^2V^{-1}s^{-1}$).[5] This lack of charge transport (either electron transport or hole transport) is due to defects in the packing.[6] Recently the group of Müllen demonstrated that discotic columnar liquid crystals could show extremely high charge transport when packing defects are suppressed.[7] Improving this parameter is a key factor to introduce elements made from organic molecules into organic-based electronic devices. An established approach to enhance the quality of the columnar organization of discotic liquid crystals is the formation of dimers with the goal to reduce the degree of freedom and stabilize the columnar organization (Figure 1).[8] This strategy has been extensively applied in the domain of *p*-type organic semiconductors.[9] Our group recently reported a successful example of increased organization in *p*-type triphenylene dimers (Scheme 1).[10]

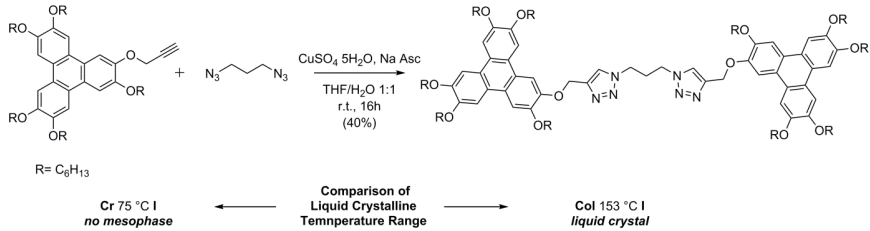

Scheme 1. Example of discotic unit dimerization by "CuAAC" chemistry employment from our research group.[10]

Unfortunately only few examples of dimers employing *n*-types discotic liquid crystals have been successfully synthesized so far. Problems related to the synthesis of the precursors and the lower stability of the molecules used affected the development of *n*-type DLC dimers.[11] Both *p*-type and *n*-type materials are needed for the construction of organic-based photovoltaic systems (Figure 1). The aggregation mechanism and the solid structures of BTA based materials are well-known, which makes them ideal candidates for the manufacturing of *n*-type organic semiconductors.

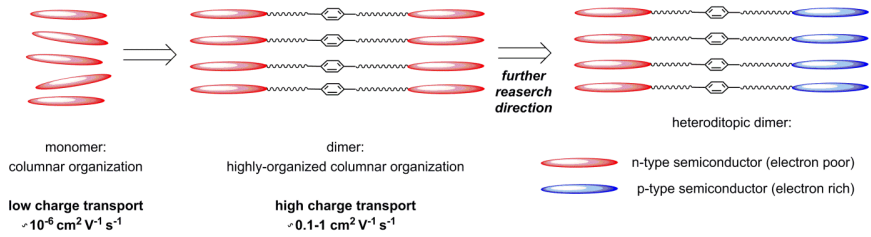

Figure 1. Schematic representation of the long term goal of this work.

Our main goal is exploiting BTAs as compounds for the fabrication of discotic columnar liquid crystalline materials. Concomitantly we wish to obtain the required material's properties based on the rational design of the dimer structures and a meticulously controlled process forming the desired supramolecular arrangement. To the best of our knowledge rules for the construction of *n*-type dimers are still missing. Once our studies will have revealed the requisite design features for reaching our goal, we will have to envisage replacing the aromatic BTAs ring with a well-known conducting *n*-type discotic system such as the *N,N*-dialkyl perylene bisimide.[12] The goal of this next step will be to transfer the lessons learned from small aromatic BTA rings to organic compounds with higher inherent conductivity.

The general design is based on the creation of ditopic, covalently linked dimers of *p*-type/*n*-type forming columnar systems suitable for the application in photovoltaics (Figure 1).

Predicted Changes in the Material Properties Induced by Dimerization

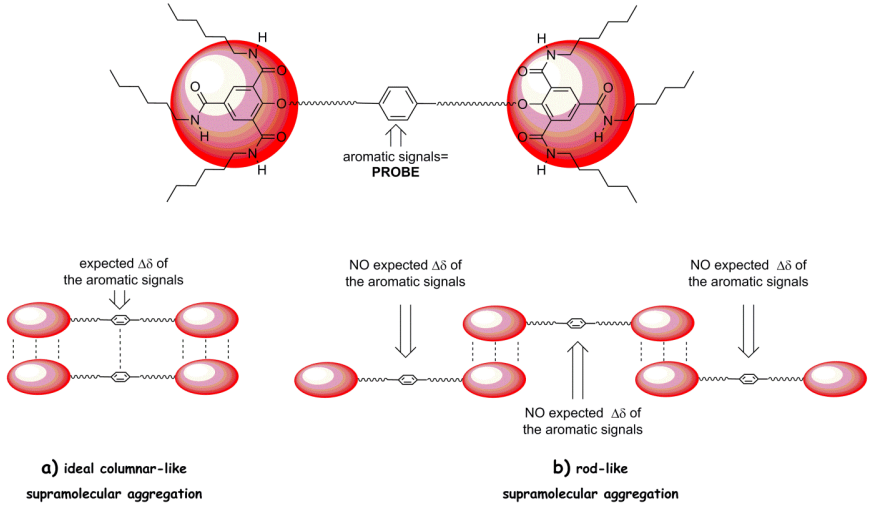

Scheme 2. Anticipated supramolecular arrangement of BTA dimers. The aromatic ring introduced in the middle of the linker will be used as a probe to study the supramolecular self-assembly. The chemical shift of the protons in the aromatic ring will be good sensors for the aggregation process. Concentration dependent NMR analysis is expected to be a sensitive and concise method to characterize the type and strength of the aggregation process.

The aromatic ring was introduced in the middle of the linker as a probe to study of the self-assembly mechanism. In the case of ideal columnar aggregation (Scheme 2a), the expected additional π–π stacking will induce shielding effect on the ^{1}H NMR signals of the aromatic ring.

Synthesis of the Dimers

The following synthetic challenges have to be solved before being able to study the material properties:

- ✓ ***Strategy***: How do we connect the discotic units?
- ✓ ***Anchoring Site***: Where do we functionalize the BTA scaffold in order to make dimers?
- ✓ ***Linker Length***: What is the optimal length of the linker?

Strategy

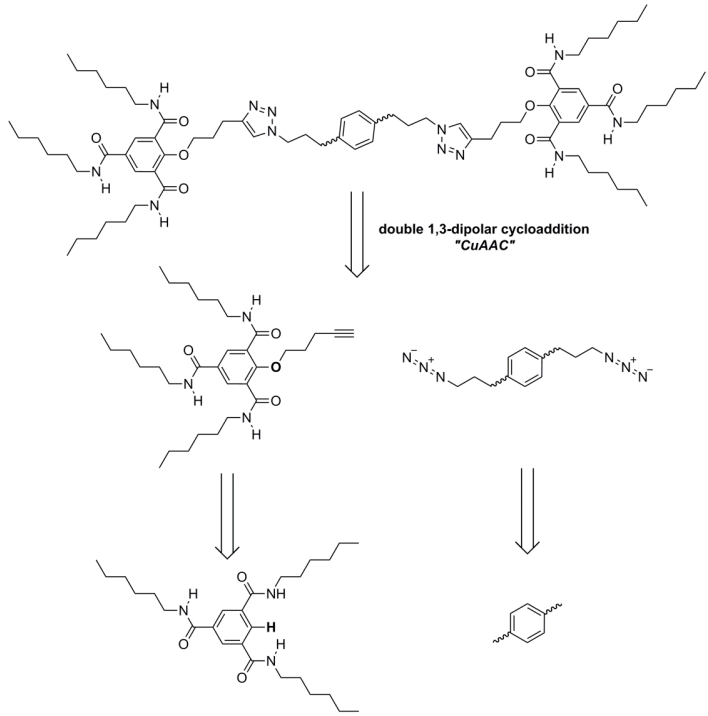

Scheme 3. Schematic representation of the synthetic approach toward the formation of covalently linked BTA dimers.

Our strategy for the synthesis of dimers is based on the copper-catalyzed click chemistry (Scheme 1). We planned to connect the two functionalized discotic units in a convergent scheme (Scheme 3) by forming the triazole moiety (*vedi infra*). This key reaction forming the dimer has great functional group tolerance. The synthesis of the two precursors is easy. The synthesis of the bisazido compounds has already been reported. Furthermore these compounds are described to be relatively stable molecules. The alkyne counterpart has not been reported and the selective mono-functionalization of the BTA scaffold might be problematic.

Choice of the Anchoring Site

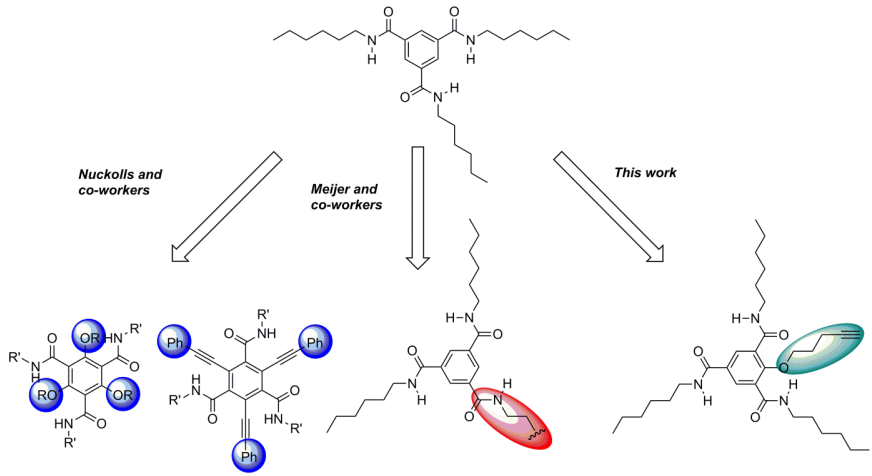

Scheme 4. Schematic representation of the possible "anchoring" sites for dimerization.

The functionalizations of BTAs scaffold and the introduction of an anchoring group is the major synthetic and design challenge. We imposed some limitations for the choice of the potential anchoring site:

- ✓ Minimum "perturbation" of the starting BTA scaffold
- ✓ Easy introduction
- ✓ Convenient modulation of the spacer length
- ✓ Facile introduction of functional groups compatible with CuAAC

The functionalization of BTAs reported so far are exploiting the lateral side chains as the "anchoring" point (see publications by Meijer[13] and Nuckolls[14]) (Scheme 4). Our design is based on the introduction of one alkoxy group, used as the connecting site for the dimer formation (Scheme 3). Alkylation of 2-hydroxy BTA derivatives can be done using an appropriate alkyne compound, introducing the triple bond required for the application of click chemistry. Nuckolls reported that the presence of alkoxy, or alkoxynyl derivatives, will increase the torsion angle of the adjacent amide groups in substituted BTA molecules, causing a strengthening of the intermolecular H-bonds.

Reflexions on the Linker Length:

The literature precedence on the dimerization of *p*-type discotic molecules gave us guidelines for the dimer construction of our *n*-type discotic BTA derived molecules.

Kumar and co-workers recently reviewed a series of triphenylene dimers highlighting the importance of the length (***a***) of the flexible linker related to the length of the aliphatic side chains (***b***) (Scheme 5).[15] The best linker length (***a***) is reached when the linker length and the length of the side chains (***b***) are comparable (ratio $\boldsymbol{a}/\boldsymbol{b} \geq 1$). Shorter linkers were found to prevent the formation of the supramolecular structures needed for obtaining mesomorphic properties.[16]

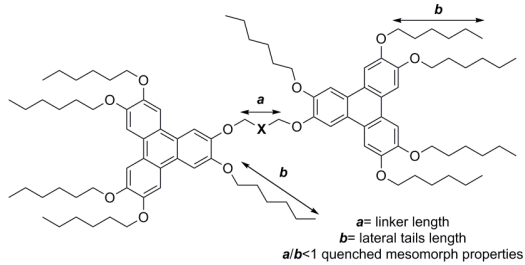

Scheme 5. Schematic explanation of the ration ***a***/***b***

Entry	**X**	***a*** (n° of carbons on the linker chain)	Phase transition (°C)
1	1	3	**Cr** 81 **I**
2	2	5	**Cr** 98 **I**
3	5	7	**Cr** 69 **I**
4	6	8	**Cr** 58 **Col$_h$** 91 **I**
5	7	9	**Cr** 72 **Col$_h$** 92 **I**
6	8	10	**Cr** 50 **Col$_h$** 104 **I**
7	10	12	**Cr** 68 **Col$_h$** 107 **I**
8	14	16	**Cr** 41 **Col$_h$** 84 **I**

Table 1. Transition temperatures of triphenylene dimers with different linker lengths as reported by Boden *et al*.[16]

Precise prediction of the best linker-design based on the actual knowledge is not possible. We therefore envisaged an empirical approach constructing a small library of dimers in order to optimize the properties "*a posteriori*".

The Concept of Click Chemistry

Introduction of the Concept of Click Reactions

In 2001 the group of Sharpless from the Scripps Research Institute presented a new concept to rapidly and easily make large libraries of molecules. They proposed what is nowadays generally called "click chemistry" approach.[17] Sharpless et al. defined as a "click chemistry" approach reactions with the following properties: wide scope of the reaction, high degree of variability, high (*stereo*)selectivity, high atom economy and high functional group tolerance on the reaction pathway. This approach favors the formation of C-X bonds (carbon-heteroatom) rather than C-C bonds. Carbon-heteroatoms bonds are generally thermodynamically and kinetically easier to make than C-C bonds. An enumeration of reactions employed in click chemistry is listed below:

- ✓ Cycloaddition like 1,3-dipolar cycloaddition reaction, Diels-Alder cycloaddition
- ✓ Nucleophilic ring-opening of strained small ring, e.g. epoxides, aziridines, etc.
- ✓ Electrophilic addition on carbon-carbon multiple bonds, e.g. epoxydation, dihydroxylation, aminohydroxylation, etc.
- ✓ Carbonyl chemistry of the non-aldol type, e.g. formation of oximes, hydrazones, etc.

Based on the goals defined by Sharpless et al. the use of Huisgen alkyne-azido 1,3-dipolar cycloaddition reactions flourished again. This reaction presents the advantage of linking two independent molecules respecting the aforementioned conditions. Before the introduction of the concept of click chemistry this reaction did not find extensive application in organic synthesis, or in biological or material sciences. The thermal instability of azido compounds was certainly one of the main reasons, why their use was limited. Since the *CuAAc* catalyzed version was introduced the number of scientific papers and citations grew spectacularly (Graph 1). Simultaneously, it was found that triazoles are interesting units in organic synthesis, medicinal chemistry [18] and material science.[19]

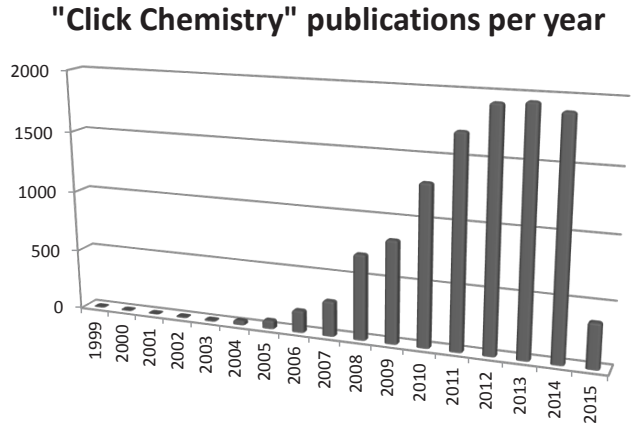

Graph 1. The graph shows the distribution of the number of scientific publications, dealing with the concept of "click chemistry" per year. The number of publications has been searched by the key word "click chemistry" using the database SciFinder® on the 1st May 2015. A total of 11627 publications were found.

Copper Catalyzed Azido-Alkyne Cycloaddition CuAAC: an Efficient Example of the Click Chemistry

In 1963 Huisgen published a review concerning the reaction between azido derivatives (R-N_3) and alkynes forming five-membered heterocyclic rings by a formal [3+2] cycloaddition (Scheme 6).[20]

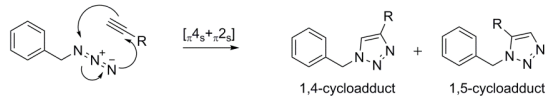

Scheme 6. Alkyne-azido [3+2] cycloaddition reported by Huisgen. The thermal version of the reaction leads to the formation of both possible regioisomers. The reaction is called [3+2] because it leads to the formation of a five-membered heterocyclic ring; however the transformation is a formal [4+2] reaction (4 π_e from the dipole and 2 π_e from the dipolarophile).

This [$\pi 4_s$ + $\pi 2_s$] transformation is allowed by the Woodward-Hofmann rules[21] and leads to heteroaromatic 1,2,3-triazoles. In the original Huisgen's version the thermal reaction proceeds without control of the regioselectivity. Substituted acetylene moieties react under thermal conditions to form both possible 1,4- and 1,5-1,2,3-triazole regioisomers (Scheme 6). The thermal azido-alkyne 1,3-DCR (DCR = dipolar cycloaddition reaction) developed by Huisgen does not fulfil the conditions for a good click reaction since both possible regioisomers are produced in comparable yields. In 2002 the group of Meldal[22] in Denmark and the group of Sharpless[23] reported independently the copper (I) catalyzed version of what is generally called "copper-catalyzed alkyne azido click chemistry" or just *CuAAC*. The addition of a catalytic amount of a copper salt enhanced dramatically the kinetics of the reaction and formed the products with high regioselectivity (only the 1,4 regioisomer is formed).

Sharpless and Fokin proposed a mechanism involving a copper (I) species (Figure 2).[24] The copper (I) inserts into the C-H alkyne bond forming an organocopper species (2). The azido compound reacts with the metallic center forming a six membered intermediate (4) that immediately rearranges to form the five-membered triazole ring maintaining the copper-carbon bond. The elimination of copper (I) regenerates the catalyst.

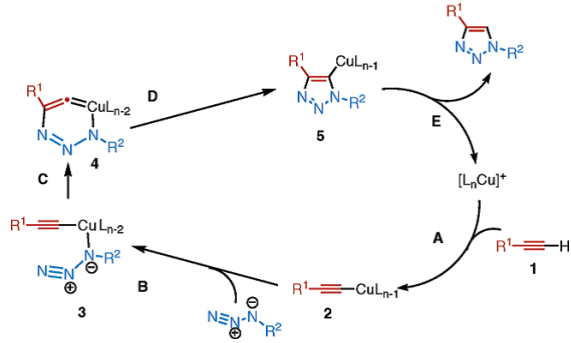

Figure 2. Schematic representation of CuAAC mechanism proposed by Sharpless and Fokin. The figure was copied from the work of Fokin and co-workers.[24]

The active catalyst in the catalyzed reaction is the copper (I) salt. A common source of copper (I) is CuI, also widely used for the generation of Gilman's cuprates.[25] Sharpless *et al*. introduced the *in situ* generation of the copper(I) species by reduction of the much less expensive and much more stable copper sulfate pentahydrate $CuSO_4$ $5H_2O$ with sodium ascorbate (NaAsc). This procedure avoids the use of the oxygen sensitive and expensive CuI.

In 2013 the group of Fokin published a detailed study on the mechanism of CuAAC (Figure 3). The group proposed the involvement of a dinuclear copper complex in the formation of the transition state by running labeling experiments and by studying the heat flow with calorimetry.[26]

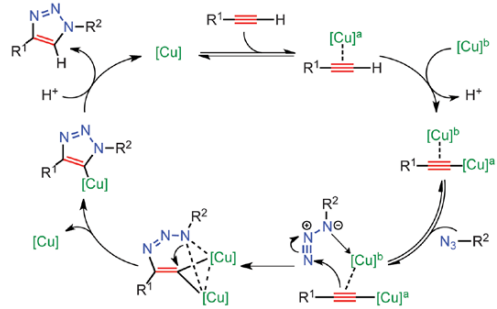

Figure 3. CuAAC dinuclear mechanism proposed by Fokin in 2013. The figure was copied from the work of Fokin and co-workers .[26]

References:

[1] a) C. F. C. Fitie, W. S. C. Roelofs, M. Kemerink, R. P. Sijbesma, *J. Am. Chem. Soc.* **2010**, *132*, 6892-6893; b) C. F. C. Fitie, W. S. C. Roelofs, P. C. M. M. Magusin, M. Wuebbenhorst, M. Kemerink, R. P. Sijbesma, *J. Phys. Chem. B* **2012**, *116*, 3928-3937.

[2] J. E. Anthony, A. Facchetti, M. Heeney, S. R. Marder, X. Zhan, *Adv. Mater.* **2010**, *22*, 3876-3892.

[3] H. Takezoe, K. Kishikawa, E. Gorecka, *J. Mater. Chem.* **2006**, *16*, 2412-2416.

[4] A. Rochefort, E. Bayard, S. Hadj-Messaoud, *Adv. Mater.* **2007**, *19*, 1992-1995.

[5] M. S. Dresselhaus, G. Dresselhaus, *Adv. Phys.* **1981**, *30*, 139-126.

[6] C. D. Sheraw, T. N. Jackson, D. L. Eaton, J. E. Anthony, *Adv. Mater.* **2003**, *15*, 2009-2011.

[7] X. Feng, V. Marcon, W. Pisula, M. R. Hansen, J. Kirkpatrick, F. Grozema, D. Andrienko, K. Kremer, K. Muellen, *Nat. Mater.* **2009**, *8*, 421-426.

[8] C. T. Imrie, P. A. Henderson, *Curr. Opin. Colloid Interface Sci.* **2002**, *7*, 298-311.

[9] a) D. Adam, P. Schumacher, J. Simmerer, L. Haeussling, W. Paulus, K. Siemensmeyer, K. H. Etzbach, H. Ringsdorf, D. Haarer, *Adv. Mater.* **1995**, *7*, 276-280; b) A. Bacher, I. Bleyl, C. H. Erdelen, D. Haarer, W. Paulus, H. W. Schmidt, *Adv. Mater.* **1997**, *9*, 1031-1035; c) W. Kranig, B. Hueser, H. W. Spiess, W. Kreuder, H. Ringsdorf, H. Zimmermann, *Adv. Mater.* **1990**, *2*, 36-40; d) A. M. Van de Craats, L. D. A. Siebbeles, I. Bleyl, D. Haarer, Y. A. Berlin, A. A. Zharikov, J. M. Warman, *J. Phys. Chem. B* **1998**, *102*, 9625-9634; e) S. Zamir, R. Poupko, Z. Luz, B. Hueser, C. Boeffel, H. Zimmermann, *J. Am. Chem. Soc.* **1994**, *116*, 1973-1980.

[10] D. Thevenet, R. Neier, *Synthesis* **2011**, 3801-3806.

[11] a) J. Zaumseil, H. Sirringhaus, *Chem. Rev.* **2007**, *107*, 1296-1323; b) W. Jiang, Y. Li, Z. Wang, *Acc. Chem. Res.* **2014**, *47*, 3135-3147.

[12] a) F. Wuerthner, *Chem. Commun.* **2004**, 1564-1579; b) H. E. Katz, A. J. Lovinger, J. Johnson, C. Kloc, T. Slegrist, W. Li, Y. Y. Lin, A. Dodabalapur, *Nature* **2000**, *404*, 478-481.

[13] J. Roosma, T. Mes, P. Leclere, A. R. A. Palmans, E. W. Meijer, *J. Am. Chem. Soc.* **2008**, *130*, 1120-1121.

[14] a) M. L. Bushey, A. Hwang, P. W. Stephens, C. Nuckolls, *J. Am. Chem. Soc.* **2001**, *123*, 8157-8158; b) M. L. Bushey, T.-Q. Nguyen, C. Nuckolls, *J. Am. Chem. Soc.* **2003**, *125*, 8264-8269; c) W. Zhang, D. Horoszewski, J. Decatur, C. Nuckolls, *J. Am. Chem. Soc.* **2003**, *125*, 4870-4873.

[15] S. Kumar, *Liq. Cryst.* **2005**, *32*, 1089-1113.

[16] N. Boden, R. J. Bushby, A. N. Cammidge, A. El-Mansoury, P. S. Martin, Z. Lu, *J. Mater. Chem.* **1999**, *9*, 1391-1402.

[17] H. C. Kolb, M. G. Finn, K. B. Sharpless, *Angew. Chem., Int. Ed.* **2001**, *40*, 2004-2021.

[18] a) S. G. Agalave, S. R. Maujan, V. S. Pore, *Chem. - Asian J.* **2011**, *6*, 2696-2718; b) F. Amblard, J. H. Cho, R. F. Schinazi, *Chem. Rev.* **2009**, *109*, 4207-4220; c) G. C. Tron, T. Pirali, R. A. Billington, P. L. Canonico, G. Sorba, A. A. Genazzani, *Med. Res. Rev.* **2008**, *28*, 278-308.

[19] a) M. G. Finn, V. V. Fokin, *Chem. Soc. Rev.* **2010**, *39*, 1231-1232; b) G. Franc, A. K. Kakkar, *Chem. Soc. Rev.* **2010**, *39*, 1536-1544; c) P. L. Golas, K. Matyjaszewski, *Chem. Soc. Rev.* **2010**, *39*, 1338-1354; d) J. E. Hein, V. V. Fokin, *Chem. Soc. Rev.* **2010**, *39*, 1302-1315; e) R. K. Iha, K. L. Wooley, A. M. Nystrom, D. J. Burke, M. J. Kade, C. J. Hawker, *Chem. Rev.* **2009**, *109*, 5620-5686; f) A. Qin, J. W. Y. Lam, B. Z. Tang, *Chem. Soc. Rev.* **2010**, *39*, 2522-2544.

[20] a) R. Huisgen, *Angew. Chem.* **1963**, *75*, 604-637; b) A. Padwa, *1,3-Dipolar Cycloaddition Chemistry, Vol. 2*, **1984**.

[21] a) R. Hoffmann, R. B. Woodward, *J. Am. Chem. Soc.* **1965**, *87*, 2046-2048; b) R. B. Woodward, R. Hoffmann, *J. Am. Chem. Soc.* **1965**, *87*, 395-397; c) R. B. Woodward, R. Hoffmann, *Angew. Chem., Int. Ed. Engl.* **1969**, *8*, 781-853.

[22] C. W. Tornoe, C. Christensen, M. Meldal, *J. Org. Chem.* **2002**, *67*, 3057-3064.

[23] V. V. Rostovtsev, L. G. Green, V. V. Fokin, K. B. Sharpless, *Angew. Chem., Int. Ed.* **2002**, *41*, 2596-2599.

[24] F. Himo, T. Lovell, R. Hilgraf, V. V. Rostovtsev, L. Noodleman, K. B. Sharpless, V. V. Fokin, *J. Am. Chem. Soc.* **2005**, *127*, 210-216.

[25] N. Krause, *Modern Organocopper Chemistry*, 1 ed., Wiley-VCH, **2002**.

[26] B. T. Worrell, J. A. Malik, V. V. Fokin, *Science* **2013**, *340*, 457-460.

BTA synthesis (monomer synthesis)

Table of Contents

Reported Synthesis of BTAs core

The synthesis of BTA scaffolds is simple and uses easily accessible starting materials and the connection between the aromatic ring and the three amide groups can be N-centered or C=O-centered. The two types of BTAs impose different synthetic strategies (Scheme 1).

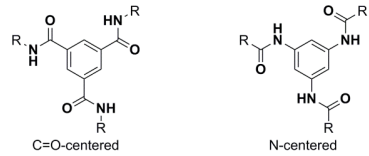

Scheme 1. General structure of C=O and N-centered BTAs.

N-centered BTAs

In our work we did not explore N-centered BTAs. For the sake of completeness we present a brief overview of the synthesis of N-centered BTAs. The first synthesis of N-centered BTAs was reported by Gill et *al*. in 1949. They performed a catalytic hydrogenation of 1,3,5-trinitrobenzene on Ni-Raney® followed by the acylation of the resulting 1,3,5-triaminobenzene giving the N-centered BTA derivative (Scheme 2).[1] Few years later palladium on carbon was used as an effective catalyst for a similar transformation.[2]

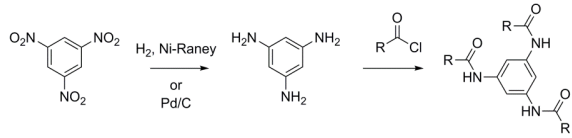

Scheme 2. Schematic synthesis of N-centered BTAs by reduction of 1,3,5-trinitrobenzene.

The manipulation of 1,3,5-trinitrobenzene is reported to be dangerous, due to the known instability and the propensity to explode of poly-nitro aromatic compounds. Moreover the 1,3,5-triaminobenzene are prone to degradation by easy oxidation. To prevent this degradation an in-situ acylation of the aromatic amines is required (Scheme 2).

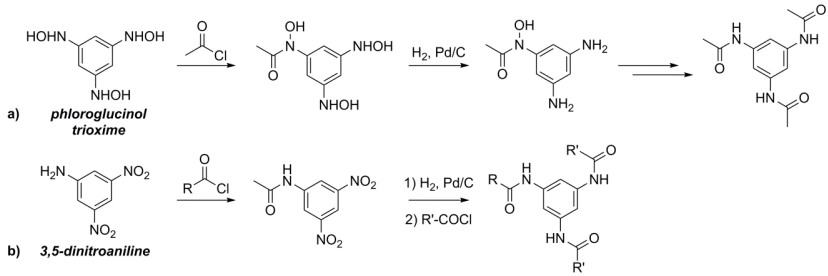

Scheme 3. a) Synthesis of N-centered BTAs by Maramatsu.[3] b) Synthesis of desymmetrized N-centered BTAs reported by Meijers and coworkers.[4]

The group of Maramatsu solved this problem, employing phloroglucinol trioxime as a safe starting material for the controlled reduction followed by acetylation (Scheme 3a).[3] The synthetic procedure

of Maramatsu allows the formation of C_3-symmetric N-centered BTA, where all three substituents must be identical. Meijer proposed an alternative approach to the synthesis of a desymmetrized N-centered BTA starting from 3,5-dinitroaniline (Scheme 3b).[4] Today these two synthetic procedures are most often used in the synthesis of N-centered BTA derivatives.

C=O-centered BTAs

Compared to the first description of BTAs, the interest of the community in BTAs and their properties came very late. Intensive studies of BTAs started in the late eighties, when the group of Matsunaga reported the capability of BTAs to form columnar LC. As a result of these extensive material property studies important improvements of the synthetic methodologies capable to prepare BTAs were reported.

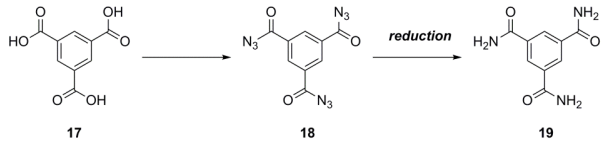

Scheme 4. Reduction of the acyl-azido **18** discovered in 1915 by Curtius.

The first synthesis of C=O-centered BTAs was accomplished by Curtius in 1915 with the synthesis of the primary benzene-tricarboxamide **19** (Scheme 4).[5] Curtius's synthesis transformed trimesic acid **17** into the triacyl azido **18** followed by reduction (Scheme 4). The major limit of this methodology is the explosive nature of the triacyl azido derivative **18** when isolated in the solid state.[6] Modern synthesis uses the thermally stable[7] benzene-1,3,5-benzentricarbonyl trichloride (or trimesoyl chloride) **21** as starting material (Scheme 5). The synthesis of **21** is accomplished from mesitylene **20**, which is oxidized to trimesic acid **17** followed by treatment with $SOCl_2$ converting it to trimesic chloride **21**. Most of the reported synthesis of C=O-centered BTAs are obtained from the reaction of trimesic chloride with an amine in presence of a base, typically a tertiary amine (Scheme 5). Trimesic acid **17** and trimesoyl chloride **21** are commercially available.

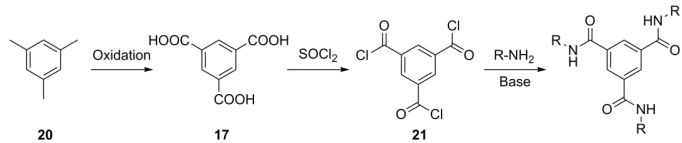

Scheme 5. General synthesis of C=O-centered BTAs.

The literature reports many examples using different amines for the preparation of a multitude of BTA derivatives. This approach allowed to introduce chiral side chains,[8] modifying the polarity using highly hydrophilic chains[9] and extending the π–system using gallic acid derivatives[10] or porphyrin derivatives[11].

This synthetic pathway can only be used to synthesize C_3-symmetric BTA derivatives. If BTAs substituted with different amines at the 1,3,5 position are needed, the synthesis is more tedious and requires additional steps. For example Meijer and coworkers reported the synthesis of a C_2-symmetric 3,5-(methoxycarbonyl)-isophthalic acid **23** from the controlled hydrolyses of trimethyl trimesic acid **22** (Scheme 6).[12]

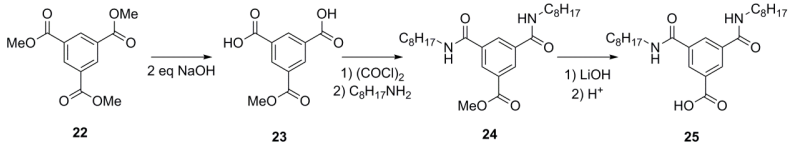

Scheme 6. Synthesis of C_2-symmetric BTA derivative **25** reported by Meijer and coworkers.[12]

This procedure allows the synthesis of desymmetrized BTAs carrying different side chains. Only a few examples are reported where the aromatic ring is functionalized.

BTA's Aromatic Core Modifications

The group of Nuckolls reported pioneering work functionalizing the aromatic core of his BTA derivatives. They synthesized a family of 2,4,6-trisubstituted N,N',N''-trialkyl 1,3,5-benezentricarboxamide, which they called "crowded arenes" (Scheme 7).[13]

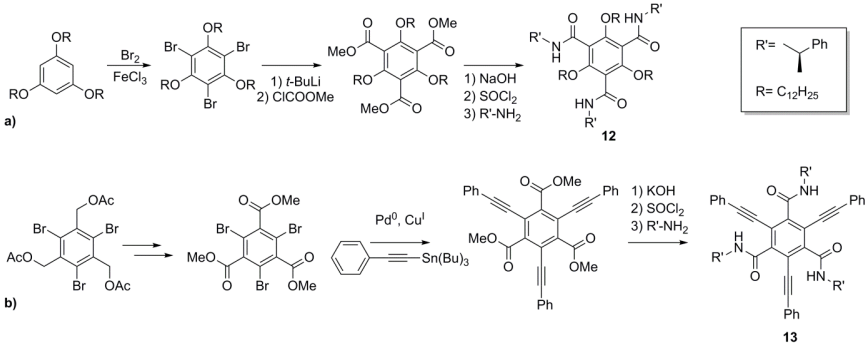

Scheme 7. a) Synthesis of 2,4,6-alkoxy-substituted-1,3,5-BTA **12**.[13a] b) Synthesis of 2,4,6-alkynyl-substituted-1,3,5-BTA **13**.[13b]

The introduced substituents in 2,4,6 position could be alkoxy groups (Scheme 7a) or alkyne groups (Scheme 7b). The work of Nuckolls allowed the formation of symmetrically fully substituted BTAs. He demonstrated that the introduction of substituents in positions 2, 4 and 6 was beneficial for the columnar organization of the obtained material (see Chapter 1). To the best of our knowledge the "Nuckolls" compounds are the only examples of fully substituted BTA reported so far in literature.

More interesting in the context of our own project is the case of 2-monosubstituted and 2,4-disubstitued BTAs. To the best of our knowledge 2,4-disubstited BTAs scaffolds have not been employed in the field of liquid crystals. No other applications of this type of compounds have been reported in literature.

Only very few examples of 2-substituted BTAs (= monosubstituted BTAs) are reported in the literature. The first example of a 2-functionalized-BTA was published in 1967 by the group of Wallenfels, synthesizing a 2-bromo-BTA **28** (Scheme 8).[14]

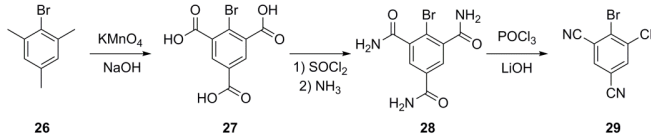

Scheme 8. 2-bromo-benzentriamide **28** synthesis reported by Wallenfels et *al.*[14]

The benzylic oxidation of the 2-bromo-mesitylene **26** furnished the triacid **27,** which was converted to the primary benzene triamide **28** (Scheme 8). The 2-bromo-tricyano benzene **29** was successively used by the group of Fendler to study the Meisenheimer complex as an intermediate in the aromatic nucleophilic substitution.[15]

The group of Raymond from Berkley reported the synthesis of the fluorescent 2-hydroxy-substituted BTA (Scheme 9). They used this fluorescent system as an "antenna" ligand for lanthanide complexation using europium or lanthanum.[16] The commercially available cresol **30** is protected as methyl ether **31** and then oxidized to the corresponding 2-methoxy-1,3,5-benzentricarboxylic acid **32** using $KMnO_4$ in basic conditions. Oxalyl chloride converted the triacid **32** to the triacyl chloride that was transformed to the corresponding 2-methoxy BTA derivative by adding the desired amine. The methyl ether cleavage was accomplished by using BBr_3 at low temperature (see Scheme 14).

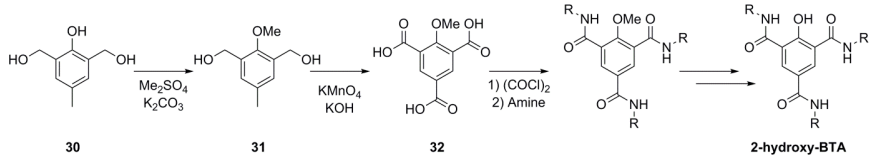

Scheme 9. Synthesis of 2-hydroxy BTA derivative reported by Raymond.[16]

The synthetic approaches reported by Wallenfels and Raymond are not suitable for the easy modification of the substituent on the aromatic ring.

Synthesis of Novel Functionalized BTA-Monomer(s)

Synthesis of 2-substituted BTAs

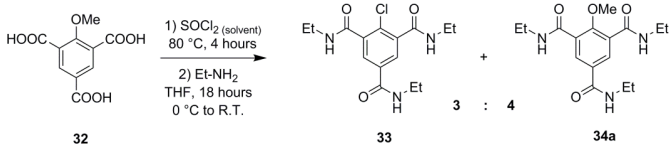

Scheme 10. Preliminary study on the activation of trimesic acid by thionyl chloride.

The synthesis of the 2-methoxy-1, 3, 5-benzenetricarboxylic acid **32** was accomplished according to the procedure published by Raymond (Scheme 9). Activation of **32** as triacyl chloride and further conversion into amides was found to be a tricky reaction. In our hands boiling **32** in thionyl chloride as solvent, followed by the addition of ethyl amine gave a mixture of the chloro-derivative **33** and the desired methoxy-BTA **34a** in ratio of 3 : 4 (Scheme 10).[17] We assumed the formation of the highly reactive triacyl chloride being the first step (Scheme 11). The excess of chloride may react as nucleophile in a $S_{N\ Aromatic}$ addition/elimination reaction generating the highly stabilized Meisenheimer complex (Scheme 11).[15] To reinstate the aromaticity either chloride or the methoxide group can be ejected leading either to the desired product **34a** or to the side product **33**. The ejected methoxide will be trapped by the excess of $SOCl_2$. We supposed that this side reaction is thermodynamically driven by the formation of chlorosulfinate **35**.

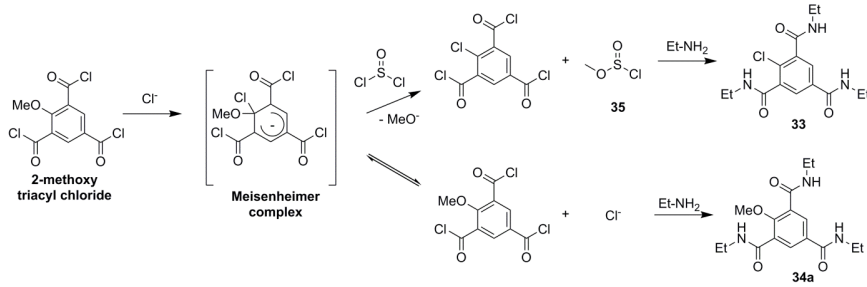

Scheme 11. Proposed mechanism of demethoxylation side reaction.

The Meisenheimer complex formation has been invoked in the thionyl chloride-mediated demethoxylation reaction reported on similar electron poor polynitro-substituited anisole (Scheme 12).[18] Indeed the addition-elimination mechanism, forming the Meisenheimer complex, in $S_{N\ Aromatic}$ can be invoked when the aromatic substrate is strongly activated (= electron poor).

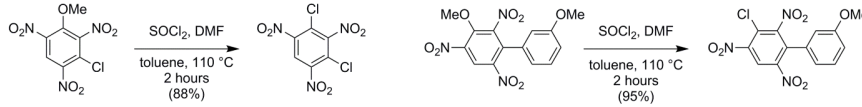

Scheme 12. Reported demethoxylation of activated aromatics described by Bellamy *et al*.[18]

The formation of the side-product was avoided by running the reaction with a stoichiometric amount of thionyl chloride. 2-methoxy-1, 3, 5-benzenetricarbonyl trichloride was isolated without

purification and the spectroscopic data (^{1}H-NMR spectra) were in agreement with the data reported by Raymond (Scheme 13).

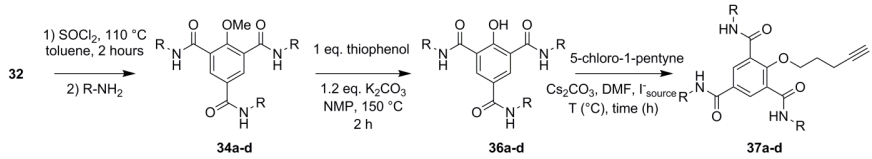

a) R= ethyl, b) R= hexyl, c) R= dodecyl, d) R= octadecyl

Scheme 13. Synthesis of 2-alkoxynyl substituted BTAs **37a-d**.

Aliphatic side chains

Formation of methoxy-BTA 34a-d

The 2-methoxy-triacyl chloride reacted with the corresponding aliphatic amines (Table 1). The acylation reactions were carried out in THF where the triacyl chloride is well soluble. In the case of the ethyl- and hexyl-amine derivatives, a large excess (eight equivalents) of the amines were used to trap the formed hydrochloric acid. When dodecyl- and octadecyl-amines were used, the hydrochloric acid was neutralized by the addition of four equivalents of triethylamine (TEA). The octadecylamine was found to be poorly soluble in THF and therefore the solvent was replaced with chloroform. The 2-methoxy BTA **34a-d** were easily purified by chromatography on silica gel (Table 1) and BTA derivatives **34a**-**c** were finally isolated in good yield. In the case of the longest octadecylamine the resulting BTA **34d** was isolated in lower yield.

BTA	amine	solvent	base	time (hours)	yield
34a	ethylamine (sol. 70% in H_2O) C_2H_5	THF/H_2O	none	4	64%
34b	hexylamine C_6H_{13}	THF	none	18	64%
34c	dodecylamine $C_{12}H_{25}$	THF	TEA	48	44%
34d	Octadecylamine $C_{18}H_{37}$	$CHCl_3$	TEA	18	16%

Table 1. Synthesis and experimental conditions of 2-methoxy BTA **34a**-**d**.

Nucleophilic Demethylation of 34a-d Affording 36a-d

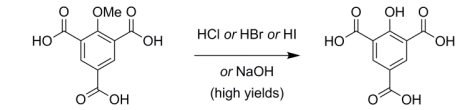

a) *Freeman*, 1950

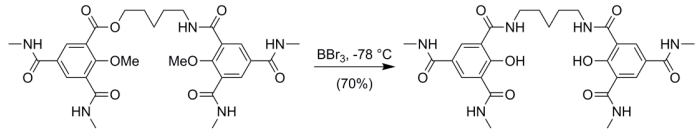

b) *Raymond*, 2009

Scheme 14. a) Demethylation conditions reported on 2-methoxy 1,3,5 tricarboxilic acid **32**.[19] The authors reported that the demethylation reaction take place under acidic or basic conditions with extreme ease. b) Demethylation condition reported for the BTA dimer derivative.[20]

The demethylation of the 2-methoxy-1,3,5-benzentricarboxylic acid **32** to the corresponding 2-hydroxytrimesic acid **38** was reported to proceed very easily by Freeman under acidic conditions (HCl, HBr or HI) or under basic condition (NaOH) (Scheme 14a).[19] In 2009 Raymond reported the demethylation reaction of a BTA dimer derivative using BBr_3 at low temperature (Scheme 14b).[20]Despite these successfully previously reported examples, our preliminary essays, on selective demethylation using these reported conditions failed. We then decided to adopt less sensitive and milder cleavage conditions. The group of Chakraborti reported a thiophenol-based nucleophilic cleavage methodology on aryl methyl ether (Scheme 15).[21]

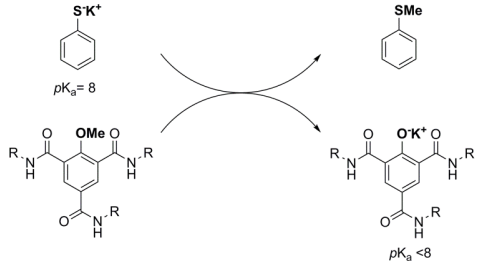

Scheme 15. Adapted demethylation mechanism according to the procedure reported by Chakraborti.[21]

The reported version of the reaction employed only a catalytic amount of base (K_2CO_3). Indeed the potassium salt of the phenol (pK_a = 10) is able to deprotonate the more acidic thiophenol (pK_a = 8) and reinstalls the thiophenolate anion. In our case we needed a stoichiometric amount of base due to the higher acidity of the corresponding 2-hydroxy-BTAs **36a-d**. The 2-hydroxy derivatives **36a-d** were then regenerated by protonation of their potassium salt format at the end of the reaction. Highly polar solvent, like *N*-methyl-2-pyrrolidone, and high temperature as 150 °C were required to run the reaction in good to excellent yields in two hours (Table 2).

BTA	R	yield
36a	C_2H_5	61%
36b	C_6H_{13}	78%
36c	$C_{12}H_{25}$	72%
36d	$C_{18}H_{37}$	90%

Table 2. Demethylation reaction of 2-methoxy BTAs **36a-d**.

Alkylation of 36a-d affording 2-pentynyloxy BTA derivatives 37a-d

The final step of the preparation of 2-alkoxynyl substituted BTAs derivatives consisted of the alkylation of **36a-d** by using 5-chloro-1-pentyne. Despite the fact that the alkylation reaction was pushed using the ion-pair separating solvent (DMF), large radii cation (Cs^+) and high temperatures, the alkylation furnished **37a-c** only in poor yields (Table 3). Moreover, the octadecyl-BTA **36d** was insoluble in DMF (event its cesium salt) therefore the alkylation did not occur. The estimated low pK_a of the phenol **36a-d** (<7.5) stabilizes the negative charge of the phenoxide and limited the alkylation of **36a-d**. We postulated that the generated negative charge on the oxygen could be stabilized by a double intramolecular H-bonds formation with the two adjacent secondary amide groups. The X-ray structures of the 2-hydroxy-isophthaloyl amide **39** and its tetramethyl ammonium salt **40** reported by Ueyama (Scheme 16) are supporting this hypothesis.[22]

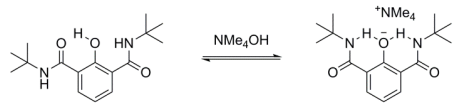

39 **40**

pK_a= 7.5

Scheme 16. Double intramolecular H-bonds formation and amide bonds rotation reported by Ueyama.[22]

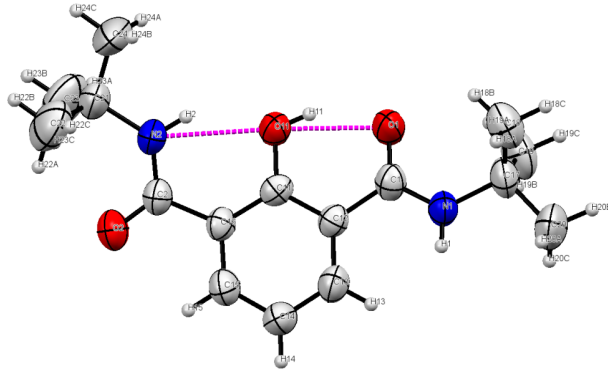

Figure 1. X-ray structure of the hydroxy-isophthaloyl amide derivative **39** reported by Ueyama.[22] Magenta dashed lines indicate intramolecular H-bonds.

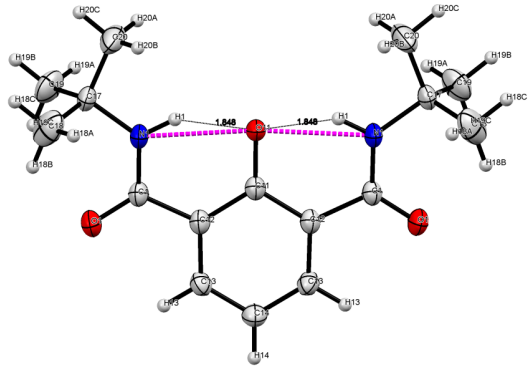

Figure 2. Double intramolecular H-bonds from a 2-oxy-isophthaloyl amide derivative **40** reported by Ueyama.[22] The tetramethylammonium counterion is missing for clarity. Magenta dashed lines indicate intramolecular H-bonds.

In the crystal structure of the deprotonated form of the 2-hydroxy-1,3-benzendicarboxamide derivative **40** the double intramolecular H-bonds (N-H--OAr *d* 1.848 Å, Figure 2) have clearly been identified.

BTA	R	T (°C)	time (hours)	yield
37a	C_2H_5	60	48	17%
37b	C_6H_{13}	60	48	42%
37c	$C_{12}H_{25}$	75	72	22%
37d	$C_{18}H_{37}$	80	96	trace

Table 3. Alkylation reaction conditions.

Other reasons that could explain the low yield of the reaction are the reversibility of the reaction and the weak electrophylicity of the alkynyl halide (Scheme 17).

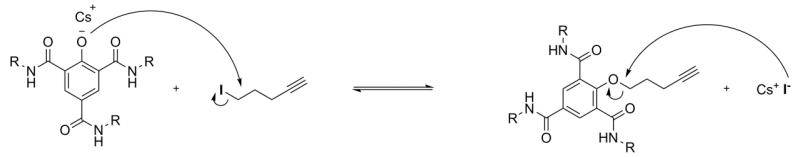

Scheme 17. Possible mechanism of ether cleavage of 2-alkoxy-BTA derivatives.

2-Bromo BTA

In order to facilitate the study of the material and self-assembly properties of **37a-c**, the synthesis of 2-bromo BTA **41** was envisaged. The bromine in **41** is not a H-bond acceptor. Compounds **41** can therefore be used as a comparison for the analysis of the 2-pentynyloxy substituted BTA derivatives. Employing transition metal-catalyzed coupling reactions the synthesis of homodimeric structures starting from the 2-bromo derivative can be envisaged. The 2-bromotrimesic acid **27** was prepared according to the work previously reported by Wallenfels.[14]

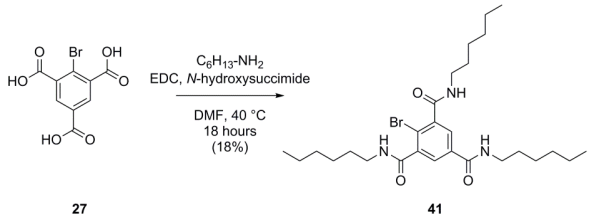

27 **41**

Scheme 18. EDC-mediated synthesis of the 2-bromo BTA derivative **41**.

The triacid **27** was converted into the tricarboxamide **41** employing 1-ethyl-3-(3-dimethylaminopropyl)carbodiimide hydrochloride EDC as coupling reagent[23] and an activating agent N-hydroxysucinimide in DMF (Scheme 21). The condensation product was isolated in acceptable yield of 18%.

Concluding Remarks

The synthetic approach based on the phenols **38** and their alkylation, introducing an alkynyl function, allowed us to synthesize three derivatives of 2-monosubstitued BTA derivatives. The length of the amide side chains can be modulated. The introduction of the pentynyloxy group made BTA derivatives available which can be used for dimer formation using click chemistry. On the other hand, the 2-bromo substituted BTA might be used in the future in the formation of dimeric structures by employing transition metal catalyzed cross-coupling transformation, such as Sonogashira type coupling.[24]

References

[1] J. E. Gill, R. MacGillivray, J. Munro, *J. Chem. Soc.* **1949**, 1753-1754.
[2] H. Stetter, D. Theisen, G. J. Steffens, *Chem. Ber.* **1970**, *103*, 200-204.
[3] I. Arai, Y. Sei, I. Muramatsu, *J. Org. Chem.* **1981**, *46*, 4597-4599.
[4] J. J. van Gorp, J. A. J. M. Vekemans, E. W. Meijer, *Mol. Cryst. Liq. Cryst.* **2003**, *397*, 491-505.
[5] T. Curtius, *J. Prakt. Chem.* **1915**, *91*, 39-102.
[6] a) J. J. van Gorp, J. A. J. M. Vekemans, E. W. Meijer, *J. Am. Chem. Soc.* **2002**, *124*, 14759-14769; b) M. C. Davis, *Synth. Commun.* **2007**, *37*, 1457-1462.
[7] According to the saftey data of different suppliers, the compound is classified as a corrosive molecule (R14, R22 and R34) but stable under normal conditions.
[8] A. R. A. Palmans, J. A. J. M. Vekemans, E. E. Havinga, E. W. Meijer, *Angew. Chem., Int. Ed. Engl.* **1997**, *36*, 2648-2651.
[9] L. Brunsveld, H. Zhang, M. Glasbeek, J. A. J. M. Vekemans, E. W. Meijer, *J. Am. Chem. Soc.* **2000**, *122*, 6175-6182.
[10] A. R. A. Palmans, J. A. J. M. Vekemans, H. Fischer, R. A. Hikmet, E. W. Meijer, *Chem. - Eur. J.* **1997**, *3*, 300-307.
[11] a) R. van Hameren, J. A. A. W. Elemans, D. Wyrostek, M. Tasior, D. T. Gryko, A. E. Rowan, R. J. M. Nolte, *J. Mater. Chem.* **2009**, *19*, 66-69; b) R. van Hameren, A. M. van Buul, M. A. Castriciano, V. Villari, N. Micali, P. Schoen, S. Speller, L. M. Scolaro, A. E. Rowan, J. A. A. W. Elemans, R. J. M. Nolte, *Nano Lett.* **2008**, *8*, 253-259.
[12] J. Roosma, T. Mes, P. Leclere, A. R. A. Palmans, E. W. Meijer, *J. Am. Chem. Soc.* **2008**, *130*, 1120-1121.
[13] a) M. L. Bushey, A. Hwang, P. W. Stephens, C. Nuckolls, *J. Am. Chem. Soc.* **2001**, *123*, 8157-8158; b) M. L. Bushey, T.-Q. Nguyen, C. Nuckolls, *J. Am. Chem. Soc.* **2003**, *125*, 8264-8269.
[14] K. Wallenfels, K. Friedrich, F. Witzler, *Tetrahedron* **1967**, *23*, 1353-1358.
[15] J. H. Fendler, E. J. Fendler, W. Ernsberger, *J. Org. Chem.* **1971**, *36*, 2333-2337.
[16] G.-L. Law, T. A. Pham, J. Xu, K. N. Raymond, *Angew. Chem., Int. Ed.* **2012**, *51*, 2371-2374.
[17] The product ratio was established on the crude raw material by ^{1}H-NMR analyses. The products of the reaction were isolated by chromatography and fully characterized.
[18] A. J. Bellamy, P. N. Hudson, *Tetrahedron* **1996**, *52*, 5639-5642.
[19] G. R. Sprengling, J. H. Freeman, *J. Am. Chem. Soc.* **1950**, *72*, 1982-1985.
[20] A. P. S. Samuel, J. Xu, K. N. Raymond, *Inorg. Chem.* **2009**, *48*, 687-698.
[21] A. K. Chakraborti, L. Sharma, M. K. Nayak, *J. Org. Chem.* **2002**, *67*, 6406-6414.
[22] D. Kanamori, A. Furukawa, T.-A. Okamura, H. Yamamoto, N. Ueyama, *Org. Biomol. Chem.* **2005**, *3*, 1453-1459.
[23] J. C. Sheehan, P. A. Cruickshank, G. L. Boshart, *J. Org. Chem.* **1961**, *26*, 2525-2528.
[24] K. Sonogashira, *J. Organomet. Chem.* **2002**, *653*, 46-49.

Association Constant Determination by Solution NMR Techniques

Table of Contents

The analysis of the chemical equilibrium is important in the study of a large variety of chemical systems such as host-guest interactions,[1] supramolecular entities (supramolecular polymers, aggregates)[2] and often to study reaction intermediates.[3] The chemical equilibrium describing the aggregation between two (or more) molecules of A_i forming the aggregated species A_{agg} is represented in Equation 1. Such equilibria can be described by defining its equilibrium (or association) constant (Equation 2):

$$A_i + A_i \underset{k_{-i}}{\overset{k_i}{\rightleftarrows}} A_{agg} \quad \textbf{(Equation 1)} \qquad K_a = \frac{[A_{agg}]}{[A_i]\,[A_i]} = \frac{1}{K_d} = \frac{k_i}{k_{-i}} \quad \textbf{(Equation 2)}$$

where A_i is the monomeric species (or more generally the non-aggregated species) and A_{agg} is the product species (aggregated form), k_i and k_{-i} are the kinetic constants, K_d is the dissociation constant for the overall equilibrium. Hereafter the equilibrium constant is called association constant K_a and it is defined as $K_a = 1/K_d$.[4] The equations are valid at constant temperature (isothermal). The challenge consists in determining the concentration of the chemical species A_i and A_{agg} involved.

Nuclear Magnetic Resonance

Nuclear Magnetic Resonance (NMR) approach for measuring K_a is based on the observation of the chemical shift variation (δ) of the chemical species present in solution as a function of the concentration of the molecule. For fast exchange processes the plot of [A] versus the chemical shift δ allows the determination of K_a.[5] These variations of the chemical shift can be induced by varying the concentration of the solutes, the temperature or by addition of external reagents (e.g. ligand). This spectroscopic technique has important advantages for the determination of binding constants.[5a] Compared to other analytical techniques (especially fluorescence and UV/Vis spectroscopy) the presence of eventual impurities minimally affects the result of the titration compared to other techniques. Moreover, the quantitative information can be obtained via integration of the signal with no need to construct a calibration curve. On the other hand, the major limitation of the NMR based techniques is the low detection limit. For example with a 400 MHz instrument the detection limit is in the range of 10^{-4} M.[6] NMR techniques can measure association constants on the order of $K_a \leq 10^5$ M^{-1}. Stronger binding constants are difficult to measure.

^{1}H is the most studied nucleus in NMR experiments due to its high abundance and sensitivity (high gyromagnetic ratio 42.576 $MHzT^{-1}$). Observations of ^{13}C nuclei are subject to practical limitations like long measuring times, low abundance of the nucleus (^{13}C is only 1% of the isotope distribution) and much smaller sensitivity compared to ^{1}H nuclei (low gyromagnetic ratio 10.705 $MHzT^{-1}$). On the other hand, experiments carried out on ^{19}F nuclei are used more frequently due to the fact that fluorine is a very sensitive nucleus (gyromagnetic ratio similar to hydrogen 40.052 $MHzT^{-1}$). The drawback is the need to introduce a fluorine atom on the molecular skeleton. The presence of fluorine can generate significant variations on the physical behavior of the molecule (solubility, lipophilicity, H-bond formations, etc.). We will concentrate our discussion on ^{1}H-NMR experiments.

^{1}H-NMR

Concentration-induced shift experiments

Here we present a typical example of concentration-induced shift experiments used to study the aggregation process driven by π-stacking and intermolecular H-bonds (Figure 1).[7] The group of Meijer synthesized a series of Ureido-Pyrimidinone derivatives and they studied the association process of the dimer formation in such molecules (Figure 1).

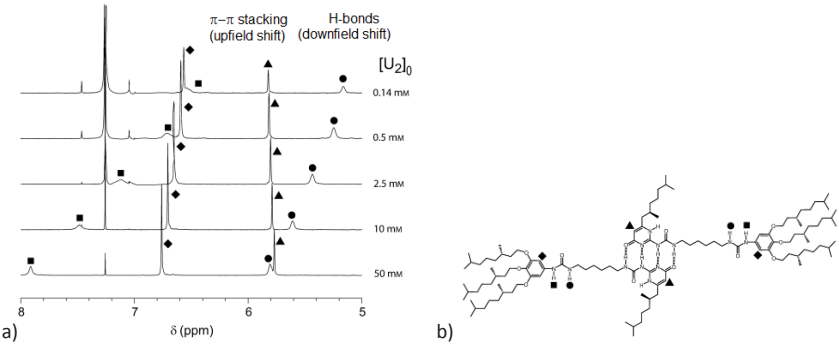

Figure 1. a) Concentration-induced ^{1}H-NMR shift experiments on ureido-pyrimidinone derivative reported by Meijer. The dimer formation (aggregation) induces downfield shifts for N-H protons (intermolecular H-bond) and upfield shift for C-H aromatic protons (π-π stacking). b) Chemical structure of the ureido-pyrimidinone dimer. The different types of protons (N-H and C-H are indicated with the symbols ●, ♦, ▲ and ▪) Both figures have been extracted and adapted from the original work of Meijer and co-workers.[7]

The dimer formation (aggregation) was studied by employing concentration-induced ^{1}H NMR. Increasing the concentration of the ureido-pyrimidinone derivative causes an enhancement of the intermolecular H-bonds between the N-H (donor) and the C=O (acceptor) groups. When a hydrogen atom is involved in H-bond interaction, the electron density on the nucleus of this atom is reduced (deshielded) consequentially its resonance frequency is downfield shifted.[8] Figure 1a shows how increasing the concentration, the N-H protons of the urea groups shift downfield ($\Delta\delta$ ~1.5 ppm for ▪ and ~1 ppm for ● from 0.14 to 50 mM in $CDCl_3$). With the aggregation process a small upfield shift for the aromatic protons of the pyrimidinone could be observed ($\Delta\delta$ ~0.1 ppm for ▲ from 0.14 to 50 mM in $CDCl_3$), whereas the aromatic protons on the benzene ring show downfield shift ($\Delta\delta$ ~0.1 ppm for ♦ from 0.14 to 50 mM in $CDCl_3$). The proposed interpretation invokes that increasing the concentration produces π-stacking resulting in a ring current effect on the pyrimidinone proton signals.[9]

Exchange rate

An important factor that can affect the concentration or temperature-induced NMR experiments is the chemical exchange rate of the reversible process under analysis. Any (reversible) chemical process is described by a thermodynamic constant K_{eq} (or K_a) and the corresponding two kinetic constants k_i and k_{-i} respectively (Equation 1 and 2). If the rate constant of the reversible association process

k ($= k_i + k_{-i}$) is much larger than the difference of the chemical shift ($\Delta\delta = \delta_{mon} - \delta_{agg}$) expressed in Herz ($k >> \Delta\delta$), we observe a situation of fast exchange (Figure 2). In this case the observed resonance signal (δ_{obs}) is the weighted average of the chemical shift of the monomer (δ_{mon}) and the aggregated (δ_{agg}) species:

$$\delta_{obs} = \delta_{mon}\chi_{mon} + \delta_{agg}\chi_{agg} \quad \textbf{(Equation 3)}$$

where $\chi_{mon,\ agg}$ are the molar fraction of the monomeric and aggregated species respectively; $\delta_{mon,\ agg}$ are the chemical shift of the monomeric and aggregated species respectively.

$$1 = \chi_{mon} + \chi_{agg} \quad \text{and} \quad \chi_{mon} = 1 - \chi_{agg} \quad \textbf{(Equation 4)}$$

Substituting Equation 4 is into Equation 3:

$$\delta_{obs} = \delta_{mon}\left(1 - \chi_{agg}\right) + \delta_{agg}\chi_{agg}$$

$$\delta_{obs} - \delta_{mon} = \chi_{agg}\left(\delta_{agg} - \delta_{mon}\right)$$

$$\Delta\delta = \chi_{agg}\left(\delta_{agg} - \delta_{mon}\right) \quad \textbf{(Equation 5)}$$

The Equation 5 links the molar fraction χ_{agg} of the aggregates present in solution with the chemical shift difference. This equation allows determining the molar fraction of monomer and aggregates present in solution. δ_{mon} and δ_{agg} can be determined by fitting of the experimental curve obtained by plotting δ_{obs} *vs*. concentration (*vide infra*).

On the other hand, when $k << \Delta\delta$ we observe a situation of slow exchange and Equation 5 is no longer valid. In this case the resonance lines of the two different components in equilibrium (monomer and aggregate) will separately appear. Under such circumstances it is possible to measure directly the concentration of A_{mon} and A_{agg} from the integral of the separated signals.[10]

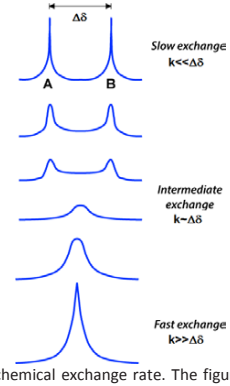

Figure 2. Schematic representation of the chemical exchange rate. The figure was extracted and modified from the web site: http://mri-q.com/chemical-exchange.html

If $k \sim \Delta\delta$ we observe the situation of intermediate exchange. In this case we typically observe the phenomenon of strong line broadening of the signals.

Data fitting

In order to solve Equation 2 and calculate K_a we need to know δ_{agg} and δ_{mon} separately. However, under conditions of fast exchange, it is not possible to measure directly both δ_{agg} and δ_{mon} from the spectra. The plot concentration of the chemical species *vs*. the observed chemical shift (δ_{obs}) gives

the binding isothermal curve for 1:1 interaction (1 monomer for 1 dimer) that describes the binding process (Figure 3b).

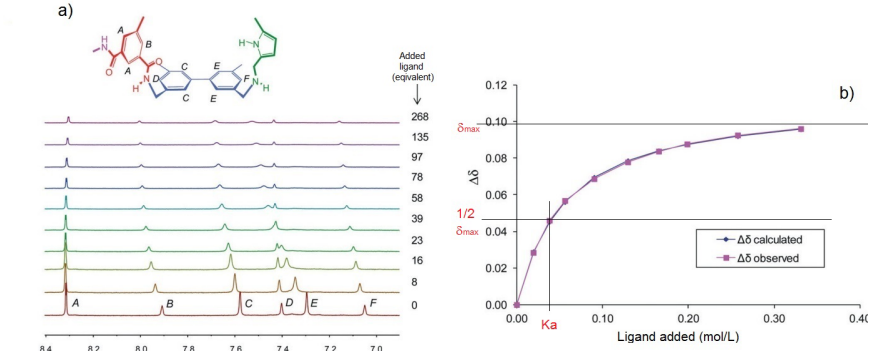

Figure 3. a) Stacked spectra of concentration-induced shift of proton NMR signals as function of the addition of a ligand. b) Overlap between experimental points and the fitting curve. The figures were extracted and modified according to the original data reported.[11]

The association (equilibrium) constant K_a is equivalent to the inverse of the concentration that produces one-half of the chemical shift variation. The way to determine this value is to fit the experimental points by the curve and to extrapolate the values of δ_{agg} and δ_{mon} from the curve fitting. In Figure 3a the stacked spectra obtained by adding a *D*-glucose to the receptor molecule are reported. The addition of the ligand produces a shift of the proton signal under a fast exchange regime. Plotting the chemical shift *vs*. the concentration is compatible with an isothermal curve describing the binding process (Figure 3b). The fitting employing non-linear least-square fitting equation simulates the experimental curve enabling the calculation of the association constant.
In our NMR study [12] we used the logistic fitting packet,[5a] of the computer program OriginLab®, for the fitting of the experimental data (Equation 7).

$$y = A_2 + \frac{(A_1 - A_2)}{\left[1+\left(\frac{x}{x_0}\right)^p\right]} \quad \text{where} \quad y(x_0) = \frac{A_1+A_2}{2} \quad \text{and} \quad x_0 = K_a \qquad \textbf{(Equation 7)}$$

where A_1 is y at x= 0, A_2 is x= ∞ and *p* is the slope or the Hill factor of the fitting curve. Replacing the value of A_1 and A_2 with δ_{mon} and δ_{agg} respectively it is possible to adapt the general logistic fitting equation to the specific case of concentration-induced NMR experiments:

$$\delta_{obs} = \delta_{agg} + \frac{(\delta_{mon} - \delta_{agg})}{\left[1+\left(\frac{c}{K_d}\right)^p\right]} \qquad \textbf{(Equation 8)}$$

The logistic fitting model has the advantage to better describe hyperbolic curves that are typical of the binding processes. Another important advantage of using the logistic fitting equation is that one obtains a value of the slope deduced from the curve. This value is interpreted as the cooperativity of the binding process. For example Hill developed this approach to determine the cooperative nature of the oxygen binding in the hemoglobin. He determined the slope of the fitted curve obtained by plotting the partial pressure of oxygen (pO_2) vs. percentage of saturation (Equation 9).[13][14]

$$\theta = \frac{[L]^p}{K_d+[L]^p} = \frac{[L]^p}{[K_a]^p+[L]^p} = \frac{1}{\left(\frac{K_a}{[L]}\right)^p+1} \qquad \textbf{(Equation 9)}$$

where ϑ is the fraction of the ligand-binding sites of the receptor occupied, [L] the concentration of the free ligand, K_a and K_d the association and the dissociation constant ($K_a=1/K_d$) and *p* is the Hill factor. This approach can be extended to study any other binding process and it is very useful to determine the cooperativity. Using this fitting approach it is possible to characterize the cooperativity *p* of an aggregation process. When *p* is >1 the aggregation shows a positive cooperativity characterized by a sigmoidal curve (hemoglobin case) and vice versa for *p*< 1 a negative cooperativity. When *p*= 1 no-cooperativity is observed for this aggregation process and in this case the curve has a hyperbolic shape. In conclusion the logistic fitting equation is broadly applicable for the fitting of different type of curves.

If the aggregation mechanism is known, equations that selectively simulate this behavior can be applied. The group of Meijer developed an *ad hoc* equation to simulate the hyperbolic curve for the isodesmic supramolecular aggregation mechanism: [7]

$$\delta_{obs} = \delta_{mon} + \left(\delta_{agg} - \delta_{mon}\right)\left(1 + \frac{1-\sqrt{4K_a+1}}{2K_a c}\right) \qquad \textbf{(Equation 10)}$$

This equation is a special case of the binding process where the slope factor is *p* =1. The isodesmic and the logistic fitting model are complementary because both they allow to discriminate the mechanism of the aggregation process.

DOSY experiments

The introduction of two-dimensional techniques drastically changed the world of NMR.[15] Using 2D methods the structure of complex natural products were solved.[16] More recently 2D methods were also applied to determine properties of molecules or aggregates. Of special interest in our studies are experiments characterizing molecular diffusion: This type of experiment is called the Diffusion-Ordered NMR spectroscopy 2D-DOSY. [17]

DOSY experiments allow to observe and to characterize the Brownian motion of molecules or aggregates in solution. The parameter observed in a DOSY experiment is the so called *self-diffusion coefficient* D. The phenomenon is described mathematically by the *Stokes-Einstein* Equation (Equation 11):[18]

$$D = \frac{k_B T}{6\pi\eta r_s} \qquad \textbf{(Equation 11)}$$

where D is the self-diffusion coefficient, measured in (m^2s^{-1});[19] k_B is the *Boltzmann* constant; *T* is the temperature (K); η is the solution viscosity and r_s is the radii of the molecule. The model used to describe the diffusion process assumes spherical molecules. The self-diffusion coefficient is therefore strictly dependent on the radii (= dimension) of the molecules (*inversely proportional*). The size of the molecules is characterized by one single parameter, the radius of the sphere representing a simplified geometrical model for the specific molecule studied. The other parameters influencing self-diffusion are the temperature and the viscosity of the solvent.

DOSY experiments have been extensively used to study metal-ligand complexation,[20] aggregations [21] and H-bonds.[22] Examples of K_a determination of macrocyclic complexes employing DOSY experiments have been reported.[17, 23] DOSY experiments allow to determine if a molecule A, with its self-diffusion coefficient D_{mon}, in a solvent at specific temperature, is forming aggregated species (according to Equation 1 and 2), by observing indirectly the molecular weight created by the aggregation process. According to the Stokes-Einstein equation (Equation 11), the diffusion

coefficient is proportional to the molecular weight and consequentially aggregated species diffuse slower in solution and the relative diffusion coefficient D_{agg} is smaller than D_{mon}. This is valid when the rate of the aggregation process is comparable (or even faster) than the NMR timescale. If the association process is in a fast exchange rate, the observed diffusion D_{obs} is the result of the weighted averaged between the diffusion of the aggregated species D_{agg} and the monomeric species D_{mon}:

$$D_{obs} = D_{mon}\chi_{mon} + D_{agg}\chi_{agg} \qquad \textbf{(Equation 12)}$$

Here we present a case study where the DOSY technique was employed for one of the first time to observe the formation of aggregated species. We analyze the case of Metolachlor, [24] a herbicide that belongs to the class of chlorocetamides.[25]

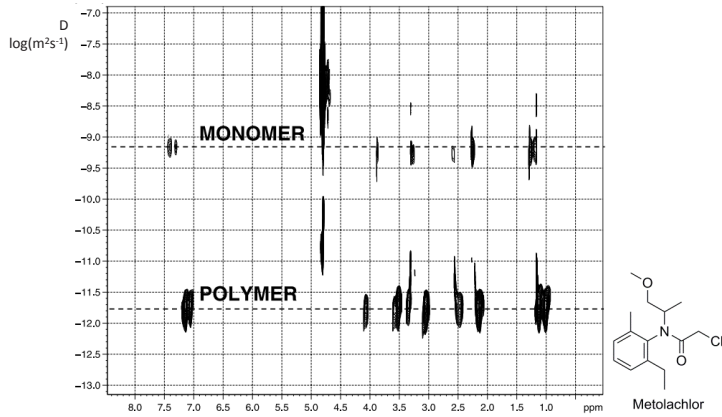

Figure 4. 2D DOSY of Metalchlor at different concentrations. The figure was extracted from the original work of Segre and co-workers.[24]

The molecule of Metolachlor is poorly soluble in water (about 1.8 mM at 25 °C). When the ^{1}H NMR experiment was carried out in D_2O at a concentration lower than the solubility limit (1.1 mM), the spectra shows well-resolved signals and the presence of two diastereoisomers (the molecule of metolachlor has a one stereogenic center and one stereogenic axis generating a couple of diastereoisomers). Increasing the concentration above the solubility produces initially a partial precipitation whereas the measured ^{1}H spectrum shows sharp lines and the appearance of new signals. As initial hypothesis the formation of dimeric structures driven by π-interactions was formulated. However, the slow exchange rate of the association and dissociation processes of this molecule prohibits the possibility to get the information from temperature-depended ^{1}H NMR experiments. The problem could be solved by running diffusion-ordered spectroscopy experiments DOSY. Indeed the DOSY spectrum at 16.9 mM shows signals with diffusion coefficients of the monomeric Metolachlor molecules, and other signals with lower diffusion coefficients compatible with the formation of aggregated structures driven by π-π interactions (Figure 4). This example elegantly shows how diffusion-ordered spectroscopy experiments can help in the analysis of aggregation processes.

References

[1] H. E. Katz, *J. Org. Chem.* **1989**, *54*, 2179-2183.

[2] T. F. A. De Greef, M. M. J. Smulders, M. Wolffs, A. P. H. J. Schenning, R. P. Sijbesma, E. W. Meijer, *Chem. Rev. (Washington, DC, U. S.)* **2009**, *109*, 5687-5754.

[3] aH. Gampp, *Inorg. Chem.* **1984**, *23*, 1553-1557; bT. M. Harris, M. P. Stone, C. M. Harris, *Chem. Res. Toxicol.* **1988**, *1*, 79-96; cL. S. Santos, L. Knaack, J. O. Metzger, *Int. J. Mass Spectrom.* **2005**, *246*, 84-104.

[4] K. A. Connors, *Binding Constants: The Measurement of Molecular Complex Stability*, **1987**.

[5] aL. Fielding, *Tetrahedron* **2000**, *56*, 6151-6170; bP. Thordarson, *Chem. Soc. Rev.* **2011**, *40*, 1305-1323.

[6] In a higher magnetic field (e. g. 600 MHz instrument) a lower concentration (10-5 molar) could be analyzed and obtain a Ka≤106 M-1.

[7] M. M. L. Nieuwenhuizen, T. F. A. de Greef, R. L. J. van der Bruggen, J. M. J. Paulusse, W. P. J. Appel, M. M. J. Smulders, R. P. Sijbesma, E. W. Meijer, *Chem. - Eur. J.* **2010**, *16*, 1601-1612, S1601/1601-S1601/1615.

[8] I. Alkorta, J. Elguero, G. S. Denisov, *Magn. Reson. Chem.* **2008**, *46*, 599-624.

[9] R. B. Martin, *Chem. Rev. (Washington, D. C.)* **1996**, *96*, 3043-3064.

[10] J. Feeney, J. G. Batchelor, J. P. Albrand, G. C. K. Roberts, *J. Magn. Reson.* **1979**, *33*, 519-529.

[11] G. Joshi, A. P. Davis, *Org. Biomol. Chem.* **2012**, *10*, 5760-5763.

[12] The NMR study will be described in the chapters 5 and 6.

[13] J. Physiol. 1910, 40, iv–vii.

[14] S. Goutelle, M. Maurin, F. Rougier, X. Barbaut, L. Bourguignon, M. Ducher, P. Maire, *Fundam. Clin. Pharmacol.* **2008**, *22*, 633-648.

[15] aW. P. Aue, E. Bartholdi, R. R. Ernst, *J. Chem. Phys.* **1976**, *64*, 2229-2246; bG. B. Richard R. Ernst, Alexander Wokaun, *Principles of Nuclear Magnetic Resonance in One and Two Dimensions*, Oxford, **1987**.

[16] R. C. Breton, W. F. Reynolds, *Nat. Prod. Rep.* **2013**, *30*, 501-524.

[17] C. S. Johnson, Jr., *Prog. Nucl. Magn. Reson. Spectrosc.* **1999**, *34*, 203-256.

[18] T. Claridge, *High-resolution NMR techniques in Organic Chemisty*, Elsevier Science Ltd ed., **2004**.

[19] On the routine DOSY the unit is log(m2s-1).

[20] aA. Pastor, E. Martinez-Viviente, *Coord. Chem. Rev.* **2008**, *252*, 2314-2345; bS. Sato, J. Iida, K. Suzuki, M. Kawano, T. Ozeki, M. Fujita, *Science (Washington, DC, U. S.)* **2006**, *313*, 1273-1276.

[21] K. F. Morris, C. S. Johnson, Jr., *J. Am. Chem. Soc.* **1993**, *115*, 4291-4299.

[22] G. S. Kapur, E. J. Cabrita, S. Berger, *Tetrahedron Lett.* **2000**, *41*, 7181-7185.

[23] aY. Cohen, L. Avram, L. Frish, *Angew. Chem., Int. Ed.* **2005**, *44*, 520-554; bO. Mayzel, Y. Cohen, *J. Chem. Soc., Chem. Commun.* **1994**, 1901-1902.

[24] S. Viel, L. Mannina, A. Segre, *Tetrahedron Lett.* **2002**, *43*, 2515-2519.

[25] H. Moser, G. Rihs, H. Sauter, *Z. Naturforsch., B: Anorg. Chem., Org. Chem.* **1982**, *37B*, 451-462.

Synthesis and NMR spectroscopic study of the self-aggregation of the 2-substituted benzene-1,3,5-tricarboxamides BTAs*

Authors: Christian Invernizzi,[a] Claudio Dalvit,[b] Helen Stoeckli-Evans[c] and Reinhard Neier*[a]

Affiliations:

[a] Institut de chimie, Université de Neuchâtel, Avenue Bellevaux 51, CH-2000 Neuchâtel

[b] NPAC, Université de Neuchâtel, Avenue Bellevaux 51, CH-2000 Neuchâtel

[c] Institut de physique, Université de Neuchâtel, Avenue Bellevaux 51, CH-2000 Neuchâtel

Corresponding Author: Reinhard.Neier@unine.ch

Keywords: self-assembly • H-bonds • π–π stacking • columnar liquid crystals • supramolecular chemistry

Abstract: The self-assembly of *N,N',N''*-trialkylbenzene-1,3,5-tricarboxyamides (BTAs) **42** or of "crowded" BTAs **12** and **13** lead to supramolecular columnar-stacked structures with attractive material properties. The introduction of three alkoxy groups is reported to reinforce the self-assembly process. The influence of a single substituent introduced on the aromatic core of BTA significantly affects the self-assembly process. The aggregation process of 2-substituted BTAs in the bulk and in solution, as studied by DSC, POM, X-ray diffraction and ^{1}H NMR experiments, is impaired by H-bond accepting substituents and strengthened by non-H-bonding substituents.

* Copy of the manuscript submitted to European Journal of Organic Chemistry on 21st April 2015

Introduction

Understanding the sequence of processes that creates order from simple molecular building-blocks is the key knowledge for deepening our insight into life and material sciences.[1] Data identifying and quantifying interactions measured in solution and correlating them with material properties help to overcome the gap between models based on the cooperative interplay between individual molecules and material properties observed in the bulk. Typically, the relatively small number of widely known interactions responsible for self-assembly is combined with the wealth of empirical data for the creation of "designed" structures with predictable shapes and properties. "*Our ability to predict the structural features and the functional outcome of the assembled materials is still limited and most of the learning is done in retrospect*".[2] The *N,N',N''*-trialkylbenzene-1,3,5-tricarboxyamides (BTAs) **42** lead to supramolecular columnar-stacked structures,[3] which show attractive material properties.[4] The observation of discotic mesophases based on the triamide structural motives has been

attributed to the occurrence of π-stacking[5] and to the simultaneous formation of the maximum number of hydrogen bonds surrounding the columns in a triple helix.[3, 6] The structural hypotheses used for rationalizing the material properties of BTAs are based on X-ray structures of simpler crystalline models and on modelling studies (Figure 4a and b, see SI).[7]

The unexpected results obtained in the context of our approach creating novel addressable organic electronic elements[9] induced us to undertake studies correlating material properties in the bulk with NMR experiments capable to distinguish the type and the force of the interactions of the building blocks in solutions. The starting point of our studies was a simple design aiming at exploring linear dimers with minimal disturbance of the benzenetriamide basic structure. The physical properties of interest in such mesomorphic materials, like 1D charge transport, strongly depend on the molecular alignment in the liquid crystalline phases.[10] Enhanced control over self-organization of discotic compounds is expected by covalently linking two discotic units via a rigid linker.[9b, 11] This approach aims at the creation of an interface between materials using nano-sized structures and microtechnology using micrometer sized connectors. The design and the synthesis of the "anchoring site" are the major challenge in this work. Predicting reliably the efficiency of the self-assembly process and as a consequence the material properties is still the biggest challenge. The first synthesis of BTAs was achieved by Curtius in 1915.[12] In his pioneering work published 1988 Matsunaga and co-workers reported the first controlled fabrication of columnar liquid crystals based on BTA as fundamental unit (Figure 1a).[3] The discovery of the liquid crystalline behaviour for **42** stimulated intense studies using BTA derivatives as building blocks. Detailed studies were carried out by the group of Meijer, elucidating the cooperative nature of supramolecular assembly using UV and CD spectroscopy to monitor the temperature-dependent titration curves of the assembly process of BTA derivatives.[13] The nucleation constant K_n and the elongation constant K_e of the cooperative aggregation process of *N,N′,N″*-trioctylbenzene-1,3,5-tricarboxyamide derivative were determined by these authors.[13b] An impressive number of modifications of BTA's have been reported mostly concentrating on variations of the lateral chains: introducing stereogenic centers in the chains,[14] changing the polarity using extended hydrophilic chains[6] and presenting gallic acid derived elements imposing the formation of additional π-stacking interactions.[15] The group of Nuckolls reported in 2001 the first modification of the central aromatic core. The 2,4,6-trialkoxy substituted BTA **12** named "crowded arenes" were described as a new class of substances forming mesomorphic materials (Figure 1b).[8a, 16] The introduction of dodecyloxy chains in the 2, 4 and 6 positions lead to considerably stronger intermolecular H-bonds. The strong shift of the amide IR absorption, when changing from the liquid crystalline phase to the isotropic phase, indicates the occurrence of the intermolecular H-bonds in the mesophase. In accordance with this observation the temperature range for the presence of the liquid crystalline phase was much larger. Nuckolls postulated that the three additional substituents were conformationally twisted out of planarity due to the steric hindrance. Molecular modelling calculations predicted larger values of the dihedral angle of the amide groups for the isolated molecule in the gas phase. The same group observed the formation of a columnar superstructure of crowded arenes, where the dodecyloxy chains have been replaced by phenyl acetylenes substituents like in compound **13** (Figure 1b).[8b, 17] For our project we proposed to introduce a single alkoxy group on the aromatic scaffold making a "minimal" structural change from the structures known in the literature (Figure 1c). The alkoxy group would be used as the linker creating covalent linear dimers hopefully maintaining the interesting material properties. To the best of our knowledge no studies of 2-monosubstituted-BTAs have been reported in the literature.

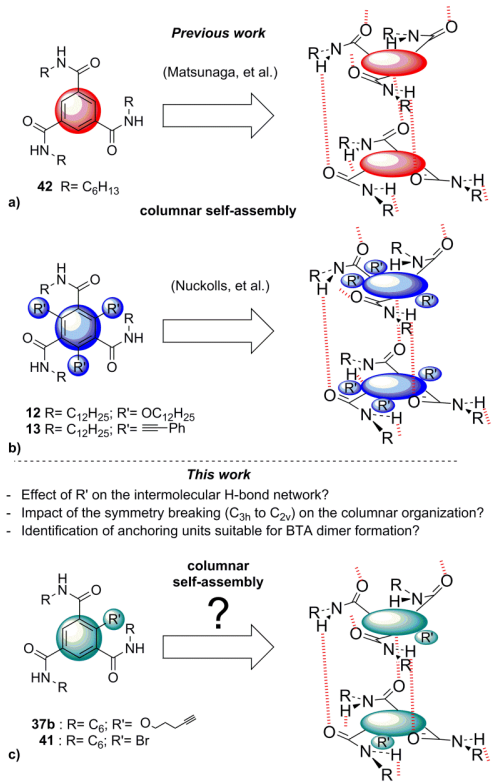

Figure 1. a) Supramolecular architectures of columnar-stacked trialkylbenzene-1,3,5-tricarboxyamide units **42** reported by Matsunaga.[3] b) Supramolecular motive of "crowded arenes" 2,4,6-trisubstituted 1,3,5-tricarboxybenzeneamides **12** and **13** proposed by Nuckolls.[8] The introduction of three additional substituents on the BTA skeleton strengthened the intermolecular interactions and lead to a wider temperature range for the occurrence of the liquid crystalline phase. c) Tentatively proposed supramolecular structure of columnar-stacked BTA derivatives substituted in the 2 position. To apply the new BTA derived design we had to explore the supramolecular assembly, the molecular properties of the novel structures and the influence of the introduction of a single, disturbing substituent into the skeleton. In all the figures 1a), b) and c), red dashed lines indicate intermolecular H-bonds.

Lacking literature precedence we had to characterize the mechanism of the self-aggregation and the structures of the aggregates of the modified BTAs before embarking on more challenging studies. With this goal in mind we decided to study the assembly of the two BTA derivatives **37b** and **41**. In this work, we present the synthesis of the monofunctionalized BTA **37b** and **41** (Scheme 1 and 2) and the analyses of their supramolecular assembly in the liquid crystalline state, carried out with differential scanning calorimetry DSC and polarized light-microscopy POM, and in the solid state carried out with X-ray diffraction of single crystals (see SI). To elucidate the aggregation mechanism of **37b** and **41**, thermodynamic data in conjunction with structural information were extracted by observing the dynamic assembly process with ^{1}H NMR in solution.[18] The two phenomena, H-bonding and π-stacking, invoked in the description of the aggregation of BTA should be easy to detect by ^{1}H NMR. The formation of intermolecular H-bonds induces a downfield shift for the amide protons,

whereas π-stacking causes an upfield shift of the aromatic protons.[19] NMR Diffusion-ordered spectroscopy (DOSY)[20] measures the changes of the diffusion coefficient and has been successfully used to evaluate the formation and the size of supramolecular aggregates,[21] dendrimers[22] and proteins.[23] The quantitative thermodynamic data, which can be derived from concentration-induced shift variation on ^{1}H NMR experiments, gives a readout on the sum of all forces in place for the aggregation process characterizing the cooperativity of the association process. The 2-substituted BTA scaffolds in **37b** and **41** are compared to the C_3-symmetric BTA **42**. A comparison of the relative capacities of these molecules to form intramolecular H-bonds measures the reducing effect induced by the alkoxynyl group in **37b** and the intensifying effect induced by the sterically demanding bromine atom in **41**.

Results and Discussion

The choice of introducing an alkoxynyl group was driven by the attractiveness of forming dimeric structures *via* "click chemistry". The terminal triple bonds can be selectively and efficiently transformed with the help of the Cu-catalysed azido-alkyne "click-chemistry" (CuAAC),[24] a strategy which has been already used in our group to form mesogenic dimeric structures.[9b] The alkoxynyl substituent can easily be introduced by phenol alkylation and varying the alkyne derivatives allows modulation of the length of the linker.

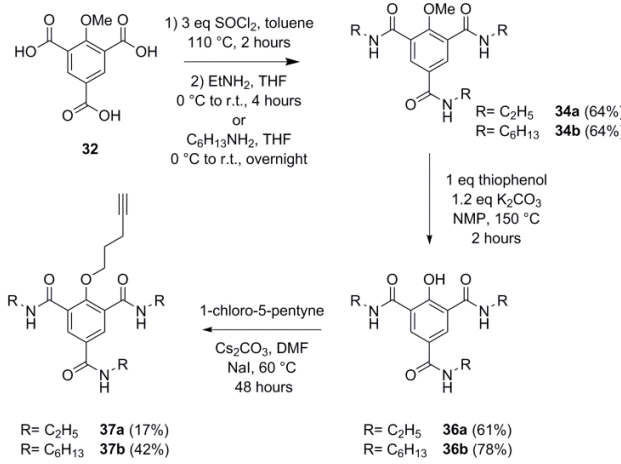

Scheme 1. Synthesis of 2-alkoxynyl-BTA derivatives **37a** and **37b**.

The study of the material and self-assembly properties of 2-bromo substituted BTA 3 was envisaged for comparison reasons with a sterically demanding but not-H-bonding substituent. The synthesis of the 2-alkoxynyl BTA scaffold started from the previously reported 2-methoxy trimesic acid **32** (Scheme 1).

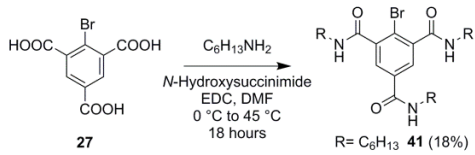

Scheme 2. Synthesis of 2-bromo-BTA derivative **41**.

The preparation of **32** was achieved according to the procedure reported by Raymond.[25] A permanganate-mediated oxidation in basic conditions of 2,6-bis-(hydroxymethyl)-*p*-cresol furnished the 2-methoxy-triacid **32** in yields comparable with the literature. The triacid **32** was converted into the corresponding triacyl chloride employing 3 equivalents of thionyl chloride and then reacted with an excess of the primary amine. The corresponding amides **34a** and **34b** were isolated in good yield over two steps. The 2-methoxy-benzamides **34a** and **34b** were deprotected by a nucleophilic methyl-ether cleavage according to the conditions reported by Chakraborti, [26] employing the potassium salt of thiophenol in *N*-methyl-2-pyrrolidone at 150 °C. The final alkylation step of the phenol derivatives **36a** and **36b** was found to be a difficult transformation. Modifying the reaction conditions moderate yields of products **37b** and **37a** (42% and 17%, respectively) were obtained, when caesium as large carbocation in DMF was used. The electronic stabilization of the phenoxide by conjugation coupled to the formation of intramolecular H-bonds affected negatively the nucleophilicity and thereby the reactivity of **36a** and **36b**. Crystallographic evidence for these strong intramolecular H-bond interactions has been reported by Ueyama, studying the deprotonated form of salicylamide derivatives.[27]

The 2-bromo BTA **41** was obtained in two-steps starting from the 2-bromo-trimesic acid **27** as described by Wallenfels (Scheme 2).[28] The triacid **27** was converted into **41** using EDC and *N*-hydroxysuccinimide in DMF in acceptable 18% yield.

Analyses in the bulk

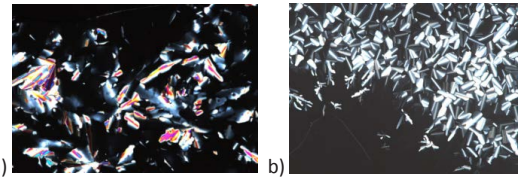

Figure 2. POM micrograph at 100x magnification. a) **37b** at 137 °C b) **41** at 202 °C.

DSC analysis:
BTA **37b** and **41** were analysed by DSC revealing polymorphism and a liquid crystalline mesophase over a broad range of temperatures for both derivatives (Table 1, for DSC spectra: see SI).
The heating cycle of **37b** presented an exothermic peak (-2.54 kJ mol^{-1}) at 64.1 °C associated to the transition from solid to mesomorphic phase. A second exothermic phase transition (-2.14 kJ mol^{-1}) was observed at 109.4 °C. The final isotropisation (141.1 °C) was associated with a strong exothermic transition with an enthalpy of -5.09 kJ mol^{-1}. Three phase transitions were measured as well in the

cooling cycle. The isotropic liquid formed the mesomorphic phase at 147.5 °C showing a strong endothermic transition (4.66 kJ mol^{-1}). A small endothermic transition (1.75 kJ mol^{-1}) at 120.3 °C indicated a change in the mesomorph organization. The final solidification of **37b** at 57.0 °C was associated with a medium intense endothermicity (2.49 kJ mol^{-1}). The heating cycle of **41** presented a very small exothermic peak (-0.48 kJ mol^{-1}) indicating the phase transition between solid and mesomorph at 70.8 °C. Two other phase modifications were observed in the heating cycle. A strong endothermic peak (18.86 kJ mol^{-1}) at 146.7 °C followed by a strong exothermic peak (-20.8 kJ mol^{-1}) at 209.1 °C. These two transitions might indicate the formation of a partially organized structure during the heating cycle (*cold crystallization*) and its relative melting. The final isotropisation of **41** was reached at 239.5 °C. The isotropic liquid underwent a phase transition (9.00 kJ mol^{-1}) toward a mesomorphic phase at 245.2 °C. The final solidification was observed at 69.5 °C associated with a very small exndothermicity (0.4 kJ mol^{-1}).

Table 1. Transition temperature (°C ± 0.2 °C) and, in parenthesis, the relative enthalpy (kJ mol^{-1}) of different BTA derivatives.

BTA	2nd heating cycle			1st cooling cycle				ΔT (°C)[a]
42[b]	99 (-12)			205 (-22)				106
37b	64.1 (-2.54)	109.4 (-2.14)		141.1 (-5.09)	147.5 (4.66)	120.3 (1.75)	57.0 (2.49)	77
41	70.8 (-0.48)	146.7 (18.86)	209.1(-20.8)	239.5 (-7.78)	245.2 (9.00)		69.5 (0.4)	168.7
12[c]	98 (-57.1)			294 (-35.1)	247 (5.6)		83 (39.1)	196

[a] Temperature range of liquid crystallinity calculated from the 2nd heating cycle. [b] Transition temperatures and enthalpy as reported by Matsunaga.[3] [c] Transition temperatures and enthalpy as reported by Nuckolls.[8a]

The temperature range of liquid crystallinity of **41** is much larger compared to the range observed for **1** (Table 1). The liquid crystallinity of **41** resembles the properties reported by Nuckolls for trialkoxy-substituted crowded derivatives **12** (Table 1).[8a] The presence of an alkoxynyl group on **37b** considerably reduced the temperature range of liquid crystallinity in comparison to **42** and BTA **41**. The enthalpy values for the transitions measured for compound **37b** resemble to those reported for compounds **42** and **12** forming columnar liquid crystals. The presence of bromine increases the solid-like behaviour of **41**, whereas the presence of the pentynyloxy group in **37b** decreases its melting point and consequentially its phase transition energies. The enthalpies for the phase transition of **37b** are smaller than those for the reference compounds **42** and **12**. In accordance with this data, the temperature for the first observed transition is lower and in parallel the range of liquid crystallinity is smaller.

Polarized Optical Microscopy:
POM analyses were carried out on BTA **37b** and **41**. Both BTA **37b** and **41** formed pseudo conic textures when cooled from their isotropic liquid phases (Figure 2). These textures are characteristic for columnar liquid crystals. DSC and POM analysis together indicate that 2-substituted BTAs, such as **37b** and **41**, presented similar mesomorphic behaviours as the unsubstituted BTA **1** and the fully substituted **12**.

Single crystal X-ray:

The group of Chu successfully crystallized the *N,N',N''*-trioctyl BTA **3** derivative reporting its chiral nanosheet arrangement.[29] Unfortunately compound **37b** did not crystallize in our hands. Replacing the hexyl chains by ethyl groups (BTA **37a**, Scheme 1), crystals suitable for X-ray diffraction could be obtained by slow evaporation from $CDCl_3$.

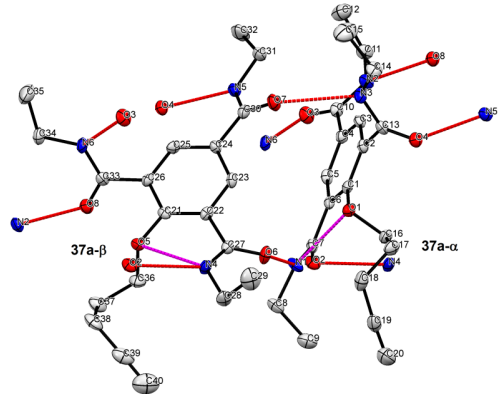

Figure 3. The crystal structure of **37a-α** and **37a-β**. Hydrogens have been omitted for clarity. Red dashed lines indicate intermolecular H-bonds. Blue dashed lines indicate intramolecular H-bonds. Oxygen atoms are highlighted in red whereas nitrogen atoms are highlighted in blue.

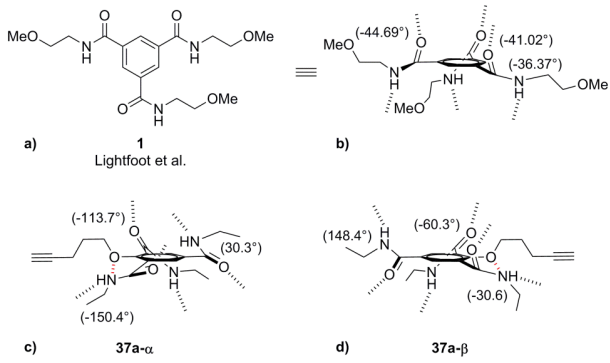

Figure 4. a) Structure of the model compound **1** reported by Lightfoot et *al.*[7a] b) Schematic representation of its X-ray structure. All the carbonyl groups are oriented toward the same face with respect to the aromatic plane. c) and d) Schematic representation of the X-ray structure of **37-α** and **37-β**. The dihedral angles of the amide groups with respect to the main plane of the aromatic core are indicated. The red dashed lines indicate intramolecular H-bonds whereas black dashed lines indicate intermolecular H-bonds.

Table 2. Measured hydrogen bond distances of molecules **37-α** and **37-β**.

Molecule	Donor (N-H)	Acceptor (C=O)	*d* (Å) [a]	Dihedral angle θ ° [b]
alpha	N1	O6	2.10(3)	C1-C6-C7-O2 -150.4(3)°
	N2 [c]	O8	1.94(3)	C5-C4-C10-O3 30.3(4)°
	N3	O7	2.06(3)	C3-C2-C13-O4 -113.7(3)°
beta	N4	O2	2.12(3)	C23-C22-C27-O6 -30.6(4)°
	N5 [c]	O4	2.12(3)	C25-C24-C30-O7 148.4(3)°
	N6	O3	2.07(3)	C21-C26-C33-O8 -60.3(4)°
Intramolecular H-bond				
alpha	NH1	O1	2.30(3)	N1-H1-O1 119°(2) [d]
beta	NH4	O5	2.27(3)	N4-H4-O5 119°(2) [d]

[a] The distance *d* refers to the H--O bond. [b] The sign of the amide dihedral angles indicates the orientation of the carbonyl (C=O) the amide group with respect to the aromatic plane. For a columnar-assembly all of the amide group have to be directed into the same orientation, leading to the same helicity of the H-bond network. [c] This interaction generates to the sheet-arrangement between the two independent molecules **37a-α** and **37a-β**. [d] Measured angle of the intramolecular H-bond.

The ethyl substituted BTA **37a** crystalized in a monoclinic unit cell containing two independent molecules in the asymmetric unit (Figure 3, molecules **α** and **β,** Figure 4c and d, See SI). All three secondary amide groups are involved in two intermolecular H-bonds, as confirmed by the measured C=O--H-N distances (Table 2, Figure 4c and d). All three measured amide torsion angles C_{ortho}-C_{ipso}-C=O, for both the independent **37a-α** and **37a-β** molecules in the crystal, are significantly twisted from coplanarity. The conformation of the amide group in *N*-alkyl benzamides is usually coplanar giving an optimal overlap between the aromatic π-system and the π-orbitals of the amide group (see SI). One of the N-H groups of **37a** in ortho position (N1 for **α** and N4 for **β**, Figure 3 and 4c and d) forms additionally an intramolecular H-bond with the oxygen of the pentynyloxy group (Figure 3 magenta dashed lines, Figure 4c and d red dashed lines, Figure 5 magenta dashed lines, See Table 2). The amides in ortho position, not involved in intramolecular H-bonds (N3 for **α** and N6 for **β**), show an unusually large torsion angle between the amide group and the plane of the aromatic ring (ca. 60°, twice as big as the other torsion angles, see Table 2). The occurrence of larger dihedral angle on "crowded arenes" was already postulated by Nuckolls.[8a] Our crystallographic results are in agreement with his hypothesis and his molecular modelling calculations.

The two *ortho*-amide groups are pointing in the same direction (same sign for the dihedral angle) compared with the plane of the aromatic ring (same helicity of the propeller-like arrangement). The *para*-amide group points into the opposite direction.

This switch of the directionality of the amide groups is in contrast to the observation of the BTA model derivative **1** reported in the literature, which form columnar mesophases (Figure 4a and b, See SI). The asymmetric unit contains two independent molecules, **α** and **β,** arranged in *pseudo-sheets* in

the crystal lattice (Figure 5). Both molecules have the maximum number of six intermolecular H-bonds each (Figure 5 blue and black dashed lines). In addition to these intermolecular H-bonds one intramolecular H-bond is formed between one of the ortho amide groups (N-H) and the oxygen of the-alkoxynyl group (see Table 2, Figure 5 magenta dashed lines). Only two out of the six intermolecular H-bonds contribute to the sheet-packing (NH5--O4 and NH2--O8, see Table 2 and Figure 5 blue dashed lines). These intermolecular interactions generate dimeric aggregates where the molecules are almost coplanar (the intra- planar dihedral angle is *ca.* 4°. See Figure 5 and SI). This arrangement allows π–π interactions and thus potentially enabling columnar organizations. The other four intermolecular interactions (Figure 5 black dashed lines) are directed out of the sheet plane generating an orthogonal packing that deviates from the potential columnar arrangement (no π–π stacking). The formation of the intramolecular H-bond perturbs the regular growing of the sheet aggregates.

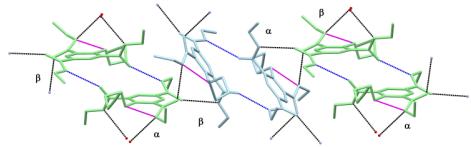

Figure 5. X-ray structure of the pseudo-sheet formed by **37a**. Hydrogens have been omitted for clarity. Magenta dashed lines refer to intramolecular H-bonds. Blue dashed lines refer to intermolecular H-bonds generating the sheets aggregation. The dimer sheet aggregates, indicated by the same colour (light green and light blue) arise from NH5--O4 and NH2--O8 H-bonds exclusively. Black dashed lines refer to intermolecular H-bonds generating quasi-orthogonal aggregates.

Despite the significant differences between the crystal structure of **37a** and the structure of the model BTA **1**, a liquid crystalline phase has been observed for **37b**. The analysis of the thermodynamic parameters of the self-assembly process in solution was needed to elucidate quantitatively the modifications on the formation of intermolecular H-bonds introduced by the additional substituent in an effort to rationalize the differences found between **42**, **237b** and **41** in the liquid crystalline state.

Analyses in diluted solution

Concentration-dependent ^{1}H-NMR dilution experiments:

^{1}H NMR experiments were performed at different concentrations of **37b** and **41** in d_2-dichloromethane as the solvent measuring the association complex constant K_a. BTA **42** was chosen as the reference compound. The association process is well studied and described in the literature.[13b] As solvent we choose d_2-dichloromethane minimising the H-bond donor or acceptor effects occurring with other solvents, like $CDCl_3$, or d_6-DMSO. The ^{1}H-NMR spectra of BTA **42** were measured at 295 K in a concentration range varying from 0.39 mM to 202 mM (Figure 6).

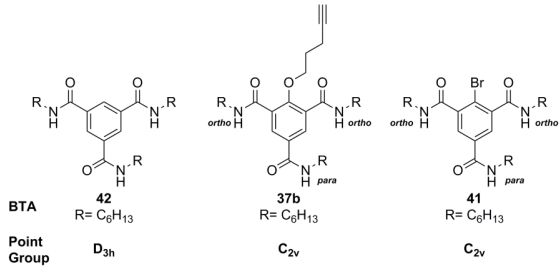

Scheme 3. Comparison of the different BTA structures **42**, **37b** and **41**. The reduced symmetry in 2-substituted BTA **37b** and **41** generates two distinct signals of amide protons (N-H_{ortho} and N-H_{para})

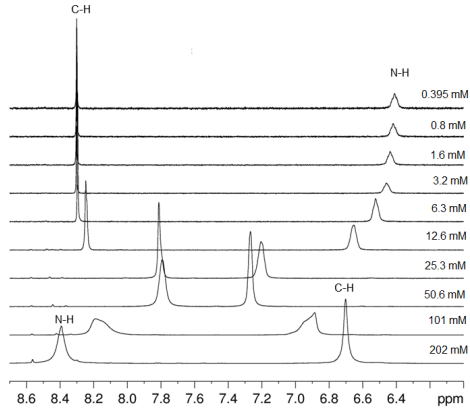

Figure 6. Concentration-induced ^{1}H-NMR experiments of **42** in CD_2Cl_2 at 295 K. The NMR spectra were measured by decreasing the concentration from 202.3 mM to 0.395 mM. In the figure only the aromatic region between 8.7-6.5 ppm is reported.

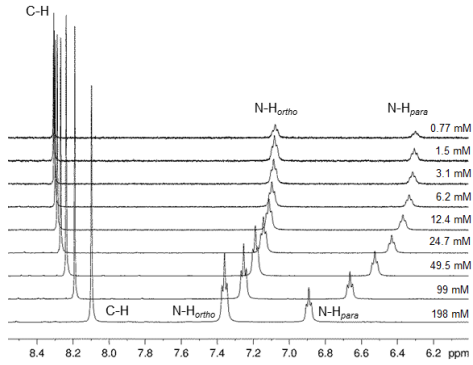

Figure 7. Concentration-induced ^{1}H-NMR experiments of **37b** in CD_2Cl_2 at 295 K. The NMR spectra were measured by decreasing the concentration from 198 mM to 0.77 mM. In the figure only the aromatic region (8.5-6.0 ppm) is reported.

Upon increasing the concentration large downfield shifts for the N-H signals ($\Delta\delta$ ~2 ppm) were observed. On the other hand a large upfield shift for the aromatic protons was measured ($\Delta\delta$ ~1.6 ppm) over the same concentration range. The concentration-induced ^{1}H-NMR shift variation of BTA **37b** was performed at 295 K in CD_2Cl_2 as well (Figure 7). The presence of the pentynyloxy substituent on the aromatic ring caused a reduction on the symmetry of the molecule (C_{2v}) generating two distinct signals for the N-H group of the three amides. For the sake of clarity, these signals are referred to N-H_{ortho} and N-H_{para}, respectively (see Scheme 3). Increasing the concentration (from 0.77 mM to 198 mM) caused an upfield shift for the aromatic protons ($\Delta\delta$ 0.21 ppm) and a downfield shift for both types of N-H protons (N-H_{ortho} $\Delta\delta$ 0.281 ppm, N-H_{para} $\Delta\delta$ 0.59 ppm). The $\Delta\delta$-values are considerably smaller than for the BTA **42**. The $\Delta\delta$-values for the N-H_{ortho} and for the C-H of the aromatic ring are similar, whereas the $\Delta\delta$-value for the N-H_{para} is twice as big, but still almost a factor of four smaller than for BTA **42**. The bromo-BTA derivative **41** had a very low solubility in CD_2Cl_2. We were forced to replace d_2-dichloromethane with d_1-chloroform. As in the case of BTA **37b**, the N-H signals are referred to N-H_{ortho} and N-H_{para}, respectively (see Scheme 3). By increasing the concentration from 0.10 mM to 82 mM a large upfield shift for the C-H ($\Delta\delta$ 0.95 ppm) was observed. A very large downfield shift was observed for the N-H protons of the amides (N-H_{ortho} $\Delta\delta$ 2.45 ppm, N-H_{para} $\Delta\delta$ 2.53 ppm) (Figure 8). The $\Delta\delta$-values for both N-H protons are even bigger, than those observed for the compound **42**, whereas the $\Delta\delta$-value for the aromatic C-H was almost a factor of 2 smaller than the values observed for our reference compound.

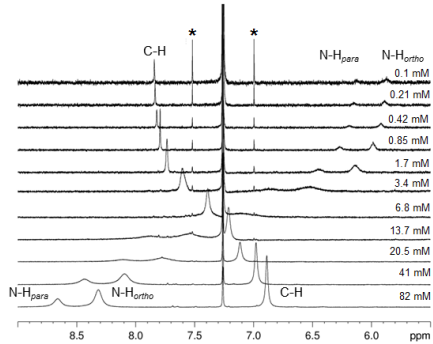

Figure 8. Concentration-induced ^{1}H-NMR experiments of **41** in $CDCl_3$ at 295 K. The NMR spectra were measured by decreasing the concentration from 82 mM to 0.10 mM. In the figure only the aromatic region (9.0-5.0 ppm) is reported. * The asterisk indicates the ^{13}C-satellite signals of the residual $CHCl_3$ in the NMR-solvent.

The NMR spectrum of **41** shows extensive line broadening at certain concentrations probably due to the intermediate exchange rate of the association process of **41**.

Globally the observed concentration-induced upfield shifting for the aromatic protons is coherent with the enhancement of the π–π interactions. According to the X-ray structures of the model tri-(2-methoxy-ethyl)-BTA derivative **1** (see SI), the short interring distance (3.62 Å) enables strong aromatic interaction (π–π stacking) along the columnar axis of the mesophase resulting in an upfield ring current shift of the aromatic protons. In the case of the amide protons the observed concentration-induced downfield shifting is consistent with the formation of intermolecular H-bond interactions. The presence of a bulky atom, such as bromine, influences the amide torsion angle. The

carbonyls of the amides are forced out of planarity despite the concomitant loss of conjugation. In the case of BTA **37b**, the concentration-induced shift for N-H_{ortho} protons is two times smaller than the shifts of the N-H_{para} and four times smaller than the shifts observed for the reference compound **42**. In the effort to explain such observation, we invoked the formation of intramolecular H-bonds by the N-H_{ortho} protons of **37b**. The dilution experiments are compatible with the occurrence of an intramolecular H-bond from the N-H_{ortho} group not only in the pure material but also in solution.

^{1}H-DOSY NMR study:

To complete the analyses of the aggregation of our BTA derivatives in solution ^{1}H 2D-DOSY experiments were executed. As for the concentration-induced shift ^{1}H-NMR experiments, BTA **1** was selected as the reference compound for 2D-DOSY experiments and d_2-dichloromethane was used as the solvent. For all three BTAs (**42**, **37b** and **41**) a reduction of the diffusion coefficient upon increasing the concentrations was observed (Table 3, Figure 9, 10 and 11).

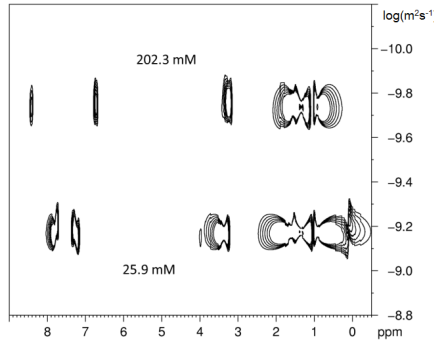

Figure 9. ^{1}H 2D-DOSY in CD_2Cl_2 of **42** at a concentration of 202.3 mM and 25.9 mM. The spectra were measured at 295 K.

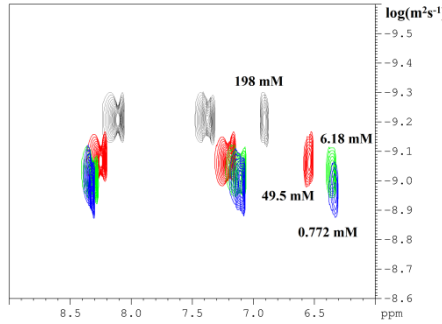

Figure 10. ^{1}H 2D-DOSY of **37b** in CD_2Cl_2: in grey at 198 mM, in red at 49.5 mM, in green at 6.18 mM, in blue at 0.772 mM at 295 K.

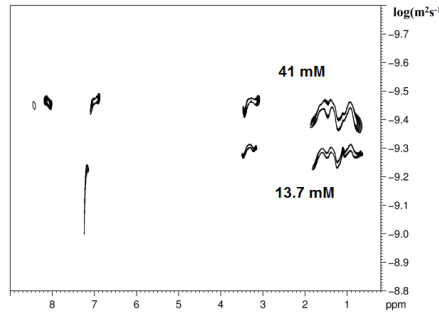

Figure 11. ^{1}H 2D-DOSY in $CDCl_3$ of **41** at 41 mM and 13.7 mM. The spectra were measured at 295 K.

These results are consistent with the formation of supramolecular aggregates, which diffuse slower than the monomeric species. In the DOSY spectrum at 13.7 mM of **41**, the signal of the amide protons are broad, whereas the aromatic proton signal partially overlaps with the residual signal of $CHCl_3$. These experimental difficulties hamper the precise measurement of the diffusion coefficient for these signals. However the diffusion coefficient of the molecule can be measured from the analysis of the signals in the aliphatic region of the spectrum (Figure 11). The observed chemical shift (δ_{obs}) is the weighted average of the chemical shifts of the monomeric species (δ_{mon}) and the aggregated species (δ_{agg}) according to Equation (1):

$$\delta_{obs} = \delta_{mon}\chi_{mon} + \delta_{agg}\chi_{agg} \qquad \textbf{(Equation 1)}$$

where χ_{mon} and χ_{agg} are the fractions of the monomer and the aggregate respectively and where $\chi_{mon} + \chi_{agg} = 1$.

Similarly, the observed diffusion coefficient (D_{obs}) is the weighted average of the diffusion coefficient of the monomer (D_{mon}) and the aggregate (D_{agg}) respectively, according to the Equation (2):

$$D_{obs} = D_{mon}\chi_{mon} + D_{agg}\chi_{agg} \qquad \textbf{(Equation 2)}$$

The limiting values of δ_{mon} and δ_{agg} could be extrapolated from the curve fitting (Figure 12, 13 and 14).

Assuming the complete aggregation (χ_{agg}=1) and the complete disaggregation (χ_{mon}=1) at the two limits of the fitting curves, an estimation of the ratio (molar fraction χ) of the aggregate and the monomer can be obtained for the measured experimental points. The monomer molar fraction χ_{mon} was calculated based on the measured shift of the N-H signal. In the case of BTA **37b** and **41** the calculation was carried out based on the shift of the N-H_{para} signal being exclusively due to intermolecular H-bond interactions (Table 3).

Simulation of the aggregation process:

The concentration-induced chemical shifts were fitted according to a nonlinear least square equation. Meijer elaborated a fitting equation to interpolate isodesmic aggregation curves, specifically excluding cooperativity.[30] However BTA **42** is known to aggregate according to a cooperative mechanism characterized by a nucleation step (K_n) and an elongation step (K_e). Therefor the general fitting procedure based on a logistic fitting function using the OrigineLab® program ($\delta_{C\text{-}H}$ and $\delta_{N\text{-}H}$ vs. [BTA]) (Equation (3)) was used giving a considerably better fit (correlation coefficients above 0.99):

$$\boldsymbol{\delta_{obs} = \delta_{agg} + \frac{(\delta_{mon} - \delta_{agg})}{\left[1 + \left(\frac{c}{K_d}\right)^{p}\right]}} \qquad \textbf{(Equation 3)}$$

Table 3. Observed Diffusion coefficient *D* value of BTA **1**, **2** and **3** at different concentrations.

	BTA **42**		BTA **37b**			BTA **41**		
[BTA][a]	202.3	25.9	198	49.5	6.18	0.772	41	13.7
D_{obs} [b]	-9.79	-9.19	-9.23	-9.08	-9.02	-8.89	-9.46	-9.22
χ_{mon} [c]	0.03	0.58[d]	0.40	0.77	0.96	0.994	0.14	0.35

[a] BTA concentration in mmol/L. [b] Diffusion coefficient measured as log(m^2s^{-1}). [c] The molar fraction of the monomer species χ_{mon} were obtained based on the extrapolated limit value (see SI) obtained from the fitting curves (Figure 12, 13 and 14). [d] Values extrapolated (see SI).

In Equation (3) *c* is the total concentration of the BTA, *p* is the slope factor of the fitting curve, δ_{mon} and δ_{agg} are respectively the extrapolated values of the chemical shifts for the monomer at infinite dilution, and the chemical shift for the aggregate obtained by the fitting procedure, K_d (mmol L^{-1}) is the dissociation constant of the aggregates. The association constants, measured as M^{-1}, were calculated based on the relation K_a (M^{-1}) = 1000/K_d (mmol L^{-1}). If the slope factor is p >1, a sigmoidal behaviour of the fitting curve is indicated compatible with positive cooperativity. Vice versa values of p <1 indicate negative cooperativity. When the value p =1 the curve assumes a hyperbolic behaviour indicating the absence of cooperativity. This statistical data fitting was applied on concentration-dependent NMR data of **42.** The best fitting (Figure 12a and b) gave a sigmoidal curve with a positive cooperativity as indicated by the slope factor of 1.8(1) for N-H, and of 2.2(2) for C-H (Table 4). The result of the statistical data analysis shows cooperativity for the aggregation of **42** in agreement with the findings reported in the literature.[13b] As our NMR results obtained for **42** are compatible with the conclusion reported in the literature, we deduced that our procedure is suitable for the analysis of the aggregation behavior of BTA derivatives. The values of K_a, 34 M^{-1} determined using the shifts of the N-H signals and 39 M^{-1} deduced using the shifts of the C-H aromatic signals are to all intend and purposes sufficiently similar, so that we assume that the aggregation observed monitoring the two separate sensors is reporting on one and the same association process. The observed association constant K_a for the three studied compounds followed the following sequence **41**>**42**>**37b** (Table 4). The relative strength of the association constant K_a follows the same trend as the material property

expressed as the temperature range of the liquid crystalline phase observed by DSC **41**>**42**>**37b** (Table 1).

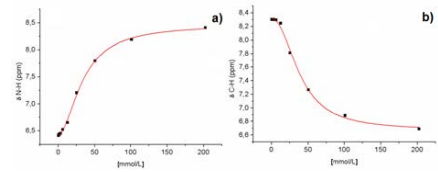

Figure 12. Curves fitted using equation 3 of the plot δ vs. [**42**]. a) N-H protons. b) C-H aromatic protons.

The unsubstituted BTA **42** has been carefully studied and characterized. Therefore we use BTA **42** as the reference compound of our studies. The association constant K_a of 2-pentynyloxy BTA **37b** is significantly smaller than the K_a of **42** (about six to eight times smaller)**.** On the other hand, the K_a found for the association process of **41** is four times bigger then **42** (Table 4). The calculated difference of ΔG (ΔG= -RT lnK_a) between **42** and **41** (4.3 kJmol^{-1} from the N-H$_{ortho}$, 4.0 kJ mol^{-1} from N-H$_{para}$, and 2.7 kJ mol^{-1} from C-H) is compatible with the loss of one H-bond interaction in **37b**.

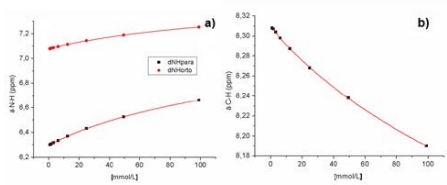

Figure 13. Curves fitted using equation 3 of the plot δ vs. [**37b**]. a) N-H protons. b) C-H aromatic protons. In both curves the asymptotes, indicating full aggregation, are not reached due to a weakness in of the binding.

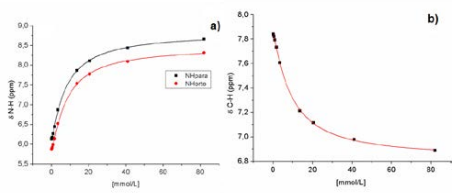

Figure 14. Curves fitted with equation 3 of the plot δ vs. [**41**]. a) N-H protons. b) C-H aromatic protons.

This observation supports the hypothesis that the formation of an intramolecular H-bond in **37b** destabilizes the columnar assembly, tentatively attributed to the occurrence of a competing intramolecular H-bond. The presence of bromine in **41** significantly stabilized the columnar association process. The large dihedral angle of at least one of the amide groups compared to the plane of the aromatic ring in BTA **41** may enhance the formation of intermolecular H-bonds. The imposed increase of this dihedral angle has been invoked as argument for the reinforced strength of self-assembly.[8a] The slope factor obtained from the fitting of the curves of the experimental data of **37b** and **41**, gave *p* values close to 1 (Table 4) indicating no or only small cooperativity. For these two

compounds using the isodesmic model (Equation (4)) for the fitting process gave results, which are not distinguishable from the results obtained from the more general approach using logistic fitting.[30]

Table 4. Thermodynamic data for the aggregation of BTA **1**, **2** and **3** calculated at 295 K applying the logistic fitting equation and the isodesmic fitting model).

Logistic [a]	BTA **42**		BTA **37b**			BTA **41**		
	N-H	C-H	N-H$_{ortho}$	N-H$_{para}$	C-H$_{arom.}$	N-H$_{ortho}$	N-H$_{para}$	C-H$_{arom.}$
K_d (mM)	34 (1)	39 (2)	196(53)	176(30)	337 (117)	8.4(3)	8.0(4)	9.3(2)
K_a (M^{-1})	29(4)	26(5)	5(1)	6(1)	3(1)	119(4)	125(6)	108(2)
R^2	0.9985	0.9968	0.9998	0.9999	0.9999	0.9994	0.9993	0.9998
p	1.8(1)	2.2(2)	0.91(4)	0.94(3)	0.90(4)	1.22(5)	1.16(5)	1.19(3)
ΔG [d]	-8.3 (1)	-8.0 (1)	-4.0(7)	-4.3(4)	-2.7(9)	-11.7(1)	-11.8(1)	-11.5(1)
Isodesmic[b]								
K_a (M^{-1})	*15(6)* [c]	*10(5)* [c]	4.7(3)	4.5(2)	3.3(2)	109(25)	120(25)	98(20)
R^2	*0.9728*	*0.9584*	0.9998	0.9999	0.9998	0.9909	0.9927	0.9928
ΔG [d]	*-7(1)*	*-6(1)*	-3.8(2)	-4(1)	-2.9(1)	-11.5(6)	-11.7(5)	-11.3(5)

[a] Calculated data from the fitting procedure using Equation (3). [b] Calculated data from the fitting procedure using Equation (4). [c] The values calculated for **42** by applying the isodesmic model are affected by a low correlation coefficient (R^2) meaning low fitting quality. [d] Gibbs Free Energy measured in kJ mol^{-1}.

$$\boldsymbol{\delta_{obs} = \delta_{mon} + \left(\delta_{agg} - \delta_{mon}\right)\left[1 + \frac{\left(1-\sqrt{4K_ac+1}\right)}{2K_ac}\right]} \qquad \textbf{(Equation 4)}$$

As indicated the application of Equation 4 to the NMR data of **42** resulted in poorer data fitting due to the cooperativity effects described (see Table 4 and SI).

Conclusions

The mono-core-functionalized BTA derivatives **37b** and **41** formed columnar mesophases over a broad temperature range. Using the C_{3v} symmetric molecule **42** as reference compound the thermodynamics of the supramolecular assembly process could be analysed Based on the concentration-dependent ^{1}H-NMR analysis. Concentration dependent shift experiments completed with DOSY experiments allowed to determine the thermodynamic strength of the supramolecular aggregation process and to differentiate between isodesmic and cooperative self-assembly. The introduction of the pentynyloxy group, an H-bond acceptor substituent, in the BTA derivative **37b** reduced in parallel the temperature range of the liquid crystalline phase and the strength of the aggregation process in solution. Both of these observations are compatible with destabilization of the intermolecular H-bonds driven supramolecular assembly by the formation on an intramolecular H-bond interaction. The introduction of bromine, on the BTA aromatic core efficiently stabilized the columnar organization and increased the strength of the aggregation in solution. In both cases, the functionalization of the aromatic core induced the loss of cooperativity during the supramolecular

assembly process. The BTA derivatives **37b** and **41** were found to aggregate according to an isodesmic self-assembly process.

Experimental Section

General Remarks: Reactions requiring anhydrous conditions were performed in oven-dried (120 °C) glassware under an inert atmosphere of dry N_2 or dry Ar. Anhydrous solvents such as toluene (≥99.7%, ≤0.005% H_2O), DMF (≥ 99.8%, ≤ 0.01% H_2O), DMSO (≥99.5%, ≤0.005 H_2O), THF (≥99.5%, ≤0.025 H_2O, stabilized WITH 0.025% 2,6-di-*t*Bu-4-methylphenol) were obtained from *Aldrich* over molecular sieves. N-methyl pyrrolidone (NMP) was purchased from Acros (purity 99%). Brine refers to a sat. aq. solution of NaCl. Petroleum ether refers to a boiling fraction of 40 °C - 60 °C. All other solvents were of technical grade and used without further purifications. ^{1}H NMR spectra and ^{13}C NMR spectra were recorded on a *Bruker Avance II-400* (400.13 MHz, ^{1}H; 100.61 MHz, ^{13}C) and on a *Bruker DPX 400* (400.13 MHz, ^{1}H; 100.61 MHz, ^{13}C) of the Neuchâtel Platform of Analytical Chemistry (NPAC) of the University of Neuchâtel. Chemical shifts (δ) are quoted (ppm) and are relative to tetramethylsilane (δ= 0 ppm) as the internal standard or the residual solvent peak in $CDCl_3$ (δ 7.26 ppm, ^{1}H; δ 77.0 ppm, ^{13}C), in dichloromethane (δ 5.32 ppm, ^{1}H; δ 53.84 ppm, ^{13}C), in methanol (δ 3.31 ppm, ^{1}H; δ 49.00 ppm, ^{13}C), in DMSO (δ 2.50 ppm, ^{1}H; δ 39.52 ppm, ^{13}C). All the deuterated NMR solvents were purchased from *Cambridge Isotope*. Multiplicities are indicated by s (singlet), d (doublet), t (triplet), q (quartet), m (multiplet) and br (broad). Coupling constants, *J*, are reported in Hertz. The assignments were verified using the following 2D-experiments if necessary: HSQC, HMBC and COSY. ^{1}H 2D-COSY experiments were performed with stimulated echo and LED schemes using bipolar gradient pulses for diffusion and two spoil gradients. The strength of the diffusion gradients was varied from 5% to 95% in 32 increments. Typically, 8 to 32 scans were recorded for each increment.[31] The length of the diffusion and spoil gradients was 2 and 1.1 ms respectively with a gradient recovery time of 200 μs. *The data matrix was 4K x32 in the time domain and 4K x512 in the processed domain. Mass spe*ctroscopy was performed at the Neuchâtel Platform of Analytical Chemistry (NPAC) of the University of Neuchatel. Electrospray (ESI (+/-)) were performed on an *API 4000 QTrap ABSciex* or *LC/MSD Trap Agilent*. The LC-MS retention times (R_t) and low resolution MS were recorded on an *UPLCUltimate 3000 Dionex - API 4000 QTrap, ABSciex*. The solvent were on UPLC grade and water was Milli-Q® grade. High resolution mass spectra were measured on *Bruker FTMS 4.7T BioAPEX II FT/ICR* using a standard electrospray ion (ESI) or MALDI source at the University of Fribourg (Switzerland) by Mr. Fredy Nydegger. Infrared spectra (IR) were recorded on a *Perkin Elmer Spectrum One FT-IR version B* spectrophotometer using the software *Spectrum version 5.0.1* for recording and treating the data. Peaks are reported in cm^{-1} with indicated relative intensities: *s* (strong, 67-100%); *m* (medium, 34-66%); *w* (weak, 0-33%). Solid samples were measured in a freshly prepared KBr pellets. Liquids were measured as films using polished KBr plates. Melting points (m.p.) were determined using a *Gallenkamp MPD 350-BM* capillary melting point apparatus in open tubes and are uncorrected. Analytical thin-layer chromatography was performed on *Merck* silica gel plates (aluminium sheets precoated with silica (60 F254)) or on *Merck* aluminium oxide plates (aluminium sheets precoated with aluminium oxide (60 F254)). Visualization was accomplished with UV light unless noted otherwise. Flash column chromatography was performed using silica gel (*Brunschwig* Silica gel 60, 32-63; or *Brunschwig* Silica gel 60, 63-200). All reaction temperatures refer to oil bath temperature measured with Heidolph EKT 3mA® thermocouples unless mentioned specifically. Differential scanning calorimetry DSC analyses were accomplished in a Mettler Toledo DSC1 STARe® instrument. The samples were prepared in an aluminium sampler. Each analysis refers to a three-cycle heating-cooling run at 10 °C/min under nitrogen flux. The reported values of temperature refer to the "onset" peak. Data were analysed on STARe software. Polarized light microscope POM analyses were performed in an Axio Scope Zeiss microscope. Samples were heated on a Linkam

THMS600® heater controlled by a Linkam 93 apparatus. POM imagines were taken by a Fujix Digital Camera HC-300Z® and theatre with Axiovision rel 4.8® software.

***N*[1],*N*[3],*N*[5]-trihexylbenzene-1,3,5-tricarboxamide (42):**
1,3,5-benzentricarbonyl trichloride (1 g, 3.77 mmol) was dissolved in dry THF (6 mL) and added drop wise to a solution of hexylamine (2.3 mL, 30.1 mmol) in dry THF (6 mL) at 0 °C under nitrogen. The reaction was stirred at 0 °C for 30 min and at room temperature for other 18 h. The organic solvent was removed under vacuum and the crude solid was diluted with HCl 2M (15 mL). The product was extracted using ethyl acetate. The resulting organic solution was washed again with HCl 2M, $NaHCO_3$ sol. 5% and with brine. The organic phase was dried over $MgSO_4$ and the solvent was removed under vacuum. The product was purified by chromatography on silica gel using cyclohexane/ethyl acetate 1:1 to afford 1.125 g of an amorphous white solid in 65% yield. R_f: (SiO_2, cyclohexane/ethyl acetate 1:1): 0.55. ^{1}H-NMR ($CDCl_3$ 400 MHz, 295 K): δ= 8.32 (s, 3H, *Ar*), 6.56 (t, $^3J_{H,H}$ = 4.5 Hz, 3H, N*H*), 3.45 (q, $^3J_{H,H}$ = 6.7 Hz, 6H, C*H*$_2$NH), 1.60 (quint, $^3J_{H,H}$ = 7.2 Hz, 6H, C*H*$_2$CH$_2$NH), 1.39-1.31 (m, 18H, C*H*$_2$), 0.89 (t, $^3J_{H,H}$ = 6.5 Hz, 9H, C*H*$_3$), ppm. ^{13}C-NMR ($CDCl_3$, 100 MHz, 295 K): δ= 165.8, 135.4, 128.1, 40.5, 31.6, 29.6, 26.8, 22.7,14.2 ppm.

2-Methoxy-1,3,5-benzentricarboxyilic acid (32): the compound was prepared according to the procedure previously reported by Raymond.[27] 2,6-bis-(hydroxymethyl)-4-methylphenol (10 g, 59.4 mmol) was dissolved in acetone (200 mL). Anhydrous K_2CO_3 (12.32 g, 89.175 mmol) was added and the suspension was stirred for 5 min. Me_2SO_4 (6.8 mL, 71.3 mmol) was added and the reaction was stirred at 70 °C for 15 h. The solid was filtered off and the solvent evaporated under vacuum to afford a white solid crude product. The product was purified by recrystallization from ethyl acetate to afford 6.4 g of a white solid in 60% yield. R_f: (SiO_2, ethyl acetate/petroleum ether 9:1): 0.57. M.p. 107 °C. ^{1}H-NMR ($CDCl_3$ 400 MHz, 295K): δ= 7.14 (s, 2H, *Ar*), 4.71 (s, 4H, *CH*$_2$), 3.84 (s, 3H, O*Me*), 2.32 (s, 3H, *Me*), 1.94 (s, 2H, OH) ppm. ^{13}C-NMR ($CDCl_3$, 100 MHz, 295K): δ= 165.8, 153.8, 134.3, 133.5, 124.3, 115.9, 62.2, 60.9, 20.8 ppm. MS (ESI): m/z (%) = 205.0 (100) $[M+Na]^+$.
KOH caps (3.8 g, 67.9 mmol) were added to a solution of (2-methoxy-5-methyl-1,3-phenylene)dimethanol (6.18 g, 33.9 mmol) in distilled water (400 mL) and stirred for 10 min. $KMnO_4$ (26.83 g, 169.7 mmol) was added portion wise and another 200 mL of distilled water were added. The dark solution was stirred at 100 °C for 7 hours. The reaction was cooled at room temperature and $Na_2S_2O_3$ powder was added until the permanganate was reduced forming a dark brown suspension. The solid residue was filtered off and the volume of water was reduced to 150 mL by distillation under vacuum. Concentrated HCl 37% was added until pH 3. The aqueous phase was saturated by adding solid NaCl. The aqueous solution was extracted with AcOEt (4 x 200 mL). The organic phases were dried over $MgSO_4$ and the solvent was removed under vacuum. The resulting white solid was dissolved in methanol and the yellowish insoluble solid was filtered off. The solvent was evaporated under vacuum to afford 6.2 g of a white solid in 76% yield. The crude product was used without further purification. ^{1}H-NMR (DMSO, 400 MHz, 295 K): δ= 8.31 (s, 2H, *Ar*), 3.85 (s, 3H, *OMe*) ppm. ^{13}C-NMR (DMSO, 100 MHz, 295K): δ= 166.6, 166.0, 161.7, 134.8, 128.1, 126.1, 63.5 ppm. MS (ESI): m/z (%) = 239.1 (100) $[M-H]^-$

***N*[1],*N*[3],*N*[5]-triethyl-2-methoxybenzene-1,3,5-tricarboxamide (34a):**
2-methoxy-1,3,5-tricarboxylic acid (**32**) (500 mg, 2.1 mmol) was suspended in dry toluene (5 mL) and $SOCl_2$ (0.53 mL, 7.3 mmol) and two drops of DMF were added. The suspension was heated at 110°C for 2 h. The yellowish solution was cooled to room temperature and volatile compounds were removed under high vacuum to furnish a pale yellow oil. The resulting acid chloride was dissolved in THF (5 mL) and added drop wise to a solution of $EtNH_2$ (1.15 mL, 14.46 mmol, sol 70% in water) dissolved in THF (5 mL) at 0 °C. After the complete addition the reaction was stirred at 0 °C for 1 h

and at room temperature for other 4 h. The solution was acidified to pH 3 by adding HCl 2M. The organic solvent was removed under vacuum and the resulting aqueous solution was diluted with water. The product was extracted with ethyl acetate. The organic phase was dried on $MgSO_4$ and the solvent removed under vacuum. The product was purified by chromatography on SiO_2 using ethyl acetate/ methanol (8:2) to afford 429 mg of a white solid in 64% yield. R_f (ethyl acetate/MeOH 9:1): 0.5. M.p. 167 – 168 °C**.** IR (KBr): 3272 *m*, 3077 *w*, 2977 *m*, 2937 *m*, 1714 *m*, 1644 *s*, 1543 *s*, 1465 *m*, 1300 *s*, 1149 *m*, 1093 *m*, 1057 *w*, 1003 *m*, 924 *w*, 656 *w*, 601 *w*. ^{1}H-NMR (CD_3OD, 400 MHz, 295 K): δ= 8.15 (s, 2H, Ar-*H*), 3.90 (s, 3H, O*CH*$_3$), 3.47-3.37 (m, 6H, *CH*$_2$-NH*)*, 1.25 (t, $^3J_{H,H}$ = 7.3 Hz, 6H, C*H*$_{3ortho}$), 1.22 (t, $^3J_{H,H}$ = 7.3 Hz, 3H, C*H*$_{3para}$) ppm. ^{13}C-NMR (CD_3OD, 100 MHz, 295 K): δ= 168.0 (C=O$_{ortho}$), 167.7 (C=O$_{para}$), 159.0 (*C*-OMe), 131.9 (*Ar*-H), 131.2 (*C*-C=O$_{para}$), 131.0 (*C*-C=O$_{ortho}$), 63.3 (O*C*H$_3$), 35.9 (*C*H$_2$-NH), 35.8 (*C*H$_2$-NH), 14.8 (*C*H$_3$-CH$_2$), 14.7 (*C*H$_3$-CH$_2$) ppm**.** MS (ESI): m/z (%) = 344.3 (100) [M+Na]$^+$**.** HRMS (ESI): Calc. for [M+Na]$^+$ 344.1581 $C_{16}H_{23}N_3O_4Na^+$; found 344.1575 [M+Na]$^+$

***N*^{1}*,N*^{3}*,N*^{5}-triethyl-2-hydroxybenzene-1,3,5-tricarboxamide (36a):**

N^1*,N*^{3}*,N*^{5}-triethyl-2-methoxybenzene-1,3,5-tricarboxamide (**34a**) (357 mg, 1.11 mmol) was dissolved in NMP (3 mL). Thiophenol (0.11 mL, 1.11 mmol) and anhydrous K_2CO_3 (184.2 mg, 1.3 mmol) were added and the solution was stirred at 150 °C for 2 hours. The reaction was cooled at room temperature and diluted with water. The resulting solution was acidified to pH 5 adding HCl 2M and the product was extracted with ethyl acetate. The organic phase was dried over $MgSO_4$ and the solvent was removed under vacuum. The product was purified by chromatography on silica gel using ethyl acetate (100%) to afford 207.3 mg of a yellowish solid in 61% yield**.** R_f (SiO_2, ethyl acetate): 0.52. M.p. 187 - 190 °C**.** IR (KBr): 3382 *w*, 3291 *m*, 3067 *w*, 2975 *w*, 2934 w, 2344 *vw*, 1663 *s*, 1630 *s*, 1579 *s*, 1541 *s*, 1459 *s*, 1336 *m*, 1285 *s*, 1196 *m*, 1146 *m*, 1062 *w*, 936 *w*, 800 *w*, 769 *w*, 692 *w***.** ^{1}H-NMR (CD_3OD, 400 MHz, 295 K): δ= 8.45 (s, 2H, Ar-H), 3.45 (q, $^3J_{H,H}$ = 7.3 Hz, 4H, C*H*$_2$-NH), 3.41 (q, $^3J_{H,H}$ = 7.3 Hz, 2H, C*H*$_2$-NH), 1.25 (t, $^3J_{H,H}$ = 7.2 Hz, 6H, C*H*$_3$-CH$_2$), 1.23 (t, $^3J_{H,H}$ = 7.2 Hz, 3H, C*H*$_3$-CH$_2$) ppm. ^{13}C-NMR (CD_3OD, 100 MHz, 295 K): δ= 168.7 (C=O$_{ortho}$), 168.3 (C=O$_{para}$), 163.6 (*C*-OH), 132.8 (*Ar*-H), 126.2 (*C*-C=O$_{para}$), 119.4 (*C*-C=O$_{ortho}$), 35.9 (*C*H$_2$-NH); 35.7 (*C*H$_2$-NH), 14.9 (*C*H$_3$-CH$_2$), 14.8 (*C*H$_3$-CH$_2$) ppm**.** MS (ESI): m/z (%) 330.3 (100) [M+Na]$^+$. HRMS (ESI): Calc. for [M+Na]$^+$ 330.1424 $C_{15}H_{21}N_3O_4Na^+$; found 330.1427 [M+Na]$^+$

***N*^{1}*,N*^{3}*,N*^{5}-triethyl-2-(pent-4-yn-1-yloxy)benzene-1,3,5-tricarboxamide (37a):** *N*^{1}*,N*^{3}*,N*^{5}-triethyl-2-hydroxybenzene-1,3,5-tricarboxamide (**36a**) (212 mg, 0.69 mmol) was dissolved in under N_2 in dry DMF (2 mL) in a vial. Cs_2CO_3 (226.9 mg, 0.69 mmol) and NaI (51.7 mg, 0.35 mmol) were added and the suspension was stirred for 5 min. at room temperature. 5-chloro-1-pentyne (0.146 mL, 141.5 mg, 1.38 mmol) was added and the vial was sealed with Teflon®-coated cap and stirred at 70 °C for 48 h. The reaction was cooled at room temperature and diluted in water. The solution was extracted with ethyl acetate and the organic phases were dried over $MgSO_4$. The solvent was removed under vacuum. The product was purified by chromatography on SiO_2 using ethyl acetate (100%) to furnish the product in 43 mg as a white solid in 17% yield. Suitable crystals for X-ray diffraction were obtained by slow evaporation from $CDCl_3$. R_f (SiO_2, ethyl acetate): 0.15. M.p. 147 - 148 °C. IR (film $CDCl_3$): 3260 *m*, 3074 *w*, 2974 *w*, 2935 *w*, 2877 *w*, 1639 *s*, 1539 *s*, 1448 *m*, 1381 *w*, 1356 *w*, 1297 *m*, 1149 *w*, 1029 *w*, 665 *w*. ^{1}H-NMR ($CDCl_3$, 400 MHz, 295 K): δ= 8.26 (s, 2H, Ar-*H*), 7.18 (t, $^3J_{H,H}$ = 5.0 Hz, 2H, N*H*$_{ortho}$), 6.46 (t, $^3J_{H,H}$ = 4.9 Hz, 2H, N*H*$_{para}$), 4.12 (t, $^3J_{H,H}$ = 6.5 Hz, 2H, ArO-C*H*$_2$-CH$_2$-CH$_2$), 3.53-3.42 (m, 6H, C*H*$_2$-NH), 2.37 (dt, $^3J_{H,H}$ = 6.9 Hz, $^4J_{H,H}$ = 2.6 Hz, 2H, CH$_2$-C*H*$_2$-C-CH), 2.03-1.96 (m, 3H, O-CH$_2$-C*H*$_2$-CH$_2$-, Alkyne-C*H*), 1.26 (t, $^3J_{H,H}$ = 7.3 Hz, 6H, C*H*$_3$-CH$_2$), 1.22 (t, $^3J_{H,H}$ = 7.3 Hz, 3H, C*H*$_3$-CH$_2$) ppm. ^{13}C-NMR ($CDCl_3$, 100 MHz, 295K): δ= 165.5 (C=O$_{para}$), 164.9 (C=O$_{ortho}$), 156.6 (*C*-O), 131.9 (*Ar*-H), 131.0 (*C*-C=O$_{para}$), 129.2 (*C*-C=O$_{ortho}$), 82.6 (*C*-CH), 75.7 (ArO-*C*H$_2$-CH$_2$-CH$_2$-), 69.8 (Alkyne-*C*H), 35.2 (*C*H$_2$-NH), 35.1 (*C*H$_2$-NH), 29.0 (ArOCH$_2$-*C*H$_2$-CH$_2$-), 15.3 (-CH$_2$-*C*H$_2$-C-CH), 14.89 (*C*H$_3$-CH$_2$), 14.86 (*C*H$_3$-CH$_2$) ppm**.** MS (ESI): m/z (%) 396.5 (100) [M+Na]$^+$ 769.8 (87) [2M+Na]$^+$ HRMS (MALDI): Calc. for [M+Na]$^+$ 396.1894 $C_{20}H_{27}N_3NaO_4^+$; found 396.1885 [M+Na]$^+$

***N*^{1},*N*^{3},*N*^{5}-trihexyl-2-methoxybenzene-1,3,5-tricarboxamide (34b):**
2-methoxy-1,3,5-tricarboxylic acid (**32**) (1.31 g, 5.46 mmol) was suspended in dry toluene (15 mL). $SOCl_2$ (1.4 mL, 19.09 mmol) and 5 drops of DMF were added. The reaction was stirred at 110°C for 2 h. Volatile compounds were removed in high vacuum to afford yellowish oil. The oil was dissolved in dry THF (10 mL) and added drop wise to a solution at 0 °C of hexylamine (5 mL, 37.8 mmol) in dry THF (10 mL). The reaction was stirred at 0 °C for 1 h and then for 15 h at room temperature. The organic solvent was removed under vacuum and the resulting crude solid was dissolved in ethyl acetate and washed with HCl 2M, $NaHCO_3$ 5% and brine. The organic phase was dried on $MgSO_4$ and the solvent was removed under vacuum. The product was purified by chromatography on silica gel using ethyl acetate/toluene (1:1) to afford 1.729 g of a white amorphous solid in 64% yield. R_f: (SiO_2, ethyl acetate/toluene 1:1): 0.36. M.p. 155.5 °C (DSC)**.** IR ($CDCl_3$ film): 3256 *m*, 3076 *w*, 2958 *s*, 2931 *s*, 2859 *m*, 2245 *w*, 1635 *s*, 1549 *s*, 1468 *m*, 1423 *w*, 1379 *w*, 1273 *w*, 1122 *vw*, 1005 *w*, 908 *s*, 735 *s*, 649 *w*. ^{1}H-NMR ($CDCl_3$, 400 MHz, 295 K): δ= 8.24 (s, 2H, Ar-*H*), 7.32 (t, $^3J_{H,H}$ = 5.5 Hz, 2H, N*H*$_{ortho}$); 6.52 (t, $^3J_{H,H}$ = 5.5 Hz, 1H, N*H*$_{para}$), 3.88 (s, 3H, O*Me*), 3.42 (q, $^3J_{H,H}$ = 6.9 Hz, 4H, C*H*$_2$-NH), 3.38 (q, $^3J_{H,H}$ = 6.9 Hz, 2H, C*H*$_2$-NH), 1.63-1.53 (m, 6H, NH-CH$_2$-C*H*$_2$-), 1.39-1.23 (m, 18H, 9xC*H*$_2$), 0.90-0.85 (m, 9H, C*H*$_3$) ppm. ^{13}C-NMR ($CDCl_3$, 100 MHz, 295 K): δ= 165.6 (C=O$_{para}$), 164.8 (C=O$_{ortho}$), 157.7 (*C*-O), 132.0 (*Ar*-H), 131.1 (*C*-C=O$_{para}$), 128.7 (*C*-C=O$_{ortho}$), 63.3 (O*Me*), 40.4 (*C*H$_2$-NH), 40.2 (*C*H$_2$-NH), 31.6 (*C*H$_2$), 29.61 (NH-CH$_2$-*C*H$_2$-), 29.56 (NH-CH$_2$-*C*H$_2$-), 26.85 (*C*H$_2$), 26.77 (*C*H$_2$), 22.68 (*C*H$_2$), 22.66 (*C*H$_2$), 14.1 (*C*H$_3$) ppm**.** MS (ESI): m/z (%) 512.5 (100) [M+Na]$^+$**.** HRMS (ESI): Calc. for [M+Na]$^+$ 512.3459 $C_{28}H_{47}N_3O_4Na^+$; found 512.3435 [M+Na]$^+$

***N*^{1},*N*^{3},*N*^{5}-trihexyl-2-hydroxybenzene-1,3,5-tricarboxamide (36b):**
N^1,*N*^{3},*N*^{5}-trihexyl-2-methoxybenzene-1,3,5-tricarboxamide (**34b**) (1.7 g, 3.47 mmol) was dissolved in *N*-methyl pyrrolidone (8 mL). Thiophenol (0.35 mL, 3.47 mmol) and anhydrous K_2CO_3 (575.8 mg, 4.16 mmol) were added and the reaction was stirred at 150°C for 2 hours. The reaction was cooled at room temperature and diluted in water. The solution was acidified to pH 3 by adding HCl conc. (37%). The product was extracted with dichloromethane. The organic phases were dried on $MgSO_4$. The solvent was removed under vacuum and the product was purified by chromatography on silica gel using cyclohexane/ ethyl acetate (6:4) to afford 1.287 g of yellowish amorphous in 78% yield. R_f (SiO_2, Cyclohexane/ethyl acetate 6:4): 0.49**.** M.p. 54 °C**.** IR(liquid film): 3306 *m*, 3081 *w*, 2957 *s*, 2930 *s*, 2858 *m*, 1634 *s*, 1579 *s*, 1542 *s*, 1464 *s*, 1415 *w*, 1378 *w*, 1287 *m*, 1194 *w*, 1149 *w*, 1063 *vw*, 932 *w*, 806 *w*, 768 *w*, 727 *w*, 674 *w*. ^{1}H-NMR ($CDCl_3$, 400 MHz, 295 K): δ= 8.57 (s, 2H, Ar-H), 7.88 (broad 2H, NH$_{ortho}$), 6.61 (t, $^3J_{H,H}$ = 5.2 Hz, 1H, NH$_{para}$), 3.47-3.37 (m, 6H, C*H*$_2$-NH), 1.63-1.52 (m, 6H, NH-CH$_2$-C*H*$_2$-), 1.37-1.26 (m, 18H, 9xC*H*$_2$), 0.90-0.85 (m, 9H, C*H*$_3$) ppm. ^{13}C-NMR ($CDCl_3$, 100 MHz, 295 K)*: δ= 166.6 (C=O$_{para}$), 163.2 (C=O$_{ortho}$), 131.9 (*C*-C=O$_{para}$ and *C*-C=O$_{ortho}$)**, 124.7 (*Ar*-H), 40.5 (*C*H$_2$-NH), 40.1 (*C*H$_2$-NH), 31.61 (*C*H$_2$), 31.58 (*C*H$_2$), 29.6 (NH-CH$_2$-*C*H$_2$-), 29.3 (NH-CH$_2$-*C*H$_2$-), 26.81 (*C*H$_2$), 26.79 (*C*H$_2$), 22.6 (*C*H$_2$), 14.1 (*C*H$_3$) ppm**.** MS (ESI): m/z (%) 499.0 (100) [M+Na]$^+$. HRMS (ESI): Calc. for [M+Na]$^+$ 498.3302 $C_{27}H_{45}N_3O_4Na^+$; found 498.3300 [M+Na]$^+$. * *C*-O aromatic signal was not detected. ** Very broad signal.

N*^{1},*N*^{3},*N*^{5}-trihexyl-2-(pent-4-yn-1-yloxy)benzene-1,3,5-tricarboxamide (37b):** *N*^{1},*N*^{3},*N*^{5}-trihexyl-2-hydroxybenzene-1,3,5-tricarboxamide (**36b**) (610 mg, 1.28 mmol) was dissolved in dry DMF (2 mL) in a vial. KI (212 mg, 1.28 mmol) and anhydrous Cs_2CO_3 (424 mg, 1.28 mmol) were added and the suspension was stirred for 5 min at room temperature. 5-chloro-1-pentyne (0.41 mL, 3.85 mmol) was added and the vial was sealed with Teflon®-coated cap and stirred at 70 °C for 48 h and for other 48 h at room temperature. The reaction was diluted in water and the solution was extracted with ethyl acetate. The organic phases were dried over $MgSO_4$ and the solvent was removed under vacuum. The product was purified by chromatography on silica gel using cyclohexane/ethyl acetate (6:4) to furnish 292 mg of a colourless solid in 42% yield. R_f (SiO_2, cyclohexane/ethyl acetate 6:4): 0.46**.** M.p. 141.1 °C (see Table 1). IR(KBr): 3246 *m*, 3079 *w*, 2930 *m*, 2859 *m*, 1634 *s*, 1552 *s*, 1451 *m*, 1376 *w*, 1297 *m*, 1033 *w*, 915 *w*, 725 *w.** ^{1}H-NMR ($CDCl_3$, 400 MHz, 295 K): δ= 8.25 (s, 2H, Ar-H), 7.17 (t, $^3J_{H,H}$ =

5.6 Hz, 2H, NH_{ortho}), 6.44 (t, $^{3}J_{H,H}$ = 5.6 Hz, 2H, NH_{para}), 4.11 (t, $^{3}J_{H,H}$ = 6.5 Hz, 2H, O-CH_2-CH_2-CH_2-), 3.46-3.37 (m, 6H, CH_2-NH), 2.35 (dt, $^{3}J_{H,H}$ = 6.9 Hz, $^{4}J_{H,H}$ = 2.6 Hz, 2H, CH_2-CH_2-C-CH), 2.01-1.93 (m, 3H, O-CH_2-CH_2-CH_2-, Alkyne-C*H*), 1.63-1.53 (m, 6H, NH-CH_2-CH_2-), 1.41-1.27 (m, 18H, 3x 6CH_2), 0.90-0.85 (m, 9H, CH_3) ppm. ^{13}C-NMR ($CDCl_3$, 100 MHZ, 295 K): δ= 165.5 (C=O_{para}), 165.0 (C=O_{ortho}), 156.5 (*C*-O), 131.8 (*Ar*-H), 131.0 (*C*-C=O_{para}), 129.2 (*C*-C=O_{ortho}), 82.6 (*C*-CH), 75.7 (O-CH_2-CH_2-CH_2-), 69.7 (Alkyne-*C*H), 40.4 (*C*H_2-NH); 40.3 (*C*H_2-NH); 31.6 (*C*H_2), 29.7 (NH-CH_2-*C*H_2-), 28.9 (OCH_2-*C*H_2-CH_2-), 26.9 (*C*H_2), 26.8 (*C*H_2), 22.68 (*C*H_2), 22.67 (*C*H_2), 15.3 (-CH_2-*C*H_2-C-CH), 14.1 (*C*H_3-CH_2) ppm**.** MS (ESI): m/z (%) 564.6 (100) $[M+Na]^+$. HRMS (MALDI): Calc. for $[M+Na]^+$ 564.3772 $C_{32}H_{51}N_3NaO_4^+$; found 564.3773 $[M+Na]^+$

Synthesis of 2-bromobenzene-1,3,5-tricarboxylic acid (27): the product was synthesized according to the procedure reported by Wallenfels *et al*.[29] 2-bromomesitylene (2.6 g, 13.07 mmol) was dissolved in a mixture of *tert*-butanol (150 mL) and distilled water (350 mL). K_2CO_3 (5.42 g, 39.21 mmol) was added and the solution was stirred for 5 min. $KMnO_4$ (20.65 g, 130.7 mmol) was slowly added and the dark violet solution was stirred at 100 °C for 9 h. The reaction was cooled to room temperature and the excess of permanganate was reduced by slowly adding solid $Na_2S_2O_3$. The brown solid was filtered off and *tert*-butanol was removed by distillation under rotatory evaporation. The water solution was acidified with HCl_{conc} (37%) until pH 3, saturated of solid NaCl and extracted with ethyl acetate. The organic phases were dried over $MgSO_4$ and the solvent was removed under vacuum. The white solid obtained was washed with dichloromethane to afford 2.3 g, of a white solid in 62 % yield. The product was used as row material without further purifications. M.p. 275 - 276 °C. IR(solid KBr): 3075 *m*, 1699 *s*, 1385 *w*, 1284 *w*, 1241 *m*, 1033 *w*, 922 *w*, 763 *w*, 674 *w*. ^{1}H-NMR (DMSO, 400 MHz, 295 K): δ= 8.15 (s, 2H, Ar-*H*) ppm**.** ^{13}C-NMR (DMSO, 100 MHz, 295 K): δ= 167.0 (*C*=O_{ortho}), 165.4 (*C*=O_{para}), 137.1 (*C*-Br); 131.0 (*Ar*-H), 130.3 (*C*-C=O_{ortho}), 121.6 (*C*-C=O_{para}) ppm.

2-bromo-N^1,N^3,N^5-trihexylbenzene-1,3,5-tricarboxamide (41):
2-bromobenzene-1,3,5-tricarboxylic acid (**27**) (80 mg, 0.277 mmol) was dissolved in dry DMF (3 mL) and cooled at 0 °C under nitrogen. EDC*HCl (191.2 mg, 0.997 mmol) and N-hydroxysuccinimide (127.5 mg, 1.108 mmol) were added and the murky solution was stirred at 0 °C for 5 min. A solution of hexylamine (0.128 mL, 0.969 mmol) dissolved in dry DMF (2 mL) was slowly added to the reaction at 0 °C. The reaction was stirred for 15 min at 0 °C and then stirred at 45 °C for 18 h. The reaction was diluted with ethyl acetate (15 mL) and the organic phase was washed with HCl 2M (2 x 15 mL), Na_2CO_3 10% (2 x 10 mL) and brine (1 x 15 mL). The organic phase was dried over $MgSO_4$ and the solvent was removed under reduced pressure. The product was purified by chromatography on silica gel using toluene/ethyl acetate (4:6) to afford 27 mg of white solid in 18% yield. R_f (SiO_2, toluene/AcOEt 4:6): 0.42. M.p. 239.5 °C (see Table 1). IR(KBr): 3271 *m*, 3081 *w*, 2957 *m*, 2929 *m*, 2857 *m*, 1639 *s*, 1553 *s*, 1467 *m*, 1378 *w*, 1304 *w*, 1149 *w*, 1028 *w*, 908 *w*, 726 *w* cm^{-1}. ^{1}H-NMR ($CDCl_3$, 400 MHz, 295 K, c= 20 mM)*: δ= 8.06 (s, 1H, NH_{para}), 7.71 (s, 2H, NH_{ortho}), 7.12 (s, 2H, Ar-*H*), 3.32-3.29 (m, 6H, CH_2-NH), 1.63-1.56 (m, 6H, NH-CH_2-CH_2-), 1.36-1.25 (m, 18H, 3x 6CH_2), 0.93-0.88 (m, 9H, CH_3) ppm. ^{13}C-NMR ($CDCl_3$, 100 MHz, 295 K, c= 20 mM)**: δ= 167.3 (*C*=O), 138.5 (*C*-Br), 127.9 (*Ar*-H), 40.6 (*C*H_2-NH), 40.3 (*C*H_2-NH), 31.7 (*C*H_2), 29.3 (NH-CH_2-*C*H_2-), 27.0 (*C*H_2), 26.9 (*C*H_2), 22.8 (*C*H_2), 14.2 (*C*H_3) ppm**.** MS (ESI): m/z (%) 560.7 (100) $[M+Na]^+$, 562.6 (100) $[M+Na]^+$. HRMS (MALDI): Calc. for $[M+H]^+$ 538.2639 and 540.2618 $[C_{27}H_{45}BrN_3O_3]^+$; found 538.2643 $[M+H]^+$ and 540.2611 $[M+H]^+$. * All the signals are broad due to intensive association of the solute. ** Two aromatic signals (*C*-C=O_{ortho} and *C*-C=O_{para}) were not detected.

Crystallographic information
CCDC 1055357 contains the supplementary crystallographic data for compound **9**. These data can be obtained free of charge via http://www.ccdc.cam.ac.uk/conts/retrieving.html, or from the Cambridge Crystallographic Data Centre, 12 Union Road, Cambridge CB2 1EZ, UK; fax: (+44) 1223-336-033; or e-mail: deposit@ccdc.cam.ac.uk. Further details of the single crystal X-ray diffraction study are provided in the supplementary information (SI).

Acknowledgements

The authors thank Dr. Armelle Vallat-Michel (NPAC University of Neuchâtel) for the assistance with the mass spectrometry and Dr. Sebastiano Guerra and Prof. Deschenaux (UniNE) for POM and DSC analysis. Financial support by the University of Neuchâtel and the Swiss National Science Foundation (grant 200020-140555) are gratefully acknowledged.

References

[1] G. M. Whitesides, M. Boncheva, *Proc. Natl. Acad. Sci. U. S. A.* **2002**, *99*, 4769-4774.

[2] S. I. Stupp, L. C. Palmer, *Chem. Mater.* **2014**, *26*, 507-518.

[3] Y. Matsunaga, N. Miyajima, Y. Nakayasu, S. Sakai, M. Yonenaga, *Bull. Chem. Soc. Jpn.* **1988**, *61*, 207-210.

[4] a) P. Besenius, J. L. M. Heynens, R. Straathof, M. M. L. Nieuwenhuizen, P. H. H. Bomans, E. Terreno, S. Aime, G. J. Strijkers, K. Nicolay, E. W. Meijer, *Contrast Media Mol. Imaging* **2012**, *7*, 356-361; b) S. Cantekin, T. F. A. de Greef, A. R. A. Palmans, *Chem. Soc. Rev.* **2012**, *41*, 6125-6137; c) T. Shikata, D. Ogata, K. Hanabusa, *J. Phys. Chem. B* **2004**, *108*, 508-514.

[5] C. A. Hunter, J. K. M. Sanders, *J. Am. Chem. Soc.* **1990**, *112*, 5525-5534.

[6] L. Brunsveld, H. Zhang, M. Glasbeek, J. A. J. M. Vekemans, E. W. Meijer, *J. Am. Chem. Soc.* **2000**, *122*, 6175-6182.

[7] a) M. P. Lightfoot, F. S. Mair, R. G. Pritchard, J. E. Warren, *Chem. Commun.* **1999**, 1945-1946; b) P. J. M. Stals, M. M. J. Smulders, R. Martin-Rapun, A. R. A. Palmans, E. W. Meijer, *Chem. - Eur. J.* **2009**, *15*, 2071-2080.

[8] a) M. L. Bushey, A. Hwang, P. W. Stephens, C. Nuckolls, *J. Am. Chem. Soc.* **2001**, *123*, 8157-8158; b) M. L. Bushey, T.-Q. Nguyen, C. Nuckolls, *J. Am. Chem. Soc.* **2003**, *125*, 8264-8269; c) M. L. Bushey, T.-Q. Nguyen, W. Zhang, D. Horoszewski, C. Nuckolls, *Angew. Chem., Int. Ed.* **2004**, *43*, 5446-5453.

[9] a) D. Thevenet, University of Neuchatel **2010**; b) D. Thevenet, R. Neier, *Synthesis* **2011**, 3801-3806.

[10] L. Schmidt-Mende, A. Fechtenkotter, K. Mullen, E. Moons, R. H. Friend, J. D. MacKenzie, *Science* **2001**, *293*, 1119-1122.

[11] S. Kumar, *Liq. Cryst.* **2005**, *32*, 1089-1113.

[12] T. Curtius, *J. Prakt. Chem.* **1915**, *91*, 39-102.

[13] a) M. M. J. Smulders, M. M. L. Nieuwenhuizen, T. F. A. de Greef, P. van der Schoot, A. P. H. J. Schenning, E. W. Meijer, *Chem. - Eur. J.* **2010**, *16*, 362-367; b) M. M. J. Smulders, A. P. H. J. Schenning, E. W. Meijer, *J. Am. Chem. Soc.* **2008**, *130*, 606-611; c) T. F. A. De Greef, M. M. J. Smulders, M. Wolffs, A. P. H. J. Schenning, R. P. Sijbesma, E. W. Meijer, *Chem. Rev.* **2009**, *109*, 5687-5754; d) A. J. Markvoort, H. M. M. ten Eikelder, P. A. J. Hilbers, T. F. A. de Greef, E. W. Meijer, *Nat. Commun.* **2011**, *2*, 1517/1511-1517/1519.

[14] A. R. A. Palmans, J. A. J. M. Vekemans, E. E. Havinga, E. W. Meijer, *Angew. Chem., Int. Ed. Engl.* **1997**, *36*, 2648-2651.

[15] A. R. A. Palmans, J. A. J. M. Vekemans, H. Fischer, R. A. Hikmet, E. W. Meijer, *Chem. - Eur. J.* **1997**, *3*, 300-307.

[16] T.-Q. Nguyen, M. L. Bushey, L. E. Brus, C. Nuckolls, *J. Am. Chem. Soc.* **2002**, *124*, 15051-15054.

[17] T.-Q. Nguyen, R. Martel, P. Avouris, M. L. Bushey, L. Brus, C. Nuckolls, *J. Am. Chem. Soc.* **2004**, *126*, 5234-5242.

[18] a) L. Fielding, *Tetrahedron* **2000**, *56*, 6151-6170; b) R. S. Macomber, *J. Chem. Educ.* **1992**, *69*, 375-378; c) P. Thordarson, *Chem. Soc. Rev.* **2011**, *40*, 1305-1323.

[19] R. B. Martin, *Chem. Rev.* **1996**, *96*, 3043-3064.

[20] a) C. S. Johnson, Jr., *Prog. Nucl. Magn. Reson. Spectrosc.* **1999**, *34*, 203-256; b) A. Macchioni, G. Ciancaleoni, C. Zuccaccia, D. Zuccaccia, *Chem. Soc. Rev.* **2008**, *37*, 479-489; c) K. F. Morris, P. Stilbs, C. S. Johnson, Jr., *Anal. Chem.* **1994**, *66*, 211-215.

[21] a) L. Allouche, A. Marquis, J.-M. Lehn, *Chem. - Eur. J.* **2006**, *12*, 7520-7525; b) A. Perez, D. de Saa, A. Ballesteros, J. L. Serrano, T. Sierra, P. Romero, *Chem. - Eur. J.* **2013**, *19*, 10271-10279.

[22] a) I. B. Rietveld, D. Bedeaux, *Macromolecules* **2000**, *33*, 7912-7917; b) A. Sagidullin, B. Fritzinger, U. Scheler, V. D. Skirda, *Polymer* **2004**, *45*, 165-170.

[23] W. S. Price, F. Tsuchiya, Y. Arata, *J. Am. Chem. Soc.* **1999**, *121*, 11503-11512.

[24] H. C. Kolb, M. G. Finn, K. B. Sharpless, *Angew. Chem., Int. Ed.* **2001**, *40*, 2004-2021.

[25] G.-L. Law, T. A. Pham, J. Xu, K. N. Raymond, *Angew. Chem., Int. Ed.* **2012**, *51*, 2371-2374.

[26] A. K. Chakraborti, L. Sharma, M. K. Nayak, *J. Org. Chem.* **2002**, *67*, 6406-6414.

[27] a) D. Kanamori, A. Furukawa, T.-A. Okamura, H. Yamamoto, N. Ueyama, *Org. Biomol. Chem.* **2005**, *3*, 1453-1459; b) D. Kanamori, T.-a. Okamura, H. Yamamoto, S. Shimizu, Y. Tsujimoto, N. Ueyama, *Bull. Chem. Soc. Jpn.* **2004**, *77*, 2057-2064; c) D. Kanamori, T.-a. Okamura, H. Yamamoto, N. Ueyama, *Angew. Chem., Int. Ed.* **2005**, *44*, 969-972.

[28] K. Wallenfels, K. Friedrich, F. Witzler, *Tetrahedron* **1967**, *23*, 1353-1358.

[29] X. Hou, M. Schober, Q. Chu, *Cryst. Growth Des.* **2012**, *12*, 5159-5163.
[30] M. M. L. Nieuwenhuizen, T. F. A. de Greef, R. L. J. van der Bruggen, J. M. J. Paulusse, W. P. J. Appel, M. M. J. Smulders, R. P. Sijbesma, E. W. Meijer, *Chem. - Eur. J.* **2010**, *16*, 1601-1612.
[31] D. Wu, A. Chen, C. S. Johnson, Jr., *J. Magn. Reson., Ser. A* **1995**, *115*, 260-264.

BTA Dimers (Part I): A review on BTA dimers and their Material Properties

Table of Contents

Literature overview on BTA dimers

We start our discussion presenting a comprehensive overview of the dimers of BTA reported in the literature and their material properties. The sequence of the literature overview starts from the non-substituted BTA derivative followed by the reports on fully-substituted crowded arenes and their dimer formation.

The group of Meijer reported the first and the only dimer of the substituted BTA **25** (Scheme 1, for the synthesis of **25**: see Scheme 6 Chapter 3).[1] The BTA discotic self-assembly units were connected using the thermoplastic elastomer, Kraton™ bisamine. The employment of such linker furnished nanorod BTA dimers showing nematic properties. In this case the thermoplastic polymeric nature of the linking unit (Kraton™ bisamine) plays a fundamental role generating a copolymer.

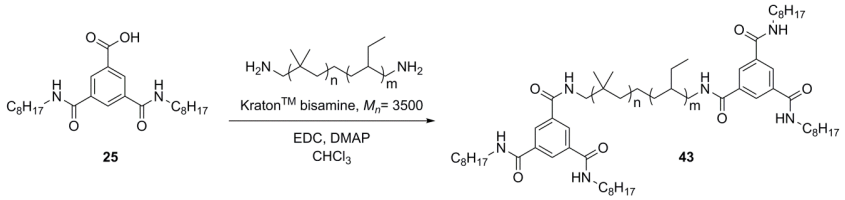

Scheme 1. Synthesis of nanorod-forming BTA dimer **43** reported by Meijers.[1] Kraton™ bisamine is a thermoplastic elastomers synthesized from the commercially available thermoplastic elasotmer diol Kraton™ L2203. Suh et al. reported a synthetic protocol to transform the diol into the diamine derivative.[2]

Up to now, no other example of dimeric structures of the benzene-1,3,5-tricarboxamide units have been reported.

Chen et *al*. reported in 2011 an example of an intramolecular helical-stacking structure, that are generally called foldamers,[3] linking two BTAs units with linear diamine linker (Scheme 2).[4] In this strategy they used 5-aminoisophthalamide (mixed N-centered, C=O-centered BTA) as the assembly unit.

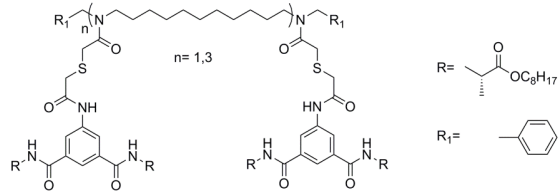

Scheme 2. Example of intramolecular-interaction foldamer made from a mixed N-centered C=O-centered BTA reported by Chen.[4] Foldamers are linear compounds that form supramolecular structures (fold) due to the intramolecular interactions, which have been installed. Foldamers are used as models helping to mimic and to simulate protein supramolecular structures.[3]

The group of Nuckolls pioneered the field of BTA-containing dimers reporting in 2003 the first example of a dimer linking two crowded BTA molecules (Scheme 3 and 4).[5]

Nuckolls employed aromatic and aliphatic types of 1,*n*-diamine derivatives, (Scheme 3), to form the connection between the two crowded arene units. Independently of the type of linker used, the dimers did not show intermolecular self-aggregation (Scheme 3).

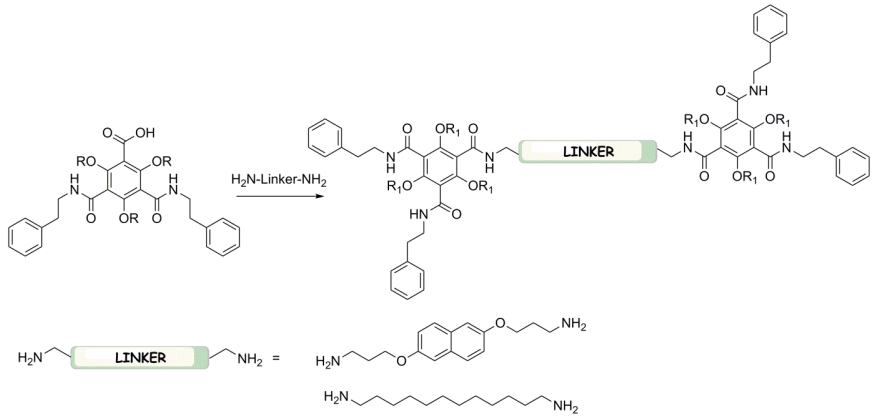

Scheme 3. Example of linearly linked crowded BTA reported by Nuckolls.[5]

When 1,8-napthalendiol or catechol were used as central element of the linker, the formation of a secondary structure attributed to strong intramolecular interactions between the two BTA units was observed (Scheme 4). The NMR analysis (concentration-induced ROESY and NOESY experiments) demonstrated the intramolecular nature of the H-bond interactions leading to the formation of foldamer aggregates.[5] No specific material properties were reported for those compounds.

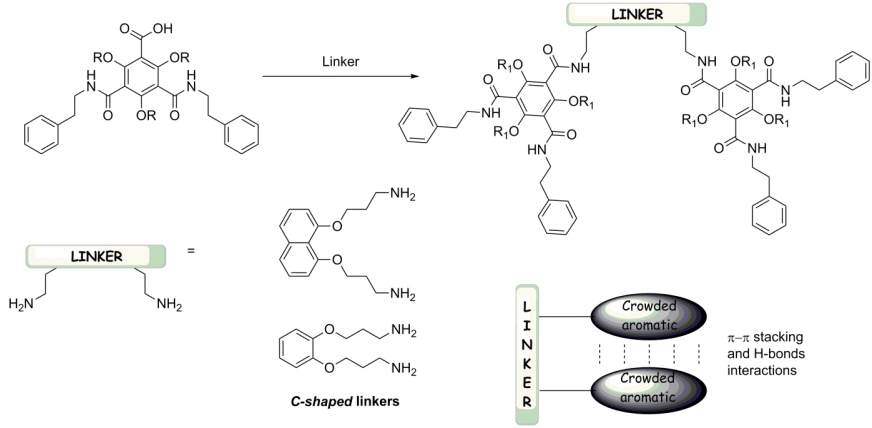

Scheme 4. Synthesis and schematic representation of "BTA-foldamer" reported by Nuckolls.[5]

The only example of 2-substituted BTA dimer reported in literature was published by Raymond.[6] The linking of the two BTAs units has been accomplished by coupling with an aliphatic diamine (Scheme 5). The goal of this work was to synthesize new structures capable of chelating Terbium ions obtaining luminescent metal-containing complexes. No mesophases were observed as expected because the N-methyl groups are too short for the formation liquid crystalline phases.

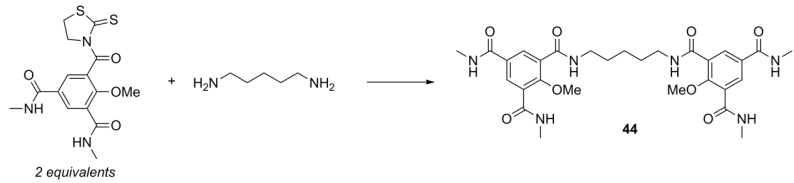

Scheme 5. Example of 2-substituted BTA dimer **44** reported by Raymond and employed into the formation of Tb-containing luminescent complexes.[6]

Small Library of BTA Dimers

The lack of literature precedents did not allow us to deduce in a rational approach the best design for the dimers needed in our project. We therefore choose empirically to test our design ideas and simultaneously to characterize their supramolecular structures. To complement the material properties data obtained from the synthesized dimers, we studied simpler model compounds, their structures and their association behaviour. We decided to construct a small library of dimers by varying the length of the linker and to observe *a posteriori* the material and aggregation properties. The general structure of the selected dimer structure is represented in Figure 1. The easy accessibility and modulation of terephthaloyl ester derivatives made this compound a perfect candidate on the screening of the length of the diazido-linker. In effect the design of the 2-pentynyloxy BTA **37b** was specifically carried out with the intent to employ the copper-catalyzed click-reaction to make dimers (see Scheme 3 on Chapter 2). Once the dimer structure is constructed, the aromatic central core of the terephthaloyl unit can be exploited as a probe to study the supramolecular self-assembly by measuring the concentration-induced NMR shifts.

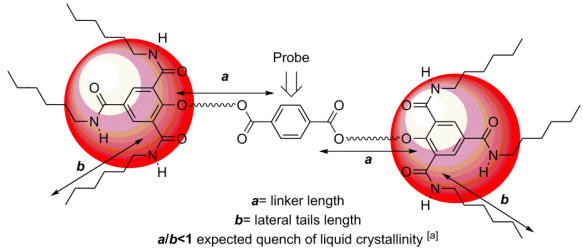

Figure 1. Schematic representation of the covalent linear dimer ***Dim***$_i$ of the BTA unit linked by an aromatic unit. [a] See Scheme 5 on Chapter 2.

Synthesis of the linkers and the BTA Dimers

A small series of diazido derivatives from the terephthaloyl acid unit, were firstly prepared (Scheme 6). The commercially available terephthaloyl chloride reacted with the *n*-bromo-alcohols (e.g. *n*= 2, 4 and 6), in the presence of a base such as trimethylamine furnishing the corresponding diester derivatives (Scheme 6). The dibromo-ester derivative **46** and the corresponding diazido derivative **47** were synthesized according to the procedure reported by June.[7] The corresponding homologs **48** and **50** (butyl and hexyl derivatives), not reported in literature, could be obtained using very similar

conditions. The esterification reaction employing the 6-bromo-1-hexanol formed the expected compound in an unsatisfactory yield of 8% probably due to the occurrence of side reactions on the bromo-alcohol.

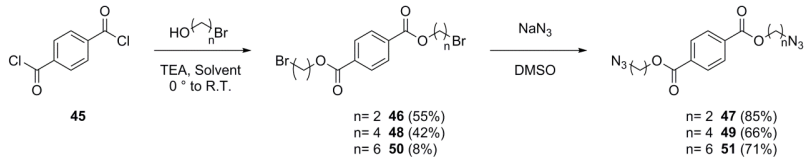

Scheme 6. Synthesis of the diazido linkers.

The small series of diazido derivatives **47**, **49** and **51** (Scheme 6) reacted under the standard copper-catalyzed azido-alkyne click chemistry.[8] In the case where the shortest diazido derivative **47** was employed, 0.2 equivalent of CuI was used as the source of copper (I). For longer diazido derivative **49** and **51** the 0.2 equivalent of the pre-catalyst copper sulfate were employed. In this case the active Cu(I) was generated by the in-situ reaction adding excess (0.6 equivalent) of the sodium salt of the ascorbic acid (the salt is used instead of the free acid for solubility reasons). For our transformation a mixture of THF and water is an effective solvent. The water is necessary to previously solubilize the salts. Both reagents are well soluble in THF.

The final dimers *Dim*$_1$ **52**, **53** and **54** were isolated in comparable and moderate non-optimized yields of 50%, 55% and 47% respectively (Scheme 7).

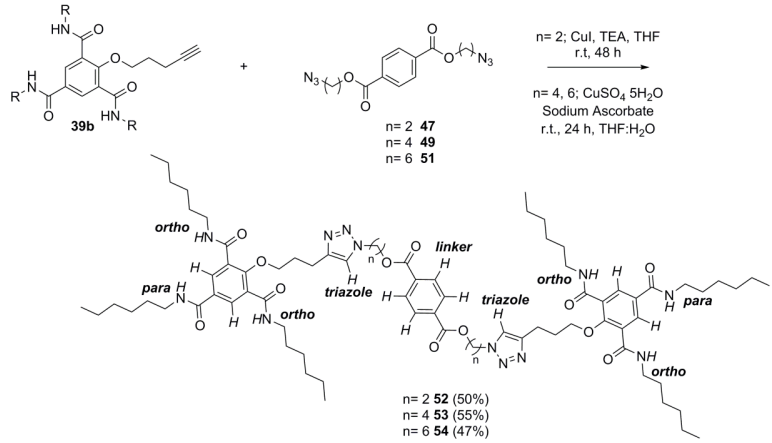

Scheme 7. Synthesis of dimers *Dim*$_1$ library by varying the length of the linker. The different types of protons are highlighted in bold.

Analyses of the Dimer's Properties

Analyses in the bulk

All three *Dim*$_i$ **52**, **53** and **54** were isolated as colorless solids, showing an amorphous aspect at room temperature. They were analyzed by means of polarized-light microscope POM. No indication of the occurrence of a liquid crystalline phase could be detected. The same unexpected results were observed when the three dimers were analyzed by differential scanning calorimetry DSC (Figure 2, 3 and 4). All samples showed a glass transition typical of amorphous solid at or around room temperature (Table 1). The highest temperature value for the glass transition was measured for the dimer **52**, where the short linker gives crystalline-like behaviors. Increasing the length of the linker (n= 4, **53**; n= 6, **54**) the temperature value of the glass transition decreased, probably due to a reduced crystallinity induced by the higher degree of freedom of the longer aliphatic linker.

Dim$_i$	Phase transition and temperature	Solid state
52	**I** 39.38 °C Glass transition	Amorphous solid
53	**I** 19.94 °C Glass transition	Amorphous solid
54	**I** 14.97 °C Glass transition	Amorphous solid

Table 1. DSC analyses of dimers *Dim*$_i$ **52**, **53** and **54**. The transition temperatures refer to the onset value measured on the 1st cooling cycle.

Combining the results obtained from the POM and the DSC analysis we conclude that the three dimers do not form columnar liquid crystalline phases. The absence of the liquid crystallinity is attributed to a lack of supramolecular organization. The strength of the intermolecular interaction in the dimer structures must be significantly smaller than the interactions in the monomer structures (e.g. **37b**). An analysis of the thermodynamic parameters of the self-assembly process in solution is needed to measure quantitatively the association constant of the dimer structures (**52**-**54**) and analyze the effects of the "dimerization" on the self-assembly process. Moreover, a comparison with the previously measured thermodynamics of the self-assembly process of the monomers **37b** and **42** could give important information and help in the process of the adequate design of the linker.

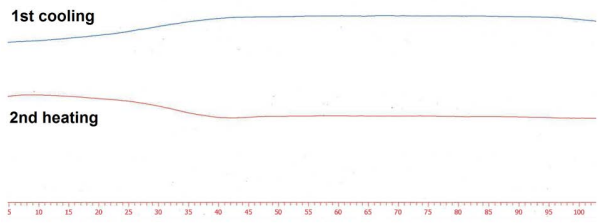

Figure 2. DSC curve (1st cooling cycle and 2nd heating cycle) of dimer **52**.

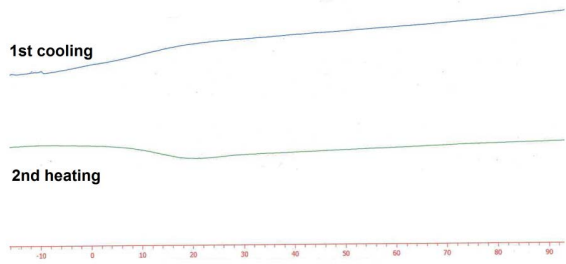

Figure 3. DSC curve (1st cooling cycle and 2nd heating cycle) of dimer **53**.

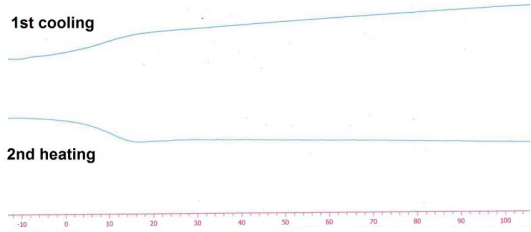

Figure 4. DSC curve (1st cooling cycle and 2nd heating cycle) of dimer **54**.

Solution analyses

Concentration-induced ^{1}H-NMR experiments

As for the concentration-induced NMR experiments of the monomeric BTA derivatives, d_2-dichloromethane (CD_2Cl_2) was chosen as the solvent in order to minimise the H-bond donor and acceptor effects from the use of other solvents (e.g. d_6-DMSO or $CDCl_3$). All three dimers *Dim*$_i$ **52**, **53** and **54** were analysed by ^{1}H NMR experiments. The chemical shift variation for concentration-induced ^{1}H-NMR experiments at 295 K was measured as a function of the concentration. The two distinct N-H signals were attributed to N-H$_{ortho}$ and N-H$_{para}$ (see the discussion of the NMR dilution experiments of **37b** and **41** on Chapter 5). The measured values of concentration-induced chemical shifts are summarized in Table 2 and the stacked spectra are reported in Figure 5, 6 and 7 respectively.

A downfield shift of N-H signals (both *ortho* and *para*) was observed by increasing the concentration for all three dimers due to the formation of strong intermolecular H-bonds. With no surprise we observed that the concentration induced shift of the N-H$_{para}$ protons was almost twice as big as the induced shift of the N-H$_{ortho}$ protons. As for BTA monomer (**45b**) we attributed these observations to the fact that N-H$_{ortho}$ forms intramolecular H-bonds. At the same time, the aromatic C-H protons of **52**, **53** and **54** shifted upfield, as a consequence of the $\pi-\pi$ stacking.

No significant shift was observed either for C-H aromatic protons of the triazole or the benzene (Table 2). None of the spectra of concentration-induced shift showed line broadening (Figure 5-7) meaning that all these observed self-assembly processes are in a fast exchange rate.

Dim_i	Δ[conc] (mmol/L)	Δδ N-H_{ortho} [a]	Δδ N-H_{para} [a]	Δδ C-H [a]	Δδ C-H_{linker} [a]	Δδ C-$H_{triazole}$ [a]
52 n=2	from 0.59 to 183	0.18	0.38	0.09	0.027	0.026
53 n=4	from 0.44 to 188.6	0.264	0.564	0.145	0.006	0.051
54 n=6	from 0.4 to 193.5	0.217	0.479	0.091	0.000	0.044

Table 2. Concentration-induced chemical shift variation at 295 K in CD_2Cl_2 at 400 MHz. [a] Measured in ppm. The size of the measured chemical shift variation in the dimer Dim_i molecules are compatible with the change of the shifts measured for the non-substituted BTA **42.**

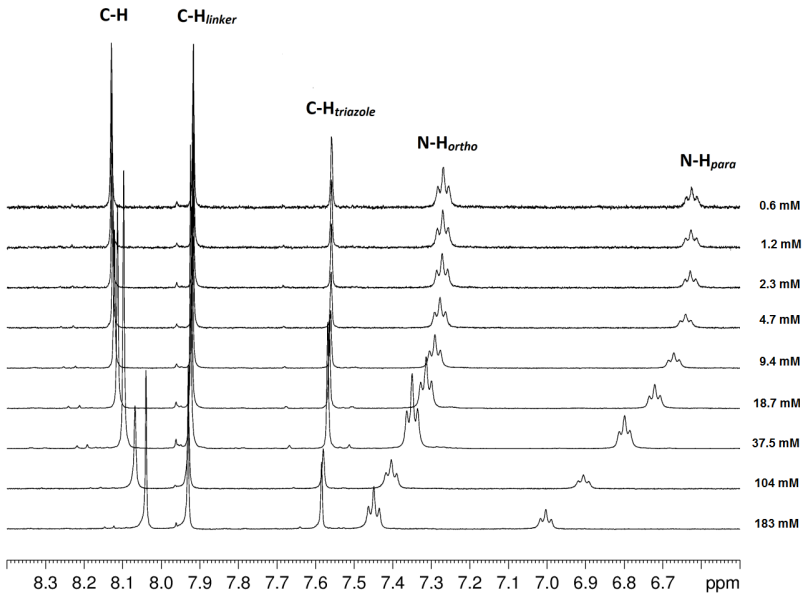

Figure 5. ^{1}H-NMR titration of **52** in CD_2Cl_2 at 295 K. The NMR spectra were measured by decreasing the concentration of **52** from 183 mM to 0.6 mM. In the figure only the aromatic region (8.4-6.5 ppm) is presented.

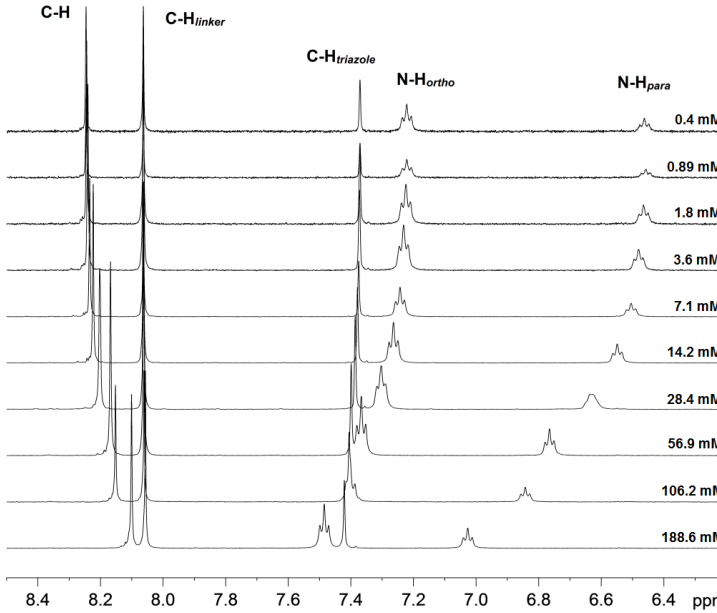

Figure 6. ^{1}H-NMR titration of **53** in CD_2Cl_2 at 295 K. The NMR spectra were measured by decreasing the concentration of **53** from 188.6 mM to 0.4 mM. In the figure only the aromatic region (8.4-6.5 ppm) is presented.

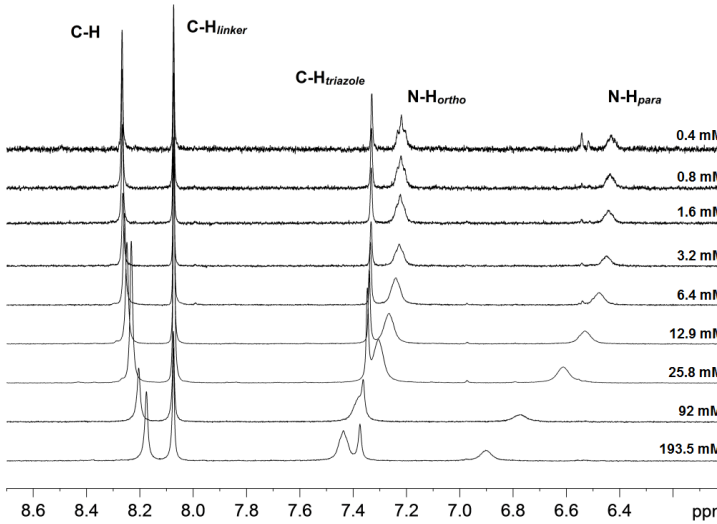

Figure 7. ^{1}H-NMR titration of **54** in CD_2Cl_2 at 295 K. The NMR spectra were measured by decreasing the concentration of **54** from 193.5 mM to 0.4 mM. In the figure only the aromatic region (8.6-6.4 ppm) is presented.

Aggregation analysis

Data fitting

The self-assembly process of the covalent linear dimers **52**-**54** (Dim_{mon}) forming the supramolecular aggregated species Dim_{agg} is a reversible process (Equation 1):

$$Dim_{mon} + Dim_{n-agg} \underset{k_{-i}}{\overset{k_i}{\rightleftarrows}} Dim_{n+1-agg} \qquad \textbf{(Equation 1)}$$

and the equilibrium constant (or association constant) can be calculated based on the Equation 2.

If this process is independent of the length of aggregate (n = any integer from 1 upwards) we describe an isodesmic process. If there are significant differences between the dimer formation (n = 1; nucleation) and the following aggregation steps (n > 2) we observe cooperative behavior.

$$K_a = \frac{[Dim_{n+1-agg}]}{[Dim_{mon}][Dim_{n-agg}]} = \frac{1}{K_d} = \frac{k_i}{k_{-i}} \qquad \textbf{(Equation 2)}$$

where Dim_{mon} is the covalent dimer **52**-**54** in the non-aggregated form; $Dim_{n+1-agg}$ is the aggregated form of the covalent dimer Dim_{mon} **52**-**54**, K_a and K_d are the association constant (M^{-1}) and dissociation constant (M) respectively.[9]

The association constants K_a were obtained, as for the BTA monomers in Figure 12, 13 and 14 Chapter 5, by fitting the plot of $\delta_{C\text{-}H}$ and $\delta_{N\text{-}H}$ vs. [*Dimer*] employing the following fitting equation:

$$\boldsymbol{\delta_{obs} = \delta_{Dim_{agg}} + \frac{\left(\delta_{Dim_{mon}} - \delta_{Dim_{agg}}\right)}{\left[1+\left(\frac{c}{K_d}\right)^p\right]}} \qquad \textbf{(Equation 3)}$$

where *c* is the total concentration, *p* is the slope factor of the fitting curve, K_d is the dissociation constant and δDim_{mon} δDim_{agg} are the extrapolated value of the chemical shift for the monomer species at infinite dilution and the chemical shift for the aggregate species obtained by extrapolation using the parameter obtained from the fitting program. The values of K_a (K_a (M^{-1}) = 1000/K_d (mM)) were measured independently for N-H_{ortho}, N-H_{para} and C-H protons for the three dimers according to the Equation 3 and are reported in Table 3.

Logistic [a]	**52** (n=2)			**53** (n=4)			**54** (n=6)		
parameters	N-H_{ortho}	N-H_{para}	C-H	N-H_{ortho}	N-H_{para}	C-H	N-H_{ortho}	N-H_{para}	C-H
K_d (mM)	37(2)	32(1)	47(3)	45(6)	44(7)	38(6)	26(1)	34(1)	28(2)
K_a (M^{-1})	27(1)	31(1)	21(1)	22(3)	23(4)	26(4)	38(1)	29(1)	36(3)
R^2	0.99923	0.99932	0.99949	0.99777	0.99659	0.99553	0.9998	0.99986	0.99921
p	1.43(8)	1.53(8)	1.50(8)	1.4(1)	1.4(2)	1.5(2)	1.46(4)	1.28(3)	1.43(8)
ΔG (kJ mol^{-1})	-8.1(1)	-8.4(1)	-7.5(2)	-7.6(3)	-7.7(9)	-8.0(8)	-9.0(1)	-8.3(7)	-8.8(6)
Isodesmic [b]									
K_a (M^{-1})	11(2)	12(3)	5(1)	9(2)	8(2)	10(3)	17(4)	13(2)	23(1)
R^2	0.99354	0.98979	0.99488	0.99373	0.99216	0.98227	0.99221	0.99687	0.9942
ΔG (kJ mol^{-1})	-5.9(5)	-6.1(6)	-4.8(3)	-5.4(6)	-5.1(6)	-5.7(8)	-7.0(6)	-6.3(4)	-7.7(1)

Table 3. Thermodynamics data (K_a, ΔG) calculated for **52**, **53** and **54** at 295 K. [a] Data calculated according to Equation 3. [b] Data calculated according to Equation 4.

Surprisingly, dimers **52**, **53** and **54** presented similar values for the association constant K_a (Table 3). A slightly smaller value of K_a was measured from the curve of dimer **53**. However, the differences in the calculated association constant were small. This observation is compatible with the hypothesis that the aggregation process of the three dimers is identical or at least very similar. The comparison of the values of K_a of the dimers **52**, **53** and **54** with the value of K_a measured for BTA **37b** is presented in Table 4. In effects, 2-pentynyloxy BTA **37b** presents the smallest association constant

compared to the other BTA monomers (e.g. **41** and **42**). The formation of covalent dimers increases the association constant of the three dimers **52**, **53** and **54** by about a factor of 5 to 6 times compared to the 2-pentynyloxy BTA **37b**. These results are in accordance with our initial hypothesis: the formation of dimeric structures stabilizes the formation of supramolecular aggregates.

	Monomer BTAs			Covalent dimers Dim_i		
parameters	**42**	**37b**	**41**	**52**	**53**	**54**
$K_a(M^{-1})^{[a]}$	29(4)	6(1)	125(6)	31(1)	23(4)	29(1)
$\Delta G(kJ\ mol^{-1})^{[a]}$	-8.3(1)	-4.3(4)	-11.8(1)	-8.4(1)	-7.7(9)	-8.3(7)

Table 4. Comparison of the thermodynamic data between BTAs monomers species and dimers Dim_i species. The table shows a comparison between the thermodynamics of the 2-substituted BTA derivatives (see also Chapter 5) and a comparison on the thermodynamics of the dimers Dim_{mon}. [a] The reported data refer to the value of K_a calculated on N-H$_{para}$ signals employing Equation 3 .

Analysis of the aggregation mechanism

The Hill factors *p* obtained from fitting of the curves are around 1.4 for the three studied compounds (Table 3). These values of *p* are clearly different from the value *p*= 1.0 deduced for the constitutive monomer (**37b**). According to the fact that the monomeric unit **37b** undergoes an isodesmic self-assembly (non-cooperative) the experimental data were also fitted with the equation simulating the isodesmic self-assembly (Equation 4) :

$$\boldsymbol{\delta_{Dim_{obs}} = \delta_{Dim_{mon}} + \left(\delta_{Dim_{agg}} - \delta_{Dim_{mon}}\right)\left(1 + \frac{1-\sqrt{4K_a+1}}{2K_a c}\right)} \qquad \textbf{(Equation 4)}$$

Fitting the experimental data with the equation describing the isodesmic self-assembly yielded association constants significantly different from those deduced using Equation 3 by logistic fitting (Table 3 and Figure 8, 9 and 10). The square of the correlation coefficient R^2 for both simulations are very near to 1.00 (> 0.99) meaning a consistent and valuable fitting process (Table 3). The calculated association constants are roughly two-times smaller than the one calculated by logistic fitting (Equation 3). The difference in calculated ΔG values is consistently around 2 kJ mol^{-1}. Based on the fitting of our data an unequivocal decision concerning the mechanism of the self-assembly process cannot be taken. A cooperative process is tentatively the preferred option.

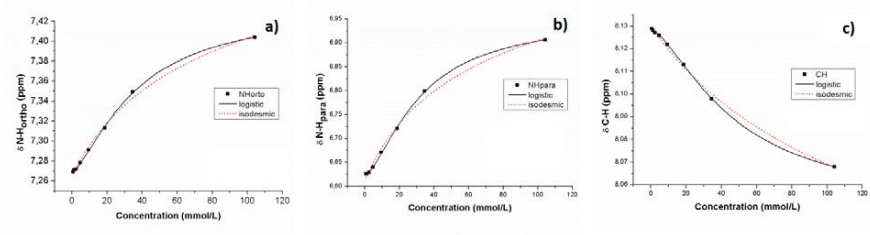

Figure 8. Fitting curves of the plot δ vs. [**52**]. a) Refers to N-H$_{ortho}$ protons. b) Refers to N-H$_{para}$ protons. c) Refers to C-H aromatic protons. Solid lines indicate fitting process according to the logistic fitting model (Equation 3). Dashed lines indicate fitting process according to the isodesmic fitting model (Equation 4).

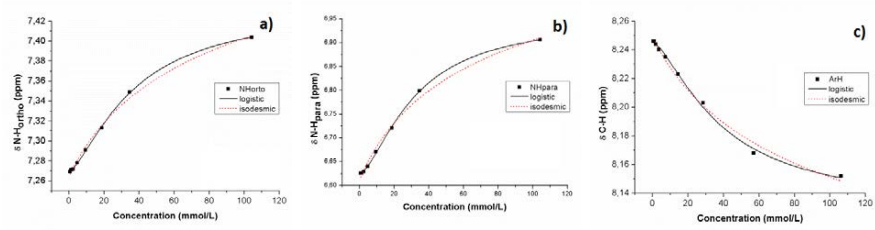

Figure 9. Fitting curves of the plot δ vs. [**53**]. a) Refers to N-H_{ortho} protons. b) Refers to N-H_{para} protons. c) Refers to C-H aromatic protons. Solid lines indicate fitting process according to the logistic fitting model (Equation 3). Dashed lines indicate fitting process according to the isodesmic fitting model (Equation 4).

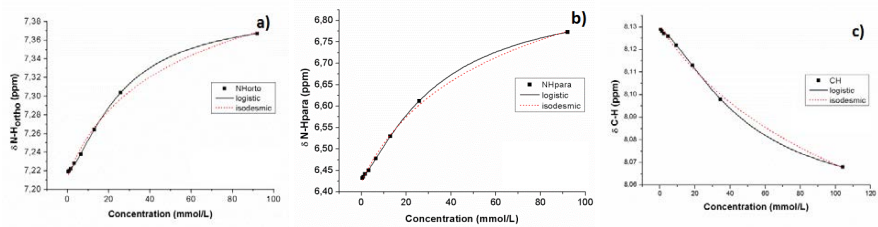

Figure 10. Fitting curves of the plot δ vs. [**54**]. a) Refers to N-H_{ortho} protons. b) Refers to N-H_{para} protons. c) Refers to C-H aromatic protons. Solid lines indicate fitting process according to the logistic fitting model (Equation 3). Dashed lines indicate fitting process according to the isodesmic fitting model (Equation 4).

The relative flexible nature of the linkers could potentially allow the formation of intermolecular interactions, generating a sort of foldamer-like structure, as previously reported by Nuckolls (Scheme 4).[5] However, our concentration-induced NMR experiments exclude the formation foldamer structures. Indeed the shift we observed in our experiments is exclusively due to intermolecular interactions as shown by the concentration dependence.

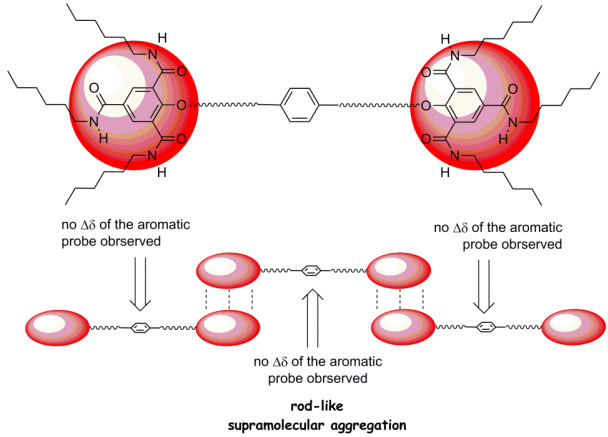

Figure 11. Proposed structure of the supramolecular aggregate. The homoditopic dimers self-assembly according to a head-to-head mechanism.

The induced shift variation was observed exclusively for the N-H (ortho and para) and C-H aromatic protons of the BTA core. Neither the C-H aromatic protons of the benzene linker nor the triazole units showed significant concentration dependent shifts. A supramolecular aggregation of our dimers following a nematic-like head-to-head aggregation mechanism is compatible with all our observations (Figure 11).

The X-ray crystal structures of the model 2-pentynyloxy BTA **37a** and of the s model BTA **1** support this hypothesis. According to the Lightfoot's model (Figure 2 in Chapter 1), the BTA's are slightly displaced and turned by 60° when moving along the column axis. If we suppose an ideal columnar-like supramolecular aggregation (Scheme 2 in Chapter 2), the BTA units cannot displace of 60° due to the rigidity imposed by the linker. On the other hand, we observed from the X-ray structure of the model compound **37a** that the pentynyloxy groups are oriented in "antiperiplanar" position in the BTA units that form the sheet dimer (Figure 12). On this way the amide groups are displaced by 60° and the stacking is perfectly allowed.

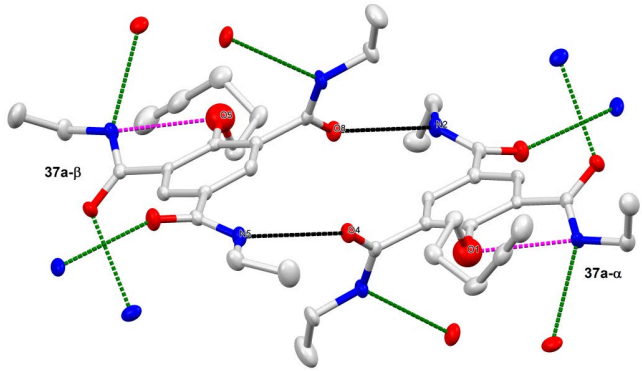

Figure 12. X-ray structure of the "antiperiplanar" sheet-forming unit of the 2-pentynyloxy BTA **37a** (**37a-α** and **37a-β**). Oxygen atoms are colored in red whereas nitrogen atoms are colored in blue. The oxygen atoms of the pentynyloxy groups (O1 and O5) are highlighted as balls. The magenta dashed lines indicate intramolecular H-bonds, black dashed lines indicate intermolecular H-bonds forming the sheet unit and dark green dashed lines indicate intermolecular H-bonds forming the bifurcation (see Figure 5 in Chapter 5).

Due to the lack literature precedence reporting BTA dimers, we cannot rely on established knowledge. The example, reported by the Meijer's group introducing a block copolymer diamine derivative (Kraton bisamine) may give hints to interpret our results (see Scheme 1). Meijer et. coll. observed the formation of nematic liquid crystalline phases in **43** without reporting information on the thermodynamics of the self-assembly process.

Combining our experimental results on the concentration-induced NMR experiments in diluted solution and the crystallography data, we conclude that the synthesized dimers probably are aggregated in a rod-like fashion. However this supramolecular arrangement is not strong enough or not ordered enough to lead to a liquid crystalline behavior of the material. The size of the association constant and the size of the free enthalpy characterizing the association process driven by the H-bonding are bigger than those values reported for the compound **37b** and slightly smaller than those values reported for compound **41** in Chapter 5. Both compound **37b** and **41** show mesomorph behavior. Our results clearly show that the occurrence of mesomorph phases is not exclusively a

consequence of the strength of the intermolecular bonding, but depends crucially on the geometric restrictions imposed by the formation of a long-range order.

Concentration-induced DOSY experiments

The diffusion coefficient of all the three dimers *Dim*$_i$ **52**, **53** and **54** increased (slightly) as a function of the concentration (Figure 13, 14 and 15). These results indicate an enhancement of the molecular weight, consistent with the formation of supramolecular aggregates.
The observed chemical shift (δ_{obs}) is the weighted average of the chemical shifts of the monomer species (δ_{mon}) and the aggregated species (δ_{agg}) according to Equation 5:

$$\delta_{obs} = \delta_{mon}\chi_{mon} + \delta_{agg}\chi_{agg} \qquad \textbf{(Equation 5)}$$

Similarly, the observed diffusion coefficient (D_{obs}) is the weighted average of the diffusion coefficient of the monomer (D_{mon}) and the aggregated (D_{agg}) species respectively, according to the Equation 5:

$$D_{obs} = D_{mon}\chi_{mon} + D_{agg}\chi_{agg} \qquad \textbf{(Equation 6)}$$

The limiting values of δ_{mon} and δ_{agg} could be extrapolated from the experimental curve fitting (Figure 8, 9 and 10). Assuming the complete aggregation (χ_{agg}=1) and the complete disaggregation (χ_{mon}=1) at the two limits of the fitting curves, an estimation of the ratio (molar fraction χ) of the aggregate and the monomer species can be obtained for the measured points (Table 5).

	52				**53**			**54**			
c[a]	183[d]	37.47	4.68	0.58	56.9	7.11	0.44	193.5[d]	25.79	6.44	0.4
D[b]	-9.487	-9.322	-9.205	-9.164	-9.404	-9.225	-9.177	-9.535	-9.315	-9.301	-9.177
χ_{agg} [c]	//[d]	0.559	0.049	0.002	0.607	0.087	0.003	//[d]	0.4148	0.107	0.0015

Table 5. Measured diffusion values *D* for the dimers **52**, **53** and **54** at 295 K. [a] Concentration (mmol/L). [b] Diffusion coefficient (log m^2s^{-1}). [c] Molar fraction of the aggregated species calculated using the N-Hpara protons as sensor. [d] These values were not taken into account in the fitting process. Due to the high concentration, they probably aggregate on the walls of the NMR tubes and the fitting process carried out including those values resulted in inconsistencies.

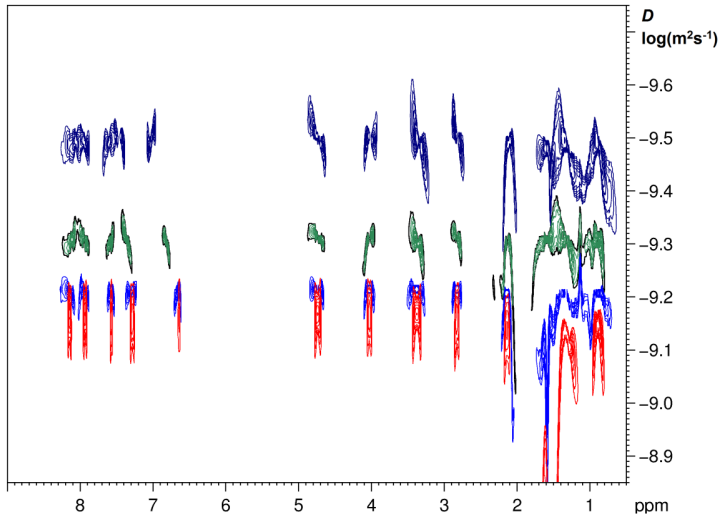

Figure 13. ^{1}H 2D-DOSY of **52** in CD_2Cl_2 at 295 K. Dark blue) at 183 mM, green) at 37 mM, blue) at 4.7 mM andred) at 0.6 mM. When the supramolecular structure is formed (dark blue trace) the diffusion is slower indicating an increased molecular weight (aggregated species).

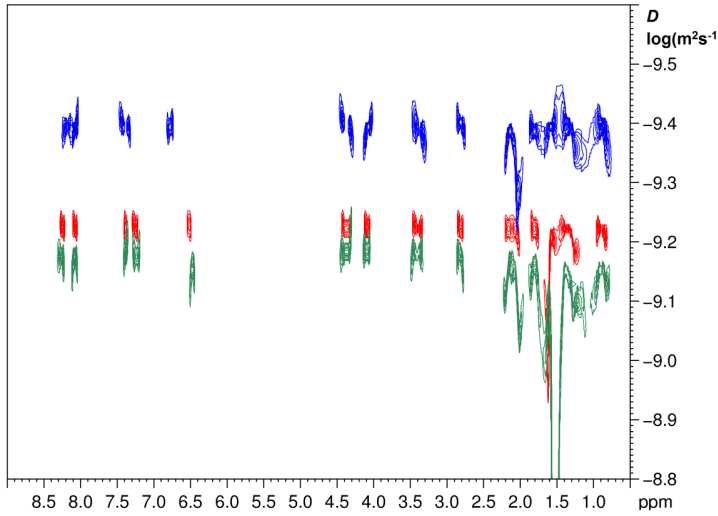

Figure 14. ^{1}H 2D-DOSY of **53** in CD_2Cl_2 at 295 K. Blue) at 57 mM, red) at 7 mM and in green) at 0.4 mM. When the supramolecular structure is formed (blue trace) the diffusion is slower indicating an increased molecular weight (aggregated species).

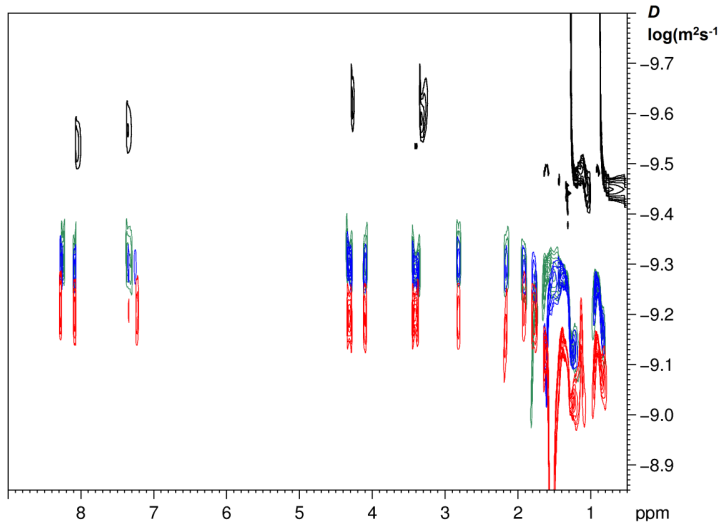

Figure 15. ^{1}H 2D-DOSY of **54** in CD_2Cl_2 at 295 K. Black) at 193 mM, green) at 26 mM, blue) at 9.3 mM and red) at 0.18 mM. When the supramolecular structure is formed (black trace) the diffusion is slower indicating an increased molecular weight (aggregated species).

In conclusion, the use of the concentration-induced DOSY experiments enables us to clearly show the formation of aggregated structures occurring due to self-assembly processes on the three synthesized covalent dimers **52**-**54**.

Concluding Remarks

The synthesis of the small library of covalent dimers was accomplished employing copper-catalyzed click chemistry. The dimers were obtained in acceptable yields (47-55%). Surprisingly, we found out that the "covalent dimerization" inhibits the formation of the columnar liquid crystalline phases. The measured free energy of the self-assembly process for the dimeric structures indicated a higher energy gain for the aggregation process compared with respect the monomeric 2-pentynyloxy BTA **37b**. The strength of the supramolecular aggregation is practically independent on the length of the linker. In accordance with our concentration-induced NMR study and comparing with the literature precedents, we hypothesized that our dimers prefer a nematic-like head-to-head supramolecular aggregation. The challenge of the liquid crystalline phase formation has to be tackled by modifying the rigidity of the linker in order to achieve a columnar-like organization. The amide side chains of the BTA unit are able to fill the empty space left from such long linkers. To optimize all elements we decided to empirically vary the different elements establishing a structure-properties relationship.

References

[1] J. Roosma, T. Mes, P. Leclere, A. R. A. Palmans, E. W. Meijer, *J. Am. Chem. Soc.* **2008**, *130*, 1120-1121.

[2] a) S. C. Suh, S. C. Shim, *Synth. Met.* **2000**, *114*, 91-95; b) H. Kautz, D. J. M. van Beek, R. P. Sijbesma, E. W. Meijer, *Macromolecules* **2006**, *39*, 4265-4267.

[3] a) R. P. Cheng, S. H. Gellman, W. F. DeGrado, *Chem. Rev.* **2001**, *101*, 3219-3232; b) D. J. Hill, M. J. Mio, R. B. Prince, T. S. Hughes, J. S. Moore, *Chem. Rev.* **2001**, *101*, 3893-4011; c) D. Seebach, A. K. Beck, M. Rueping, J. V. Schreiber, H. Sellner, *Chimia* **2001**, *55*, 98-103.

[4] Z. Chen, N. D. Urban, Y. Gao, W. Zhang, J. Deng, J. Zhu, X. C. Zeng, B. Gong, *Org. Lett.* **2011**, *13*, 4008-4011.

[5] W. Zhang, D. Horoszewski, J. Decatur, C. Nuckolls, *J. Am. Chem. Soc.* **2003**, *125*, 4870-4873.

[6] A. P. S. Samuel, J. Xu, K. N. Raymond, *Inorg. Chem.* **2009**, *48*, 687-698.

[7] S. M. June, P. Bissel, T. E. Long, *J. Polym. Sci., Part A: Polym. Chem.* **2012**, *50*, 3797-3805.

[8] a) H. C. Kolb, M. G. Finn, K. B. Sharpless, *Angew. Chem., Int. Ed.* **2001**, *40*, 2004-2021; b) V. V. Rostovtsev, L. G. Green, V. V. Fokin, K. B. Sharpless, *Angew. Chem., Int. Ed.* **2002**, *41*, 2596-2599; c) C. W. Tornoe, C. Christensen, M. Meldal, *J. Org. Chem.* **2002**, *67*, 3057-3064.

[9] For a complete analysis of the aggregation process, see chapter 4

BTA Dimers (Part II): Structure-Properties Relationships

Table of Contents

Our studies on the self-assembly of 2-substituted BTAs derivatives allowed us to gain insight on the thermodynamics and part of the mechanistic aspects of the supramolecular aggregation of 2-substituited BTA monomers (see Chapter 5). The analysis of the thermodynamics was then extended to the dimeric structures (**52**, **53** and **54**). The association constant and the free energy ΔG of the dimers were considerably larger than the values observed for the corresponding monomers; however no liquid crystallinity could be observed. With our dimers we achieved the task to increase the strength of the self-assembly process but we failed in obtaining a supramolecular assembly giving a mesophase. In order to shed light on this dichotomy, we decided to screen the structural parameters of the dimeric molecule hoping to solve this enigma. Since the discovery of the liquid crystals, chemists tried to figure out rules on how to get mesophases,[1] however an empirical approach is in most case still inevitable.

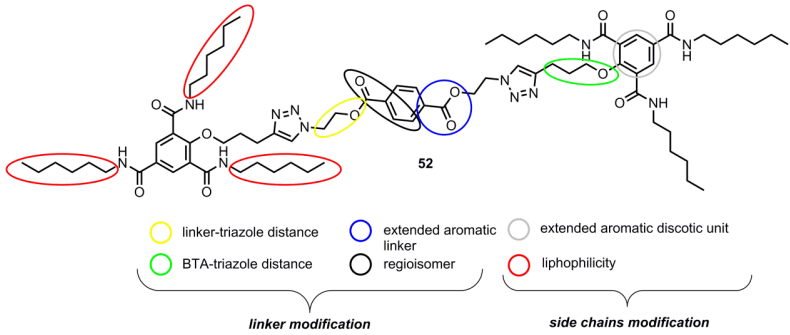

Figure 1. Schematic overview of the proposed structural modifications on **52**.

Our screening approach uses the shortest dimer **52** as the starting point to formulate rational and systematic modifications of the dimeric scaffold in order to be able to construct a structure-properties relationship (Figure 1). We identified two reasonably different approaches:

- ✓ Modification of the linker
- ✓ Modification of the side chains

In Chapter 6, we demonstrated that the length of the linker (linker-triazole distance, Figure 1 yellow) does not play a fundamental rule on the thermodynamics of the self-assembly strength of our dimers **52**-**54**. Therefore we envisaged modifications that provide variation on the rigidity-flexibility and on the geometry of the resulting dimeric structure. On the other hand, the fact that side chains play a fundamental role on the supramolecular association of BTA derivatives has been well established (see Figure 11 Chapter 1). For this reason, a second type of approach envisages modification on the side chains of the monomer BTA derivatives with the intent to impose liquid crystallinity to the resulting dimer.

Linker Modifications

Aromatic Linker (Employment of 1,4-bis(5-azidopent-1-yn-1-yl)-2,5-difluorobenzene)

We observed in Chapter 6 that the π-interactions between the aromatic rings of the linker are absent or very weak in compound **52**, **53** and **54** connected aromatic ester linkers. We focused our first modification on the stabilization of the columnar organization by enhancing the intermolecular interactions of the aromatic core present in the linkers. This following modification aimed to enhance the aromatic linker interaction as an indirect strategy to stabilize the columnar organization of the discotic units. We decided to extend the planarity and the stiffness of the benzene central core by connecting the spacer alkyl chain using planar alkyne groups (Figure 2). The dialkyne groups in 1,4-positions could be easily introduced starting from a 1,4-dibromo benzene derivative. The introduction of alkyne groups increases the rigidity and the stiffness of the linker reducing the possibility that the mesogenic units (BTAs) interact intramolecularly forming a sort of foldamer structure (see Scheme 4 Chapter 6).

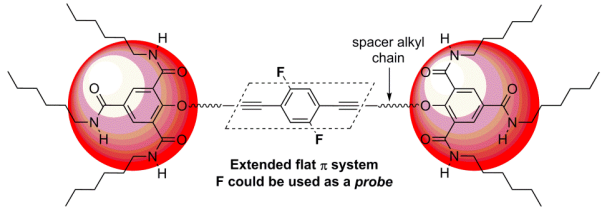

Figure 2. Representation of the extended flat π-system of 1,4-dialkyne benzene derivative. The enhanced planarity should facilitate the interactions between the central aromatic linkers stabilizing the columnar stack of the BTA units.

The synthesis of 1,4-dialkyne benzene derivative was carried out employing a double Sonogashira cross-coupling reaction[2] between 4-pentyne-1-ol on 2,6-difluoro-1,4-dibromobenze **55**. This fluorinated substrate was chosen because ^{19}F is a NMR active nuclei and it is known to be very sensitive toward structural modification and it could be used as probe capable of measuring the occurrence of the self-aggregation process.[3]

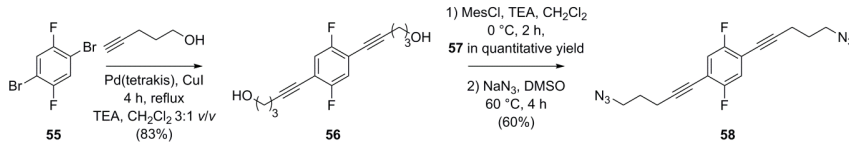

Scheme 1. Synthesis of the fluorinated 1,4-dialkyne benzene derivative **58**.

The reaction was carried out adapting the conditions reported by Ueda *et al*. to our fluorinated substrate (Schem 1).[4] The diol **56** was isolated in a very good yield for the double cross coupling reaction. The product was crystalized by slow evaporation from $CDCl_3$. The solid state structure determined by X-ray diffraction indicated a staggered packing of the aromatic rings which are in π-π

stacking distance (Figure 3). The planes of the aromatic rings are tilted by 18.08° between next neighbours. The mesured short intering distances is compatible with the formation of strong π–π stacking (~3.6 Å, Figure 3). The X-ray diffraction analysis of the crystal clearly demonstrates the presence of the π-π stacking interactions in our dialkyne linker. Unfortunately we cannot quantify these intermolecular interactions. We do not know the relative importance of the π-π stacking compared to the H-bonding.

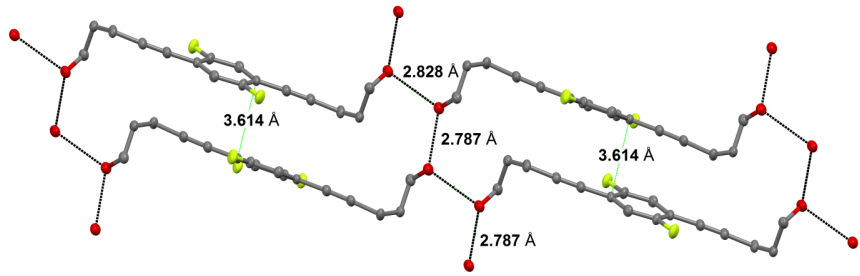

Figure 3. X-ray of the crystal packing of **56**. The structure indicates short interring distance compatible with strong π–π stacking formation (light green dashed lines). Black dashed lines indicate the formation of intermolecular H-bond.

The conversion of the primary alcohol to the azido group was achived by transformaiton of the alcohol to the mesylate **57**, followed by nucleophylic displacment with sodium azide (Scheme 1). The diazido **58** was treated with two equivalents of the 2-alkoxynyl BTA derivative **37b** under the well-established "click conditions" (e.g. copper sulfate and sodium ascorbate). The dimer **59** was obtained in a non-optimized yield of 35% and then analyzed in the bulk by means of POM and DSC analyses.

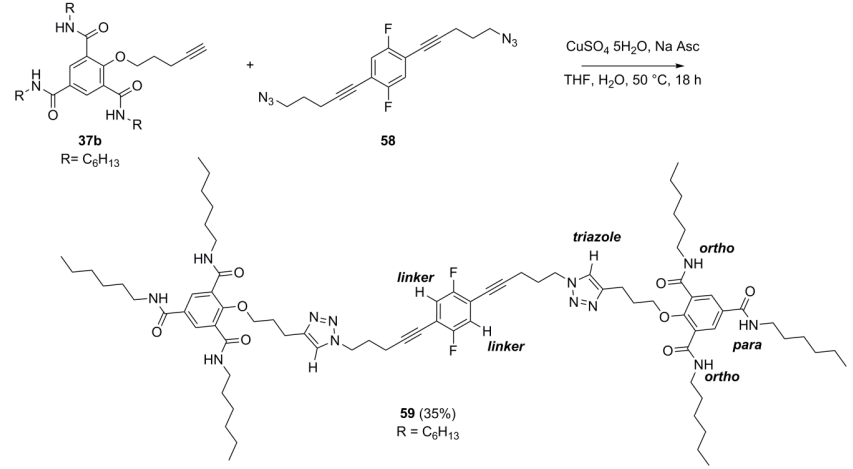

Scheme 2. Synthesis of rigid dimer **59** by using a fluorinated aromatic linker.

Analyses in the bulk (POM and DSC)

When the dimer **59** was analyzed by means of POM, no typical textures of columnar liquid crystals were observed. The DSC thermal analysis carried out on **59** confirmed the absence of mesophase formation. A glass phase transition, typical of amorphous solids, was measured at 23.4 °C at the first cooling cycles (Table 1 and Figure 4).

Compound	Linker type	Phase transition and temperature	Solid state
59	rigid	**I** 23.41 °C Glass transition	Amorphous solid

Table 1. Thermal analyses of dimer **59**. No mesophases were observed for both synthesized derivatives.

In analogy with the dimers **52**-**54**, the analysis of the thermodynamics of the association process of **59** in solution was needed to characterize the aggregation behavior.

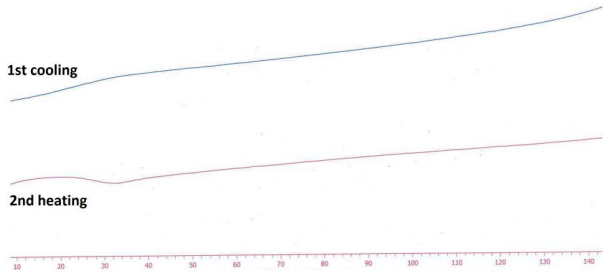

Figure 4. DSC curve (1st cooling cycle and 2nd heating cycle) of dimer **59**.

Solution analyses

Concentration-induced ^{1}H NMR experiments

The aggregation process was studied by concentration dependent NMR measurements in d_2-dichloromethane (see pages 86 and 87 Chapter 6). The NMR spectra were recorded at 295 K (Figure 5). The two distinct N-H signals were attributed to N-H$_{ortho}$ and N-H$_{para}$ as for the dimers **52**-**54.** Table 2 lists the values of the concentration-induced chemical shift measured for **59**. A downfield shift of N-H signals (both for the *ortho* and *para* protons) was observed by increasing the concentration from 0.5 mM to 184 mM. This shift is attributed to the formation of strong intermolecular H-bonds interactions. As in the previous cases, the N-H$_{para}$ protons shifted (measured in ppm) almost twice as much as the respective N-H$_{ortho}$ protons. The C-H aromatic protons of **59** shifted upfield as the consequence of the increased π–π stacking interactions. As in the cases of the dimers **52**, **53** and **54** reported in Chapter 6, neither significant concentration-induced shift variations of the C-H$_{linker}$ nor on the ^{19}F were observed. Combining these observations with the absence of mesophases, we can conclude the occurrence of a head-to-head nature of the supramolecular aggregation (see Figure 11 Chapter 6).

Dimer	Δ[**59**][a]	Δδ N-H$_{ortho}$[b]	Δδ N-H$_{para}$[b]	Δδ C-H[b]	Δδ C-H$_{linker}$[b]	Δδ C-H$_{triazole}$[b]	Δδ F[b]
59	from 0.5 to 184	0.266	0.572	0.128	0.002	0.048	0.052

Table 2. Concentration-induced chemical shift variation of **59** at 295 K in CD_2Cl_2 at 400 MHz. [a] mmol/L. [b] ppm.

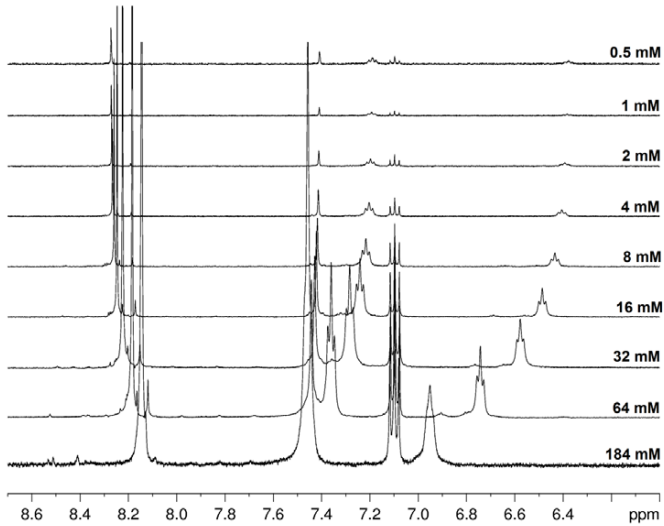

Figure 5. ^{1}H-NMR titration of **59** in CD_2Cl_2 at 295 K. The NMR spectra were measured by decreasing the concentration of **59** from 184 mM to 0.5 mM. In the figure only the aromatic region (8.6-6.4 ppm) is presented.

Data analysis

The analysis of the supramolecular aggregation of dimer **59** was carried out using the same fitting equations (Equation 3 and 4) used for the analysis of dimers **52**-**54** in Chapter 6. The association constants K_a were obtained by fitting the plot of $\delta_{C\text{-}H}$ and $\delta_{N\text{-}H}$ vs. [*Dimer*].

Logistic[a]	Dimer **59**		
parameters	N-H$_{ortho}$	N-H$_{para}$	C-H
K_d (mM)	69(12)	71(10)	52(5)
K_a (M^{-1})	14(3)	14(2)	19(1)
R^2	0.99649	0.9978	0.99743
p	1.2(1)	1.2(1)	1.4(1)
Temperature (K)	295.15	295.15	295.15
ΔG (kJ mol^{-1})	-6.6(4)	-6.5(4)	-7.5(2)
Isodesmic[b]			
K_a (M^{-1})	7(1)	7(1)	9(2)
R^2	0.99405	0.99532	0.98971
ΔG (kJ mol^{-1})	-4.8(4)	-4.8(4)	-5.4(6)

Table 3. Thermodynamics data (K_a, ΔG) calculated for **59**. [a] Data calculated according to Equation 3 in Chapter 6. [b] Data calculated according to Equation 4 in Chapter 6.

The values of K_a (K_a= 1000/K_d) were calculated independently for N-H$_{ortho}$, N-H$_{para}$ and C-H aromatic protons. According to the logistic fitting equation (Equation 3, Chapter 6), the fluorinated dimer **59** presented a higher association constant with respect to the monomer unit (2-pentynyloxy BTA **37b**) by a factor of 2 (Table 4), but smaller when compared to the ester-linked dimers **52**, **53** and **54** by a factor of 2 as well (Table 4).

BTA	59	37b	52	53	54
K_d (mM)[a]	71(10)	176(30)	32(1)	44(7)	34(1)
K_a(M^{-1})[a]	14(2)	6(1)	31(1)	23(4)	29(1)
ΔG(kJ mol^{-1})[a]	-6.5(4)	-4.3(4)	-8.4(1)	-7.7(9)	-8.3(7)
p[a]	1.2(1)	0.94(3)	1.53(8)	1.4(2)	1.28(3)

Table 4. Comparison of the thermodynamic data between monomers and dimers calculated according to the logistic fitting equation (Equation 3, Chapter 6). **[a]** The data refers to the N-H_{para} signals. A cooperative process is tentatively the preferred option.

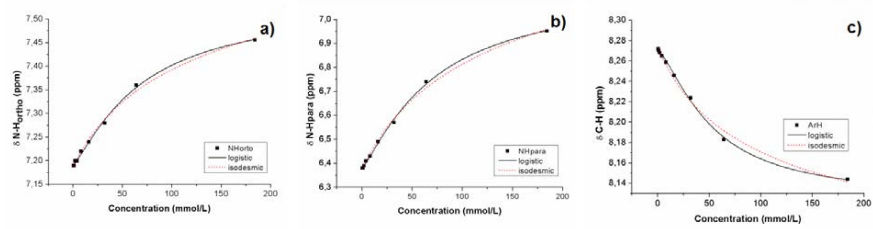

Figure 6. Fitting curves of the plot δ vs. [**59**]. a) Refers to N-H_{ortho} protons. b) Refers to N-H_{para} protons. c) Refers to C-H aromatic protons. Solid lines indicate fitting process according to the logistic fitting model (Equation 3, Chapter 6). Dashed lines indicate fitting process according to the isodesmic fitting model (Equation 4, Chapter 6).

Analysis of the Mechanism

The curves, obtained using the logistic fitting equation (Equation 3 in Chapter 6), provided a slop factor *p* slightly bigger than the value of 1.0 (Table 3). These values are compatible with the absence of cooperativity (*p*= 1). In order to confirm the occurrence of the isodesmic aggregation model on the self-assembly process of **59**, we simulated the experimental data applying the isodesmic model (Equation 4 Chapter 6) (Figure 6a, b and c). The isodesmic curve consistently simulated the experimental data (R^2 >0.99); however the obtained value of K_a were significantly different from the values obtained from the logistic fitting equation (Table 3). As in the previous case of the dimers **52**-**54**, the data can be fitted with both models for the supramolecular aggregation mechanism for **59**. We tend to prefer the data obtained through the logistic fitting showing a moderate cooperativity (small difference between nucleation and oligomerization).

In conclusion, the use of a flat and stiffer linker did not lead to the wanted columnar-aggregation of the dimer derivative **59**. The free energy of the supramolecular association process measured for molecule **59** is less favorable than free energy measured for the ester-connected dimers **52**-**54**. Moreover, the absence of concentration-induced shift of the aromatic linker core is once again compatible with the occurrence of a rod-like aggregation mechanism.

Flexible linker (Employment of 1,4-bis(2-azidoethoxy)benzene)

In the previous case of **59**, we observed that the more rigid linker did not lead to a columnar organization of the dimer structure. Moreover a reduction of the association constant, with respect to the ester-linked dimers **52**-**54**, was measured for **59**. We decided to test electronic effects employing an electron rich hydroquinone-type linker where the stiff alkyne moiety was replaced by a short, flexible chain (Scheme 3).

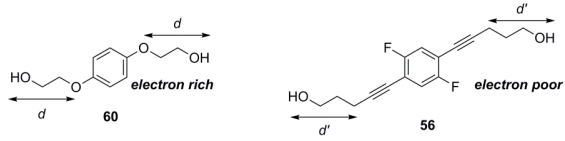

Scheme 3. Schematic representation of the short electron rich hydroquinone-type linker **60**. The length of the flexible part in both linkers is similar (*d* ~ *d'*).

The hydroquinone-type linker was synthesized according the procedure reported by Beer (Scheme 4).[5]

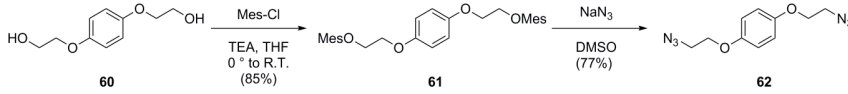

Scheme 4. Synthesis of the hydroquinone-type linker **62** according to the procedure reported by Beer.[5]

The dimer **63** was synthesized using CuI as the source of the active Cu(I) species in anhydrous and degassed reaction conditions to afford **63** in 55% (Scheme 5).

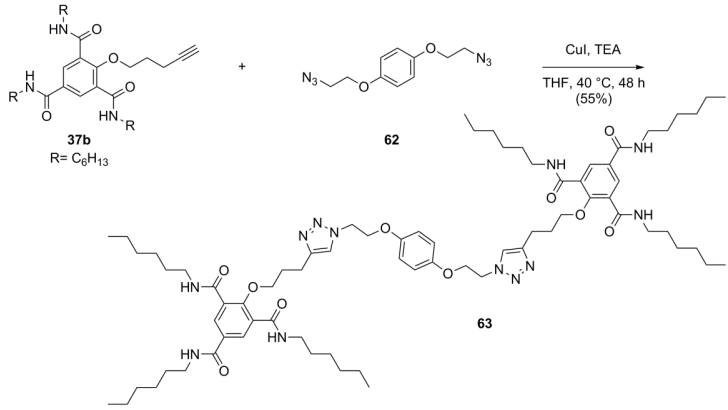

Scheme 5. Synthesis of the dimer **63**.

The dimeric compound presented a similar glass-like aspect as the other synthesized dimers **52**-**54** and **59**.

POM and DSC analyses

Polarized-light microscope analysis did not show the formation of textures indicating the absence of columnar or other types of mesophases.
The DSC analysis run on **63** indicated only a glass transition at 31.56 °C characteristic of the presence of amorphous solids (Table 5).

Dimer	Linker type	Phase transition and temperature	Solid state
63	flexible	**I** 31.56 °C Glass transition	Amorphous solid

Table 5. Thermal analyses of dimer **63**. No mesophases were observed for both synthesized derivatives.

Despite the fact the molecular weight of **63** is smaller than **59**, the temperature value of the measured glass transition of this dimeric structure is higher than the glass transition measured for dimer **59**. This means that the intermolecular interactions between molecules in the neat compound are stronger when this electron rich hydroquinone-type linker is incorporated. If bigger intermolecular interactions between the molecules has to be achieved the hydroquinone-type linker should be preferred compared to the ester-connected linkers.

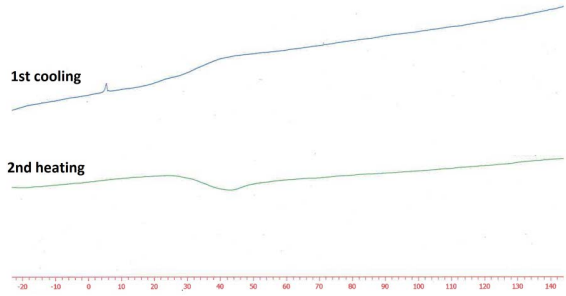

Figure 7. DSC curve (1st cooling cycle and 2nd heating cycle) of dimer **63**.

Modification of the linker regiochemistry (Employment of bis(2-azidoethyl) terephthalate)

The use of 1,4-disubstituted aromatic ring as central element of the linker structure allows the construction linear dimers. Replacing the para substituted benzene by a 1,3-disubstituted benzene ring could induce the formation of bended dimers (Scheme 6). For example, Kumar synthesized a series of triphenylene dimers connected by the isophthaloyl unit. They observed a inhibition of the liquid crystallinity of the monomers when connected by a 1,3-linking unit.[6]

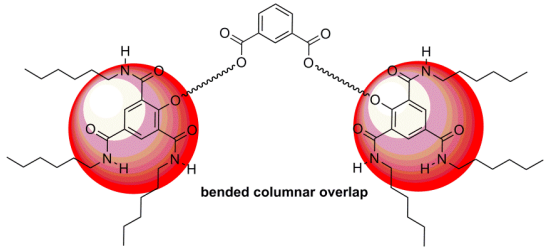

Scheme 6. Structure of the bended BTA dimer.

According to our working hypothesis the 2-pentynloxy substituted BTAs prefer to aggregate in a linear ("antiperplanar") mode, thereby hampering the formation of a liquid crystalline phase (Figure 12 in Chapter 6). Forcing the dimer out of linearity it should destabilize the linear aggregation modes. As a correlate the columnar self-assembly might then become favored rather than the head-to-head assembly observed when linear linkers (linear dimers induced by 1,4-aromatic derivatives) are used.
Nuckolls reported the induction of strong intramolecular interactions in crowded arene dimers when a 1,2-dihydroxybenzene units (pyrocatechol) or 1,8-dixydroxynapthalene units were used as central elements of the linker (Scheme 2 Chapter 6). Our goal is to avoid intramolecular interactions as we would expect using phthalic acid derivatives. We therefore tested the 1,3-connecting units (isophthaloyl) as linkers for the dimerization of BTA (Scheme 6).
The bended diazido isophthaloyl linker derivative **66** was synthesized by a modification of the procedure reported by June.[7] Commercially available isophthaloyl chloride **64** reacted with 2-bromoethanol followed by a double nucleophilic displacement of the bromine by sodium azide in DMSO (Scheme 7).

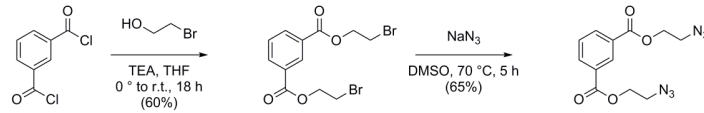

Scheme 7. Synthesis of 1,3-regioisomer spacer **66** (isophthalic derivative).[7]

The double click reaction was carried out according to the well-established methodology to furnish the bended dimer **67** in moderate yield of 32% (Scheme 8). Interestingly, the dimer **67** was isolated as a yellowish liquid at ambient temperature after the purification. The POM analysis confirmed the occurrence of the isotropic phase at ambient temperature.
In this specific case, it is remarkable to note that the dimers **67** and **52** have the same type of connection (ester function), the same distance ***a*** between the aromatic linker and the discotic units but different melting point. The change of the geometry of the connection induced a major change in

the macroscopic behavior. The variation of the regiochemistry produced probably a reduction of the intermolecular interactions and this geometrical arrangement could prevent the formation of a dense crystal packing as observed for dimer **52**.

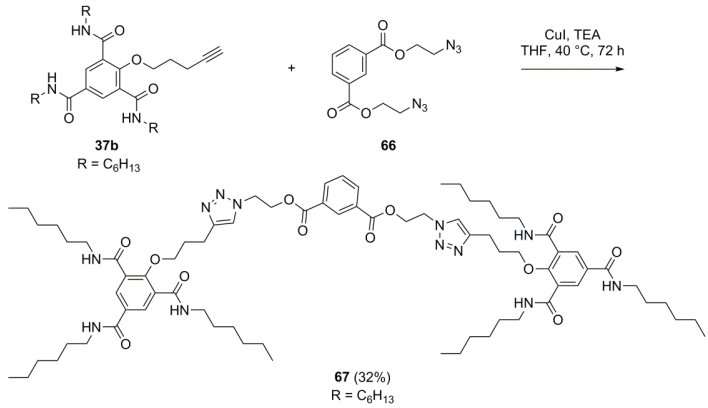

Scheme 8. Synthesis of banded dimer **67**.

The reduction of intermolecular interactions and of the lattice energy of the crystal was expected and in accordance with the knowledge from literature and the simple model we are using. As this part of our screening effort yielded the "predicted", uninspiring material properties, we did not characterize the aggregation in solution. Suffice it say, that we validated the observation of Kumar: bent linkers (1,3-substituted aromatic core element) do not lead to mesophases.

Short alkyne derivative (Employment of 2-propargyloxy substituted BTA)

The supramolecular aggregation of our BTA dimers does not depend on the length of the linker, at least not in the cases studied (Chapter 6). The literature reports that too short linkers can exercise an inhibitory effect on the occurrence of liquid crystalline phases from triphenylene-dimers (Scheme 5 Chapter 2). From the data available there is no clear, unequivocal correlation between the linker length and the observation of the desired columnar-like supramolecular interactions. We therefore decided to study the influence of reducing the degree of freedom (rotation and translation) by decreasing the length of the linker. Replacing the pentynyloxy function with a shorter alkoxynyl group will reduce the degrees of conformational freedom hopefully without preventing the possibility to form supramolecular aggregates.

2-propargyloxy BTA unit

Synthesis of the monomer

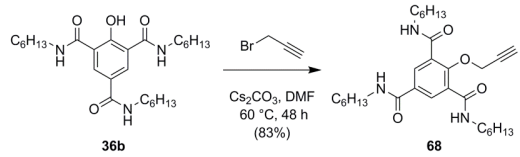

Scheme 9. Synthesis of the 2-propargyloxy BTA derivative **68**.

We introduced the propargyl moiety on the 2-hydroxy BTA **36b** by a simple alkylation with propargyl bromide (Scheme 9). The highly reactive propargyl bromide was employed in the alkylation of the 2-hydroxy derivative **36b**. The final propargyl ether derivative **68** was isolated in excellent 83% yield (Scheme 9). The higher reactivity of the propargyl derivative induced a better chemical yield compared with 5-chloro-1-pentyne (Table 3 Chapter 3).

DSC and POM analysis of the 2-propargyloxy BTA

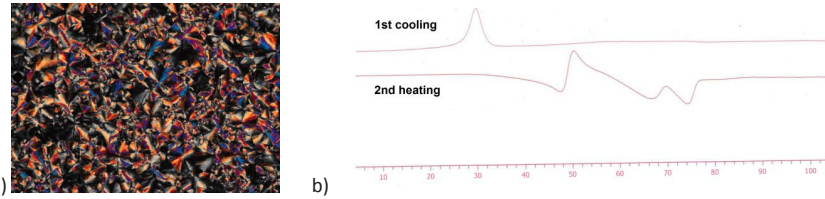

Figure 8. a) POM pictures of pseudo-focal conic texture of **68** at 67.6 °C (magnification x100). b) DSC curve of **68**.

Upon cooling from its isotropic phase (liquid) BTA **68** forms birefringent pseudo-focal conic texture typical of columnar liquid crystals (Figure 8a), whereas the liquid crystalline phase was analysed with the help of the DSC (Figure 8b). The second heating DSC cycle showed the polymorph nature of 2-propargyloxy BTA **68**. A first exothermic transition phase at 38.78 °C (-2.35 $kJmol^{-1}$) was followed by an endothermic transition at 50.40 °C (0.98 $kJmol^{-1}$) and an exothermic transition at 57.88 °C

(-1.71 kJmol^{-1}). The combination of these last two transition phases (exo/endothermic) could indicate the formation of a partially organized structure on the heating cycle (*cold crystallization*) and its relative melting. The final melt occurs at 69.97 °C associated with an expected exothermic transition phase (-1.86 kJmol^{-1}). On the other hand, only a transition phase indicating the final solidification at 32.53 °C (2.53 kJ mol^{-1}) was detected upon the cooling cycle.

Synthesis of the dimer

The click reaction was carried out according to the previously used conditions. Surprisingly, the major product isolated was the "depropargylated" 2-hydroxy-BTA **36b** in 60 % yield rather than the expected dimer (Scheme 10, Table 6 Entry 3).

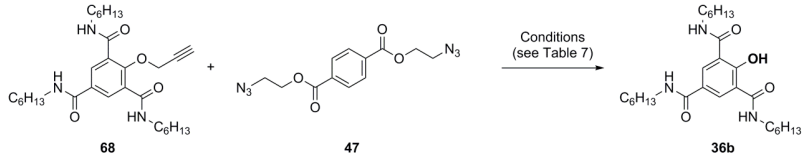

Scheme 10. Click reaction on the 2-propargyloxy BTA derivative **68**. Experimental conditions are listed in Table 6.

Entry	Reagent	Equivalents	Solvent	Diazido	T (°C)	time (hours)	Yield %
1	Cu_2SO_4 [a]	0.4	THF/H_2O	//	40	76	//
2	NaAsc [a]	0.8	THF/H_2O	//	40	76	//
3	Cu_2SO_4/NaAsc [b]	0.4 Cu, 0.8 NaAsc	THF/H_2O		40	76	60
4	CuI, TEA	0.2	THF		40	76	50
5	(COD)Ru(II)Cl_2	0.05	DMF		65	96	60
6	Ni(II)$(PPh_3)_3Cl_2$	0.05	DMF		65	96	64

Table 6. Screening of click chemistry conditions. [a] Control reactions. Yields refer to the 2-hydroxy BTA **36b**.

Different reaction conditions were tested trying to avoid this undesired side reaction. When the 2-propargynyloxy-BTA **68** was treated exclusively with the reducing agent (sodium ascorbate) or with copper (II) ($CuSO_4$ $5H_2O$) no reaction took place and the starting material was recovered (Entry 1 and 2). Copper (II) species do not form an acetylide derivative with triple bonds and in the absence of alkyne activation no depropargylation of the substrate could be observed. On the contrary, good yield of depropargylated product **36b** was observed when a source of copper (I) was employed (CuI, Entry 4). When other transition metals, capable to active the triple bond such as ruthenium or nickel complexes were employed the depropargylated derivative **36b** was isolated in good yield (Entry 5 and 6). Under these conditions the depropargylation reaction is favored (*fast*) compared to the cycloaddition. The nature of the metal, or of the catalyst, does not influence the pathway of the reaction as long as the alkyne-activation takes place.

Analysis of the depropargylation mechanism

The use of the propargyl moiety as a protecting group for alcohol or amine groups and its removal has been studied by different research groups.[8] The cleavage of the propargyl moiety are often performed using highly activated reagents such as low-valent titanium,[9] tetrathiomolybdate,[10] nickel catalyzed electroreductive propargyl ether cleavage[11] or using carbene ruthenium

complexes.[12] Recently Pal *et al*. proposed a mild propargyl ether cleavage using a palladium catalyst (Scheme 9).[13]

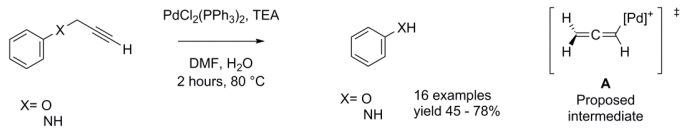

Scheme 11. Propargyl ether cleavage proposed by Pal *et al*.[13]

The authors proposed a formation of the *allenyl-pallada* species **A** as the active intermediate (Scheme 11).[14] The postulated intermediate **A** adds a molecule of water on the central *sp* carbon and thereby regenerates the active Pd(0) species. Palladium in known to form η^3-complexes on triple bonds, thereby catalyzing the depropargylation process.[15]

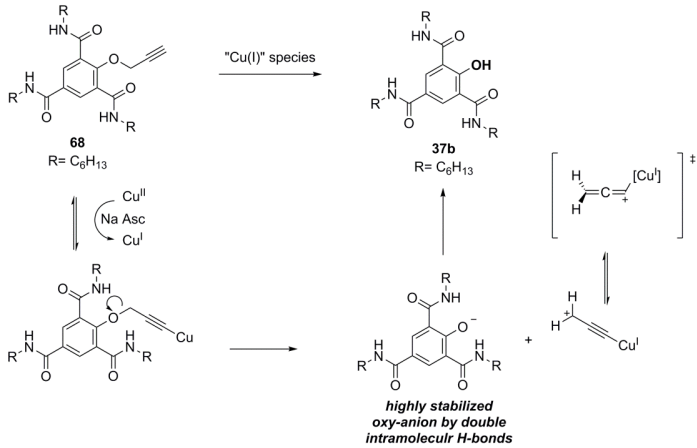

Scheme 12. Proposed Cu-mediated propargyl ether cleavage.

The formation η^3-complexes starting with copper (I) species has been less often postulated, than the formation of the corresponding palladium complexes. On the other hand many examples are known in the literature, where a C-H activation of an acetylenic C-H bond has been postulated using copper (I). We therefore propose the following catalytic cycle for the observed depropargylation (Scheme 12). We assume that the first step is the insertion of the copper (I) species into C-H acetylene bond forming the *copper-acetylide* species, followed by the oxygen-carbon bond breakage.

The generated phenolate species is strongly stabilized by the double intramolecular H-bonds between the charge on the phenolate and the two adjacent N-H groups (see Figure 2 Chapter 3). Moreover, the low pK_a of the conjugate phenol **36b** means high stability of the deprotonated **36b**. The formed organometallic fragment is stabilized by the presence of the low-valent copper (carbenoid species). Reacting with water or other nucleophiles present in solution may regenerate the catalytic active Cu(I) species. The presence of the paramagnetic copper species prevents studies of the reaction pathway by NMR spectroscopy.

The depropargylation was not the "desired reaction". We made some preliminary studies of the scope of this transformation. We tested the in situ generated copper(I) species toward the depropargylation of a few substrates (Scheme 13). The Cu-mediated depropargylation only works well when the phenyl ring is electron poor (Table 7). In conclusion the depropargylation condition using copper (I) species is limited to examples, where the generated phenoxide is extremely stabilized.

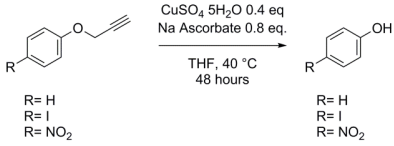

Scheme 13. Study of the reaction scope.

R	Yield[a]	Yield[b]
H	No reaction	75
I	No reaction	51
NO_2	8%[c]	74

Table 7. Experimental data comparison between our depropargylation and Pal's work. [a] Our condition. [b] Pal's condition. [c] NMR measured yield.

The propargyl derivative, compound BTA **68**, could not be used in the click reaction under the conditions tested. This diagnosis leads to the conclusion that we have to stay with the pentynyloxy group as element for the click chemistry.

Side Chain Modifications

Lipophilicity enhancement (Employment of BTA containing dodecyl-substituted alkyl side chains)

Up to now we were seeking to impose liquid crystallinity in our dimer structures by modifying the aromatic linker. As next step we focus our attention on the modification of the side chains (amide group substituent) of the BTA core. The nature of the side chain plays a fundamental role on the supramolecular organization of the resulting BTA derivatives. For example, branched aliphatic lateral chains induce organogel formation rather than liquid crystalline phases. All the examples of 2-substituted BTA derivatives used so far employed the hexyl group as lateral chain. According to the systematic work of Matsunaga, the length of the linear aliphatic lateral chains has not a fundamental role on the liquid crystallinity as long as its length is more than five carbons (see Table 3 Chapter 1). On the other hand, the group of Lillya reported an insightful study on the effects of branching and rigidifying the side chains on the discotic liquid crystal behavior.[16] They concluded their study by saying: *The crystal-to-discotic phase transition involves disordering of the side chains. The temperature at which side-chains disordering take place is lowered by incorporating branch points*.[16] They also reported that: *If the disordering temperature of the side chains is higher than that at which the cores remain stacked, the crystal will melt directly to the isotropic phase*.[16]

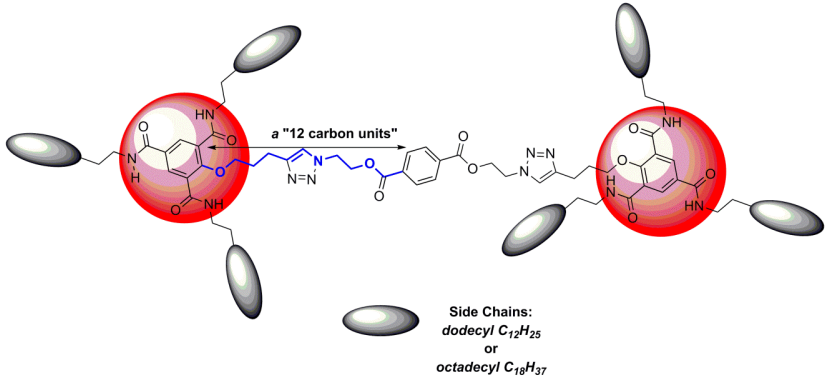

Scheme 14. Schematic representation of the space filling by a longer aliphatic side chains.

Based on Lillya's work and the fact we observed that the dimerization of the 2-pentynyloxy BTA **37b** is an effective strategy to improve the self-assembly, we decided to study the influence of the side chains. The goal of the approach is to decrease the "disordering temperature" by introducing disordered long alkyl chains (see Scheme 14). In this way the temperature for the transition from an ordered to an disorderd state will be lowered. Based on the conclusions cited above this change in properties should promote the mesophase formation. We decided to study the synthesis of 2-pentynyloxy BTA derivatives substituted with longer aliphatic lateral chains such as dodecyl ($C_{12}H_{25}$) **37c** or octadecyl ($C_{18}H_{37}$) **37d**.

Introduction of long aliphatic side-chains in 2-pentynyloxy BTA derivatives

The synthesis of the dodecyl side chains substituted BTA **37c** has been previously reported in Chapter 3 (Scheme 13), whereas the octadecyl side chain substituted BTA derivative **37d** could not be prepared due to solubility issues of the phenol precursor **36d**.

POM and DSC analysis of the monomers

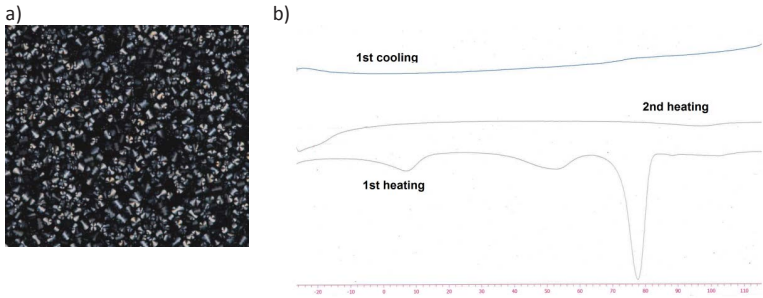

Figure 9. POM pictures of pseudo-focal conic texture of BTAs derivative **37c** at 55 °C (magnification x10). b) DSC curve of **37c**. The first heating cycle shows three transition phases that were not observed in any other heating/cooling cycle. The energies and the temperatures measured in the first heating cycle are known not to be reliable.

POM analysis showed the formation of pseudo-focal conic textures indicating the occurrence of the columnar liquid crystalline phase (Figure 9a). Surprisingly, the thermal analyses of the **37c** could only partially confirm such result. Indeed the DSC analysis could detect the transition phases, and relative enthalpies, exclusively at the first heating run (Figure 9b). Temperature and enthalpy values determined in the 1st run are not reliable. Despite this general rule this values can furnish an indication on the type of mesophase present. The temperature measured during the 1st run for the liquid crystalline formation is -2.50 °C (-3.47 kJmol^{-1}). A second exothermic peak was observed at 40.20 °C (-4.21 kJmol^{-1}) probably associated to a phase transition indicating the polymorph nature of **37c**. The final isotropisation occurred at 72.47 °C and this transition is associated to an intense exothermic peak (-19.91kJmol^{-1}).

Synthesis of the dimers

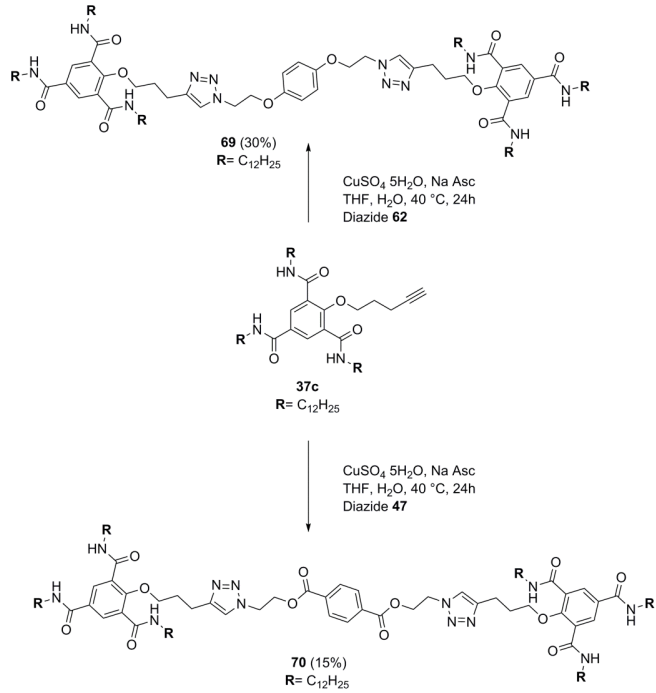

Scheme 15. Synthesis of the dodecyl-side chains substituted dimers **69** and **70**.

The double click cycloaddition reaction was tested on two different aromatic linkers (electron poor **47** and electron rich **62**) using the previously extensively used Sharpless conditions. The unoptimized cycloaddition furnished dimers **69** and **70** in 30% and 15% yield respectively as amorphous solids (Scheme 15).

POM and DSC analysis

POM analysis carried out on both synthesized dimers **69** and **70** did not show the occurrence of the textures characteristic for the presence of liquid crystalline mesophase. After the isotropisation of the solids, no textures could be observed upon the cooling process.

The DSC analyses indicated the occurrence of a glass transition for both dimers typical of amorphous solids (Figure 10 and 11).

Compound	Phase transition and temperature[a]	Solid state
69	**I** 78.78 °C Glass transition	Amorphous solid
70	**I** 58.81 °C Glass transition	Amorphous solid

Table 8. Transition temperatures and solid phase analyses. [a] Measured on the 1st cooling cycle.

The temperature value of the glass transition of **69** and **70** is increased when compared to the one of the analogues substituted with hexyl chains **52** and **63**. The introduction of disordering lateral chains did not change the materials properties enough: no formation of mesophases could be observed. The difference of the temperature of the glass transition of the two dimeric structures is interesting. The electron rich aromatic hydroquinone-type linker consistently shows higher glass transition. The difference of 20 °C between **69** and **70** (Table 8) is another empirical data substantiating this empirical rule.

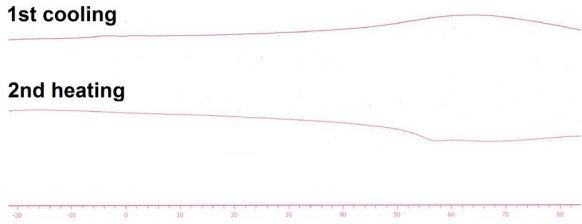

Figure 10. DSC heating/cooling cycles of **69**.

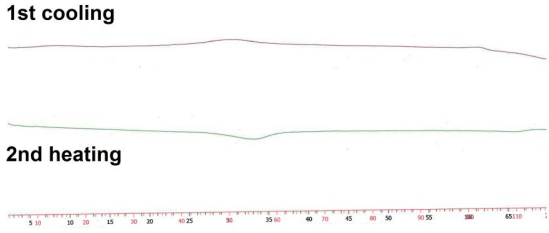

Figure 11. DSC heating/cooling cycles of **70**.

Aromaticity enhancement (Employment of Gallic Acid Derivative as BTAs side chains)

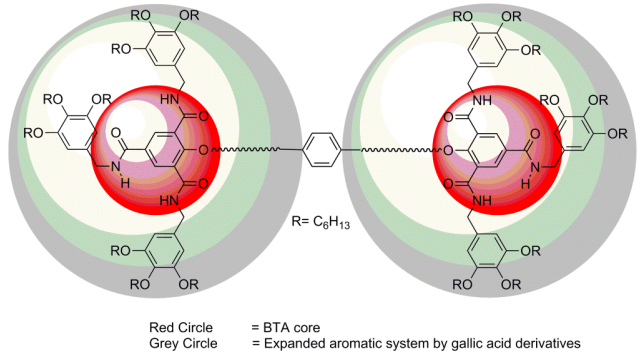

Scheme 16. Schematic representation of the expanded-aromatic system of BTAs derivatives.

In our studies we have been able to proof, that mono-substituted BTA derivatives can and do form mesophases. However, our efforts to create dimers using different linker designs always lead to compounds which showed exclusively a glass to liquid transition. We have not been able to induce the presence of a columnar mesophase. This observation is all the more amazing, as our studies of the thermodynamic strength of the association process in solution showed, that the dimers form aggregates, which are at least as thermodynamically stable as the monomeric precursors.
We therefore decided to induce the formation of mesophases by introducing lateral chains known to "stabilize" may be even to "impose" columnar liquid crystalline phases. The group of Meijer reported the use of pyrogallol derivative as an effective columnar mesophases stabilizing substituent. Introducing pyrogallol groups as end groups of the side chains as in **71** doubled the temperature range of the liquid crystalline phase compared to the BTA **3** substituted with aliphatic side chains (Scheme 17 and Table 9).[17]

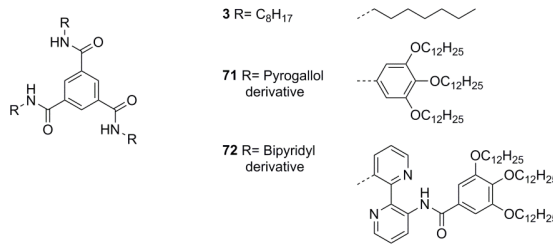

Scheme 17. Schematic representation of BTAs substituted with different side chain reported in the literature.[17]

BTA	R	Transition Temperature °C (ΔH J mol^{-1})	ΔT	Ref.
3	C_8H_{17}	**Cr** 102(19) **Col** 204(17) **I**	102	[18]
71	Pyrogallol derivative	**Cr** -4(44) **Col** 178(27) **I**	182	[17a]
72	Bipyridyl derivative	**Cr** 9(56) **Col** 355(27) **I**	346	[17d]

Table 9. Transition Temperature and Enthalpy of different side tails substituted BTAs.

Synthesis of the gallic acid derivative

Synthesis of the gallic acid derivative amine

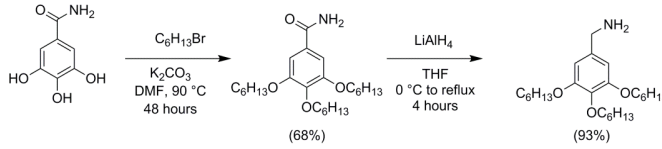

Scheme 18. Synthesis of the gallic acid derivative amine **75**.

We decided to use in our study the benzyl amine derivative **75** rather than the pyrogallol derivative used in BTA **71** (Scheme 17). The synthesis of **75** was already reported by Percec, however their synthetic pathway is tedious.[19] We decided to develop a more efficient synthetic pathway starting from the commercially available 3,4,5-trihydroxy benzamide **73** (gallic acid derivative, Scheme 18). The tri-hydroxyl groups of **73** were alkylated with 1-bromohexane furnishing **74** in good yield (68%). The benzamido group was reduced to the corresponding benzylamine **75** in excellent yield (93%) using $LiAlH_4$ (Scheme 18).

Synthesis of the (gallic acid substituted)-2-pentynyloxy BTA derivative

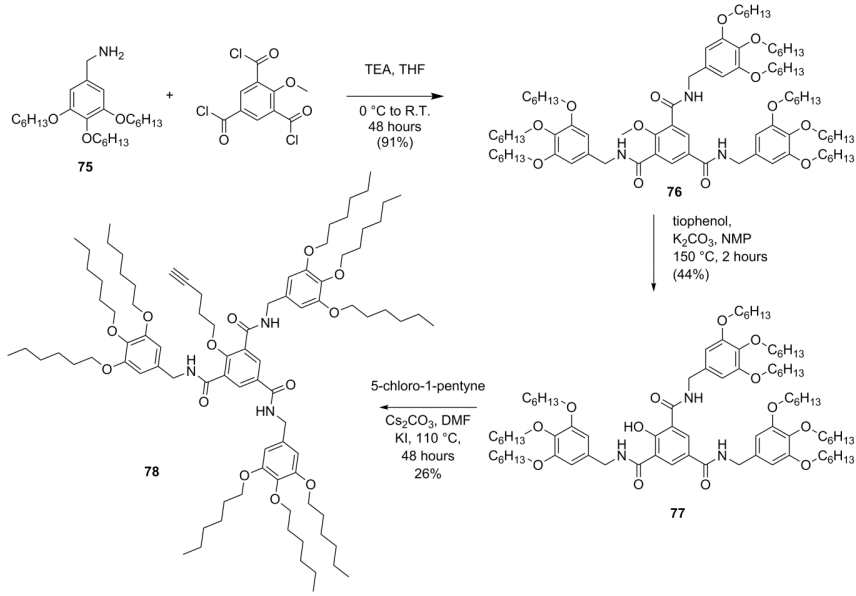

Scheme 19. Synthesis of gallic acid derivative-substituted (GAD) BTA **78**.

The 2-methoxy-1,3,5-benzentricarboxylic acid **32** reacted with 3,4,5-trihexyloxybenzylamine **75** (by previous activation to the corresponding 2-methoxy triacyl chloride) to furnish the expected

substituted BTA **76** in excellent yield (Scheme 19). The raw material was pure enough to be used in the following demethylation step without chromatographic purifications. The demethylation did not proceed as smoothly as for the simpler BTAs. The corresponding 2-hydroxy BTA **77** was obtained in 44% yield. The tri-hexyloxy substituent on the gallic acid residue could be "*dehexyloxylated*" as well using the demethylation conditions. Polyhydroxy benzene derivatives are known to be not very stable, especially under oxidative conditions. It is plausible that a competitive dehexyloxylation lead to an instable polyhydroxy derivative reducing the yield.
The alkylation of **77** required long reaction times (48 hours) and high temperature (110 °C) to obtain the pentynyloxy derivative **78** in an expected low yield of 26%.

POM and DSC analysis

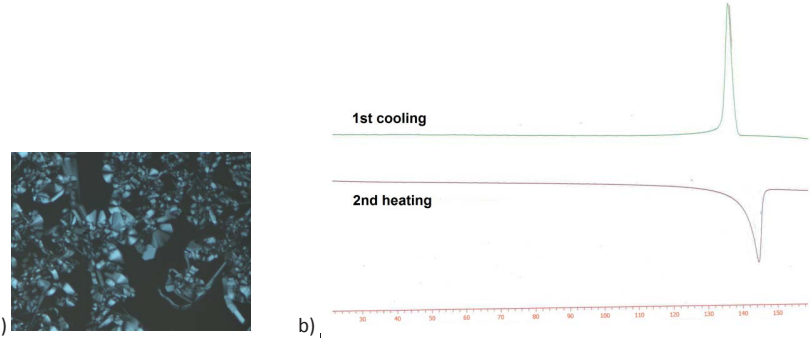

Figure 12. a) POM pictures of pseudo-focal conic texture of BTAs **78** at 134.6 °C (magnification x200). b) First cooling and second heating cycle of the DSC analysis of **78**.

Upon cooling from its isotropic phase (liquid) BTA **78** forms birefringent pseudo-focal conic texture typical of columnar liquid crystals (Figure 12a). The liquid crystalline phase was analysed with the help of the DSC. The gallic acid functionalized BTA **78** presented a strong exothermic peak at 140.9 °C (-28.87 $kJmol^{-1}$) indicating the phase transition between liquid crystallinity and isotropic liquid. A strong endothermic peak was registered as well upon cooling at 138.5 °C (30.87 $kJ\ mol^{-1}$). These observations are consistent with the formation of a columnar mesophase. These intense phase transitions indicate the high stability gained in the mesomorphic phase by the introduction of the gallic acid substituents into **78**. The phase transition to the solid state could be detected neither in the heating nor in the cooling cycles.

Synthesis of the dimers

The double cycloaddition click reaction was carried out on a series of diazido **47**, **49** and the fluorinated **58** derivatives (Scheme 20).

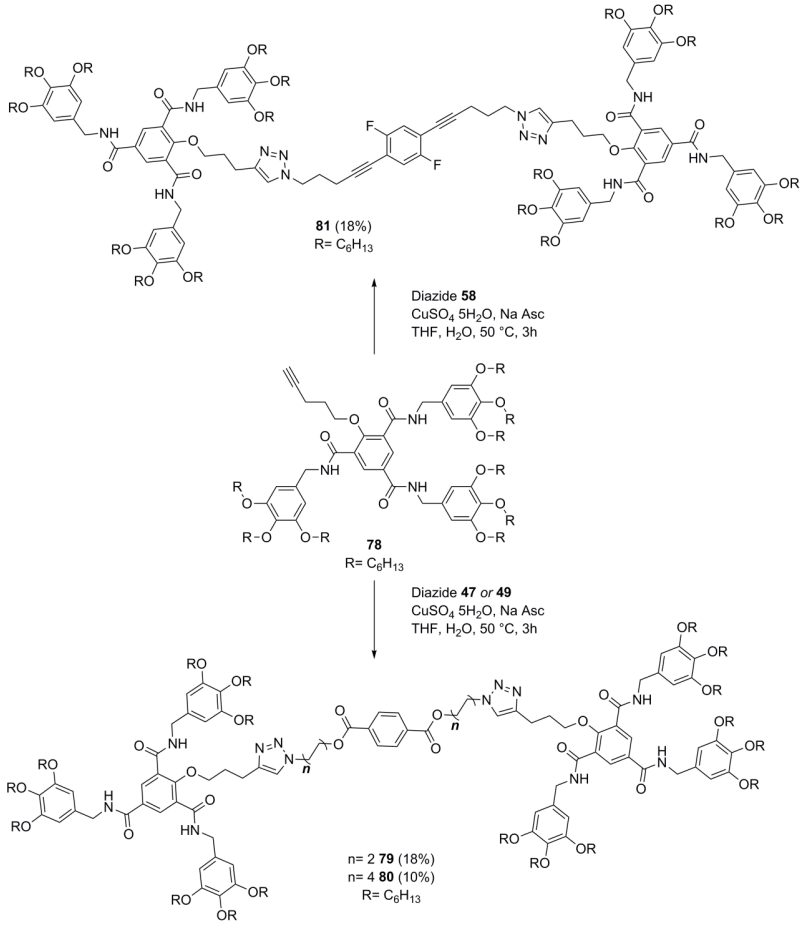

Scheme 20. Synthesis of the aromatic extended core BTAs dimers **79**, **80** and **81**.

The amount of the transition-metal catalyst (copper) and the reducing agent (sodium ascorbate) were increased compared to the aliphatic-substituted BTA (0.5 eq. rather than 0.3 eq. for Cu and 1 eq. rather than 0.6 eq. for sodium ascorbate). The purification step of the dimers was very tedious which drastically affected the yields of the isolated final products.

POM and DSC analysis

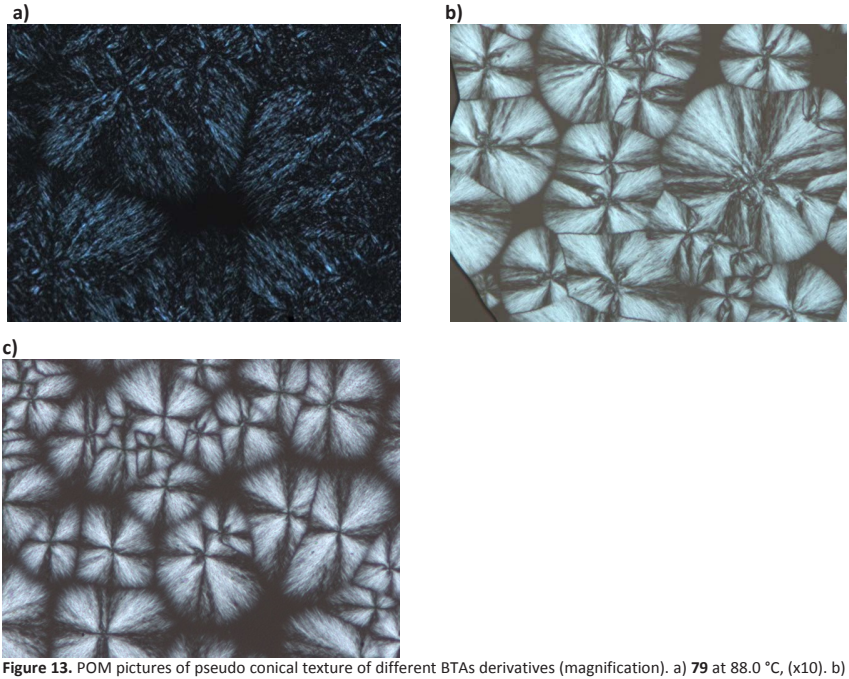

Figure 13. POM pictures of pseudo conical texture of different BTAs derivatives (magnification). a) **79** at 88.0 °C, (x10). b) **80** at 71.4 °C (x200). c) **81** at 75.5 °C (x20).

Finally all the three dimers **79**, **80** and **81** presented a birefringence at room temperature without well-defined textures. After isotropization at melting point, the dimers were cooled down and texture formation took place (Figure 13a, b and c). The mesomorph natures of the textures were confirmed by submitting the samples at mechanical stress. The pressed texture showed reversibility from the deformation stress, a characteristic of liquid crystals.

BTA	R	2nd heating cycle[a]	1st cooling cycle[a]
79 (n=2)	C_6H_{13}	89.17(-30.97)	90.8(38.10)
80 (n=4)	C_6H_{13}	80.07(-27.80)	59.83(26.26)
81 (fluoro)	C_6H_{13}	50.2[b] 77.7(-16.35)	63.4(17.16) 46.4(3.54)

Table 10. [a] Transition temperatures (°C) and enthalpy (kJ mol^{-1}). [b] Glass transition.

In the DSC analysis of the ester-linked dimers **79** and **80** only the isotropization temperatures were detectable both on the heating and on the cooling cycle (Figure 14 and 15). Both dimers presented a different isotropization temperature when measured either on the cooling or on the heating run. This is probably due to the high viscosity of these compounds when heated upon forming the mesophase. All the detected phase transitions presented an intensive peak in the DSC measurements (Table 10). These energy values are coherent with the typical energy values reported for columnar liquid crystals in the literature for similar molecules.[17a, 17d, 18] The DSC curve of the fluorinate-dimers **81** presented some differences with respect to the other dimers **79** and **80**. In the first cooling cycle a quite intensive peak (17.16 kJ mol^{-1}) was measured at 63.4 °C followed by a small transition peak

(3.54 kJ mol^{-1}) at 46.4 °C. The first intensive peak can be attributed to the mesophase formation whereas the second smaller peak is typical for a glass transition. The second heating cycle presented a small glass transition at 50.2 °C indicating the mesophase formation. A more intense second peak was measured at 77.7 °C (16.35 $kJmol^{-1}$) indicating the isotropization temperature (=melting point).

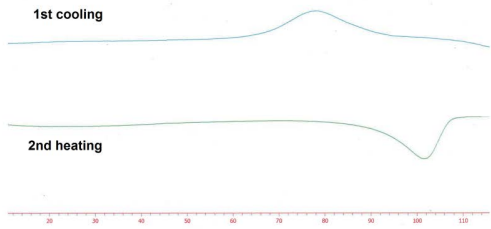

Figure 14. DSC curve (1st cooling cycle and 2nd heating cycle) of dimer **79**.

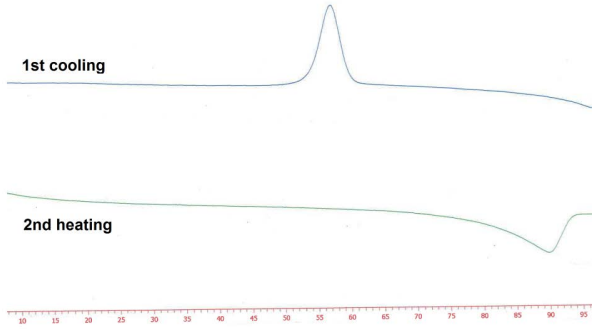

Figure 15. DSC curve (1st cooling cycle and 2nd heating cycle) of dimer **80**.

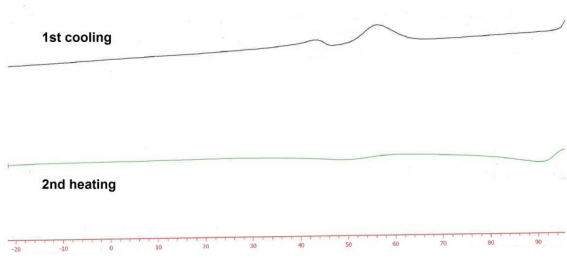

Figure 16. DSC curve (1st cooling cycle and 2nd heating cycle) of dimer **81**.

The introduction of the gallic acid substituents as the amide lateral chains into the 2-substituted BTA derivatives induced the formation of columnar mesophases both in the monomeric and in the dimeric structures **79**-**81**. At this point we only have the experimental results from the studies of the

material properties. We do not know if the columnar mesophase imposed by the presence of the gallic acid units orders also our central dimeric BTA unit in a supramolecular column. The conclusion of these experiments is: We need an extremely strong inducer of mesophase formation in order to force our dimeric BTA derivatives into a columnar supramolecular arrangement.

References

[1] H. Kelker, R. Hatz, *Handbook of Liquid Crystals* Wiley-VCH Verlag GmbH **1980**.

[2] aR. Chinchilla, C. Najera, *Chem. Soc. Rev.* **2011**, *40*, 5084-5121; bK. Sonogashira, *J. Organomet. Chem.* **2002**, *653*, 46-49; cK. Sonogashira, Y. Tohda, N. Hagihara, *Tetrahedron Lett.* **1975**, 4467-4470.

[3] W. R. J. Dolbier, *Guide to Fluorine NMR for Organic Chemists*, **2009**.

[4] T. Ueda, N. Kanomata, H. Machida, *Org. Lett.* **2005**, *7*, 2365-2368.

[5] D. E. Phipps, P. D. Beer, *Tetrahedron Lett.* **2009**, *50*, 3454-3457.

[6] S. K. Gupta, V. A. Raghunathan, V. Lakshminarayanan, S. Kumar, *J. Phys. Chem. B* **2009**, *113*, 12887-12895.

[7] S. M. June, P. Bissel, T. E. Long, *J. Polym. Sci., Part A: Polym. Chem.* **2012**, *50*, 3797-3805, S3797/3791-S3797/3798.

[8] P. G. M. Wuts, T. W. Greene, *Protective Groups in Organic Synthesis*, 3rd ed., John Wiley, New York, **1999**.

[9] aS. M. Kadam, S. K. Nayak, A. Banerji, *Tetrahedron Lett.* **1992**, *33*, 5129-5132; bS. K. Nayak, S. M. Kadam, A. Banerji, *Synlett* **1993**, 581-582.

[10] aS. Sinha, P. Ilankumaran, S. Chandrasekaran, *Tetrahedron Lett.* **1999**, *40*, 771-774; bV. M. Swamy, P. Ilankumaran, S. Chandrasekaran, *Synlett* **1997**, 513-514.

[11] S. Olivero, E. Dunach, *Tetrahedron Lett.* **1997**, *38*, 6193-6196.

[12] D.-W. Hahn, D.-M. Byun, J. Tae, *Eur. J. Org. Chem.* **2004**, 63-67.

[13] M. Pal, K. Parasuraman, K. R. Yeleswarapu, *Org. Lett.* **2003**, *5*, 349-352.

[14] aN. Monteiro, A. Arnold, G. Balme, *Synlett* **1998**, 1111-1113; bJ.-R. Labrosse, P. Lhoste, D. Sinou, *Tetrahedron Lett.* **1999**, *40*, 9025-9028.

[15] aS. Ogoshi, K. Tsutsumi, H. Kurosawa, *J. Organomet. Chem.* **1995**, *493*, C19-21; bS. Doherty, J. F. Corrigan, A. J. Carty, E. Sappa, *Adv. Organomet. Chem.* **1995**, *37*, 39-130; cA. Wojcicki, *New J. Chem.* **1994**, *18*, 61-68.

[16] D. M. Collard, C. P. Lillya, *J. Am. Chem. Soc.* **1991**, *113*, 8577-8583.

[17] aJ. J. van Gorp, J. A. J. M. Vekemans, E. W. Meijer, *J. Am. Chem. Soc.* **2002**, *124*, 14759-14769; bL. Brunsveld, H. Zhang, M. Glasbeek, J. A. J. M. Vekemans, E. W. Meijer, *J. Am. Chem. Soc.* **2000**, *122*, 6175-6182; cM. H. C. J. van Houtem, R. Martin-Rapun, J. A. J. M. Vekemans, E. W. Meijer, *Chem. - Eur. J.* **2010**, *16*, 2258-2271, S2258/2251-S2258/2259; dA. R. A. Palmans, J. A. J. M. Vekemans, H. Fischer, R. A. Hikmet, E. W. Meijer, *Chem. - Eur. J.* **1997**, *3*, 300-307.

[18] Y. Matsunaga, N. Miyajima, Y. Nakayasu, S. Sakai, M. Yonenaga, *Bull. Chem. Soc. Jpn.* **1988**, *61*, 207-210.

[19] V. Percec, H.-J. Sun, P. Leowanawat, M. Peterca, R. Graf, H. W. Spiess, X. Zeng, G. Ungar, P. A. Heiney, *J. Am. Chem. Soc.* **2013**, *135*, 4129-4148.

Conclusions and Perspective

Conclusions

The synthetic objectives of this work, the introduction of an "anchoring site" on BTA cores and the synthesis of dimeric BTA structures, were achieved. The central element of our design was the introduction of a hydroxyl group in position 2 of the BTA core as anchoring site. Our synthesis of 2-hydroxy BTA derivatives is based on reported methodologies adapting them to our specific target molecules. Our synthesis allowed an easy modification of the amide side chains introducing ethyl, hexyl, dodecyl, octadecyl and gallic acid substituents. The 2-alkoxynyl derivatives were found to show mesomorphic behavior over a broad temperature range. We demonstrated that the alkoxynyl substituent tilts the amide bonds (torsion angle) out of coplanarity with the aromatic ring. This behavior has been previously predicted by molecular modeling for the fully substituted crowded arenes. The strong intramolecular H-bonds formed between the adjacent amide proton and the alkoxynyl oxygen reduced drastically the supramolecular aggregation strength in dichloromethane solution. As a consequence of this competitive intramolecular interaction not only the aggregation strength as measured as change in the free energy but also the liquid crystalline behavior was negatively affected. The detailed supramolecular aggregation analysis indicated that, the presence of the pentynyloxy group not only induces the formation of intramolecular H-bonds competing with the desired intermolecular H-bonds, but it also changes the supramolecular aggregation mechanism. Indeed normally the self-assembly of BTA derivatives follows a cooperative process induced by the joint formation of three helices of H-bonds surrounding the column held together by π-π stacking. The 2-pentynyloxy BTA **37b** was found to aggregate according to an isodesmic model. The modification of the aggregation mechanism indicates the drastic effect of the intramolecular H-bond formation on the aggregation mechanism in the bulk. The presence of an H-bond acceptor as anchoring site reduces the efficiency of the BTA self-aggregation.

On the other hand, the dimerization using the ester connected diazido derivatives afforded dimers **52**-**54** that showed an expected increased association strength with respect to the constitutive monomer **37b** by a factor of 5-6 times, measured as the association constant K_a. The association strength is essentially independent of the length of the linker in the limits we studied. Despite the strengthening of the association, as observed in our solution experiment, none of the dimeric structures showed the formation of a liquid crystalline phase in the bulk. The absence of liquid crystallinity in our dimer structures is not correlated with the strength of the self-assembly process as expressed by the free energy change. Our screening efforts with the goal to establish an empirical structure-property relationship correlating the different design of the side chains in our quest to obtain dimers showing liquid crystalline mesophases allowed to derive a series of empirical rules, without giving us a complete analytical picture of the factors influencing the material properties.

Perspective

Three main directions for future work can be identified.

With first priority, the modification of the anchoring site should be studied in order to prevent intramolecular H-bond formation. According to the examples reported by Nuckolls (Figure 13 Chapter 1), we can employ a Stille-type cross coupling reaction on the 2-bromo-substituted BTA derivative and construct dimeric structures. The alkyne groups will enable an easy construction of dimeric structures.

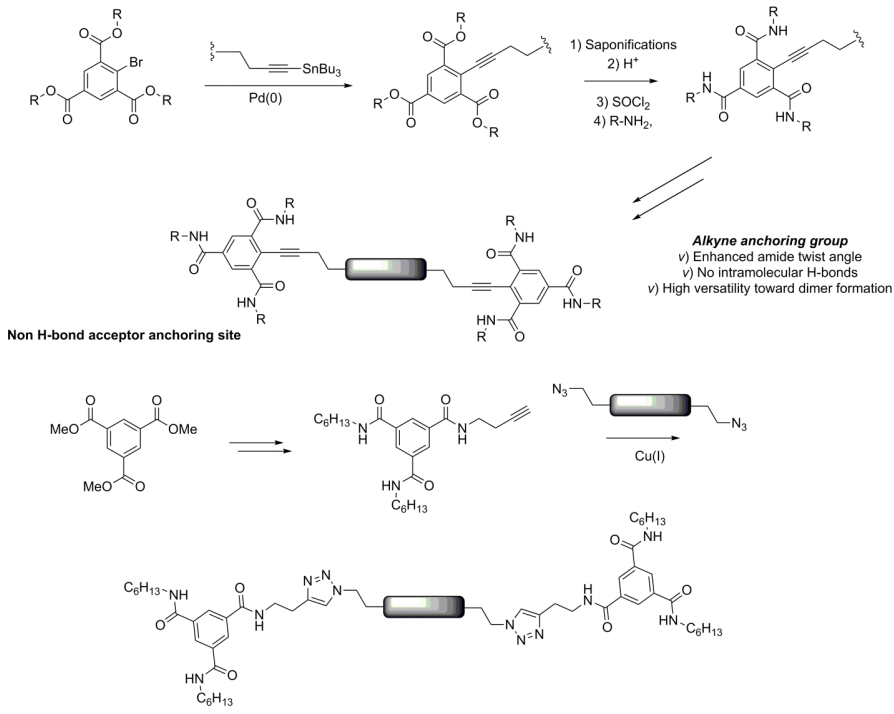

Scheme 1. Possible alkyne-anchoring function synthesis.

The second approach consists of changing the position of the anchoring site moving the linker chain to one of the amide groups. This design should not affect the strength of the intermolecular H-bond. This type of functionalization is quite tedious (from a synthetic point of view). The studies carried out by Meijer et coll. on the aggregation mechanism are a good precedent allowing to compare the new compounds with models. The interpretation and the comparison of the data will thereby be facilitated.

The last proposal consists of the introduction of the bypyridyl side chain (Figure 11 Chapter 1) that forms intramolecular H-bonds with the amide group and drives the self-assembly by π-interactions (Figure 1). In this case all the H-bond interactions are intramolecular, avoiding the formation of the

intermolecular H-bond. Replacing the intermolecular H-bonds by intramolecular bonds avoids the need to form a network of helical intermolecular H-bonds around the column. The disturbance introduced by the substituent in position 2 does not affect in the same crucial way the self-assembly process as it has been found for **37b** (see Chapter 5). The self-assembly will be mainly driven by π-π stacking and not any more by the H-bonding.

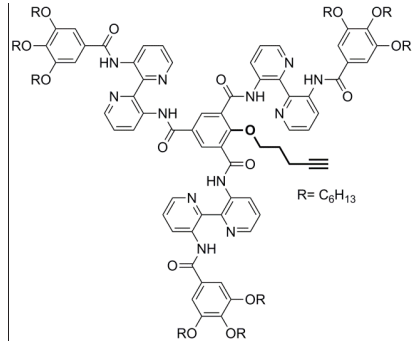

Figure 1. Example of 2-pentynyloxy BTA where the amide lateral chains are substituted with the bipyridine derivatives. In this case the all the H-bonds are intramolecular and therefore the alkoxynyl group could not affect the strength of the intermolecular H-bond.

Experimental Part and Additional Information

Table of Contents

Experimental Part

General Remarks

Safety Information:

We reported the synthesis and employments of different diazido derivatives. Some of those compounds were prepared according to reported procedures, where the authors did not report dangerous decompositions. The compounds were synthesized, purified and isolated as pure materials. In all the cases we did not observed explosions or dangerous decompositions. However, due to the intrinsic hazardous nature of azido compounds careful and small operational scales are recommended.

Glassware and heating system: Reactions requiring anhydrous conditions were performed in oven-dried (120 °C) glassware under an inert atmosphere of dry N_2 or dry Ar. All reaction temperatures refer to oil bath temperature measured with Heidolph EKT 3mA thermocouples unless other noted.

Chromatography: Analytical thin-layer chromatography (*TLC*) was performed on *Merck* silica gel plates (aluminum sheets precoated with silica (60 F254)) or on *Merck* aluminum oxide plates (aluminum sheets precoated with aluminum oxide (60 F254)). Preparative thin-layer chromatography was performed on silica gel supported on glass plates (20 cm x 20 cm precoated with 60 F254) or neutral aluminum oxide supported on glass plates (20 cm x 20 cm preacoated with 60 F254). Visualization was accomplished with UV light or potassium permanganate solution stain unless other noted. Flash column chromatography was performed using silica gel (*Brunschwing* Silica gel 60, 63-200) employing technical grade solvents.

NMR spectroscopy: ^{1}H NMR spectra and ^{13}C NMR spectra were recorded on a *Bruker Avance II-400* (400.13 MHz, ^{1}H; 100.61 MHz, ^{13}C) and on a *Bruker DPX 400* (400.13 MHz, ^{1}H; 100.61 MHz, ^{13}C) of the Neuchâtel Platform of Analytical Chemistry (*NPAC*) of the University of Neuchâtel. Chemical shifts (δ) are quoted (ppm) and are relative to tetramethylsilane (δ= 0 ppm) as the internal standard or the residual solvent peak in $CDCl_3$ (δ 7.26 ppm, ^{1}H; δ 77.0 ppm, ^{13}C), in dichloromethane (δ 5.32 ppm, ^{1}H; δ 53.84 ppm, ^{13}C), in methanol (δ 3.31 ppm, ^{1}H; δ 49.00 ppm, ^{13}C), in DMSO (δ 2.50 ppm, ^{1}H; δ 39.52 ppm, ^{13}C). All the deuterated NMR solvents were purchased from *Cambridge Isotope*. Multiplicities are indicated by *s* (singlet), *d* (doublet), *t* (triplet), *q* (quartet), *quint* (quintet), *m* (multiplet), *br* (broad), *dd* (doublet of doublet) and *dt* (doublet of triplet). Scalar coupling constants, *J*, are reported in Hertz. The assignments were verified using the following 2D-experiments if necessary: HSQC, HMBC, COSY and ROESY. ^{1}H 2D-DOSY experiments were performed with stimulated echo and LED schemes using bipolar gradient pulses for diffusion and two spoil gradients. The strength of the diffusion gradients was varied from 5% to 95% in 32 increments. Typically, 8 to 32 scans were recorded for each increment.[1] The length of the diffusion and spoil gradients was 2 and 1.1 ms respectively with a gradient recovery time of 200 μs. The data matrix was 4K x32 in the time domain and 4K x512 in the processed domain.

Solvent	Abbrev.	% deuterium
d_1-chloroform	$CDCl_3$	*d* 99.8%
d_6-dimethylsulphoxyde	d_6-DMSO	*d* 99.9%
d_4-methanol	CD_3OD	*d* 99.8%
d_2-dichloromethane	CD_2Cl_2	*d* 99.9%
d_2-water	D_2O	*d* 99.9%

Table 1. Deuterated solvents list. All of solvents were purchased from Cambridge Isotope Laboratories.

Mass spectroscopy: Mass spectroscopy was performed by the Neuchâtel Platform of Analytical Chemistry (*NPAC*) of the University of Neuchâtel. Electrospray (ESI (+/-)) were performed on a *API 4000 QTrap ABSciex* or *LC/MSD Trap Agilent*. The LC-MS retention times (R_t) and low resolution MS were recorded on a *UPLCUltimate 3000 Dionex - API 4000 QTrap, ABSciex*. The solvent were on ULC grade and water was milli-q grade. High resolution mass spectra were measured on *Bruker FTMS 4.7T BioAPEX II FT/ICR* using a standard electrospray ion source (ESI) or MALDI at the University of Fribourg (Switzerland) by Mr. F. Nydegger.

Infrared spectroscopy: Infrared spectra (IR) were recorded on a *Perkin Elmer Spectrum One FT-IR version B* spectrophotometer using the software *Spectrum version 5.0.1* for recording and treating the data. Peaks are reported in cm^{-1} with indicated relative intensities: *s* (strong, 67-100%); *m* (medium, 34-66%); *w* (weak, 0-33%). Solid samples were measured in a freshly prepared KBr pellet. Liquids were measured as films using polished KBr plates. * The asterisk refers to measurements carried out on a Thermo Scientific Nicolet iS5 iD5 ATR instrument.

DSC and POM analyses: Differential scanning calorimetry DSC analyses were accomplished on a Mettler Toledo DSC1 STARe instrument. The samples were prepared in aluminum sampler. Each analysis refers to a three-cycle heating-cooling running at 10 °C/min under nitrogen flux. Data were analyzed on STARe software. Melting glass transition point temperature refers to the *onset* value. Polarized light microscope POM analyses were performed in an Axioscope Zeiss microscope. Samples were heated on a Linkam THMS 600 heater controlled by a Linkam 93 apparatus. POM images were taken by a Fujix Digital Camera HC-300Z and treated with Axio vision Rel 4.8 program. DSC and POM analysis were performed in the group of Prof. Deschneaux's group at the Institute of Chemistry of the University of Neuchâtel.

Melting points: M.p. were determined using a *Gallenkamp MPD 350-BM* capillary melting point apparatus in open tubes and are uncorrected.

Chemicals

Product	abbreviation	quality
Triethyl amine	TEA	Acros 99%
4-Dimethylammino-pyridine	DMAP	Fluka, puriss. 99%
sodium bicarbonate	$NaHCO_3$	Technical grade
Magnesium Sulphate	$MgSO_4$	puriss.
Sodium Azide	NaN_3	Fluka, purum 99%
Copper sulphate pentahydrate	$CuSO_4\ 5H_2O$	Technical grade
Sodium Ascorbate	NaAsc	Acros 99%
Mesyl chloride	MsCl	Fluka, 99.5%
Pyridine	Py	Fluka, 99.8%
Copper (I) Iodide	CuI	Fluka, purum 98%
Propargyl bromide	C_3H_3Br	Acros, 80% toluene
Neutral allumina	Al_2O_3	Fluka, purum 95%
Methyl sulphate	Me_2SO_4	Fluka, purum 95%
Potassium carbonate	K_2CO_3	Fluka, puriss. 99%
Potassium permanganate	$KMnO_4$	Fluka, purum 99%
Potassium hydroxide	KOH	Fluka, purum 85%
Sodium chloride	NaCl	Technical grade
Thionyl chloride	$SOCl_2$	Fluka, purum 99%
Ethyl amine	$EtNH_2$	Fluka

Thiophenol	Ph-SH	Aldrich, 99%
Tetrabutyl ammonium iodide	TBAI	Fluka, 98%
Hexyl amine	$C_6H_{13}NH_2$	Fluka, 99%
3,4,5-trihydroxybenzamide	$C_7H_7NO_4$	Alfa Aesar, 98%
Dodecyl amine	$C_{12}H_{25}NH_2$	Acros, 98%
Octadecyl amine	$C_{18}H_{35}NH_2$	Alfa Aesar, 98%
2,5-difluoro-1,4-dibromobenzene	$C_6H_2Br_2F_2$	Fluorochem, 98%
N-hydroxysuccinimide	NBS	Fluka, 95%
Palladium tetrakis	$Pd(PPh_3)_4$	Fluka, purum >97% (Pd)
Lithium aluminum hydride	$LiAlH_4$	Aldrich, (2.4M in THF)
Sodium Iodide	NaI	Riedel-de- Haen puriss.
Potassium Iodide	KI	Fluka, puriss. 99%
Cesium Carbonate	Cs_2CO_3	Alfa Aesar, 99.9%
Sodium sulfate	Na_2SO_4	purris.
5-chloro-1-pentyne	C_5H_7Cl	Apollo Scientific
1-bromo hexane	$C_6H_{13}Br$	Acros, 98%
2-bromo-1-ethanol	C_2H_5BrO	Acros, 97%
4-bromo-1-butanol	C4H9BrO	Aldrich, 85%
6-bromo-1-hexanol	$C_6H_{13}BrO$	Alfa Aesar, 97%
Therphthaloyl chloride	$C_8H_4Cl_2O_2$	Aldrich, 99%
Hydroquinone *bis*(2-hydroxyethyl) ether	$C_{10}H_{14}O_4$	Acros, 99%
Isophthaloyl chloride	$C_8H_4Cl_2O_2$	Aldrich, 99%

Table 2. List of chemicals and the corresponding suppliers and purities.

Solvents: Anhydrous solvents were purchased over molecular sieves and used without any further purification: toluene (≥99.7%, ≤0.005% H_2O, Aldrich), DMF (≥ 99.8%, ≤ 0.01% H_2O, Aldrich), DMSO (≥99.5%, ≤0.005 H_2O, Aldrich), THF (≥99.5%, ≤0.025 H_2O, stabilized WITH 0.025% 2,6-di-*t*Bu-4-methylphenol, Aldrich). Brine refers to a sat. aq. solution of NaCl. Petroleum ether refers to a boiling fraction of 40 ° - 60 °C. The other solvents used for reactions are listed in Table 3. All other solvents were of technical grade and used without further purifications. Degassed solvents refers to a freshly degassed solvents prepared by bubbling dried nitrogen for at least 20 min.

Solvents	abbreviation	quality	Supplier
Diethyl ether	Et_2O	*p.a.*	Honeywell
Dichloromethane	DCM or CH_2Cl_2	*p.a.*	Honeywell
Chloroform	$CHCl_3$	*p.a.*[a]	Honeywell
Tetrahydrofurane	THF	>99.5%	VWR
Ethanol	EtOH	*p.a.*	Honeywell
Methanol	MeOH	99.9%	VWR
Toluene	Toluene	*p.a.*	Honeywell
N-methyl pyrrolidone	NMP	99%	Acros
Water	H_2O	milli-q water[b]	

Table 3. List of non-dry solvent used for reactions. [a] Stabilized by 1% of ethanol. [b] Refers to a reverse osmosis filtered water by employing Merck Millipore® system. The notation *p.a.* means for analyses.

Synthetic procedures

Synthesis of the aromatic linkers

Synthesis of compound **46**

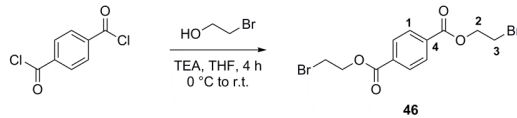

46

2-bromo-ethanol (0.38 mL, 5.4 mmol) and TEA (1.03 mL, 7.4 mmol) were dissolved in dry THF (5 mL) and cooled at 0 °C. Terephtaloyl chloride (500 mg, 2.46 mmol) was dissolved in dry THF (3 mL) and added dropwise to the reaction. The reaction was stirred at 0 °C for 1 hour and then for 3 hours at r.t. The organic solution was removed under vacuum and the resulting white solid was dissolved in AcOEt. The organic phase was washed with Hydrochloric acid 0.5 M (2 x 20 mL), with a solution of $NaHCO_3$ 5% and then with brine. The organic phase was dried with $MgSO_4$ and the solvent was evaporated under vacuum. The product was recrystallized from isopropyl ether to afford 516.3 mg of a white solid in 55% yield. Spectroscopic data were in agreement with the literature.

R_f (EDP/ethyl acetate 7:3): 0.82

M.p.: 93 ° - 94 °C

^{1}H-NMR ($CDCl_3$, 400 MHz, 295K): δ= 8.15 (s, 4H, H1), 4.66 (*t*, $^3J_{H\text{-}H}$ = 6.0 Hz, 4H, H2), 3.66 (t, $^3J_{H\text{-}H}$ = 6.0 Hz, 4H, H2) ppm.

^{13}C-NMR ($CDCl_3$, 100 MHz, 295K): δ= 165.3 (*C*=O), 133.8 (*C*4), 129.4 (*C*1), 64.7 (*C*2), 28.7 (*C*3) ppm.

Synthesis of compound **47**

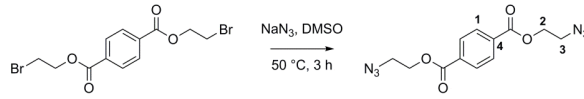

46 **47**

NaN_3 (102.6 mg, 1.58 mmol) was dissolved in dry DMSO (2 mL) after stirring for 30 min at 50 °C. The dibromo derivative **46** (100 mg, 0.26 mmol) was dissolved in dry DMSO (1 mL) and added to the solution. The reaction was stirred at 50 °C for 3 hours. The solution was cooled at r.t. and diluted in water (20 mL). The aqueous phase was extracted with Et_2O (3 x 20 mL), the organic phase was dried over $MgSO_4$ and the solvent evaporated at ambient pressure to afford a white solid in 85% yield. The product was used without further purification.

R_f (EDP/ethyl acetate 7:3): 0.67

M.p.: 81 ° - 82 °C

^{1}H-NMR ($CDCl_3$, 400 MHz, 295K): δ= 8.15 (s, 4H, H1), 4.53 (*t*, $^3J_{H\text{-}H}$ = 5.0 Hz, 4H, H2), 3.63 (*t*, $^3J_{H\text{-}H}$ = 5.0 Hz, 4H, H3) ppm.

^{13}C-NMR ($CDCl_3$, 100 MHz, 295K): δ= 165.3 (*C*=O), 133.5 (*C*4), 129.8 (*C*1), 64.00 (*C*2), 49.8 (*C*3) ppm.

Synthesis of compound **48**

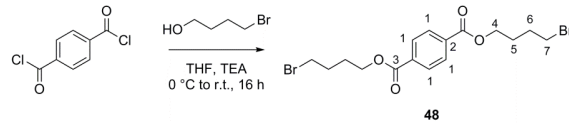

4-bromo-1-butanol (0.19 mL, 329.9 mg, 2.16 mmol) was dissolved in dry THF (5 mL) and cooled at 0 °C. TEA (0.4 mL, 2.94 mmol) was added and a white solid formation took place. Terephthaloyl chloride (200 mg, 0.98 mmol) was dissolved in dry THF (5 mL) and added dropwise to the reaction. The reaction was stirred at 0 °C for 1 hour and then for 16 hours at r.t. The solvent was removed under vacuum and the resulting solid was dissolved in AcOEt. The organic phase was washed with Hydrochloric acid 2M, then with $NaHCO_3$ 5% and finally with brine. The organic phases were dried over $MgSO_4$. The product was purified by chromatography on silica gel using cyclohexane/ethyl acetate 8:2 to afford 181 mg of white solid product in 42% yield.

R_f (cyclohexane/ethyl acetate 8:2): 0.51

^{1}H-NMR ($CDCl_3$, 400 MHz, 295K): δ= 8.07 (*s*, 4H, H1), 4.36 (*t*, $^3J_{H,H}$ = 6.2 Hz, 4H, H4), 3.46 (*t*, $^3J_{H,H}$ = 6.4 Hz, 4H, H7), 2.05-1.90 (*m*, 8H, H5-H6) ppm.

^{13}C-NMR ($CDCl_3$, 100 MHz, 295K): δ= 165.7 (*C*=O), 134.1 (*C2*), 129.6 (*C1*), 64.5 (*C4*), 33.1 (*C7*), 29.4 (*C*), 27.4 (*C*) ppm**.**

Synthesis of compound **49**

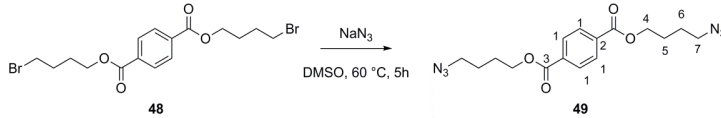

NaN_3 (148 mg, 2.28 mmol) was dissolved in dry DMSO (3 mL) by heating at 60 °C for 30 min. The dibromo derivative **48** was added to the reaction and stirred at 60 °C for 5 hours. The reaction was cooled to r.t. and diluted with water. The aqueous phase was extracted with Et_2O and the organic phases were dried over $MgSO_4$. The solvent was evaporated and the product was obtained as a 91.1 mg of brownish oil in 66% yield.

R_f (cyclohexane/ethyl acetate 8:2): 0.45

IR (Film $CDCl_3$): 2930 *m*, 2859 *w*, 2096 *m*, 1718 *s*, 1635 *w*, 1591 *w*, 1557 *w*, 1505 *w*, 1440 *w*, 1408 *w*, 1380 *w*, 1268 *s*, 1112 *s*, 1019 *m*, 910 *w*, 875 *w*, 796 w, 730 *s*.

^{1}H-NMR ($CDCl_3$, 400 MHz, 295K): δ= 8.08 (*s*, 4H, H1), 4.36 (*t*, $^3J_{H,H}$ = 6.3 Hz, 4H, H4), 3.36 (*t*, $^3J_{H,H}$ = 6.7 Hz, 4H, H7), 1.89-1.84 (*m*, 4H, H5), 1.79-1.71 (*m*, 4H, H6) ppm.

^{13}C-NMR ($CDCl_3$, 100 MHz, 295K): δ= 165.8 (C=O), 134.1 (*C2*), 129.6 (*C1*), 64.8 (*C4*), 51.1 (*C7*), 26.1 (*C*5), 25.7 (*C*6) ppm**.**

MS (ESI): m/z (%)= 383.8(100) $[M+Na]^+$

HR-ESI MS: Calc. for $[M+Na]^+$ $C_{16}H_{20}N_6NaO_4^+$ 383.1438; found 383.1440 $[M+Na]^+$

Synthesis of compound **50**

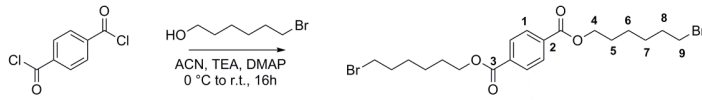

50

6-bromo-1-hexanol (0.64 mL, 4.92 mmol) was dissolved in acetonitrile (15 mL) and the solution was cooled at 0 °C. TEA (1.02 mL, 7.38 mmol) and DMAP (60.11 mg, 0.49 mmol) were added and the solution was stirred for 5 min. Terephthaloyl chloride (500 mg, 2.46 mmol) was dissolved in acetonitrile (10 mL) and slowly added to the solution. The reaction was stirred for 1 hour at 0 °C and for other 16 hours at r.t. The organic solvent was removed under vacuum and the resulting solid was dissolved in ethyl acetate. The organic phase was washed with hydrochloric acid 2M, $NaHCO_3$ 5% and finally with brine. The organic phases were dried over $MgSO_4$ and the product was purified by chromatography on silica gel using cyclohexane/ ethyl acetate 85:15 to afford 97.6 mg of a white solid product in 8% yield.

R_f (Cy/AcOEt 8:2): 0.68

IR (Film $CDCl_3$): 2932 *w*, 2856 *w*, 1717 *s*, 1267 *s*, 1463 *w*, 1408 *w*, 1270.33 *m*, 1118 *s*, 1103 *s*, 1108 *m*, 959 *w*, 875 *w*, 730 *w*.

^{1}H-NMR ($CDCl_3$, 400 MHz, 295K): δ= 8.10 (*s*, 4H, H1), 4.34 (*t*, $^3J_{H,H}$ = 6.6 Hz, 4H, H4), 3.41 (*t*, $^3J_{H,H}$ = 6.7 Hz, 4H, H9), 1.90 (*quint*, $^3J_{H,H}$ = 6.7 Hz, 4H, H8), 1.81 (*quint*, $^3J_{H,H}$ = 6.7 Hz, 4H, H5), 1.57-1.44 (*m*, 8H, H6 and H7) ppm.

^{13}C-NMR ($CDCl_3$, 100 MHz, 295K): δ= 165.9 (*C*=O), 134.2 (*C2*), 129.6 (*C1*), 65.4 (*C4*), 33.8 (*C9*), 32.7 (*C8*), 28.6 (*C*5), 27.9 (*C*6 or *C7*), 25.4 (*C*6 or *C7*) ppm**.**

MS (ESI): m/z (%)= 515.3(100) $[M+Na]^+$

HRMS: Calc. for $[M+Na]^+$ $C_{20}H_{28}Br_2NaO_4^+$ 513.0247; found 513.0246 $[M+Na]^+$

Synthesis of compound **51**

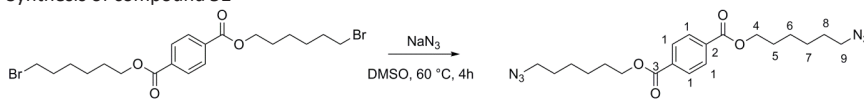

50 **51**

NaN_3 (69.3 mg, 1.87 mmol) was dissolved in dry DMSO (2 mL) by stirring for 30 min at 60 °C. The dibromo derivative **50** (87.3 mg, 0.178 mmol) was added and the reaction was stirred at 60 °C for 4 hours. The reaction was cooled to r.t. and diluted with water. The aqueous phase was extracted with Et_2O (2 x 5 mL). The organic phases were dried over $MgSO_4$ and the solvent was evaporated. The product was purified by chromatography on silica gel using Cyclohexane/ ethyl acetate 8:2 as the eluent. The product was obtained as colorless oil in 52.3 mg in 71% yield.

R_f (Cy/AcOEt 8:2): 0.49

IR (film $CDCl_3$)*: 2930 *m*, 2858 *w*, 2093 *s*, 1719 *s*, 1463 *w*, 1408 *w*, 1268 *s*, 1119 *s*, 1102 *s*, 1018 *m*, 875 *w*, 731 *s*.

^{1}H-NMR ($CDCl_3$, 400 MHz, 295K): δ= 8.08 (*s*, 4H, H1), 4.35 (*t*, $^3J_{H,H}$ = 6.6 Hz, 4H, H4), 3.28 (*t*, $^3J_{H,H}$ = 6.9 Hz, 4H, H9), 1.78 (*quint*, $^3J_{H,H}$ = 6.6 Hz, 4H, H5), 1.61 (*quint*, $^3J_{H,H}$ = 6.9 Hz, 4H, H8), 1.50-1.41 (*m*, 8H, H6 and H7) ppm.

^{13}C-NMR ($CDCl_3$, 100 MHz, 295K): δ= 166.0 (*C*=O), 134.3 (C2), 129.6 (C1), 65.4 (C4), 51.5 (C9), 28.9 (*C*5), 28.7 (*C*8), 26.6 (*C*6 or *C*7), 25.8 (*C*6 or *C*7) ppm.

MS (ESI): m/z (%)= 439.4(100) $[M+Na]^+$

HRMS (ESI): Calc. for $[M+Na]^+$ $C_{20}H_{28}N_6NaO_4^+$ 439.2064; found 439.2064 $[M+Na]^+$

Synthesis of compound **65**

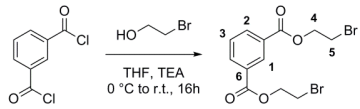

64 **65**

Isopthaloyl chloride **64** (1 g, 4.92 mmol) was dissolved in dry THF (10 mL) and added dropwise to a dry THF solution (10 mL) of 2-bromoethanol (1.4 mL, 19.7 mmol) and TEA (3.4 mL, 24.6 mmol) at 0 °C. The reaction was stirred at 0 °C for 1 hour and at r.t. for 18 hours. The solvent was removed under vacuum and the resulting solid was dissolved in DCM and washed with hydrochloric acid 2M. The organic phase was dried over $MgSO_4$. The solvent was removed under vacuum and the resulting solid was recrystallized from iPr_2O to afford 1.1323 g of a white solid in 60% yield. The spectroscopic dates are in agreement with the literature.[2]

R_f (Cy/AcOEt 1:1): 0.44

M.p.: 60.7 °C

^{1}H-NMR ($CDCl_3$, 400 MHz, 295K): δ= 8.73 (s, 1H, H1), 8.28 (*dd*, $^4J_{H,H}$ = 7.8 Hz, $^5J_{H,H}$ = 0.86 Hz, 2H H2), 7.57 (d*t*, $^3J_{H,H}$ = 7.8 Hz, $^5J_{H,H}$ = 2.8 Hz, 1H, H3), 4.67 (*t*, $^3J_{H,H}$ = 6.1 Hz, 4H, H4), 3.66 (*t*, $^3J_{H,H}$ = 6.1 Hz, 4H, H5) ppm.

^{13}C-NMR ($CDCl_3$, 100 MHz, 295K): δ= 165.26 (*C*=O), 134.39 (*C*2), 131.16 (*C*1) 130.33 (*C*6), 128.80 (*C*3), 64.65 (*C*4), 28.67 (*C*5) ppm.

Synthesis of compound **66**

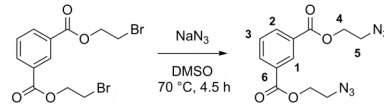

65 **65**

NaN_3 (718.5 mg, 11.05 mmol) was dissolved in dry DMSO (9 mL) by stirring and heating for 30 min at 70 °C. Dibromo derivative **65** (700 mg, 1.84 mmol) was added to the solution and stirred at 70 °C for 4.5 h. The reaction was cooled to r.t. and diluted with water. The aqueous solution was extracted with Et_2O and the organic phases were dried over $MgSO_4$. The solvent was removed under vacuum and the crude was recrystallized from isopropyl ether to afford 361.7 mg of a white powder in 65% yield. The spectroscopic dates were in agreement with the literature.[2]

R$_f$ (cyclohexane/ethyl acetate 8:2): 0.29

M.p.: 78 °C

^{1}H-NMR ($CDCl_3$, 400 MHz, 295K): δ= 8.74 (s, 1H, H1), 8.28 (*d*, $^4J_{H,H}$ = 7.8 Hz, 2H H2), 7.58 (*t*, $^3J_{H,H}$ = 7.8 Hz, 1H, H3), 4.53 (*t*, $^3J_{H,H}$ = 4.8 Hz, 4H, H4), 3.62 (*t*, $^3J_{H,H}$ = 4.9 Hz, 4H, H5) ppm.

^{13}C-NMR ($CDCl_3$, 100 MHz, 295K): δ= 165.44 (*C*=O), 134.44 (*C*2), 131.18 (*C*1), 130.25 (*C*6), 129.05 (*C*3), 64.19 (*C*4), 49.95 (*C*5) ppm.

Synthesis of compound **61**

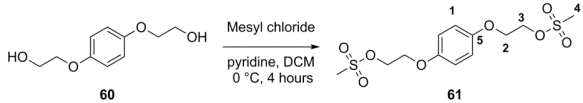

60 **61**

Hydroquinone *bis*(2-hydroxyethyl) **60** (300 mg, 1.51 mmol) was dissolved in dry DCM (3 mL) and the solution was cooled at 0 °C. Pyridine (0.49 mL, 6.05 mmol) was added and the solution was stirred for 5 min. Methanesulfonyl chloride (0.35 mL, 4.54 mmol) was added dropwise and the reaction was stirred at 0 °C for 4 hours. The organic solution was diluted with DCM and washed with hydrochloric acid 2M, $NaHCO_3$ 5% and with brine. The organic phase was dried over $MgSO_4$ and the solvent was evaporated under vacuum to afford 451 mg of a white solid in 85% yield. The product was used in the further step without any other purification. The measured spectral data are in agreement with the data reported in literature.[3]

M.p.: 100 ° – 101 °C

***R*$_f$** (EDP/AcOEt 7:3): 0.46

^{1}H-NMR ($CDCl_3$, 400 MHz, 295K): δ= 6.85 (*s*, 4H, H1), 4.55 (AA'BB' *coupling system*, 4H, H3), 4.20 (AA'BB' *coupling system*, 2H, H2), 3.08 (*s*, 6H, H4) ppm.

^{13}C-NMR ($CDCl_3$, 100 MHz, 295K): δ= 152.9 (*C*5), 115.9 (*C*1), 68.2 (*C*3), 66.7 (*C*2), 37.9 (*C*4) ppm**.**

Synthesis of compound **62**

61 **62**

NaN_3 (218.4 mg, 3.36 mmol) was dissolved in dry DMSO (2 mL) at 50 °C. The solution became homogenous after stirring for ca. 30 min. Compound **61** (200 mg, 0.56 mmol) was dissolved in dry DMSO (1 mL) and added to the solution. The reaction was stirred for 4 hours at 50 °C. The solution was cooled to r.t. and diluted with water. The aqueous phase was extracted with Et_2O and the organic phases were dried over $MgSO_4$. The solvent was removed under vacuum to afford 107 mg of a white solid in 77% yield.
The measured spectral data are in agreement with the data reported in literature.[3]

M.p.: 50 °C

***R*$_f$** (EDP/AcOEt 8:2): 0.9

^{1}H-NMR ($CDCl_3$, 400 MHz, 295K): δ= 6.87 (s, 4H, H1), 4.11 (*t*, $^{3}J_{H,H}$ = 5.0 Hz, 4H, H2), 3.37 (*t*, $^{3}J_{H,H}$ = 5.0 Hz, 4H, H3) ppm.

^{13}C-NMR ($CDCl_3$, 100 MHz, 295K): δ= 153.0 (*C*4), 115.8 (*C*1), 67.7 (*C*2), 50.3 (*C*3) ppm.

Synthesis of compound **56**

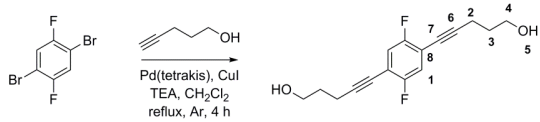

55 **56**

The cross-coupling conditions were used from similar reaction described in literature.[5] 1,4-dibromo-2,6-difluorobenzene **55** (500 mg, 1.84 mmol) was dissolved in a freshly degassed dichloromethane (5 mL). CuI (17.5 mg, 0.092mmol) and freshly degassed TEA (15 mL) were added to the solution. 4-pentyne-1-ol (0.51 mL, 5.52 mmol) was added and the solution was stirred for 5 min. $Pd(PPh_3)_4$ (106.3 mg, 0.092 mmol) was added and the reaction was stirred at 60 °C for 4 hours. The reaction was cooled to r.t., diluted with AcOEt (30 mL) and washed with hydrochloric acid 2M (2 x 20 mL). The organic phases were dried over $MgSO_4$ to afford a brownish crude solid. The product was purified by chromatography on silica gel using Cy/AcOEt 1:1 to afford 426.7 mg of brown solid in 83% yield.

R_f (cyclohexane/ethyl acetate 1:1): 0.24

M.p.: 100 ° - 102 °C

IR (solid KBr): 3370 *s*, 2939 *m*, 2890 *w*, 2234 *w*, 1616 *w*, 1497 *s*, 1414 *s*, 1349 *w*, 1312 *w*, 1277 *w*, 1226 *w*, 1168 *m*, 1072 s, 1045 *s*, 975 *m*, 918 *m*, 889 *s*. 852 *w*, 801 *w*, 703 *w*.

^{1}H-NMR ($CDCl_3$, 400 MHz, 295K): 7.04 (*t*, $^{3}J_{H,F}$ = 7.5 Hz, $^{4}J_{H,F}$ = 7.5 Hz, 2H, H1), 3.81 (*t*,$^{3}J_{H,H}$ = 6.1 Hz, 4H, H4), 2.58 (*t*, $^{3}J_{H,H}$ = 6.9 Hz, 4H, H2), 1.87 (*quint*, $^{3}J_{H,H}$ = 6.5 Hz, 4H, H3), 1.52 (*s*, 2H, H5) ppm.

^{13}C-NMR ($CDCl_3$, 100 MHz, 295K): δ= 119.46 (*dd*, $^{3}J_{F,C}$ = 17.8 Hz, $^{4}J_{F,C}$ = 9.7 Hz, *C*1), 113.14 (*dd*, $^{2}J_{F,C}$ = 12.2 Hz, $^{3}J_{F,C}$ = 3.9 Hz, *C7*)*, 97.49 (*C*6), 73.70 (*C7*), 61.71 (*C*4), 31.71 (*C*3), 16.34 (*C*2) ppm. Some aromatic signals were not detected. * The signal was measured and attributed by HMBC experiments.

^{19}F-NMR ($CDCl_3$, 400 MHz, 295K): δ= -118.22 ppm.

MS (ESI): m/z (%)= 301.3(100%) $[M+Na]^+$ 279.3(3%) $[M+H]^+$

HRMS (MALDI): Calc. for $[M+Na]^+$ $C_{16}H_{16}F_2NaO_2^+$ 301.1011; found 301.1009 $[M+Na]^+$

Synthesis of compound **57**

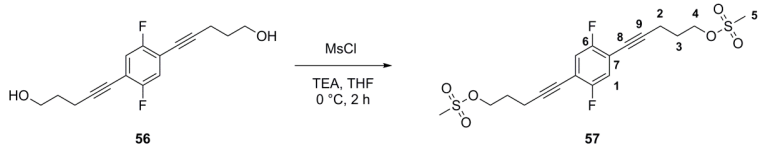

56 **57**

Compound **56** (300 mg, 1.08 mmol) and TEA (0.6 mL, 4.32 mmol) were dissolved in dry THF (5 mL) under nitrogen and cooled to 0 °C. Mesyl chloride (0.25 mL, 3.24 mmol) was added dropwise over 5 min. and the reaction was stirred at 0 °C for 2 hours. The solution was diluted with AcOEt (20 mL)

and washed with hydrochloric acid 2M, $NaHCO_3$ and brine. The organic phase was dried over $MgSO_4$ and the solvent was removed under vacuum to afford 552.4 mg of a white solid in quantitative yield. The product was used to the following step without any other purification.

R_f (cyclohexane/AcOEt 1:1): 0.41

M.p.: 77 °C – 78 °C

IR (KBr solid): 3424 *w*, 3020 *w*, 2971 *w*, 2944 *w*, 2237 *w*, 1737 *w*, 1504 *m*, 1472 *w*, 1446 *w*, 1416 *s*, 1386 *w*, 1346 *s*, 1277 *w*, 1246 *w*, 1224 *w*, 1165 *s*, 1175 *s*, 1089 *w*, 1052 *w*, 1013 *m*, 982 *s*, 969 *m*, 934 *s*, 880 *m*, 822 *m*, 802 *m*, 781 *m*, 765 *m*, 730 *m*, 719 *w*, 531 *s*, 470 *w*.

^{1}H-NMR ($CDCl_3$, 400 MHz, 295K): 7.05 (*t*, $^3J_{H,F}$ = 7.4 Hz, $^4J_{H,F}$ = 7.4 Hz, 2H, H1), 4.40 (*t*,$^3J_{H,H}$ = 6.0 Hz, 4H, H4), 3.04 (*s*, 6H, H5), 2.64 (*t*, $^3J_{H,H}$ = 6.8 Hz, 4H, H2), 2.06 (*quint*, $^3J_{H,H}$ = 6.8 Hz, 4H, H3) ppm.

^{13}C-NMR ($CDCl_3$, 100 MHz, 295K): 158.52 (*dd*, $^1J_{F,C}$ = 248.7 Hz, $^4J_{F,C}$ = 3.7 Hz, *C*6), 119.53 (*dd*, $^3J_{F,C}$ = 17.9 Hz, $^4J_{F,C}$ = 9.7 Hz, *C*1), 112.91 (*dd*, $^2J_{F,C}$ = 12.5 Hz, $^3J_{F,C}$ = 3.8 Hz, *C*7), 95.81 (C9), 74.51 (C8), 68.37 (C4), 37.39 (C5), 27.90 (C3), 16.08 (C2) ppm.

^{19}F-NMR ($CDCl_3$, 400 MHz, 295K): δ= -117.84 ppm

MS (ESI): m/z (%)= 457.4 (100) $[M+Na]^+$

HRMS (ESI): Calc. for $[M+Na]^+$ 457.0562 $[C_{18}H_{20}F_2NaO_6S_2]^+$; found 457.0562 $[M+Na]^+$

Synthesis of compound **58**

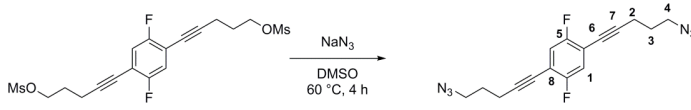

57 **58**

NaN_3 (358.8 mg, 5.52 mmol) was dissolved in dry DMSO (7 mL) by stirring the heterogeneous mixture at 60 °C for 1 hour. Compound **57** (381 mg, 0.88 mmol) was added to the solution and the reaction was stirred at 60 °C for 4 hours. The reaction cooled to r.t, diluted with water and extracted with Et_2O. The organic phases were dried over $MgSO_4$ and the solvent was removed under vacuum. The product was purified by chromatography on silica gel using Cy/AcOEt 8:2 to afford 172.7 mg of yellowish oil in 60% yield.

R_f (cyclohexane/ethyl acetate 8:2): 0.75

IR (Film $CDCl_3$): 2932.02 *w*, 2253.06 *w*, 2101.54 *m*, 1501.97 *w*, 1416.14 *w*, 1175.52 *w*, 908.21 *m*, 733.24 *m*, 650.72 *w*.

^{1}H-NMR ($CDCl_3$, 400 MHz, 295K): 7.05 (*t*, $^3J_{H,F}$ = 7.5 Hz, $^4J_{H,F}$ = 7.5 Hz, 2H, H1), 3.48 (*t*,$^3J_{H,H}$ = 6.6 Hz, 4H, H4), , 2.58 (*t*, $^3J_{H,H}$ = 6.9 Hz, 4H, H2), 1.88 (*quint*, $^3J_{H,H}$ = 6.7 Hz, 4H, H3) ppm.

^{13}C-NMR ($CDCl_3$, 100 MHz, 295K): δ= 158.51 (*dd*, $^1J_{F,C}$ = 248.6 Hz, $^4J_{F,C}$ = 4.1 Hz, *C*5), 119.5 (*dd*, $^3J_{F,C}$ = 17.7 Hz, $^4J_{F,C}$ = 9.8 Hz, *C*1), 113.08 (*dd*, $^2J_{F,C}$ = 13.3 Hz, $^3J_{F,C}$ = 32 Hz, *C*8), 96.4 (*C*7), 74.2 (*C*6), 50.3 (*C*4), 27.8 (*C*2), 17.1 (*C*3) ppm.

^{19}F-NMR ($CDCl_3$, 400 MHz, 295K): δ= -117.97 ppm

MS (ESI): m/z (%)= 351.3(100) $[M+Na]^+$

Synthesis of 2-substituted BTA derivatives

Synthesis of compound **33**

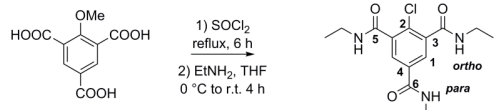

32 **33**

2-methoxy 1,3,5-tricarboxylic acid **32** (100 mg, 0.41 mmol) was suspend in $SOCl_2$ (2 mL). Two drops of DMF were added and the mixture was heated at 80 °C for 6 hours. Volatile compounds were removed under high vacuum to afford a pale yellow oil. In a two necked flask, $EtNH_2$ (0.23 mL, 2.87 mmol, sol 70% in water) was dissolved in THF (2 mL) and cooled to 0 °C. The acid chloride was dissolved in THF (5 mL) and added dropwise to the solution. The reaction was stirred at 0 °C for 1 hour and at r.t. for other 4 hours. The solution was acidified with hydrochloric acid 2M to pH 3 and the organic solvent was removed under vacuum. The resulting aqueous solution was extracted with AcOEt (4 x 20 mL). The organic phases were dried on $MgSO_4$ and the solvent removed under vacuum. The product was purified by chromatography on SiO_2 using AcOEt/ MeOH 9:1 as the eluent to afford34.5 mg of a white solid in 26% yield.

R_f (AcOEt/MeOH 8:2): 0.68

M.p.: 264 ° - 268 °C

IR (KBr): 3437 *m*, 3248 *w*, 3082 *w*, 2978 *w*, 2918 *w*, 2381 *w*, 2372 *w*, 2346 *w*, 1630 *s*, 1560 *w*, 1463 *m*, 1413 *w*, 1384 *w*, 1353 *w*, 1301 *w*, 1149 *w*, 999 *w*, 911 *w*, 697 *w*, 528 *w*.

^{1}H-NMR (CD_3OD, 400 MHz, 295K): δ= 7.93 (s, 2H, H1), 7.15 (*t*, $^3J_{H,H}$ = 5.5 Hz, 2H, N-H_{ortho}), 6.25 (*t*, $^3J_{H,H}$ = 5.7 Hz, 1H, N-H_{para}), 3.34-3.38 (*m*, 6H, H7), 1.26-1.20 (*m*, 6H, H7) ppm.

^{13}C-NMR (CD_3OD, 100 MHz, 295K): δ= 168.6 (*C*5), 167.0 (*C*6), 139.15 (*C*2), 134.6 (*C*3), 131.7 (*C*4), 129.1 (*C*1), 36.0 (*C*7), 35.8 (*C*7), 14.7 (*C*8), 14.6 (*C*8) ppm.

MS (ESI): m/z (%)= 348.2(80) $[M+Na]^+$

HRMS (MALDI): Calc. for $[M+Na]^+$ $C_{15}H_{20}ClN_3NaO_3^+$ 348.1085; found 348.1083 $[M+Na]^+$

Synthesis of compound **34d**

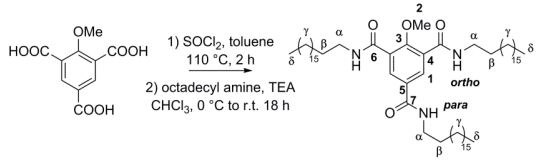

32 **34d**

2-methoxy trimesic acid **32** (2.37 g, 9.87 mmol) was suspended in dry toluene (60 mL) and two drops of DMF were added. $SOCl_2$ (2.4 mL, 32.6 mmol) was added and the suspension was stirred at 110 °C for 2 hours. The resulting homogenous solution was cooled to r.t. and the volatiles were removed under high vacuum (0.01 mbar). The resulting pale yellow oil was dissolved in $CHCl_3$ (20 mL) and added dropwise to a solution at 0 °C of TEA (5.5 mL, 39.5 mmol) and octadecyl amine (8.8 g, 32.6 mmol) in $CHCl_3$ (30 mL). The reaction was stirred at 0 °C for 1 hour and then for 18 hours at r.t. The white amorphous solid was filtered off and the organic phase was washed with hydrochloric acid 2M (3 X 30 mL). The organic phase was then dried over $MgSO_4$. The product was purified by chromatography on silica gel using cyclohexane/ethyl acetate 1:1 to afford 1.559 g of amorphous white solid in 16 % yield.

R_f (cyclohexane/AcOEt 1:1): 0.79

M.p. (DSC 4th heating cycle): 141.41 °C

IR (Film $CDCl_3$): 3255 *m*, 3067 *w*, 2956 *m*, 2918 *s*, 2850 *s*, 1638 *s*, 1552 *m*, 1473 *m*, 1464 *m*, 1428 *w*, 1376 *w*, 1314 w, 1289 *w*, 1257 *w*, 1082 *w*, 1012 *w*, 907 *w*, 807 *w*, 720 *w* 660 *w*, 597 *w*.

^{1}H-NMR ($CDCl_3$, 400 MHz, 295K): δ= 8.38 (s, 2H, H1), 7.17 (*t*, $^3J_{H,H}$ = 5.5 Hz, 2H, N-H_{ortho}), 6.25 (*t*, $^3J_{H,H}$ = 5.7 Hz, 1H, N-H_{para}), 3.91 (*s*, 3H, H2), 3.50-3.40 (*m*, 6H, Hα), 1.66-1.55 (m, 6H, Hβ), 1.41-1.25 (m, 84H, Hγ), 0.88 (*t*, $^3J_{H,H}$ = 6.7 Hz, 9H, Hδ) ppm.

^{13}C-NMR ($CDCl_3$, 100 MHz, 295K): δ= 165.6 (*C*7), 164.8 (*C*6), 157.7 (*C*3), 131.9 (*C*4), 130.9 (*C*5), 128.6 (*C*1), 63.2 (*C*2), 40.4 (*C*α), 40.2 (*C*α), 32.0 (*C*γ), 29.81-29.66 (*C*γ and *C*β), 29.6 (*C*γ), 29.5 (*C*γ), 27.22 (*C*γ), 27.16 (*C*γ), 22.8 (*C*γ), 14.2 (*C*δ) ppm.

MS (ESI): m/z (%)= 1017.4(100) $[M+Na]^+$

HRMS (MALDI): Calc. for $[M+H]^+$ $C_{64}H_{120}N_3O_4^+$ 994.9273; found 994.9276 $[M+H]^+$

Synthesis of compound **36d**

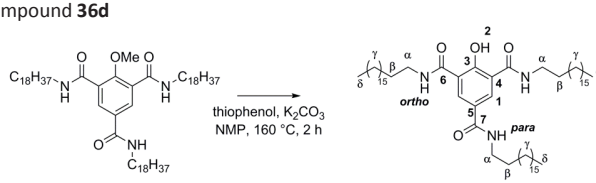

34d **36d**

2-methoxy BTA derivative **34d** (1.3 g, 1.31 mmol) was suspended in NMP (10 mL). K_2CO_3 (270.9 mg, 1.96 mmol) and thiophenol (0.15 mL, 1.44 mmol) were added and the reaction was stirred at 160 °C for 2 hours. The resulting dark homogenous solution was cooled to r.t., diluted with water and acidified to pH= 2 using concentrated hydrochloric acid. The aqueous phase was extracted with $CHCl_3$

(3 x 50 mL) and the organic phases were dried over $MgSO_4$. The solvent was evaporated under vacuum and the product was purified by chromatography on silica gel using cyclohexane/ethyl acetate 7:3 to afford 1.16 g of an amorphous light brown solid in 90% yield.

R_f (cyclohexane/ethyl acetate 7:3): 0.73

M.p.: 48 °C – 50 °C

IR (Film $CDCl_3$): 3292 *m*, 2920 *s*, 2851 s, 1640 *s*, 1548 *s*, 1468 *s*, 1287 *m*, 1190 *w*, 938 *w*, 806 *w*, 769 *w*, 721 *w*, 676 *w*.

^{1}H-NMR ($CDCl_3$, 400 MHz, 295K): δ= 8.51 (*s*, 2H, H1), 6.47 (*t*, $^3J_{H,H}$ = 5.5 Hz, N-H_{para}), 3.48-3.40 (m, 6H, Hα), 1.65-1.54 (m, 6H, Hβ), 1.37-1.25 (m, 84H, Hγ), 0.88 (*t*, $^3J_{H,H}$ = 6.6 Hz, 9H, Hδ) ppm.
^{13}C-NMR ($CDCl_3$, 100 MHz, 295K)*: δ= 165.7 (*C*7), 163.0 (*C*6), 124.3 (*C*1), 40.4 (*C*α), 40.2 (*C*α), 32.1 (*C*γ), (29.86-29.81, 29.76, 29.69, 29.52, 29.48, 29.45, 27.2 *C*γ and *C*β), 22.9 (*C*γ), 14.3 (*C*δ) ppm. * The signals of the aromatic C3, C4 and C5 were not observed.

MS (ESI): m/z (%)= 979.3(100) $[M-H]^-$

HRMS (MALDI): Calc. for $[M-H]^- C_{63}H_{116}N_3O_4^-$ 978.8971; found 978.8974 $[M-H]^-$

Synthesis of compound **34c**

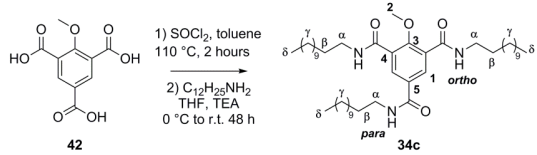

42 **34c**

2-methoxy trimesic acid **32** (3.8 g, 15.8 mmol) was suspended in dry toluene (60 mL) and two drops of DMF were added. $SOCl_2$ (3.5 mL, 47.5 mmol) was added and the suspension was stirred at 110 °C for 2 hours. The resulting homogenous solution was cooled to r.t. and the volatiles were removed under high vacuum (0.01 mbar). The resulting pale yellow oil was dissolved in dry THF (50 mL) and added over 30 min. to a dry THF (50 mL) solution at 0 °C of TEA (8.8 mL, 63.3 mmol) and dodecyl amine (8.8 g, 63.28 mmol) . The reaction was stirred at 0 °C for other 30 min. and then for 48 hours at r.t. The organic solvent was evaporated under vacuum and the resulting solid was dissolved in ethyl acetate. The organic phase was washed with hydrochloric acid 2M, then with $NaHCO_3$. The white solid was filtered off by filtration through celite filter. The organic phase was then washed with brine and dried over $MgSO_4$. The product was purified by chromatography on silica gel using cyclohexane/ethyl acetate 6:4 to afford 5.2 g of amorphous solid in 44% yield.

R_f (toluene/AcOEt 7:3): 0.31

M.p.: 157 °C – 159 °C

IR (Film $CDCl_3$): 3436 *w*, 3019 *m*, 2928 *m*, 2856 *m*, 2400 *w*, 1662 *m*, 1523 *m*, 1464 *w*, 1216 *s*, 929 w, 669 *m*.

^{1}H-NMR ($CDCl_3$, 400 MHz, 295K): δ= 8.34 (*s*, 2H, H1), 7.22 (*t*, $^3J_{H,H}$ = 5.5 Hz, 2H, N-H_{ortho}), 6.33 (*t*, $^3J_{H,H}$ = 5.6 Hz, 1H, N-H_{para}), 3.90 (*s*, 3H, H2), 3.48-3.39 (*m*, 6H, Hα), 1.65-1.55 (*m*, 6H, Hβ), 1.40-1.25 (*m*, 54H, Hγ), 0.87 (*t*, $^3J_{H,H}$ = 6.7 Hz, 9H, Hδ) ppm.

^{13}C-NMR ($CDCl_3$, 100 MHz, 295K): δ= 165.49 (*C*=O), 164.7 (*C*=O), 157.8 (C3), 132.2 (*C*1), 131.3 (*C*5), 128.7 (*C*4), 63.5 (*C*2), 40.3 (*C*α), 40.3 (*C*α), 32.0 (*C*γ), 29.78-29.77-29.75-29.71-29.67 (*C*γ), 29.49-29.46 (Cβ), 27.22 (*C*γ), 27.14 (*C*γ), 22.8 (*C*γ), 14.3 (*C*δ) ppm.

MS (ESI): m/z (%)= 765.1(100) $[M+Na]^+$

HRMS (ESI): Calc. for $[M+H]^+$ $C_{46}H_{83}N_3NaO_4^+$ 764.6276; found 764.6273 $[M+Na]^+$

Synthesis of compound **36c**

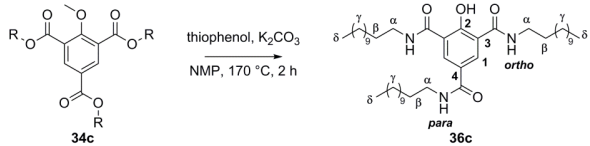

2-methoxy BTA derivative **34c** (4.33 g, 5.84 mmol) was dissolved in NMP (25 mL). K_2CO_3 (1.21 g, 8.76 mmol) and thiophenol (0.72 mL, 7.00 mmol) were added and the reaction was stirred at 170 °C for 2 hours. The reaction was cooled to r.t. and diluted with water (50 mL). The solution was acidified to pH= 2 using concentrated hydrochloric acid. The aqueous phase was extracted with DCM and the organic phase was dried over $MgSO_4$. The solvent was evaporated and the product was purified by chromatography on silica gel using cyclohexane/ethyl acetate 8:2 as the eluent to afford 3.09 g of a dark brown solid in 72% yield.

R_f (cyclohexane/ethyl acetate 8:2): 0.42

M.p.: 72 ° - 75 °C

IR (Solid deposition): 3282 *w*, 2916 *s*, 2849 *s*, 1727 *w*, 1662 *m*, 1638 *m*, 1538 *s*, 1465 *s*, 1329 *m*, 1311 *m*, 1281 *m*, 1156 *m*, 950 *w*, 720 *m*.

^{1}H-NMR ($CDCl_3$, 400 MHz, 295K): δ= 8.68 (*s*, 2H, H1), 8.16 (*broad s*, 2H, N-H_{ortho}), 7.11 (*broad s*, 1H, N-H_{para}), 3.43-3.40 (*m*, 6H, Hα), 1.61-1.52 (*m*, 6H, Hβ), 1.30-1.24 (*m*, 54H, Hγ), 0.87 (*t*, $^3J_{H,H}$ = 6.7 Hz, 9H, Hδ) ppm.

^{13}C-NMR ($CDCl_3$, 100 MHz, 295K)*: δ= 166.5 (*C*=O), 163.5 (*C*=O), 132.1 (*C*1),[a] 40.7 (*C*α), 40.2 (*C*α), 32.0 (*C*γ), 29.77-29.43 (*C*β and *C*γ), 27.2 (*C*γ), 22.8 (*C*γ), 14.3 (*C*δ) ppm. * The signals of the aromatic C2, C3 and C4 were not observed. **Chemical shift estimated by HMBC experiment.

MS (ESI): m/z (%)= 751.0(100) $[M+Na]^+$

HRMS (MALDI): Calc. for $[M+H]^+$ $C_{45}H_{82}N_3O_4^+$ 728.6300; found 762.6286 $[M+H]^+$

Synthesis of compound **37c**

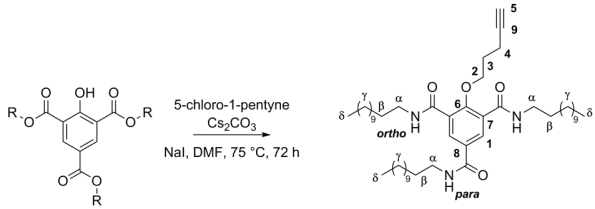

36c
R= $C_{12}H_{25}$

37c

2-hydroxy BTA derivative **36c** (636 mg, 0.87 mmol) was dissolved in dry DMF (2 mL) in a vial. Cs_2CO_3 (286.1 mg, 0.87 mmol) and NaI (65.2 mg, 0.435 mmol) were added forming a heterogeneous solution. 5-chloro-1-pentyne (0.18 mL, 1.75 mmol) was added and the vial was sealed with Teflon®-coated cap and stirred at 75 °C for 72 hours. The reaction was cooled to r.t., diluted with water and the aqueous solution was extracted with ethyl acetate. The organic phases were dried on $MgSO_4$ and the solvent was evaporated under vacuum. The product was purified by chromatography on silica gel using toluene/ethyl acetate 8:2 to afford 150 mg of an amorphous solid in 22% yield.

R_f (toluene/AcOEt 8:2): 0.35

M.p.: 99 ° - 100 °C

IR (Solid deposition): 2920 *s*, 2852 *m*, 1654 *m*, 1638 *s*, 1628 *s*, 1539 *m*, 1454 *m*, 1297 *m*, 718 *m*, 667 *m*, 631 *m*.

^{1}H-NMR ($CDCl_3$, 400 MHz, 295K): δ= 8.33 (*s*, 2H, 1H), 7.05 (*t*, $^3J_{H,H}$ = 5.6 Hz, 2H, N-H_{ortho}), 6.25 (*t*, $^3J_{H,H}$ = 5.6, 1H, N-H_{para}), 4.14 (*t*, $^3J_{H,H}$ = 6.5 Hz, 1H, H2), 3.49-3.40 (*m*, 6H, Hα), 2.36 (*dt*, $^3J_{H,H}$ = 6.9 Hz, $^4J_{H,H}$ = 2.7 Hz, 2H, H4), 2.03-1.97 (*m*, 3H, H3 and H5), 1.65-1.55 (*m*, 8H, Hβ), 1.35-1.26 (*m*, 54H, Hγ), 0.88 (*t*, $^3J_{H,H}$ = 6.7 Hz, 9H, Hδ) ppm.

^{13}C-NMR ($CDCl_3$, 100 MHz, 295K): δ= 164.4 (*C*=O), 164.9 (*C*=O), 156.6 (*C*6), 131.9 (*C*1), 131.3 (*C*8), 129.4 (*C*7), 82.6 (*C*9), 75.9 (*C*2), 69.8 (*C*5), 40.43 (*C*α), 40.37 (*C*α), 32.1 (*C*γ), 29.79-29.68 (*C*γ), 29.49 (*C*β), 29.43 (*C*β), 28.97 (*C*3), 27.3 (*C*γ), 27.1 (*C*γ), 22.8 (*C*γ), 15.4 (*C*4), 14.3 (*C*δ) ppm.

MS (ESI): m/z (%)= 817.3(100) $[M+Na]^+$

HRMS (MALDI): Calc. for $[M+Na]^+$ $C_{50}H_{87}N_3NaO_4^+$ 816.6590; found 816.6582 $[M+Na]^+$

Synthesis of compound **68**

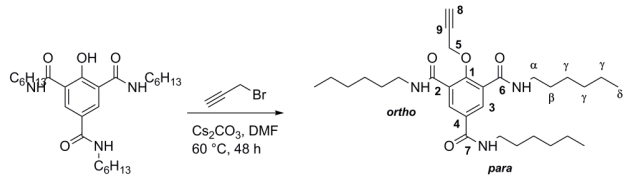

36b

68

2-hydroxy BTA derivative **36b** (500 mg, 1.05 mmol) was dissolved in dry DMF (2 mL) in a vial. Cs_2CO_3 (342.1 mg, 1.05 mmol) was added forming a heterogeneous solution. Propargyl bromide (sol. 80% in toluene, 0.23 mL, 2.1 mmol) was added and the vial was sealed with Teflon®-coated cap and stirred at 60 °C for 48 hours. The reaction was cooled to r.t., diluted with water and extracted with

dichloromethane. The organic phases were dried on $MgSO_4$ and the solvent was evaporated under vacuum. The product was purified by chromatography on silica gel using cyclohexane/ethyl acetate 6:4 to afford 462 mg of an amorphous yellowish solid in 83% yield.

R_f (cyclohexane/AcOEt 6:4): 0.36

M.p. (DSC 2nd heating cycle): 69.97 °C

IR (Film $CDCl_3$): 3243 *m*, 3075 *w*, 2929 *m*, 2858 *w*, 1630 *s*, 1552 *m*, 1458 *w*, 1306 *w*, 1004 *w*, 726 *w*.

^{1}H-NMR ($CDCl_3$, 400 MHz, 295K): δ= 8.35 (*s*, 2H, H3), 7.14 (*t*, $^3J_{H,H}$ = 5.6 Hz, 2H, N-H_{ortho}), 6.35 (*t*, $^3J_{H,H}$ = 5.7 Hz, 1H, N-H_{para}), 4.73 (*d*, $^4J_{H,H}$ = 2.5 Hz, 2H, H5), 3.49-3.40 (*m*, 6H, Hα), 2.61 (*t*, $^4J_{H,H}$ = 2.5 Hz, 1H, H8), 1.67-1.55 (*m*, 6H, Hβ), 1.42-1.25 (*m*, 18H, Hγ), 0.92-0.87 (*m*, 9H, Hδ) ppm.

^{13}C-NMR ($CDCl_3$, 100 MHz, 295K): δ= 165.53 (*C*=O), 164.8 (*C*=O), 154.7 (*C*1), 131.4 (*C*3), 131.2 (*C*4), 129.2 (*C*2), 77.4 (*C*9), 77.1 (*C*8), 63.2 (*C*5), 40.3 (*C*α), 40.1 (*C*α), 31.5 (*C*γ), 29.4 (*C*β), 29.2 (*C*β), 26.8 (*C*γ), 26.7 (*C*γ), 22.5 (*C*γ), 14.0 (*C*δ) ppm.

MS (ESI): m/z (%)= 536.9(100%) $[M+Na]^+$

HRMS (ESI): Calc. for $[M+Na]^+$ $C_{30}H_{47}N_3NaO_4^+$ 536.3460; found 536.3455 $[M+Na]^+$

Synthesis of compound **74**

73 **74**

3,4,5-trihydroxy-benzenamide **73** (2 g, 11.8 mmol) was dissolved in dry DMF (20 mL). K_2CO_3 (10.73 g, 77.88 mmol) was added and the heterogeneous suspension was stirred for 10 min. 1-bromohexane (5.5 mL, 39.02 mmol) was added and the resulting suspension was stirred at 90 °C for 48 hours. The reaction was cooled to r.t. and diluted with water (200 mL). The brown precipitate was filtered and dried under vacuum. The product was purified by chromatography on silica gel using cyclohexane/ethyl acetate 1:1 as the eluent to afford 3.389 g of a white solid in 68% yield. The spectroscopic data were in agreement with the literature.[6]

R_f (Cy/AcOEt 1:1): 0.54

M.p.: 95 ° - 96 °C

^{1}H-NMR ($CDCl_3$, 400 MHz, 295K): δ= 7.00 (*s*, 2H, H-Ar), 6.06-5.49 (*broad*, 2H, N-*H*), 4.01 (*t*, $^3J_{H,H}$ = 6.6 Hz, 6H, H4 and H4'), 1.85-1.70(*m*, 6H, H5 and H5'), 1.49-1.43 (m, 6H, H6), 1.34-1.32 (m, 12H, H7 and H7', H8 and H8'), 0.90 (*t*, $^3J_{H,H}$ = 6.5 Hz, 9H, H9 and H9') ppm.

^{13}C-NMR ($CDCl_3$, 100 MHz, 295K): δ= 165.9 (*C*=O), 153.3 (*C*2 and *C*2'), 116.1 (*C*3), 106.4 (*C*1), 73.7 (*C*4'), 69.6 (*C*4), 31.9 (*C*8'and *C*7'), 31.7 (*C*8 and *C*7), 30.4 (*C*5'), 29.4 (*C*5), 25.87 (*C*6), 25.84 (*C*6'), 22.82 (*C*8'and *C*7'), 22.76 (*C*8 and *C*7), 14.23 (*C*9'), 14.17 (*C*9) ppm.

MS (ESI): m/z (%)= 444.7(27%) $[M+Na]^+$ 866.2(100%) $[2M+Na]^+$ 1287.1(27) $[3M+Na]^+$

Synthesis of compound **75**

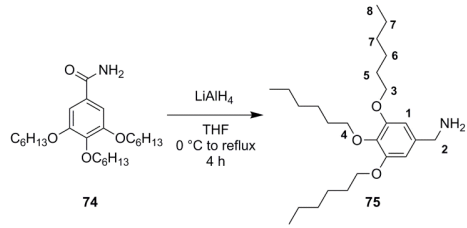

$LiAlH_4$ (8 mL, 19.27 mmol, 2.4M in THF) was diluted with dry THF (10 mL) under Ar and cooled to 0 °C. Benzamide derivative **74** (4.063 g, 9.636 mmol) was dissolved in dry THF (20 mL) and added dropwise to the solution of $LiAlH_4$. The homogenous solution was stirred at 0 °C for 30 min. and then stirred at 70 °C for 4 hours. A white solid formation took place. The reaction was cooled to 0 °C and the excess of the hydride was quenched by slowly adding a solution of Na_2CO_3 5%. The solid was filtered off over a celite filter. The filter was washed with THF and the liquor was extracted with dichloromethane. The organic phases were dried over Na_2SO_4 and the solvent was removed under vacuum to afford 3.663 g of a white amorphous solid in 93% yield. The product resulted pure enough to be employed in the further synthetic step. The spectroscopic data were in agreement with the literature.[7]

R_f (AcOEt/MeOH 6:4): 0.38

^{1}H-NMR ($CDCl_3$, 400 MHz, 295K): δ= 6.51 (*s*, 2H, H1), 3.97 (*t*, $^3J_{H,H}$ = 6.5 Hz, 4H, H3), 3.93 (t, $^3J_{H,H}$ = 6.7 Hz, 2H, H4), 3.78 (*s*, 2H, H2), 1.83-1.70 (*m*, 6H, H5), 1.51-1.43 (*m*, 6H, H6), 1.36-1.30 (*m*, 12H, H7), 0.90 (*t*, $^3J_{H,H}$ = 7.45 Hz, 9H, H8) ppm.

MS (ESI): m/z (%)= 431.0(27%) $[M+Na]^+$

Synthesis of compound **76**

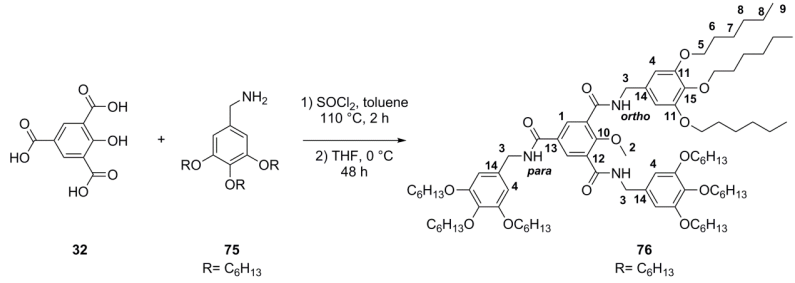

2-methoxy trimesic acid **32** (1.18 g, 4.9 mmol) was suspended in toluene (20 mL) and two drops of DMF were added. $SOCl_2$ (1.07 mL, 15.7 mmol) was added and the suspension was stirred at 110 °C for 2 hours. The resulting homogenous solution was cooled to r.t. and the volatiles were removed under high vacuum (0.01 mbar). The resulting pale yellow oil was dissolved with dry THF (15 mL) and added dropwise to a solution at 0 °C of TEA (2.73 mL, 19.6 mmol) and benzyl amine derivative **75** (6 g, 14.72 mmol) in dry THF (40 mL). The reaction was stirred at 0 °C for 30 min. and then for 48 hours at r.t. The organic solvent was evaporated under vacuum and the resulting solid was dissolved in ethyl acetate. The organic phases was washed with hydrochloric acid 2M, then with $NaHCO_3$ 5% and finally with brine. The organic phase was dried over $MgSO_4$ and the solvent evaporated under vacuum to afford 6.25 g of a yellowish amorphous solid in 91 % yield. The product was pure enough to be employed in the further synthetic step.

R_f (Cy/AcOEt 7:3): 0.5

M.p.: 215 ° - 220 °C (DSC)

IR (Solid deposition)*: 2928 *m*, 2858 *m*, 1640 *m*, 1589 *m*, 1554 *w*, 1504 *m*, 1466 *w*, 1440 *m*, 1385 *w*, 1328 *m*, 1307 w, 1251 *m*, 1232 *m*, 1109 *s*, 1052 *w*, 1014 *w*, 926 *w*, 905 *w*, 799 *w*, 725 *w*, 692 *w*, 602 *w*.

^{1}H-NMR ($CDCl_3$, 400 MHz, 295K): δ= 8.48 (*s*, 2H, H1), 7.38 (*t*, $^3J_{H,H}$ = 5.6 Hz, 2H, N-H_{ortho}), 6.51 (*s*, 6H, H4), 6.46 (*t*, $^3J_{H,H}$ = 5.4, 1H, N-H_{para}), 4.53-4.50 (*m*, 6H, H3), 3.98-3.90 (*m*, 18H, H5), 3.72 (*s*, 3H, H2), 1.82-1.69 (*m*, 18H, H6), 1.50-1.42 (*m*, 18H, H7), 1.35-1.30 (*m*, 36H, H8), 0.91-0.87 (*m*, 27H, H9) ppm.

^{13}C-NMR ($CDCl_3$, 100 MHz, 295K): δ= 164.2 (*C*=O), 158.1 (*C*10), 153.6 (*C*11), 138.0 (*C*15), 132.91 (*C*14) 132.88 (C14), 132.66 (*C*13), 128.6 (*C*12), 106.98 (*C*4), 106.85 (*C*4), 73.60 (*C*5), 69.42 (*C*5), 69.34 (*C*5), 63.7 (*C*2), 45.0 (*C*3), 44.8 (*C*3), 31.9 (*C*8), 31.7 (*C*8), 30.4 (*C*6), 29.5 (*C*6), 25.9 (*C*7), 22.83 (*C*8), 22.77 (*C*8), 22.76 (*C*8), 14.23 (*C*9), 14.17 (*C*9) ppm.

MS (ESI): m/z (%)= 1432.3(100) $[M+Na]^+$

HRMS (MALDI): Calc. for $[M+Na]^+$ $C_{85}H_{137}N_3NaO_{13}^+$ 1431.0044; found 1431.0071 $[M+Na]^+$

Synthesis of compound **77**

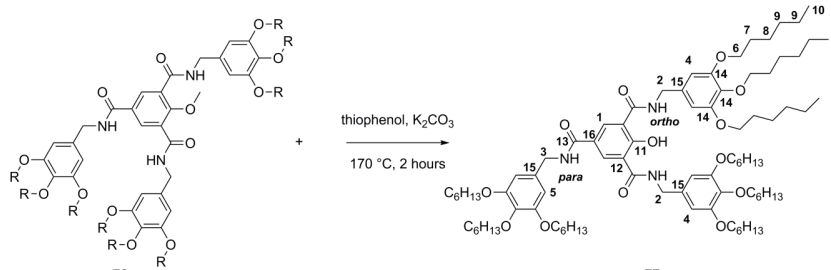

76
R= C_6H_{13}

77
R= C_6H_{13}

2-methoxy BTA derivative **76** (6.25 g, 4.48 mmol) was dissolved in NMP (15 mL). K_2CO_3 (928.7 mg, 6.72 mmol) was added and the solution turned green. Thiophenol (0.55 mL, 5.4 mmol) was added and the reaction was stirred at 170 °C for 2 hours. The reaction was stirred for other 48 hours at r.t. The reaction was diluted with water (100 mL) and acidified until pH= 1 with hydrochloric acid 37%. The aqueous phase was extracted with DCM and the organic phases were dried over $MgSO_4$ and the solvent removed under vacuum. The product was purified by chromatography on silica gel using cyclohexane/ethyl acetate 75:25 to afford 2.766 g of very viscous pale yellow oil in 44% yield.

R_f (cyclohexane/ethyl acetate 7:3): 0.61

IR (Film $CDCl_3$): 3316 *m*, 2957 *s*, 2932 *s*, 2872 *m*, 2860 *m*, 2251 *w*, 1658 *m*, 1591 *m*, 1538 *m*, 1505 *m*, 1466 *m*, 1439 *m*, 1384 *m*, 1354 *m*, 1331 *m*, 1280 *w*, 1264 *m*, 1113 *s*, 908 *s*, 824 *w*, 804 *w*, 734 *s*, 651 *m*.

^{1}H-NMR ($CDCl_3$, 400 MHz, 295K): δ= 8.56 (*s*, 2H, 1H), 6.89 (*t*, $^3J_{H,H}$ = 4.8 Hz, 1H, N-H_{para}), 6.51 (*s*, 4H, H4), 6.47 (*s*, 2H, H5), 4.51 (*d*, $^3J_{H,H}$ = 5.3 Hz, 4H, H2), 4.44 (*d*, $^3J_{H,H}$ = 5.3 Hz, 4H, H3), 3.97-3.88 (*m*, 18H, H6), 1.82-1.68 (*m*, 18H, H7), 1.52-1.39 (*m*, 18H, H8), 1.37-1.24 (*m*, 36H, H9), 0.91-0.87 (*m*, 27H, H10) ppm.

^{13}C-NMR ($CDCl_3$, 100 MHz, 295K):* δ= 163.2 (*C*=O), 153.5 (*C*14), 138.0 (*C*14), 132.6 (*C*1), 106.8 (*C*5), 106.7 (*C*4), 73.6 (*C*6), 69.35 (*C*6), 69.31 (*C*6), 44.9 (*C*3), 44.5 (*C*2), 31.9 (*C*9), 31.7 (*C*9), 30.4 (*C*7), 29.5 (*C*7), 27.0 (*C*8), 25.9 (*C*8), 22.8 (*C*9), 22.7 (*C*9), 14.2 (*C*10), 14.1 (*C*10) ppm. * The signals of the aromatic C11, C12 and C16 were not observed.

MS (ESI): m/z (%)= 1416.9(100) $[M+Na]^+$

HRMS (MALDI): Calc. for $[M+Na]^+$ $C_{84}H_{135}N_3NaO_{13}^+$ 1416.9887; found 1417.0010 $[M+Na]^+$

Synthesis of compound **78**

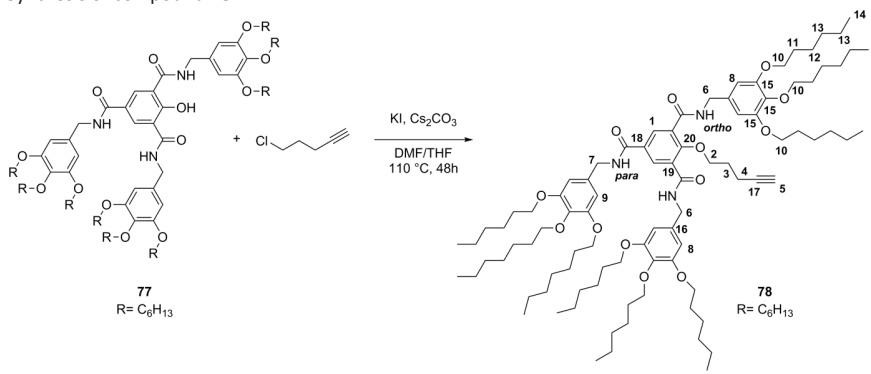

2-hydroxy BTA derivative **77** (2.766 g, 1.983 mmol) was dissolved in dry DMF (5 mL). THF (2 mL) was added to increase the solubility of **77**. Cs_2CO_3 (977.8 mg, 2.97 mmol) and KI (329.1 mg, 1.983 mmol) were added forming a heterogeneous solution. 5-chloro-1-pentyne (0.42 mL, 3.965 mmol) was added and the reaction was stirred at 110 °C under nitrogen for 18 hours. Another portion of 5-chloro-1-pentyne (0.21 mL, 1.98 mmol) was added and the reaction was stirred for other 30 hours at 110 °C. The reaction was cooled to r.t. and the volatiles were removed under vacuum. The crude mixture was directly purified on alumna column chromatography using cyclohexane/ethyl acetate 6:4 to afford 744 mg of amorphous pale yellow solid in 26% yield.

R_f (cyclohexane/ethyl acetate 7:3): 0.68

M.p. (DSC 2nd heating cycle): 140.87 °C

IR (Solid deposition): 3245 *w*, 2952 *m*, 2928 *m*, 2856 *m*, 1667 *w*, 1632 *m*, 1591 *m*, 1537 *m*, 1504 *m*, 1439 *m*, 1383 *w*, 1328 *m*, 1232 *m*, 1109 *s*, 1010 *m*, 632 *w*.

^{1}H-NMR ($CDCl_3$, 400 MHz, 295K): δ= 8.45 (*s*, 2H, 1H), 7.37 (*t*, $^3J_{H,H}$ = 5.6 Hz, 2H, N-H_{ortho}), 6.56 (*t*, $^3J_{H,H}$ = 5.4, 1H, N-H_{para}), 6.52 (*s*, 4H, H9), 6.50 (*s*, 2H, H8), 4.53-4.49 (*m*, 6H, H6 + H7), 3.93 (*quint*, $^3J_{H,H}$ = 7.3 Hz, 20H, H10 and H2), 2.04 (*dt*, $^3J_{H,H}$ = 6.8 Hz, $^4J_{H,H}$ = 2.6 Hz, 2H, H4), 1.92 (*t*, $^3J_{H,H}$ = 2.6 Hz, 1H, H5), 1.82-1.69 (*m*, 18H, H11), 1.57 (*quint*, $^3J_{H,H}$ = 6.8 Hz, 2H, H3), 1.50-1.41 (*m*, 18H, H112), 1.36-1.30 (*m*, 36H, H13), 0.91-0.87 (*m*, 27H, H14) ppm.

^{13}C-NMR ($CDCl_3$, 100 MHz, 295K): δ= 165.0 (*C*=O), 164.3 (*C*=O), 156.8 (*C*20), 153.59 (*C*15), 153.55 (*C*15), 138.04 (*C*15), 137.95 (*C*15), 132.8 (*C*16), 132.7 (*C*1), 131.1 (*C*18), 128.9 (*C*19), 107.2 (*C*8), 106.9 (*C*9), 82.5 (*C*17), 76.3 (*C*2), 73.6 (*C*10), 69.9 (*C*5), 69.4 (*C*10), 69.3 (*C*10), 44.9 (*C*7), 44.8 (*C*6), 31.9

(*C*13), 31.7 (*C*13), 30.40 (*C*11), 29.5 (*C*11), 28.3 (*C*3), 25.9 (*C*12), 22.8 (*C*13), 22.7 (*C*13), 15.2 (*C*4), 14.20 (*C14*), 14.13 (*C*14) ppm.

MS (ESI): m/z (%)= 1484.4(100) $[M+Na]^+$

HRMS (MALDI): Calc. for $[M+Na]^+$ $C_{89}H_{141}N_3NaO_{13}^+$ 1483.0357; found 1483.0406 $[M+Na]^+$

Synthesis of the dimers

Synthesis of compound **52**

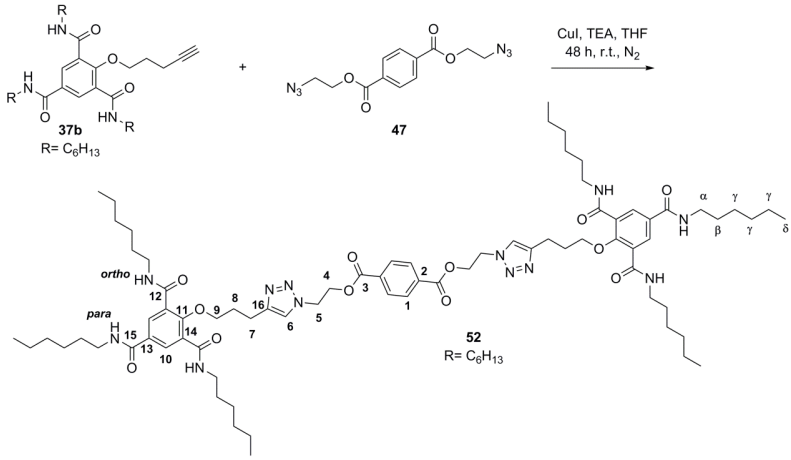

2-pentynyloxy BTA derivative **37b** (100 mg, 0.185 mmol) was dissolved in freshly degassed THF (2 mL). Diazido derivative **47** (28.14 mg, 0.095 mmol) and TEA (15 μL, 0.095 mmol) were added and the solution was stirred for 5 min. CuI (3.5 mg, 0.0185 mmol) was added and the solution was stirred for other 48 hours at r.t. The crude was directly purified by chromatography on silica gel using ethyl acetate 100% to afford 63 mg of a colorless amorphous solid in 50% yield.

R_f (ethyl acetate 100%): 0.35

M.p. (DSC 1st cooling cycle): 39.38 °C

IR ($CHCl_3$ film): 3271 *m*, 3079 *w*, 2956 *m*, 2930 *s*, 2858 *m*, 1727 *m*, 1638 *s*, 1541 *m*, 1449 *m*, 1409 w, 1384 w, 1269 *s*, 1121 *m*, 1020 *w*, 756 *w*, 731 *w*.

^{1}H-NMR ($CDCl_3$, 400 MHz, 295K): δ= 8.09 (*s*, 4H, H10), 7.89 (*s*, 4H, H1), 7.55 (*s*, 2H, H6), 7.29 (*t*, $^3J_{H,H}$ = 5.6 Hz, 4H, N-H_{ortho}), 6.70 (*t*, $^3J_{H,H}$ = 5.6 Hz, 2H, N-H_{para}), 4.74-4.69 (*m*, 8H, H4 and H5), 3.99 (*t*, $^3J_{H,H}$ = 6.5 Hz, 4H, H9), 3.34 (*quint*, $^3J_{H,H}$ = 7.7 Hz, 12H, Hα), 2.81 (*t*, $^3J_{H,H}$ = 7.1 Hz, 4H, H7), 2.10 (*quint*, $^3J_{H,H}$ = 6.9 Hz, 4H, H8), 1.59-1.49 (*m*, 12H, Hβ), 1.32-1.22 (*m*, 36H, Hγ), 0.87-0.82 (*m*, 18H, Hδ) ppm.

^{13}C-NMR ($CDCl_3$, 100 MHz, 295K): δ= 165.65 (*C*=O), 165.14 (*C*=O), 165.11 (*C*=O), 156.4 (*C*11), 146.8 (*C*16), 133.4 (*C*2), 131.4 (*C*10), 130.7 (*C*13), 129.74 (*C*1), 129.25 (*C*14), 121.9 (*C*6), 75.9 (*C*9), 63.5 (*C*4), 49.0 (*C*5), 40.4 (*C*α), 40.2 (*C*α), 31.58 (*C*γ), 31.54 (γ), 29.57 (*C*8), 29.54 (*C*β), 26.82 (*C*γ), 26.77 (*C*γ), 22.6 (*C*7), 21.9 (*C*γ), 14.1 (*C*δ) ppm.

MS (ESI): m/z (%)= 1410.2(100%) $[M+Na]^+$

HRMS (MALDI): Calc. for $[M+Na]^+$ $C_{76}H_{114}N_{12}NaO_{12}^+$ 1409.8571; found 1409.8578 $[M+Na]^+$

Synthesis of compound **53**

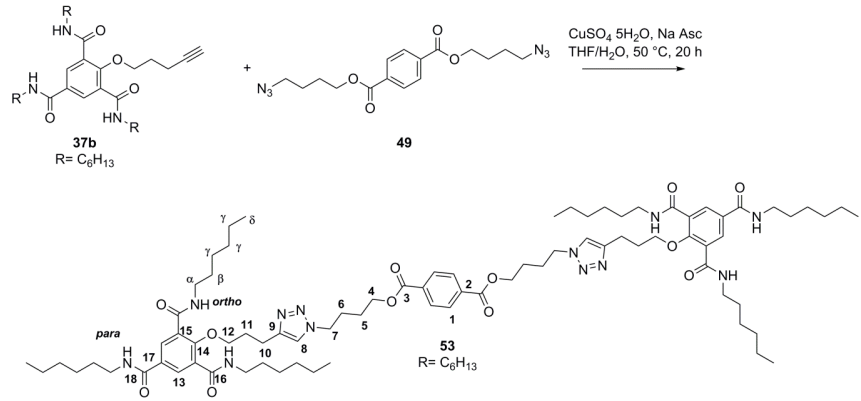

2-pentynyloxy BTA derivative **37b** (89.9 mg, 0.166 mmol) and diazido derivative **49** (30 mg, 0.083 mmol) were dissolved in THF (1 mL). A solution of sodium ascorbate (6.6 mg, 0.033 mmol in 100 μL of H_2O) was added to the reaction forming a homogenous solution. A solution of $CuSO_4$ $5H_2O$ (4 mg, 0.017 mmol in 200 μL of H_2O) was added to the reaction. The reaction was stirred at 50 °C for 20 hours. The crude was directly purified by chromatography on silica gel starting from ethyl acetate 100% to ethyl acetate/MeOH 95:5 as the eluent to afford 65.7 mg of amorphous white solid in 55% yield.

R_f (ethyl acetate/MeOH 95:5): 0.71

M.p. (DSC 1st cooling cycle): 19.94 °C

IR (film $CHCl_3$): 3435 *w*, 3019 *w*, 2960 *w*, 2932 *w*, 2860 *w*, 2401 *w*, 1717.27 *w*, 1660 *m*, 1525 *w*, 1445 *w*, 1384 *w*, 1271 *w*, 1216 *s*, 1122 *w*, 1049 *w*, 1019 *w*, 929 *w*, 876 *w*, 759 *s*, 669 *m*, 626 *w*.

^{1}H-NMR ($CDCl_3$, 400 MHz, 295K): δ= 8.20 (*s*, 4H, H13), 8.04 (*s*, 4H, H1), 7.37 (*s*, 2H, H8), 7.24 (*t*, $^3J_{H,H}$ = 5.7 Hz, 4H, N-H_{ortho}), 6.52 (*t*,$^3J_{H,H}$ = 5.7 Hz, 2H, N-H_{para}), 4.38 (*t*, $^3J_{H,H}$ = 7.1 Hz, 4H, H4), 4.34 (*t*, $^3J_{H,H}$ = 6.3 Hz, 4H, H7), 4.07 (*t*, $^3J_{H,H}$ = 6.6 Hz, 4H, H12), 3.41-3.35 (*m*, 12H, Hα), 2.81 (*t*, $^3J_{H,H}$ = 7.4 Hz, 4H, H10), 2.14 (*quint*, $^3J_{H,H}$ = 6.9 Hz, 4H, H11), 2.05 (*quint*, $^3J_{H,H}$ = 7.2 Hz, 4H, H5), 1.79 (*quint*, $^3J_{H,H}$ = 6.3 Hz, 4H, H6), 1.56 (*quint*, $^3J_{H,H}$ = 7.0 Hz, 12H, Hβ), 1.35-1.21 (*m*, 36H, Hγ), 0.89-0.83 (*m*, 18H, Hδ) ppm.

^{13}C-NMR ($CDCl_3$, 100 MHz, 295K): δ= 165.72 (*C*=O), 165.55 (*C*=O), 165.11 (*C* =O), 156.5 (*C*14), 146.5 (*C* 9), 134.0 (*C*2), 131.6 (*C*13), 130.9 (*C*17), 129.6 (*C*1), 129.3 (*C*15), 121.1 (*C*8), 76.1 (*C*12), 64.5 (*C*7), 49.8 (*C*4), 40.37 (*C*α), 40.24 (*C*α), 31.58 (*C*γ), 31.56 (*C*γ), 29.68 (*C*11), 29.60 (*C*β), 29.58 (*C*β), 27.12 (*C*5), 26.84 (*C*γ), 26.76 (*C*γ), 25.88 (*C*6), 22.6 (γ), 22.0 (*C*10), 14.1 (*C*δ) ppm.

MS (ESI): m/z (%)= 1466.4(100%) $[M+Na]^+$ 1444.3(26%)$[M+H]^+$

HRMS (MALDI): Calc. for $[M+H]^+ C_{80}H_{123}N_{12}O_{12}^+$ 1443.9378; found 1443.9383 $[M+H]^+$

Synthesis of compound **54**

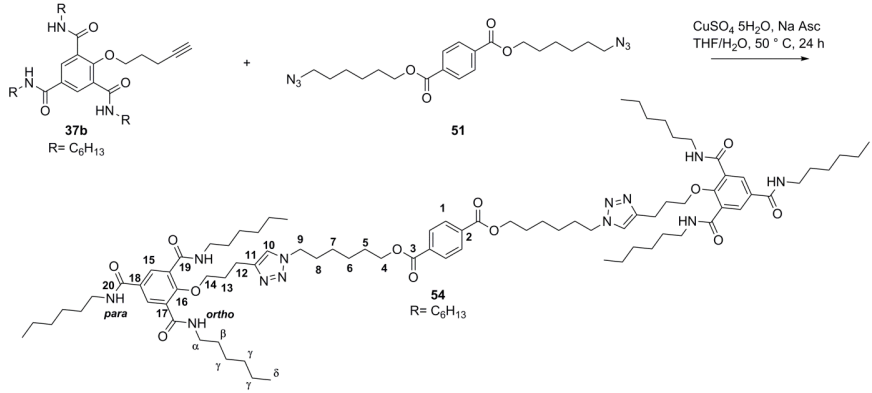

2-pentynyloxy BTA derivative **37b** (104 mg, 0.252 mmol) and the diazido derivative **51** (52.5 mg, 0.126 mmol) were dissolved in THF (2 mL). A solution of sodium ascorbate (14.9 mg, 0.075 mmol in 300 μL of H_2O) was added to the reaction forming a homogenous solution. A solution of $CuSO_4$ $5H_2O$ (6.3 mg, 0.0252 mmol in 200 μL of H_2O) was added to the reaction. The reaction was stirred at 50 °C for 24 hours. The crude was directly purified by chromatography on silica gel starting from ethyl acetate 100% to ethyl acetate/MeOH 95:5 as the eluent to afford 89.1 mg of amorphous white solid in 47% yield.

R_f (ethyl acetate/MeOH 95:5): 0.4

M.p. (DSC 1st cooling cycle): 14.97 °C

IR (film $CHCl_3$): 3402 m, 3018 *m*, 2932 *s*, 2860 *m*, 1716 *m*, 1652 *s*, 1531 *m*, 1446 *m*, 1383 *w*, 1272 *m*, 1216 *s*, 1123 *w*, 1019 *w*, 668 *m*.

^{1}H-NMR ($CDCl_3$, 400 MHz, 295K): δ= 8.21 (*s*, 4H, H15), 8.05 (*s*, 4H, H1), 7.35 (*s*, 2H, H10), 7.28 (*t*, $^3J_{H,H}$ = 5.4 Hz, 4H, N-H_{ortho}), 6.56 (*t*,$^3J_{H,H}$ = 5.5 Hz, 2H, N-H_{para}), 4.32-4.29 (*m*, 8H, H9 and H4), 4.07 (*t*, $^3J_{H,H}$ = 6.4 Hz, 4H, H14), 3.38 (*quint*, $^3J_{H,H}$ = 6.4 Hz, 12H, Hα), 2.81 (*t*, $^3J_{H,H}$ = 7.3 Hz, 4H, H12), 2.13 (*quint*, $^3J_{H,H}$ = 6.9 Hz, 4H, H13), 1.91 (*quint*, $^3J_{H,H}$ = 7.3 Hz, 4H, H8), 1.75 (*quint*, $^3J_{H,H}$ = 6.9 Hz, 4H, H5), 1.64-1.50 (*m*, 12H, Hβ), 1.49-1.43 (*m*, 4H, H7), 1.40-1.21 (*m*, 40H, Hγ and H6), 0.87-0.83 (*m*, 18H, Hδ) ppm.

^{13}C-NMR ($CDCl_3$, 100 MHz, 295K): δ= 165.9 (*C*3), 165.6 (*C*20), 165.14 (*C*19), 156.5 (*C* 16), 146.3 (*C* 11), 134.2 (*C*2), 131.6 (*C*15), 130.8 (*C*18), 129.6 (*C*1), 129.3 (*C*17), 121.1 (*C*10), 76.1 (*C*14), 64.2 (*C*4), 50.2 (*C*9), 40.37 (*C*α), 40.25 (*C*α), 31.57 (*C*γ), 30.28 (*C*8), 29.69 (*C*β), 29.59 (*C*β), 28.6 (*C*5), 26.85 (*C*γ), 26.76 (*C*γ), 26.3 (*C*6), 25.6 (H7), 22.65 (*C*γ), 21.98 (*C*12), 14.13 (*C*δ) ppm.

MS (ESI): m/z (%)= 1522.5(100%) $[M+Na]^+$

HRMS (ESI): Calc. for $[M+H]^+$ $C_{84}H_{130}N_{12}NaO_{12}^+$ 1521.9823; found 1521.9811 $[M+H]^+$

Synthesis of compound **59**

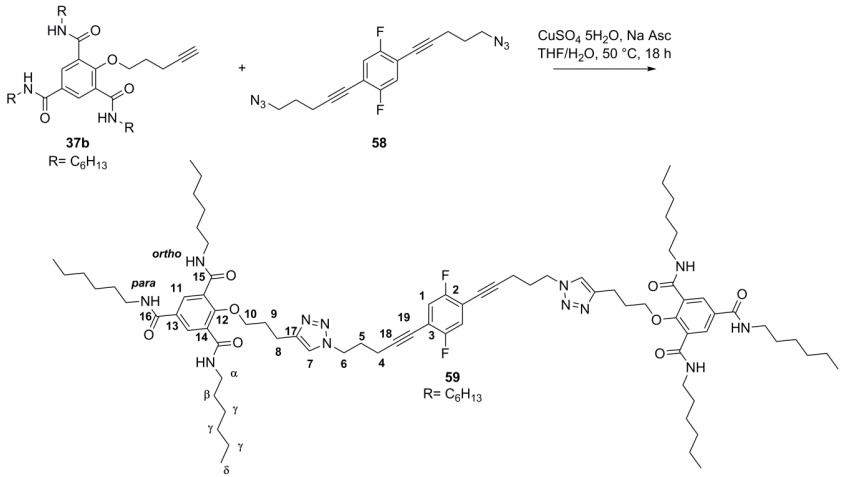

2-pentynyloxy BTA derivative **37b** (188 mg, 0.45 mmol) and diazido derivative **58** (73.9 mg, 0.225 mmol) were dissolved in THF (2 mL). A solution of sodium ascorbate (26.7 mg, 0.135 mmol in 500 μL of H_2O) was added to the reaction. A solution of $CuSO_4$ $5H_2O$ (11.2 mg, 0.045 mmol in 400 μL of H_2O) was added and the reaction was stirred at 50 °C for 18 hours. The crude was directly purified by chromatography on silica gel starting from ethyl acetate 100% as the eluent to afford 111 mg of amorphous white solid in 35% yield.

R_f (ethyl acetate/MeOH 95:5): 0.8

M.p. (DSC 1st cooling cycle): 33.38 °C

IR (film $CHCl_3$): 3272.42 *m*, 3076 *w*, 2957 *s*, 2931 *s*, 2859 *s*, 2242 *m*, 2101 *w*, 1777 *w*, 1651 *s*, 1538 *s*, 1503 *m*, 1467 *s*, 1448 *s*, 1416 *m*, 1379 *w*, 1275.90 *m*, 1176 *w*, 1130 *w*, 1050 *w*, 1024 *w*, 909 *s*, 783 w, 733 *s*, 647 *m*.

^{1}H-NMR ($CDCl_3$, 400 MHz, 295K): δ= 8.20 (*s*, 4H, H11), 7.43 (*s*, 2H, H7), 7.28 (*t*, $^3J_{H,H}$ = 5.2 Hz, 4H, N-H_{ortho}), 7.05 (*t*, $^3J_{H,F}$ = 7.4 Hz, $^4J_{H,F}$ = 7.4 Hz, 2H, H1), 6.54 (*t*,$^3J_{H,H}$ = 5.5 Hz, 2H, N-H_{para}), 4.49 (*t*, $^3J_{H,H}$ = 6.5 Hz, 4H, H6), 4.07 (*t*, $^3J_{H,H}$ = 6.0 Hz, 4H, H10), 3.37 (*quint*, $^3J_{H,H}$ = 7.3 Hz, 12H, Hα), 2.81 (*t*, $^3J_{H,H}$ = 6.7 Hz, 4H, H8), 2.46 (*t*, $^3J_{H,H}$ = 6.6 Hz, 4H, H4), 2.22-2.12 (*m*, 8H, H5 and H9), 1.59-1.54 (*m*, 12H, Hβ), 1.33-1.26 (*m*, 36H, Hγ), 0.86-0.83 (*m*, 18H, Hδ) ppm.

^{13}C-NMR ($CDCl_3$, 100 MHz, 295K): δ= 165.5 (*C*=O), 165.1 (*C*=O), 158.5 (*dd*, $^1J_{F,C}$ = 247.9 Hz, $^4J_{F,C}$ = 3.9 Hz, *C*2), 156.5 (*C*12), 146.4 (*C*17), 131.6 (*C*11), 130.8 (*C*13), 129.2 (*C*15), 121.7 (*C*7), 119.4 (*dd*, $^2J_{F,C}$ = 17.5 Hz, $^3J_{F,C}$ = 9.6 Hz, *C*1), 112.9 (*dd*, $^2J_{F,C}$ = 16.2 Hz, $^3J_{F,C}$ = 12.5 Hz, *C*3), 95.8 (*C*18), 76.1 (*C*19), 74.7 (*C*10), 48.8 (*C*6), 40.4 (*C*α), 40.2 (*C*α), 31.6 (*C*γ), 29.7 (*C*9), 29.6 (*C*β), 28.6 (*C*5), 26.8 (*C*γ), 26.7 (*C*γ), 22.6 (*C*γ), 22.0 (*C*8), 16.9 (*C*4), 14.1 (*C*δ) ppm.

^{19}F-NMR ($CDCl_3$, 400 MHz, 295K): δ= -116.71 ppm.

MS (ESI): m/z (%)= 1434.4(100%) $[M+Na]^+$ 1412.3(0.03%) $[M+H]^+$

HRMS (ESI): Calc. for $[M+H]^+$ $C_{80}H_{117}F_2N_{12}O_8^+$ 1411.9080; found 1411.9079 $[M+H]^+$

Synthesis of compound **63**

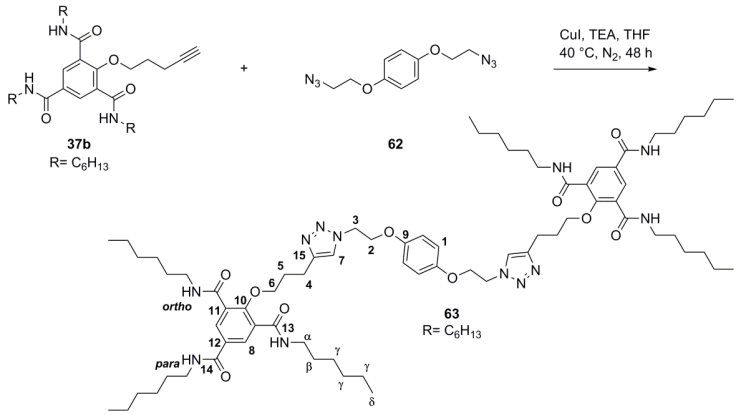

2-pentynyloxy BTA derivative **37b** (100 mg, 0.185 mmol) was dissolved in freshly degassed THF (2 mL). Diazido derivative **62** (22.9 mg, 0.093 mmol) and TEA (13 μL, 0.092 mmol) were added. CuI (3.5 mg, 0.0185 mmol) was added and the solution was stirred for 6 hours at 40 °C. Another portion of CuI was added (5 mg, 0.026 mmol) and the reaction was stirred for other 42 hours at 40 °C under nitrogen. The crude was directly purified by chromatographic on silica gel using a gradient from ethyl acetate 100% to ethyl acetate/methanol 95:5 to afford 67.8 mg of a colorless amorphous solid in 55% yield.

R_f (ethyl acetate 100%): 0.17

M.p. (DSC 1st cooling cycle): 40.16 °C

IR (Film $CHCl_3$): 3261 w, 2924 *s*, 2854 *m*, 1634 *s*, 1533 *m*, 1507 *s*, 1448 *m*, 1377 *w*, 1269 *m*, 1227 *s*, 1046 *m*, 911 *m*, 826 *m*, 725 *m*, 698 *m* , 668 *m*.

^{1}H-NMR ($CDCl_3$, 400 MHz, 295K): δ= 8.20 (*s*, 4H, H8), 7.53 (*s*, 2H, H7), 7.24 (*t*, $^3J_{H,H}$ = 5.7 Hz, 4H, NH_{ortho}), 6.72 (*s*, 4H, H1), 6.54 (*t*, $^3J_{H,H}$ = 5.6 Hz, 2H, NH_{para}), 4.67 (*t*, $^3J_{H,H}$ = 4.9 Hz, 4H, H2), 4.25 (*t*, $^3J_{H,H}$ = 4.90 Hz, 4H, H3), 4.06 (*t*, $^3J_{H,H}$ = 6.6 Hz, 4H, H6), 3.38 (*q*, $^3J_{H,H}$ = 6.8 Hz, 12H, Hα), 2.82 (*t*, $^3J_{H,H}$ = 7.3 Hz, 4H, H4), 2.14 (*quint*, $^3J_{H,H}$ = 7.0 Hz, 4H, H5), 1.56-1.51 (*m*, 12H, Hβ), 1.34-1.24 (*m*, 36H, Hγ), 0.88-0.83 (m, 18H, Hδ) ppm.

^{13}C-NMR ($CDCl_3$, 100 MHz, 295K): δ= 165.6 (*C*=O), 165.1 (*C*=O), 156.6 (*C*10), 152.8 (*C*9), 146.5 (*C*15), 131.6 (*C*8), 130.8 (*C*12), 129.2 (*C*11), 122.3 (*C7*), 115.8 (*C*1), 76.1 (*C*6), 67.2 (*C*3), 49.8 (*C*2), 40.4 (*C*α), 40.2 (*C*α), 31.6 (*C*γ), 31.6 (*C*γ), 29.7 (*C*5), 29.6 (*C*β), 29.6 (*C*β), 26.8 (*C*γ), 26.8 (*C*γ), 22.7 (*C*γ), 22.0 (*C4*), 14.1 (Cδ) ppm.

MS (ESI): m/z (%)=1354.2 (100%) $[M+Na]^+$ 1332.2(6.7%) $[M+H]^+$

HRMS (ESI): Calc. for $[M+Na]^+$ $C_{74}H_{114}N_{12}NaO_{10}^+$ 1353.8673; found 1353.8660 $[M+Na]^+$

Synthesis of compound **67**

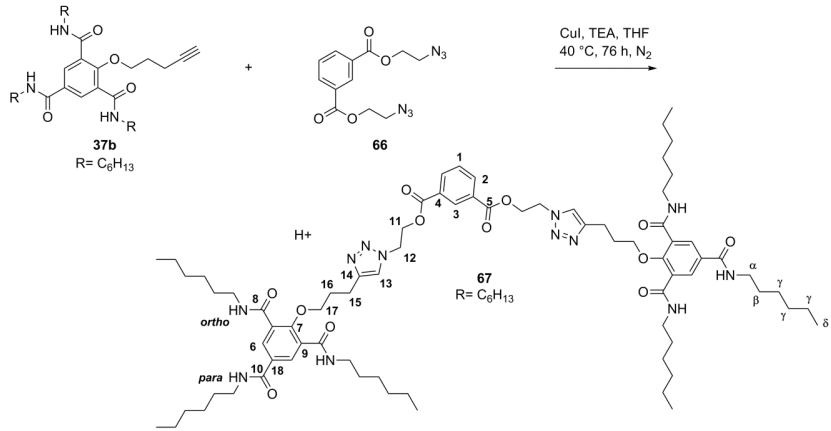

2-pentynyloxy BTA derivative **37b** (100 mg, 0.18 mmol) and diazido derivative **66** (28.1 mg, 0.092 mmol) were dissolved in a dry and freshly degased THF (1.75 mL) under nitrogen. TEA (19.2 μL, 0.138 mmol) was added and the solution was stirred for 5 min. CuI (3.5 mg, 0.018 mmol) was dissolved in dry and freshly degased THF (0.25 mL) and added to the reaction. The reaction was stirred under nitrogen at 40 °C for 76 hours. The solution was directly purified by chromatography on silica gel using AcOEt 100%. A second purification on silica gel chromatography was carried out using AcOEt/MeOH 95:5 to afford 77 mg of yellowish oil in 32% yield.

R_f (AcOEt/MeOH 95:5): 0.61

IR(solid deposition)*: 3271 w, 2955 *w*, 2927 *m*, 2854 *m*, 1728 *m*, 1638 *s*, 1537 *s*, 1447 *m*, 1295 *s*, 1232 *s*, 1026 *m*, 729 *s*, 678 *m*.

^{1}H-NMR ($CDCl_3$, 400 MHz, 295K): δ= 8.40 (*t*, $^3J_{H,H}$ = 1.5 Hz, 1H, H3), 8.11 (*s*, 4H, H6), 8.07 (*dd*, $^3J_{H,H}$ = 7.8 Hz, $^4J_{H,H}$ = 1.7 Hz, 2H, H2), 7.61 (*s*, 2H, H13), 7.43 (*t*, $^3J_{H,H}$ = 7.7 Hz, 1H, H1), 7.24 (*t*, $^3J_{H,H}$ = 5.7 Hz, 4H, N-H_{ortho}), 6.60 (*t*, $^3J_{H,H}$ = 5.6 Hz, 2H, N-H_{para}), 4.76 (*t broad*, $^3J_{H,H}$ = 4.5 Hz, 4H, H11), 4.69 (*t broad*, $^3J_{H,H}$ = 4.5 Hz, 4H, H12), 4.02 (*t*, $^3J_{H,H}$ = 6.7 Hz 4H, H17), 3.40-3.32 (*m*, 12H, Hα), 2.86 (*t*, $^3J_{H,H}$ = 7.2 Hz, 4H, H15), 2.13 (*quint*, $^3J_{H,H}$ = 6.8 Hz, 4H, H16), 1.61-1.50 (*m*, 12H, Hβ), 1.33-1.23 (*m*, 36H, Hγ), 0.89-0.83 (*m*, 18H, Hδ) ppm.

^{13}C-NMR ($CDCl_3$, 100 MHz, 295K): δ= 165.6 (*C*=O), 165.1 (*C*=O), 165.0 (*C*=O), 156.4 (*C*7), 147.00(*C*14), 134.3 (*C*2), 131.5 (*C*6), 130.8 (*C*9 and *C*18), 130.7 (*C*3), 129.8 (*C*4), 129.1 (*C*1), 122.2 (*C*13), 76.0 (*C*17), 63.4 (*C*12), 49.2 (*C*11), 40.41 (*C*α), 40.24 (*C*α), 31.62 (*C*γ), 31.58 (*C*γ), 29.63 (*C*16), 29.60 (*C*β), 26.85 (*C*γ), 26.81 (*C*γ), 22.67 (*C*γ), 22.0 (*C*15), 14.1 (*C*δ) ppm.

MS (ESI): m/z (%)= 1410.7(100%) $[M+H]^+$ 1432.4 (6.7%) $[M+Na]^+$

HRMS (ESI): Calc. for $[M+H]^+$ $C_{76}H_{115}N_{12}O_{12}^+$ 1387.8752; found 1387.8750 $[M+H]^+$

Synthesis of compound **70**

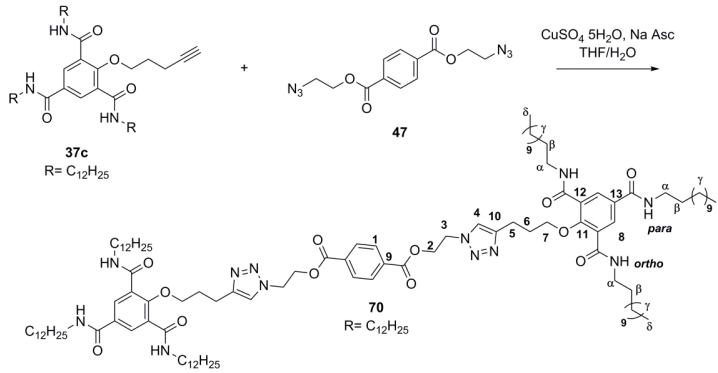

2-pentynyloxy BTA derivative **37c** (100 mg, 0.126 mmol) and diazido derivative **47** (19.1mg, 0.063 mmol) were dissolved in a vial in THF (1 mL). A solution of sodium ascorbate (12.47 mg, 0.063 mmol in 100 μL of H_2O) was added forming a homogenous solution. A solution of $CuSO_4$ $5H_2O$ (7.9 mg, 0.032 mmol dissolved in 75 μL of H_2O) was added to the reaction and stirred at 50 °C for 18 hours. The crude was filtered on silica filter using ethyl acetate/cyclohexane 7:3. The solvent was removed under vacuum and the product was purified on a preparative TLC-plate of silica gel using pentane/ethyl acetate 3:7 to afford 21.3 mg of a colorless amorphous solid in 18% yield.

R_f (Cy/AcOEt 3:7): 0.42

M.p. (DSC 1st cooling cycle): 58.81 °C

IR (Film $CDCl_3$)*: 2922 *s*, 2853 *m*, 2360 *w*, 2341 *w*, 1728 *m*, 1635 *s*, 1557 *m*, 1456 *m*, 1376 *w*, 1269 *m*, 1120 *w*, 1021 *w*, 911 *w*, 731 *w*, 668 *w*.

^{1}H-NMR ($CDCl_3$, 400 MHz, 295K): δ= 8.15 (*s*, 4H, H8), 7.91 (*s*, 4H, H1), 7.56 (*s*, 2H, H4), 7.19 (*t*, $^3J_{H,H}$ = 5.7 Hz, 4H, N-H_{ortho}), 6.50 (*t*, $^3J_{H,H}$ = 5.6 Hz, 2H, N-H_{para}), 4.74 (s, 8H, H2 and H3), 4.03 (*t*, $^3J_{H,H}$ = 6.6 Hz, 4H, H7), 3.43-3.35 (*m*, 12H, Hα), 2.84 (*t*, $^3J_{H,H}$ = 7.2 Hz, 4H, H5), 2.15 (*quint*, $^3J_{H,H}$ = 7.0 Hz, 4H, H6), 1.58-1.53 (*m*, 12H, Hβ), 1.37-1.25 (*m*, 108H, Hγ), 0.87 (*t*, $^3J_{H,H}$ = 6.8 Hz, 4H, Hδ) ppm.

^{13}C-NMR ($CDCl_3$, 100 MHz, 295K): δ= 165.6 (*C*=O), 165.2 (*C*=O), 165.1 (*C*=O), 156.5 (*C*11), 146.9 (*C*10), 133.5 (*C*9), 131.6 (*C*8), 130.9 (*C*13), 129.8 (*C*1), 129.4 (*C*12), 122.0(C4), 76.0 (*C*7), 63.6 (*C*2 or *C*3), 49.16 (*C*2 or *C*3), 40.48 (*C*α), 40.31 (*C*α), 32.07 (*C*γ), 29.85-29.63 (*C*β and *C*6), 29.51 (*C*β), 22.84(*C*γ), 22.0 (*C*5), 14.3 (*C*δ)ppm.

MS (ESI): m/z (%)= 1915.6(100%) $[M+Na]^+$

HRMS (MALDI): Calc. for $[M+Na]^+$ $C_{112}H_{186}N_{12}NaO_{12}^+$ 1914.4205; found 1914.4206 $[M+Na]^+$

Synthesis of compound **69**

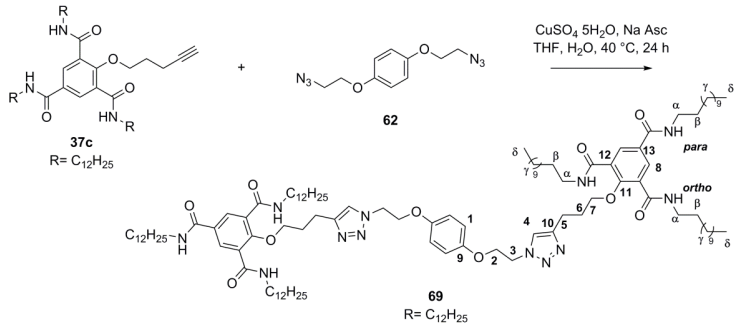

2-pentynyloxy BTA derivative **37c** (250 mg, 0.315 mmol) and diazido derivative **62** (39 mg, 0.094 mmol) were dissolved in a vial in THF (2 mL). A solution of sodium ascorbate (11.1 mg, 0.094 mmol in 150 μL of H_2O) was added forming a homogenous solution. A solution of $CuSO_4$ $5H_2O$ (7.8 mg, 0.031 mmol dissolved in 150 μL of H_2O) was added to the reaction and stirred at 40 °C for 24 hours. The crude was directly purified by chromatography on silica using ethyl acetate 100% and then the product was purified by a second silica gel chromatography using pentane/ethyl acetate 3:7 to afford 86.1 mg of a colorless amorphous solid in 30% yield.

R_f (AcOEt 100%): 0.57

M.p. (DSC 1st cooling cycle): 78.78 °C

IR (Solid deposition)*: 2922 *s*, 2852 *m*, 1633 *s*, 1547 *m*, 1453 *m*, 1227 *m*, 1045 m, 720 *m*.

^{1}H-NMR ($CDCl_3$, 400 MHz, 295K): δ= 8.21 (*s*, 4H, H8), 7.58 (*s*, 2H, H4), 7.20 (*t*, $^3J_{H,H}$ = 5.6 Hz, 4H, NH_{ortho}), 6.70 (*s*, 4H, H1), 6.46 (*t*, $^3J_{H,H}$ = 5.4 Hz, 2H, NH_{para}), 4.69 (*t*, $^3J_{H,H}$ = 5.0 Hz, 4H, H2), 4.26 (*t*, $^3J_{H,H}$ = 5.0 Hz, 4H, H3), 4.06 (*t*, $^3J_{H,H}$ = 6.6 Hz, 4H, H7), 3.39 (*q*, $^3J_{H,H}$ = 6.7 Hz, 12H, Hα), 2.85 (*t*, $^3J_{H,H}$ = 7.2 Hz, 4H, H5), 2.16 (*quint*, $^3J_{H,H}$ = 6.9 Hz, 4H, H6), 1.57-1.53 (*m*, 12H, Hβ), 1.31-1.24 (*m*, 108H, Hγ), 0.87 (*t*, $^3J_{H,H}$ = 6.8 Hz, 18H, Hδ) ppm.

^{13}C-NMR ($CDCl_3$, 100 MHz, 295K): δ= 165.6 (*C*=O), 165.1 (*C*=O), 156.6 (*C*11), 152.8 (*C*9), 146.4 (*C*10), 131.7 (*C*8), 130.8 (*C*12), 129.3 (*C*13), 122.6 (*C*4), 115.8 (*C*1), 76.0 (*C*7), 67.2 (*C*3), 50.0 (*C*2), 40.4 (*C*α), 40.3 (*C*α), 32.05 (*C*γ), 29.80-29.77-29.73-29.70-29.63-29.49 (*C*β and *C*6), 27.25 (*C*γ), 27.17 (*C*γ), 22.8 (*C*γ), 22.0 (*C*5), 14.3 (*C*δ) ppm.

MS (ESI): m/z (%)= 1859.8(100%) $[M+Na]^+$

HRMS (MALDI): Calc. for $[M+Na]^+$ $C_{110}H_{186}N_{12}NaO_{10}^+$ 1858.4307; found 1858.4304 $[M+Na]^+$

Synthesis of compound **79**

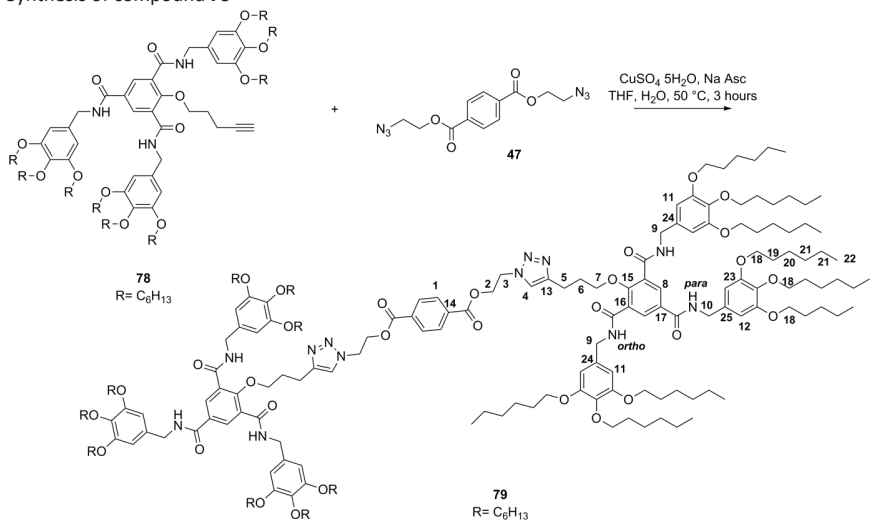

2-pentynyloxy BTA derivative **78** (200 mg, 0.136 mmol) and diazido derivative **47** (20.8 mg, 0.07 mmol) were dissolved in a vial in THF (1.5 mL). A solution of sodium ascorbate (13.5 mg, 0.07 mmol in 150 μL of H_2O) was added forming a homogenous solution. A solution of $CuSO_4$ $5H_2O$ (8.5 mg, 0.035 mmol dissolved in 150 μL of H_2O) was added and the resulting solution became dark brown before and yellow later. The reaction was stirred at 50 °C under nitrogen for 3 hours. The reaction was directly purified by chromatographic on silica gel using pentane/ethyl acetate 1:1 to afford 40 mg of an amorphous colorless solid in 18% yield.

R_f (cyclohexane/ethyl acetate 1:1): 0.61

M.p. (DSC 1st cooling cycle): 89.17 °C

IR (Film, CD_2Cl_2)*: 3272 *m*, 3067 *w*, 2955.25 *s*, 2929.99 *s*, 2859.71 *s*, 1730.90 *m*, 1660.87 *s*, 1634.29 *s*, 1592.26 *s*, 1531.94 *m*, 1505.22 *s*, 1467 *m*, 1440.35 *s*, 1384.15 *m*, 1329.57 *m*, 1266.24 *s*, 1247.45 *s*, 1113.36 *s*, 1045 *w*, 1020 *w*, 925 *w*, 822 *w*, 730.39 *w*, 582 *w*.

^{1}H-NMR (CD_2Cl_2, 400 MHz, 295K): δ= 8.34 (*s*, 4H, H8), 7.87 (*s*, 4H, H1), 7.60 (*t*, $^3J_{H,H}$ = 5.7 Hz, 4H, N-H_{ortho}), 7.27 (*s*, 2H, H4), 6.92 (*t*, $^3J_{H,H}$ = 5.6 Hz, 2H, N-H_{para}), 6.56 (*s*, 8H, H11), 6.54 (*s*, 4H, H12), 4.70-4.66 (AA'BB' *coupling system*, 8H, H2 and H3), 4.46 (*t*, $^3J_{H,H}$ = 5.3 Hz, 12H, H9 and H10), 3.95-3.85 (*m*, 40H, H18 and H7), 2.57 (*t*, $^3J_{H,H}$ = 7.2 Hz, 4H, H5), 1.85-1.65 (*m*, 40H, H19 and H6), 1.45-1.39 (*m*, 36H, H20), 1.34-1.27 (*m*, 72H, H21), 0.92-0.81 (*m*, 54H, H22) ppm.

^{13}C-NMR (CD_2Cl_2, 100 MHz, 295K): δ= 165.54 (*C*=O), 165.43 (*C*=O), 164.7 (*C*=O), 157.38 (*C*15), 153.90 (*C*23), 153.87 (*C*23), 147.1 (*C*13), 137.9 (*C*23), 134.01 (*C*14), 133.95 (*C*24), 133.85 (*C*25), 132.9 (*C*8), 131.2 (*C*17), 130.1 (*C*1), 129.3 (*C*16), 122.1 (*C*4), 107.09 (*C*11), 106.84 (*C*12), 77.4 (*C*7), 73.91 (*C*18), 73.87 (*C*18), 69.63 (*C*18), 69.59 (*C*18), 63.9 (*C*2 or *C*3), 49.4 (*C*2 or *C*3), 45.0 (*C*10), 44.9 (*C*9), 32.36 (*C*21), 32.35 (*C*21), 32.19 (*C*21), 32.17 (*C*21), 30.88 (*C*19), 30.86 (*C*19), 30.00 (*C*19), 29.98 (*C*19), 29.75 (*C*6), 26.4 (*C*20), 23.26 (*C*21), 23.19 (*C*21), 22.5 (*C*5), 14.43 (*C*22), 14.38 (*C*22) ppm.

HRMS (MALDI): Calc. for $[M+Na]^+$ $C_{190}H_{294}N_{12}NaO_{30}^+$ 3247.1741; found 3247.1827 $[M+Na]^+$

Synthesis of compound **80**

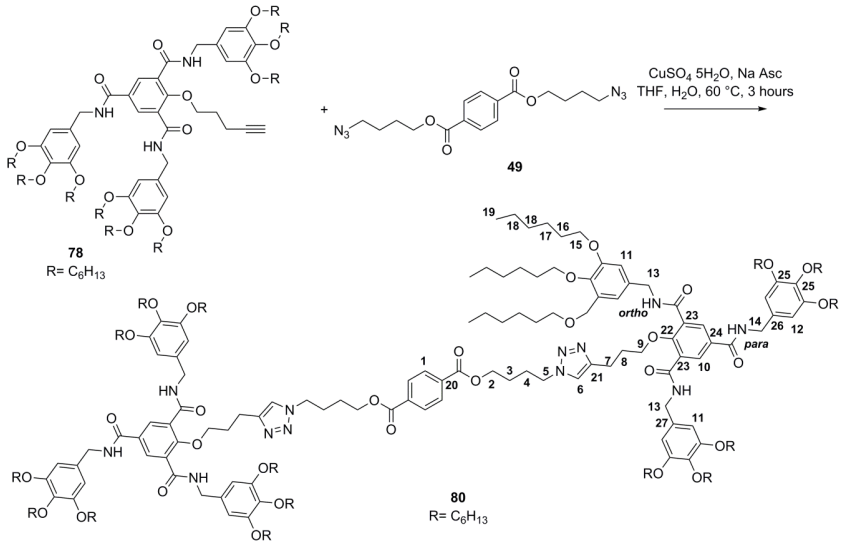

2-pentynyloxy BTA derivative **78** (150 mg, 0.102 mmol) and diazido derivative **49** (18.5 mg, 0.051 mmol) were dissolved in a vial in THF (1 mL). A solution of sodium ascorbate (10.2 mg, 0.05 mmol in 100 μL of H_2O) was added forming a homogenous solution. A solution of $CuSO_4$ $5H_2O$ (6.4 mg, 0.026 mmol dissolved in 100 μL of H_2O) was added and the reaction was stirred at 60 °C under nitrogen for 3 hours. The reaction was directly purified by chromatographic on silica gel using cyclohexane/ethyl acetate 4:6 and a second silica gel chromatography using toluene/ethyl acetate 1:1. The product was obtained as a 17.6 mg of amorphous colorless solid in 10% yield.

R_f (pentane/ethyl acetate 3:7): 0.56

M.p. (DSC 1st cooling cycle): 59.83 °C

IR (Film CD_2Cl_2)*: 2952 *m*, 2926 *m*, 2859 *m*, 1726 *w*, 1633 *m*, 1591 *w*, 1504 *w*, 1438 *m*, 1328 *w*, 1266 *m*, 1110 *s*, 1021 *m*, 730 *m*.

^{1}H-NMR (CD_2Cl_2, 400 MHz, 295K): δ= 8.43 (*s*, 4H, H10), 8.07 (*s*, 4H, H1), 7.59 (*t*, $^3J_{H,H}$ = 5.6 Hz, 4H, N-H_{ortho}), 7.15 (*s*, 2H, H6), 6.74 (*t*, $^3J_{H,H}$ = 5.3 Hz, 2H, N-H_{para}), 6.56 (*s*, 8H, H11), 6.53 (*s*, 4H, H12), 4.50-4.49 (*m*, 12H, H13 and H14), 4.34 (*q*, $^3J_{H,H}$ = 7.0 Hz, 8H, H2 and H5), 3.97-3.85 (*m*, 40H, H15 and H9), 2.53 (*t*, $^3J_{H,H}$ = 7.5 Hz, 4H, H7), 2.07-1.99 (*m*, 4H, H3 or H4), 1.83-1.65 (*m*, 44H, H16, H3 or H4 and H8), 1.50-1.44 (*m*, 36H, H17), 1.32-1.26 (m, 72H, H18), 0.89-0.86 (*m*, 54H, H19) ppm.

^{13}C-NMR (CD_2Cl_2, 100 MHz, 295K): δ= 166.0 (*C*=O), 165.3 (*C*=O), 164.6 (*C*=O), 157.4 (*C*22), 153.9 (*C*25), 146.7 (*C*21), 137.9 (*C*25), 134.6 (*C*20), 133.9 (*C*27), 133.7 (*C*26), 133.1 (*C*10), 131.4 (*C*23), 130.0 (*C*1), 129.3 (C24), 121.5 (*C*6), 106.9 (*C*11), 106.8 (*C*12), 77.5 (*C*9), 73.9 (*C*15), 69.6 (*C*15), 65.0 (*C*2 or *C*5), 50.1 (*C*2 or *C*5), 45.0 (*C*14), 44.9 (*C*13), 32.33 (*C*18), 32.15 (*C*18), 30.87 (*C*16), 30.83 (C16), 30.25-29.95-29.85-27.51 (*C*16, *C*3, *C*4 and *C*8), 26.3 (*C*17), 23.25 (*C*18), 23.18 (*C*18), 22.5 (*C*7), 14.42 (*C*19), 14.37 (*C*19) ppm.

HRMS (MALDI): Calc. for $[M+Na]^+$ $C_{194}H_{302}N_{12}NaO_{30}^+$ 3303.2367; found 3303.2323 $[M+Na]^+$

Synthesis of compound **81**

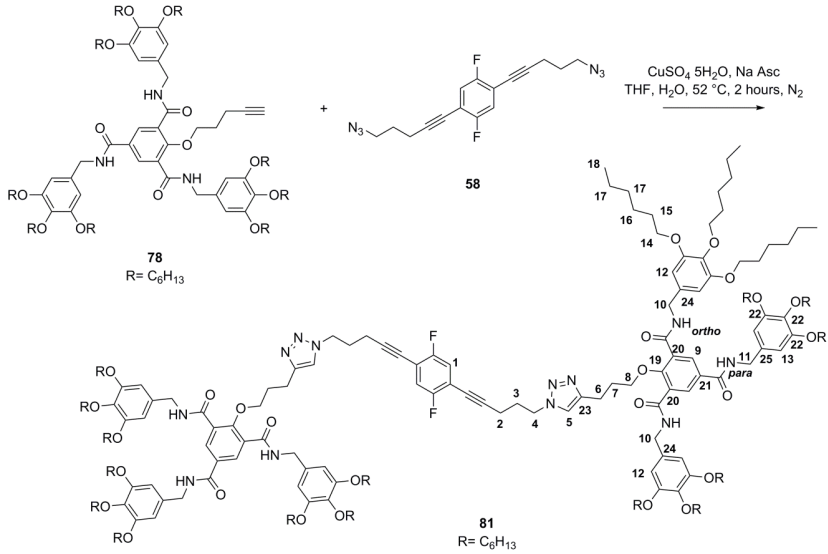

2-pentynyloxy BTA derivative **78** (200 mg, 0.136 mmol) and diazido compound **58** (22.5 mg, 0.07 mmol) were dissolved in a vial in THF (1.5 mL). A solution of sodium ascorbate (15 mg, 0.07 mmol in 150 μL of H_2O) was added forming a homogenous solution. A solution of $CuSO_4$ $5H_2O$ (10 mg, 0.035 mmol dissolved in 150 μL of H_2O) was added to the reaction stirred at 55 °C under nitrogen for 2 hours. The crude was directly purified by silica gel chromatographic using cyclohexane/ethyl acetate 4:6. The product was purified by a second silica gel column chromatography using toluene/ethyl acetate 6:4 as the eluent, and then by a preparative TLC plate using chloroform/ethyl acetate 9:1. The product was obtained as a 39.9 mg of amorphous colorless solid in 18% yield.

***R*$_f$**(cyclohexane/AcOEt 4:6): 0.56; ($CHCl_3$/AcOEt 9:1): 0.07

M.p. (DSC 1st cooling cycle): 63.45 °C

IR(Film, CD_2Cl_2)*: 2923 *m,* 2855 *m*, 1733 *w*, 1669 *w*, 1633 *m*, 1591 *m*, 1504 *m*, 1439 *m*, 1259 *w*, 1229 *m*, 1109 *s*, 1016 *m*, 925 *w*, 881 *w*, 801 *w*, 724 *w*, 668 *w*, 600 *w*.

^{1}H-NMR (CD_2Cl_2, 400 MHz, 295K): δ= 8.45 (*s*, 4H, H9), 7.59 (*t*, $^3J_{H,H}$ = 5.7 Hz, 4H, N-*H$_{ortho}$*), 7.19 (*s*, 2H, H5), 7.08 (*t*, $^3J_{F,H}$ = 7.5 Hz, $^4J_{F,H}$ = 7.5 Hz, 2H, H1), 6.75 (*t*, $^3J_{H,H}$ = 5.6 Hz, 2H, N-*H$_{para}$*), 6.56 (*s*, 8H, H12), 6.54 (*s*, 4H, H13), 4.49 (*t*, $^3J_{H,H}$ = 4.9 Hz, 12H, H10 and H11), 4.44 (*t*, $^3J_{H,H}$ = 6.9 Hz, 4H, H8), 3.98-3.85 (*m*, 40H, H14 and H4), 2.54-2.48 (*m*, 8H, H6 and H2), 2.18 (*quint*, $^3J_{H,H}$ = 6.8 Hz, 4H, H7), 1.84-1.65 (*m*, 40H, H15 and H3), 1.50-1.40 (*m*, 36H, H16), 1.36-1.26 (*m*, 72H, H17), 0.91-0.86 (*m*, 54H, H18) ppm.

^{13}C-NMR (CD_2Cl_2, 100 MHz, 295K): δ= 165.3 (*C*=O), 164.6 (*C*=O), 157.5 (*C*19), 153.9 (*C*22), 153.9 (*C*22), 146.7 (*C*23), 137.95 (*C*22), 137.92 (*C*22), 133.9 (*C*24), 133.8 (*C*25), 133.1 (*C*9), 131.4 (*C*21), 129.3 (*C*20), 121.8 (*C*5), 107.0 (*C*12), 106.8 (*C*13), 77.6 (*C*4), 73.9 (*C*14), 69.6 (*C*14), 49.3 (*C*8), 45.0 (*C*11), 44.9 (*C*10), 32.35 (*C*17), 32.16 (*C*17), 30.88 (*C*17), 30.85 (*C*17), 29.97-29.89 (*C*15 and *C*3), 29.45 (*C*7), 26.35 (*C*16), 23.26 (*C*17), 23.19 (*C*17), 22.5 (*C*2 or *C*6), 17.5 (*C*2 or *C*6), 14.42 (*C*18), 14.37 (*C*18) ppm.

^{19}F-NMR (CD_2Cl_2, 400 MHz, 295K): δ= -117.25 ppm

HRMS (MALDI): Calc. for $[M+Na]^+$ $C_{194}H_{296}F_2N_{12}NaO_{26}^+$ 3271.2069; found 3271.2063 $[M+Na]^+$

Additional Information

^{1}H-NMR titration data

Fitting curves were obtained by a non-linear least squares interpolation on experimental NMR data using OriginPro 8® program.

[**42**][a]	δ N-H	δ_{theor} N-H[b]	χ_{agg}[c]	χ_{mon}[d]	δ C-H	δ_{theor} C-H[d]	D[f]
202.3	8.41	8.385	0.975	0.025	6.687	6.716	-9.79
101.15	8.192	8.216	0.869	0.131	6.886	6.856	
50.575	7.792	7.793	0.673	0.327	7.268	7.269	
25.9[g]	*7.283*	*7.187*	*0.423*	*0.577*	*7.268*	*7.839*	*-9.19*
25.287	7.205	7.166	0.385	0.615	7.813	7.856	
12.64	6.652	6.704	0.114	0.886	8.248	8.188	
6.32	6.525	6.508	0.051	0.949	8.296	8.289	
3.16	6.455	6.446	0.017	0.983	8.302	8.313	
1.58	6.437	6.427	0.008	0.992	8.302	8.318	
0.79	6.425	6.422	0.002	0.998	8.302	8.320	
0.395	6.41	6.421	0.000	1.005	8.302	8.320	
δ_{mon}[h]	6.42				8.32		
δ_{agg}[i]	8.46				6.67		
K_d[l]	34.125				39.03		
p[m]	1.8351				2.1652		

Table 4. Concentration-induced chemical shift variation of BTA **42** measured in CD_2Cl_2 at 295 K. [a] [mmo/L]. [b] Chemical shift values calculated from the simulating equation.[c] Aggregated species molar fraction calculated on the N-H signals.[d] Monomer species molar fraction ($1-\chi_{agg}$).[f] Diffusion coefficient measured as $\log(m^2s^{-1})$.[g] This value of chemical shift was not used in the fitting process. The values of χ were extrapolated from the fitting curve. [h] The value refers to the extrapolated chemical shift at the lowest concentration, where molecules are assumed to be fully monomer species. [i] The value refers to the extrapolated chemical shift at the highest concentration, where molecules are assumed to be fully aggregate. [l] Dissociation constant (mmol/L). [m] Slope factor of the fitting curve.

[**37b**] [a]	δ N-H$_{ortho}$	δ_t N-H$_{ortho}$ [b]	χ_{agg} N-H$_{ortho}$ [c]	χ_{mon} N-H$_{ortho}$ [d]	δ N-H$_{para}$	δ_t N-H$_{para}$ [e]	χ_{agg} N-H$_{para}$ [f]	χ_{mon} N-H$_{para}$ [g]	δ C-H	δ_t C-H [h]	D [i]
198.8 [l]	7.359	7.3313	0.558	0.442	6.892	6.8247	0.596	0.404	8.098	8.1251	-9.23
99	7.253	7.2530	0.349	0.651	6.663	6.6628	0.368	0.632	8.190	8.1901	
49.5	7.188	7.1883	0.221	0.779	6.526	6.5269	0.231	0.769	8.238	8.2376	-9.08
24.75	7.143	7.1424	0.133	0.867	6.432	6.4303	0.137	0.863	8.268	8.2685	
12.37	7.113	7.1134	0.074	0.926	6.369	6.3699	0.074	0.926	8.287	8.2871	
6.18	7.096	7.0964	0.040	0.960	6.334	6.3351	0.039	0.961	8.298	8.2977	-9.02
3.09	7.087	7.0869	0.022	0.978	6.317	6.3160	0.023	0.977	8.304	8.3036	
1.545	7.083	7.0817	0.014	0.986	6.306	6.3057	0.012	0.988	8.307	8.3068	
0.772	7.078	7.0789	0.005	0.995	6.30	6.3003	0.006	0.994	8.308	8.3085	-8.89
δ_{mon} [m]	7.0757				6.29441				8.31055		
δ_{agg} [n]	7.58302				7.29724				7.82693		
K_d [o]	195.50318				175.98083				336.883		
p [p]	0.91353				0.94469				0.90102		

Table 5. Concentration-induced chemical shift variation of BTA **37b** measured in CD_2Cl_2 at 295 K. [a] [mmo/L]. [b] Chemical shift values calculated from the simulating equation for N-H$_{ortho}$ signal. [c] Aggregated species molar fraction calculated for N-H$_{ortho}$ signals. [d] Monomer species molar fraction calculated for N-H$_{ortho}$ signals (1-χ_{agg}). [e] Chemical shift values calculated from the simulating equation for N-H$_{para}$ signals. [f] Aggregated species molar fraction calculated for N-H$_{para}$ signals. [g] Monomer species molar fraction calculated for N-H$_{para}$ signals (1-χ_{agg}). [h] Chemical shift values calculated from the simulating equation for C-H signals. [i] Diffusion coefficient measured as log(m^2s^{-1}). [l] This value was not taken into account on the fitting process due to an inconsistency with the fitting process. The values of χ were extrapolated from the fitting curve. [m] The value refers to the extrapolated chemical shift at the lowest concentration, where molecules are assumed to be fully monomer species. [n] The value refers to the extrapolated chemical shift at the highest concentration, where molecules are assumed to be fully aggregate. [o] Dissociation constant (mmol/L). [p] Slope factor of the fitting curve.

[**41**] [a]	δ N-H $_{ortho}$	δ_t N-H$_{ortho}$ [b]	χ_{agg} N-H$_{ortho}$ [c]	χ_{mon} N-H$_{ortho}$ [d]	δ N-H $_{para}$	δ_t N-H$_{para}$ [e]	χ_{agg} N-H $_{para}$ [f]	χ_{mon} N-H $_{para}$ [g]	δ C-H	δ_t C-H [h]	D [i]
82	8.317	8.2954	0.950	0.050	8.660	8.6400	0.9442	0.0558	6.888	6.893	
41	8.096	8.1195	0.865	0.135	8.438	8.4563	0.8623	0.1377	6.979	6.971	-9.46
20.5	7.777	7.7934	0.742	0.258	8.110	8.1287	0.7413	0.2587	7.115	7.110	
13.666 6	7.540	7.5234	0.651	0.349	7.874	7.8625	0.6543	0.3457	7.213	7.219	-9.22
3.4166 6	6.525	6.4987	0.260	0.740	6.873	6.8358	0.2851	0.7149	7.606	7.608	
1.700	6.137	6.1724	0.111	0.889	6.447	6.4857	0.1280	0.8720	7.734	7.727	
0.850	5.986	5.9984	0.053	0.947	6.272	6.2874	0.0634	0.9366	7.793	7.791	
0.425	5.922	5.9154	0.028	0.972	6.183	6.1873	0.0306	0.9694	7.821	7.821	
0.2106	5.885	5.8777	0.014	0.986	6.154	6.1394	0.0199	0.9801	7.835	7.836	
0.106	5.871	5.8616	0.008	0.992	6.130	6.1179	0.0111	0.9889	7.841	7.842	
δ_{mon} [l]	5.84927				6.100				7.847		
δ_{agg} [m]	8.44648				8.81137				6.821		
K_d [n]	8.39493				8.011				9.315		
p [o]	1.22176				1.15913				1.189		

Table 6. Concentration-induced chemical shift variation of BTA **41** measured in $CDCl_3$ at 295 K. [a] [mmo/L]. [b] Chemical shift values calculated from the simulating equation for N-H$_{ortho}$ signal. [c] Aggregated species molar fraction calculated for N-H$_{ortho}$ signals. [d] Monomer species molar fraction calculated for N-H$_{ortho}$ signals (1-χ_{agg}). [e] Chemical shift values calculated from the simulating equation for N-H$_{para}$ signals. [f] Aggregated species molar fraction calculated for N-H$_{para}$ signals. [g] Monomer species molar fraction calculated for N-H$_{para}$ signals (1-χ_{agg}). [h] Chemical shift values calculated from the simulating equation for C-H signals. [i] Diffusion coefficient measured as log(m^2s^{-1}). [l] The value refers to the extrapolated chemical shift at the lowest concentration, where molecules are assumed to be fully monomer species. [m] The value refers to the extrapolated chemical shift at the highest concentration, where molecules are assumed to be fully aggregate. [n] Dissociation constant (mmol/L). [o] Slope factor of the fitting curve.

[**52**] [a]	δ N-H ortho	δ_t N-H [b] ortho	χ_{agg} N-H [c] ortho	χ_{mon} N-H [d] orto	δ N-H para	δ_t N-H [e] para	χ_{agg} N-H [f] para	χ_{mon} N-H [g] para	δ C-H	δ_t C-H [h]	Linker [i]	*D* [l]
183.34 [m]	7.449				7.003				8.040		7.931	-9.49
104.24	7.404	7.404	0.814	0.186	6.906	6.906	0.859	0.141	8.068	8.068	7.930	
37.47	7.349	7.353	0.482	0.518	6.799	6.808	0.559	0.441	8.098	8.096	7.924	-9.32
18.73	7.313	7.315	0.264	0.736	6.721	6.724	0.304	0.696	8.113	8.113	7.921	
9.367	7.291	7.290	0.131	0.869	6.671	6.668	0.131	0.869	8.122	8.122	7.919	
4.683												
5	7.278	7.278	0.053	0.947	6.640	6.641	0.050	0.950	8.126	8.126	7.917	-9.20
2.34	7.272	7.272	0.016	0.984	6.629	6.630	0.018	0.982	8.127	8.128	7.917	
1.17	7.271	7.270	0.010	0.990	6.626	6.626	0.006	0.994	8.128	8.128	7.917	
0.585	7.269	7.270	-0.002	1.002	6.626	6.625	0.002	0.998	8.129	8.128	7.917	-9.16
δ_{mon} [n]	7.26929				6.624				8.1284			
δ_{agg} [o]	7.4347				6.9525				8.0496			
K_d [p]	36.86702				32.093				47.191			
p [q]	1.42853				1.53403				1.5037			

Table 7. Concentration-induced chemical shift variation of dimer **52** measured in CD_2Cl_2 at 295 K.[a] [mmo/L]. [b] Chemical shift values calculated from the simulating equation for N-H_{ortho} signal. [c] Aggregated species molar fraction calculated for N-H_{ortho} signals. [d] Monomer species molar fraction calculated for N-H_{ortho} signals (1-χ_{agg}). [e] Chemical shift values calculated from the simulating equation for N-H_{para} signals. [f] Aggregated species molar fraction calculated for N-H_{para} signals. [g] Monomer species molar fraction calculated for N-H_{para} signals (1-χ_{agg}). [h] Chemical shift values calculated from the simulating equation for C-H signals. [i] Measure chemical shift of the aromatic C-H protons of the linker unit. [l] Diffusion coefficient measured as log(m^2s^{-1}). [m] This value was not taken into account on the fitting process due to an inconsistency with the fitting process. The values of χ were extrapolated from the fitting curve. [n] The value refers to the extrapolated chemical shift at the lowest concentration, where molecules are assumed to be fully monomer species. [o] The value refers to the extrapolated chemical shift at the highest concentration, where molecules are assumed to be fully aggregate. [p] Dissociation constant (mmol/L). [q] Slope factor of the fitting curve.

[**53**] [a]	δ N-H ortho	δ_t N-H ortho [b]	χ_{agg} N-H [c] ortho	χ_{mon} N-H [d] orto	δ N-H para	δ_t N-H [e] para	χ_{agg} N-H [f] para	χ_{mon} N-H [g] para	δ C-H	δ_t C-H [h]	Linker [i]	*D* [l]
188.59 [m]	7.485				7.027				8.101		8.056	
106.19	7.406	7.408	0.756	0.244	6.843	6.847	0.763	0.237	8.152	8.15	8.061	
56.9	7.367	7.363	0.596	0.404	6.765	6.755	0.607	0.393	8.168	8.17	8.062	-9.40
28.45	7.303	7.307	0.333	0.667	6.627	6.638	0.331	0.669	8.203	8.20	8.062	
14.225	7.264	7.264	0.173	0.827	6.549	6.548	0.175	0.825	8.223	8.22	8.063	
7.112	7.243	7.240	0.087	0.913	6.505	6.499	0.087	0.913	8.235	8.24	8.063	-9.22
3.556	7.232	7.229	0.041	0.959	6.481	6.476	0.040	0.960	8.24	8.24	8.063	
1.778	7.224	7.225	0.009	0.991	6.465	6.467	0.008	0.992	8.244	8.24	8.063	
0.889	7.222	7.223	0.000	1.000	6.457	6.464	-0.008	1.008	8.246	8.24	8.063	
0.444	7.221	7.222	-0.004	1.004	6.463	6.462	0.004	0.996	8.246	8.24	8.063	-9.12
δ_{mon} [n]	7.222				6.461				8.245			
δ_{agg} [o]	7.466				6.961				8.130			
K_d [p]	44.992				44.117				38.386			
p [q]	1.354				1.380				1.471			

Table 8. Concentration-induced chemical shift variation of dimer **53** measured in CD_2Cl_2 at 295 K.[a] [mmo/L]. [b] Chemical shift values calculated from the simulating equation for N-H_{ortho} signal. [c] Aggregated species molar fraction calculated for N-H_{ortho} signals. [d] Monomer species molar fraction calculated for N-H_{ortho} signals (1-χ_{agg}). [e] Chemical shift values calculated from the simulating equation for N-H_{para} signals. [f] Aggregated species molar fraction calculated for N-H_{para} signals. [g] Monomer species molar fraction calculated for N-H_{para} signals (1-χ_{agg}). [h] Chemical shift values calculated from the simulating equation for C-H signals. [i] Measure chemical shift of the aromatic C-H protons of the linker unit. [l] Diffusion coefficient measured as log(m^2s^{-1}). [m] This value was not taken into account on the fitting process due to an inconsistency with the fitting process. The values of χ were extrapolated from the fitting curve. [n] The value refers to the extrapolated chemical shift at the lowest concentration, where molecules are assumed to be fully monomer species. [o] The value refers to the extrapolated chemical shift at the highest concentration, where molecules are assumed to be fully aggregate. [p] Dissociation constant (mmol/L). [q] Slope factor of the fitting curve.

[**54**] [a]	δ N-H ortho	δ_t N-H ortho [b]	χ_{agg} N-H ortho [c]	χ_{mon} N-H orto [d]	δ N-H para	δ_t N-H para [e]	χ_{agg} N-H para [f]	χ_{mon} N-H para [g]	δ C-H	δ_t C-H [h]	Linker [i]	*D* [l]
193.46 [m]	7.487				5.773				7.205		8.074	-9.53
92.062	7.367	7.367	0.862	0.138	6.773	6.773	0.784	0.216	8.205	8.20	8.074	
25.79	7.304	7.304	0.495	0.505	6.612	6.612	0.415	0.585	8.232	8.23	8.073	-9.31
12.895	7.264	7.264	0.262	0.738	6.530	6.530	0.227	0.773	8.249	8.25	8.073	
6.447	7.238	7.239	0.110	0.890	6.478	6.478	0.107	0.893	8.258	8.26	8.073	-9.30
3.2237	7.228	7.227	0.052	0.948	6.450	6.452	0.043	0.957	8.264	8.26	8.073	
1.6118	7.222	7.222	0.017	0.983	6.442	6.440	0.025	0.975	8.265	8.26	8.073	
0.806	7.220	7.220	0.005	0.995	6.435	6.435	0.008	0.992	8.266	8.27	8.073	
0.403	7.219	7.219	0.000	1.000	6.432	6.433	0.002	0.998	8.267	8.27	8.073	-9.18
δ_{mon} [n]	7.219				6.431				8.267			
δ_{agg} [o]	7.391				6.867				8.194			
K_d [p]	26.227				33.669				27.841			
p [q]	1.458				1.284				1.427			

Table 9. Concentration-induced chemical shift variation of dimer **54** measured in CD_2Cl_2 at 295 K.[a] [mmo/L]. [b] Chemical shift values calculated from the simulating equation for N-H_{ortho} signal. [c] Aggregated species molar fraction calculated for N-H_{ortho} signals. [d] Monomer species molar fraction calculated for N-H_{ortho} signals (1-χ_{agg}). [e] Chemical shift values calculated from the simulating equation for N-H_{para} signals. [f] Aggregated species molar fraction calculated for N-H_{para} signals. [g] Monomer species molar fraction calculated for N-H_{para} signals (1-χ_{agg}). [h] Chemical shift values calculated from the simulating equation for C-H signals. [i] Measure chemical shift of the aromatic C-H protons of the linker unit. [l] Diffusion coefficient measured as log(m^2s^{-1}). [m] This value was not taken into account on the fitting process due to an inconsistency with the fitting process. The values of χ were extrapolated from the fitting curve. [n] The value refers to the extrapolated chemical shift at the lowest concentration, where molecules are assumed to be fully monomer species. [o] The value refers to the extrapolated chemical shift at the highest concentration, where molecules are assumed to be fully aggregate. [p] Dissociation constant (mmol/L). [q] Slope factor of the fitting curve.

[**59**] [a]	δ N-H ortho	δ_t N-H ortho [b]	χ_{agg} N-H ortho [c]	χ_{mon} N-H_{orto} [d]	δ N-H para	δ_t N-H para [e]	χ_{agg} N-H para [f]	χ_{mon} N-H para [g]	δ C-H	δ_t C-H [h]	δ Linker [i]	δ ^{19}F
184.												
15	7.456	7.457	0.770	0.230	6.952	6.954	0.763	0.237	8.144	8.14	7.098	-117.21
64	7.36	7.355	0.490	0.510	6.74	6.731	0.479	0.521	8.183	8.18	7.096	-117.24
32	7.28	7.287	0.257	0.743	6.57	6.585	0.252	0.748	8.224	8.22	7.096	-117.24
16	7.24	7.240	0.140	0.860	6.49	6.484	0.145	0.855	8.246	8.25	7.096	-117.25
8	7.22	7.214	0.082	0.918	6.43	6.428	0.065	0.935	8.259	8.26	7.097	-117.25
4	7.2	7.201	0.024	0.976	6.41	6.402	0.038	0.962	8.265	8.27	7.097	-117.25
2	7.2	7.196	0.024	0.976	6.39	6.390	0.012	0.988	8.268	8.27	7.097	-117.27
1	7.19	7.194	-0.005	1.005	6.38	6.385	-0.002	1.002	8.270	8.27	7.097	-117.26
0.5	7.19	7.193	-0.005	1.005	6.38	6.383	-0.002	1.002	8.272	8.27	7.097	-117.26
δ_{mon} [m]	7.192				6.381				8.270			
δ_{agg} [n]	7.535				7.130				8.123			
K_d [o]	69.023				71.031				51.679			
p [p]	1.245				1.237				1.432			

Table 10. Concentration-induced chemical shift variation of dimer **59** measured in CD_2Cl_2 at 295 K.[a] [mmo/L]. [b] Chemical shift values calculated from the simulating equation for N-H_{ortho} signal. [c] Aggregated species molar fraction calculated for N-H_{ortho} signals. [d] Monomer species molar fraction calculated for N-H_{ortho} signals (1-χ_{agg}). [e] Chemical shift values calculated from the simulating equation for N-H_{para} signals. [f] Aggregated species molar fraction calculated for N-H_{para} signals. [g] Monomer species molar fraction calculated for N-H_{para} signals (1-χ_{agg}). [h] Chemical shift values calculated from the simulating equation for C-H signals. [i] Measure chemical shift of the aromatic C-H protons of the linker unit. [l] Diffusion coefficient measured as log(m^2s^{-1}). [m] The value refers to the extrapolated chemical shift at the lowest concentration, where molecules are assumed to be fully monomer species. [n] The value refers to the extrapolated chemical shift at the highest concentration, where molecules are assumed to be fully aggregate. [o] Dissociation constant (mmol/L). [p] Slope factor of the fitting curve.

References

[1] D. Wu, A. Chen, C. S. Johnson, Jr., *J. Magn. Reson., Ser. A* **1995**, *115*, 260-264.

[2] S. M. June, P. Bissel, T. E. Long, *J. Polym. Sci., Part A: Polym. Chem.* **2012**, *50*, 3797-3805, S3797/3791-S3797/3798.

[3] D. E. Phipps, P. D. Beer, *Tetrahedron Lett.* **2009**, *50*, 3454-3457.

[4] M. Pal, K. Parasuraman, K. R. Yeleswarapu, *Org. Lett.* **2003**, *5*, 349-352.

[5] T. Ueda, N. Kanomata, H. Machida, *Org. Lett.* **2005**, *7*, 2365-2368.

[6] A. Kraft, F. Osterod, R. Froehlich, *J. Org. Chem.* **1999**, *64*, 6425-6433.

[7] V. Percec, H.-J. Sun, P. Leowanawat, M. Peterca, R. Graf, H. W. Spiess, X. Zeng, G. Ungar, P. A. Heiney, *J. Am. Chem. Soc.* **2013**, *135*, 4129-4148.